

Copy No.

47

Issue Date: 12 February 1963

X 63 14387

Code 2dr

LIQUID ROCKET PLANT

Report No. LRP 297, Volume II

Prepared by
AEROJET-GENERAL CORPORATION
Liquid Rocket Plant

Contract NAS8-2599
Purchase Order No. 6403-SC (STL)

Prepared for
SPACE TECHNOLOGY LABORATORIES, INC.
One Space Park
Redondo Beach, California

63-257



AEROJET-GENERAL CORPORATION

SACRAMENTO, CALIFORNIA

FOREWORD

This study was sponsored by the Future Projects Office, Marshall Space Flight Center, NASA, Huntsville, Alabama as a portion of its large booster feasibility and system cost study program. It is an extension of Contract NAS8-2599 with Space Technology Laboratories, Inc., Aerojet-General Corporation is the major subcontractor under this study program.

Previous studies have indicated that application of sea borne techniques to very large launch vehicles may offer a more effective solution to the launch of very large unit payloads when compared to other booster concepts. This study will describe a sea launch booster system, define a vehicle and its performance, and apply developed costing techniques to show what economies may be expected when vehicle size is increased rapidly, vehicle simplicity is emphasized, and vehicle recovery and reuse is exploited. The use of the sea launch technique is primarily to permit latitude in the choice of vehicle size, simplicity of design, handling and launch, and simplicity in recovery techniques.

TABLE OF CONTENTS

	<u>PAGE NO.</u>
I. INTRODUCTION	I-1
II. VEHICLE DESCRIPTION	II-1
A. GENERAL FEATURES AND FUNCTION	II-1
B. OPERATIONAL SEQUENCE	II-5
C. SYSTEM PERFORMANCE	II-6
III. VEHICLE SUBSYSTEMS	III A-1
A. STAGE I PROPULSION SYSTEM	III A-1
B. STAGE II PROPULSION SYSTEM	III B-1
C. INTERSTAGE STRUCTURE ASSEMBLIES	III C-1
D. PAYLOAD	III D-1
E. CONTROL SYSTEM	III E-1
F. GUIDANCE SYSTEM	III F-1
G. RECOVERY SYSTEM	III G-1
H. SECONDARY SUBSYSTEMS	III H-1
I. BALLAST UNIT	III I-1

TABLE OF CONTENTS (cont.)

	<u>PAGE NO.</u>
IV. VEHICLE STRUCTURAL CHARACTERISTICS	IV-1
V. VEHICLE ANALYSIS	V A-1
A. SYSTEM PERFORMANCE	V A-1
B. VEHICLE LOADS AND DYNAMICS	V B-1

APPENDIXES

	<u>APPENDIX NO.</u>
TANKAGE MATERIALS	II-1
COMBUSTION STABILITY	II-2
SECOND-STAGE CHAMBER AND NOZZLE COOLING	II-3
INSULATION	II-4
AUTOGENOUS PRESSURIZATION SYSTEM	II-5
EXPANDABLE NOZZLE	II-6
IGNITION SYSTEM AND IGNITION SEQUENCE	II-7
FILL, VENT, AND DUMP SYSTEMS	II-8

TABLE OF CONTENTS (cont.)

	<u>APPENDIX NO.</u>
FIRST-STAGE NOZZLE DESIGN ANALYSIS	II-9
AN ALTERNATE FIRST-STAGE TVC SYSTEM	II-10
RE-ENTRY FLARE DESIGN	II-11
ACCURACY ANALYSES AND GUIDANCE EQUATIONS	II-12
COMPONENT DESIGN DATA	II-13
CHECKOUT AND GSE	II-14
EXPERIMENTAL WATER ENTRY PROGRAM	II-15
ASCENT TRAJECTORY, ATMOSPHERIC MODE	II-16
CONSIDERATIONS PERTAINING TO STAGE SEPARATION	II-17
DESIGN ANGLE OF ATTACK AND HISTORIES OF THRUST DEFLECTION CAUSED BY WINDS	II-18
TOWING CABLE DYNAMICS	II-19
EXAMPLE OF RESPONSE TO WAVE MOTION	II-20
LAUNCH DYNAMICS	II-21
IMPACT DYNAMICS	II-22
PROPELLANT SLOSHING	II-23
SEA DRAGON ACOUSTIC NOISE STUDY	II-24
NOZZLE FLUTTER	II-25

TABLE LIST

	<u>Table No.</u>
Summary of Sea Dragon Vehicle Characteristics	II-A-1
Stage I Weight Breakdown	II-A-2
Stage II Weight Breakdown	II-A-3
Sequence of Operations	II-B-1
Tank Design	III-A-1
Tank Pressures Required to React Vehicle Body Loads	III-A-2
Stage I Propulsion System Weight, Recoverable Vehicle	III-A-3
Stage II Propulsion System Weight Breakdown	III-B-1
Weight and Performance Data	V-A-1
Comparison of Continuous Burn Ascent Trajectory to Restart Trajectory	V-A-2
Acoustic Environment Experienced by Structure	V-B-1

FIGURE LIST

	<u>Figure No.</u>
Sea Dragon Vehicle Schematic	II-A-1
Sea Dragon Vehicle--External View	II-A-2
Sea Dragon Vehicle--Internal View	II-A-3
Sea Dragon Launch Sequence	II-A-4
Sea Dragon Flight Sequence	II-A-5
Stage I Trajectory Parameters	II-C-1
Stage II Trajectory Parameters	II-C-2
Stage I Propulsion System Layout Drawing	III-A-1
Stage I Propellant Performance	III-A-2
Stage I Nozzle Types	III-A-3
Stage I Engine Contour	III-A-4
Chamber Pressure versus Propellant Consumption (Stage I)	III-A-5
Stage I Injector	III-A-6

FIGURE LIST (cont.)

	<u>Figure No.</u>
Alternate Thrust Chamber Coolant Designs	III-A-7
Gimbal Actuator Flow System	III-A-8
Mass Fraction versus Tank Material	III-A-9
Stage I Pressurization System	III-A-10
Profile of Pressure Drops	III-A-11
Stage I LO ₂ Tank Pressure versus Time	III-A-12
Stage I RP-1 Tank Pressures	III-A-13
Specific Impulse versus Chamber Pressure (Stage I)	III-A-14
Stage II Propulsion System Layout Drawing	III-B-1
Stage II Engine Contour	III-B-2
Stage II Injector	III-B-3
Stage II Pressurization System	III-B-4
TVC Engine Pressurization System	III-B-5
Specific Impulse versus Mixture Ratio (TVC Engine)	III-B-6

FIGURE LIST (cont.)

	<u>Figure No.</u>
Thrust versus Mixture Ratio (TVC Engine)	III-B-7
Specific Impulse versus Altitude (TVC Engine)	III-B-8
Stage II Propellant Performance	III-B-9
Large Expandable Nozzle Currently Undergoing Altitude Tests	III-B-10
Interstage Assembly	III-C-1
Staging Sequence Schematic	III-C-2
Angles and Forces Acting on Vehicle	III-E-1
Characteristics of Simplified Autopilot	III-E-2
Root Locus for Autopilot with Undamped Sloshing Dipoles	III-E-3
Self-Alignment Mode	III-F-1
Flight Navigation Mode	III-F-2
Permissible Error in Velocity at Injection versus Probability of Not Exceeding Tolerances in Eccentricity	III-F-3

FIGURE LIST (cont.)

	<u>Figure No.</u>
Tolerance in Radial Position at Injection versus Probability of Not Exceeding Given Eccentricity	III-F-4
Basic Loop of Inertial Guidance System	III-F-5
General Concept of Flight Mode Guidance	III-F-6
Block Diagram of L-90 Computer	III-F-7
Deceleration versus Time	III-G-1
Tank Pressure versus Critical Impact Velocity	III-G-2
Pressure Distribution at Various Core Immersion Depths	III-G-3
Water Entry Parameters versus Entry Time	III-G-4
Impact Acceleration versus Time	III-G-5
Stage I Recoverable Configuration	III-G-6
Weight Distribution at Liftoff	IV-1
EA vs Length	IV-2
EI vs Length	IV-3
Bending Modes At Launch	IV-4
Bending Modes while Empty	IV-5

FIGURE LIST (cont.)

	<u>Figure No.</u>
Thrust-Weight Optimization	V-A-1
Staging Ratio Optimization	V-A-2
Stage I Area Ratio Optimization	V-A-3
Drag Coefficient vs Mach Number	V-A-4
Underwater Trajectory	V-A-5
Net Pressure on Skirt	V-A-6
Performance Parameters Stage I	V-A-7
Trajectory Parameters Stage I	V-A-8
Performance Parameters Stage II, High Thrust	V-A-9
Trajectory Parameters Stage II, High Thrust	V-A-10
Performance Parameters Stage I, Low Thrust	V-A-11
Trajectory Parameters Stage I, Low Thrust	V-A-12
Staging Data, Separation Time versus Stroke Length	V-A-13
Staging Data, Displacement versus Separation Distance	V-A-14
Bending Moment Diagram--Still Water, Loaded, Sealed Interstage	V-B-1
Shear Curve--Hogging Condition	V-B-2
Bending Moment--Hogging Condition	V-B-3
Shear Curve--Sagging Condition	V-B-4
Bending Moment--Sagging Condition	V-B-5
Loading During Erection (2.5×10^6 lb Ballast)	V-B-6
Bending Moment During Erection (2.5×10^6 lb Ballast)	V-B-7
Loading During Erection (5×10^6 lb Ballast)	V-B-8
Bending Moment During Erection (5×10^6 lb Ballast)	V-B-9

FIGURE LIST (cont.)

	<u>Figure No.</u>
Axial Load vs Station (Sea State 6)	V-B-10
Shear versus Station (Sea State 6)	V-B-11
Moment versus Station (Sea State 6)	V-B-12
Axial Load vs Station (Sea State 7)	V-B-13
Shear Load vs Station (Sea State 7)	V-B-14
Moment versus Station (Sea State 7)	V-B-15
Pitching Amplitude vs Wind Velocity	V-B-16
Heave Amplitude vs Wind Velocity	V-B-17
Sea State vs Wind Velocity	V-B-18
Bending Moment, Maximum Dynamic Pressure	V-B-19
Impact Forces	V-B-20
Impact Accelerations	V-B-21
Impact Dynamic Loads	V-B-22
Frequency versus Fluid Depth Stage I Fuel Tank	V-B-23
Frequency versus Fluid Depth Stage I LO ₂ Tank	V-B-24
Frequency versus Fluid Depth Stage II Fuel Tank	V-B-25
Frequency versus Fluid Depth Stage II Oxidizer Tank	V-B-26
Near Field Sound Level	V-B-27
Near Noise Field after Water Exit	V-B-28

I. INTRODUCTION

This volume discusses the vehicle system that has been defined and analyzed as a result of the Sea Dragon study.

The technical approach was taken for several reasons:

1. The time available was limited -- four months for the complete task.
2. Basic data defining the vehicle portion of the overall system was needed early in the course of the study as input to supplementary investigations in such phases as manufacturing and operational support.
3. To analyze potential problems in depth, it was necessary to establish a detailed preliminary vehicle design.

These factors pointed to the necessity for freezing basic design parameters early in the study. The design decisions made at this point were on the basis of previous studies, first level optimization studies,

I, Introduction (cont.)

and to some extent on arbitrary engineering judgments. Using this information, a preliminary expendable vehicle configuration (No. 132) was developed by three weeks after the start of the study. This basic design was refined and detailed in a later version (No. 134) released midway through the study. The final recoverable design (No. 135), which is discussed in the vehicle description section, was produced one month before the completion of the study. All of these configurations are basically similar; various supporting studies and analyses were on the basis of the design available at the time the analysis had to be initiated to meet study deadlines. Wherever possible, the analyses have been modified to show how they relate to Configuration No. 135.

Because of the design approach followed, the degree of optimization possible was obviously limited. Results of the design study and analyses show that in some phases of the study, improvement in technical approach is possible. Where these problems can be defined, the avenues to possible improvement are discussed.

II. VEHICLE DESCRIPTION

A. GENERAL FEATURES AND FUNCTION

The Sea Dragon is a very large sea-launched two stage liquid propellant rocket vehicle that will be used to inject into earth orbit large payloads. As presently designed, the vehicle has a gross liftoff weight of 40 million lb and is capable of propelling a payload of approximately 1,100,000 lb to a circular orbit of 300 nm altitude. The payload was assumed to be liquid hydrogen for this study, but it could be other material or equipment, or additional propulsion stages. A command module of the Apollo type provides the guidance, control, and communication functions; it will be capable of separation, re-entry and recovery as well as abort functions.

The vehicle as shown in Figure II-A-1, II-A-2, and II-A-3 is nominally 75 ft in diameter and 500 ft long. Tables II-A-1, II-A-2, and II-A-3 list other principle characteristics of the vehicle. Detailed propulsion system (stage) drawings are included in Parts 3A and B.

II, A, General Features and Function (cont.)

The major components of the vehicle, such as the first stage, second stage, and payload will be separately towed by sea to the assembly site where they will be assembled in the horizontal position while floating in a quiet lagoon. Small components that might be better transported by land or air will be installed and checked out at the assembly site. The vehicle will be capable of being serviced and operated in moderately heavy seas. To achieve proper flotation and stability characteristics during towing and while in the vertical prelaunch attitude, the vehicle will be equipped with a ballast unit. During the launch sequence, the ballast unit is released and later taken in tow for reuse.

The first stage of the vehicle is recoverable and reuseable. After staging, the re-entry flight is passively controlled by an inflated drag device that limits its velocity at water impact so that the structure is not damaged and can be recovered and reused with minimal refurbishments. Figures II A-4 and II A-5 depict the vehicle flight operations functions.

II, A, General Features and Function (cont.)

The main vehicle structure consists of pressure stabilized tanks. This structure is pressurized at levels that prevent the development of compressive instability during all modes of sea handling, propellant loading, erection, flight, and recovery. The propellant tanks are provided with lines for controlled pressure loading and venting in both horizontal and vertical positions. Cryogenic tanks and lines are insulated. One large regeneratively-cooled combustion chamber and conventional De Laval nozzle comprise the first-stage engine. It uses RP-1 fuel pressurized by CH_4 from a separate tank. The oxidizer is liquid oxygen pressurized by an autogenous system utilizing a heat exchanger on the engine. The mixture ratio is controlled by the autogenous pressurizing gas flow. The first-stage engine thrust vector is controlled by gimbaling the thrust chamber with actuators using RP-1 fuel at tank pressure. Roll control is provided during both stages of flight by four auxiliary engines on the second stage. These engines also provide pitch and yaw control for the second stage as well as assisting in orbital injection.

II, A, General Features and Function (cont.)

The main second-stage engine has a fixed alignment and utilizes an expandable nozzle. Propellants are liquid oxygen and liquid hydrogen. The oxygen is pressurized by its own vapor pressure plus acceleration head. The hydrogen tank pressure is obtained by flow from the engine heat exchangers. Thus, one of the main features of the entire propulsion system is its simple pressurization system, which avoids use of turbopumps. The expandable nozzle on the second stage provides a method of conforming to a conventional configuration envelope while still producing a large expansion ratio when opened (compared to equivalent fixed nozzles).

An all-inertial guidance system is incorporated in the vehicle's command module; it returns with the module for recovery. Self-checking and sequencing functions are included in the guidance system.

II, Vehicle Description (cont.)

B. OPERATIONAL SEQUENCE

The operational sequence of the vehicle is considered to start after the vehicle has been assembled, checked out, and is ready for fueling. After propellant servicing, the vehicle is towed to the launch site and erected. Operational readiness is verified and the launch sequence is started. The main events in the launch sequence are illustrated in Figure II-A-4 and the flight sequence in Figure II-A-5.

A list of the major vehicle operations is presented in Table II-B-1. More detailed plans and descriptions of the equipment for the entire Sea Dragon operation are presented in the Operational Plan section of this report. Detailed operational sequences or discussions of the operation of the major subsystems are included in corresponding portions of this report.

The recovery of the Apollo-type command module will be similar to that in current earth orbital programs and is also illustrated in Figure II-A-5.

II, B, Operational Sequence (cont.)

The ballast unit will be recovered by inflating flotation bags on the unit after launch of the vehicle. Prior to launch, the unit will be attached to a buoy by means of a line, and an air hose to the flotation bag on the ballast unit is supported by the same line. After launch, the air hose will be connected to a service vessel for the ballast recovery operations. Retrieval of both the ballast and the first stage, after return from flight, is discussed in the section on the Operational Plan.

C. SYSTEM PERFORMANCE

As presently conceived, the recoverable version of Sea Dragon will place into earth orbit a useful payload of 1,100,000 lb in addition to the spent second stage. An orbital altitude of 300 nm with a maximum eccentricity of 0.005 and an inclination of 28° will be achieved by launching along the Atlantic Missile Range from a launch point 40 mi from Cape Canaveral. Orbit injection will occur 22.4 min after launch at a point 4,100 nm downrange.

II, C, System Performance (cont.)

After 81 sec of propulsion, the first-stage booster will separate at an altitude of 125, 000 ft and a velocity of 5,800 ft/sec, having reached a peak acceleration of 4.2 g and after passing a peak q of 1,600 lb/ft² (Figure II-C-1). The first-stage booster will coast to an altitude of 335,000 ft after staging. During this period, inflation of the conical flare will be initiated. Approximately 200 sec later, the flare will be fully inflated and atmospheric re-entry will begin, decelerating the first stage at a maximum of 6.5 g to an impact velocity of 300 ft/sec at a location 175 mi downrange of the launch site. Water penetration of 75% of one body length occurs after impact and causes loading in the tankage, which is adequately balanced by the 100 psi minimum internal pressure. Because an inflatable flare and special structural reinforcement is not needed for an expendable configuration, a higher stage propellant mass fraction is achievable, and additional payload can be delivered into orbit. The payload capability of Sea Dragon with an expendable first stage will be 1,121,000 lb or an increase of 21,000 lb for equivalent launch and orbit conditions.

II, C, System Performance (cont.)

The second-stage booster propels the vehicle with its main engine for 260 sec, assisted by the low thrust auxiliary TVC engines, which continue burning to orbit injection 1,344 sec after launch.

The nominal performance characteristics of the system are shown in Table II-A-1. The trajectory characteristics are shown in Figure II-C-2. Also in Section V. are presented discussions of the performance analyses that have been conducted to evaluate the vehicle propulsion, loads, and dynamics in its main modes of operation. It is shown therein that the main propulsion system has been optimized for a staging ratio of 1.92:1, a first-stage area ratio of 5.10:1 and a thrust-to-weight ratio of 2:1. Limited analyses have shown that the underwater launch causes a payload penalty of about 3% when compared to surface launch; however, an optimum launch mode has not been determined. The combined effects of sea state, wind and thrust perturbations have been found to cause launch dispersion effects within the corrective

II, C, System Performance (cont.)

capability of the first-stage control system. Subsequent flight maneuvers and wind influences, together with longitudinal acceleration, give rise to a structural loading that exceeds those developed in the most severe water environment prior to flight. Whereas the first-stage control system capability is found to be adequate, the auxiliary engines for the second stage, as presently sized, appear marginal. Improvement to an adequate level of TVC capability represents no basic problem.

The nature of the assumed Sea Dragon mission is such as to require only normal performance of a present day inertial guidance system. An error analysis has shown that prelaunch accuracy requirements on alignment, position, and velocity are $1/3$ min of arc, .33 nm and 3.16 knots respectively. With present day systems, these can be achieved easily except for the initial alignment accuracy even though the vehicle is in constant motion. Thus it can be concluded that no serious performance penalties need be paid to acquire the many advantages of sea-launched and sea-recovered vehicles of Sea Dragon type.

TABLE II-A-1

SUMMARY OF SEA DRAGON VEHICLE CHARACTERISTICS, CONFIGURATION NO. 135

<u>Item</u>	<u>Propulsion</u> <u>Main Stage Engines</u>		<u>TVC</u>
	<u>Stage I</u>	<u>Stage II</u>	<u>(4) Engines</u>
Nominal Thrust - lb	80×10^6 (s.L.)	14.12×10^6 (vac.)	53,200 (ea.)
Operating Time - sec	81	260	1,340
Nominal Chamber Pressure - psia	300	75	75
Nozzle Area Ratio	5.0	20 (exp. nozz.)	20
Oxidizer	LO ₂	LO ₂	LO ₂
Weight Oxidizer - Full Tank (lb)	17,617,568	8,005,045	583,000
Fuel	RP-1	LH ₂	LH ₂
Weight Fuel - Full Tank (lb)	7,659,812	1,601,009 (& line)	116,000 (total)
Mixture Ratio - Oxidizer/Fuel	2.3	5	4.0
Stage Propellant Mass Fraction	.888	.887	---

AEROJET-GENERAL CORPORATION

TABLE II-A-1 (cont.)Vehicle Weight (lb)

<u>Item</u>	<u>Recoverable</u>	<u>Expendable</u>
Payload (nominal)	1,100,000*	1,121,000
Stage I At Launch (full tanks)	28,217,195	27,961,397
Stage I Empty (dry) (2,939,715)	(2,684,017)	
Stage II At Launch (full tanks)	10,631,893	10,631,893
Stage II Empty (dry) (1,025,839)	(1,025,839)	
Nominal Total Take-off Weight	<u>39,950,000</u>	<u>39,710,000</u>

* This figure includes the beneficial effect of an eastward launch. It includes allowance for a payload decrement of 3.16% for under-water performance losses and 7.66% for a continuous burn vs. restart trajectory (total penalty = 10.8%). It should be recognized that the preliminary staging ratio selection of 1.92 results in a payload 7% lower than the optimum value of 1.4. Use of a more optimum staging ratio would result in a payload of approximately 1,170,000 lb for the recoverable vehicle.

TABLE II-A-1 (cont.)

	<u>Vehicle Performance</u>	
	<u>Stage I</u>	<u>Stage II</u>
Velocity Increment (ft/sec)	5,800	17,630**
Maximum Acceleration (g)	4.21	5.2***
Altitude at Burnout (ft)	125,000	750,000 (150 nm)
Altitude at Injection (ft)		1,822,800 (299.8 nm)

** The performance given is for the recoverable vehicle. The data for the expendable vehicle does not differ significantly.

*** At completion of the high thrust phase.

TABLE II-A-2

STAGE I SEA DRAGON WEIGHT, CONFIGURATION NO. 135

	<u>Weight (lb)</u>	<u>Totals (lb)</u>
Propellants		
LO ₂	17,617,568	
RP-1	<u>7,659,812</u>	25,277,380
Tankage		
RP-1 tank	420,496	
RP-1 slosh baffles	33,200	
LO ₂ tank (includes common blkhd)	948,678	(874,280)*
LO ₂ slosh baffles	40,000	
LO ₂ tank insulation	18,000	
Insulation, common bulkhead	9,479	
Encapsulation skin	13,428	
Insulation (methane RP-1)	1,760	
Encapsulation skin	<u>2,493</u>	1,487,534 (1,413,136)
Skirts, Lines, and Structure		
Forward skirt and separation equip	29,200	(15,000)
Aft tank support skirt	39,000	
Structure between gimbal and injector	54,000	
Oxidizer line from tank to injector	59,000	
Fuel line from tank to chamber	40,900	
LO ₂ fill and vent system	500	
RP-1 fill and vent system	500	
Oxidizer pressurization equip	<u>3,160</u>	226,260 (212,060)

* The figures in parenthesis refer to weight charges for an expendable version of Configuration No. 135.

AEROJET-GENERAL CORPORATION

TABLE II-A-2 (cont.)

	<u>Weight (lb)</u>	<u>Totals (lb)</u>
Engine System		
Gimbal	122,600	
Actuators	44,000	
Injector assy	88,500	
Thrust chamber	180,000	
Ballast mounting structure	18,400	
LO ₂ valve	23,400	
RP-1 valve	25,600	
Oxidizer pressurant	236,000	
Heat exchanger	8,200	
Fuel pressurant	178,000	
Fuel pressurization equip	700	
Fuel trapped in tubes	<u>100,000</u>	
		1,025,400
Miscellaneous		
Recovery flare and equip	124,200 (0)	
Insulation on LO ₂ line	2,104	
Insulation on pressurant line	840	
Misc. weight (5% tankage)	73,477	200,621
Impact load structural strengthening not required for expendable vehicle	-- (-43,000)	<u>(33,421)*</u>
	TOTAL SYSTEM WEIGHT	28,217,195 (27,961,397)
Total Propellant Weight	25,277,380	
Less Outage	252,774	
Plus TVC Burned in 1st State	<u>42,000</u>	
Total Usable Propellant	25,066,406	
Stage Mass Fraction =	$\frac{25,066,406}{28,217,195} = 0.888 (0.896)$	

* The figures in parenthesis refer to weight charges for an expendable version of Configuration No. 135.

AEROJET-GENERAL CORPORATION

TABLE II-A-3

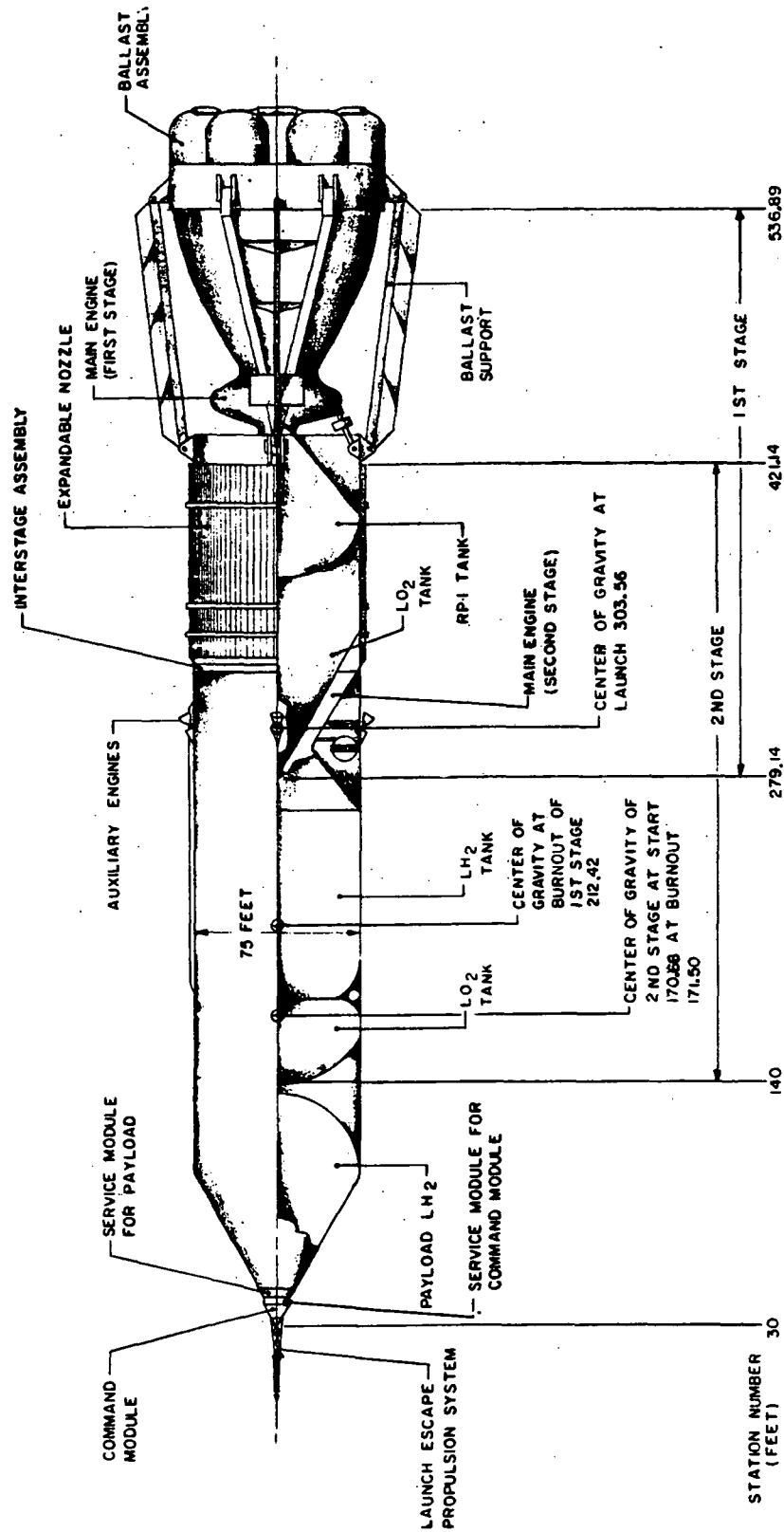
STAGE II SEA DRAGON WEIGHT, CONFIGURATION NO. 135

	<u>Weight (lb)</u>	<u>Totals (lb)</u>
Propellants		
LO ₂		
In tank	7,918,356	
In line to chamber	<u>86,689</u>	
		8,005,045
LH ₂		
In tank	<u>1,601,009</u>	
		<u>1,601,009</u>
	TOTAL	<u>9,606,054</u>
Tankage		
LO ₂ tank	123,310	
LH ₂ tank (includes bulkhead)	318,396	
Encapsulation skin	13,428	
Insulation on bulkhead	<u>9,479</u>	
		464,613
Skirts, Lines, and Structure		
Aft tank skirt	211,984	
Skirt between LO ₂ -LH ₂ tank	27,137	
LO ₂ line to chamber	4,700	
LH ₂ line to chamber	1,360	
Vortex structure	2,700	
LO ₂ and LH ₂ fill and vent system	1,525	
Fuel pressurizing equipment	<u>1,820</u>	
		251,226
Engine System		
Injector assembly	10,000	
Thrust chamber	51,400	
Expandable nozzle	71,500	
TVC system (structure, engine, mounts)	5,300	
LO ₂ valve	3,640	
LH ₂ valve	4,480	
Heat exchanger	13,400	
TVC pressurization system	14,550	
Oxidizer pressurization gases	52,000	
Fuel pressurization gases	<u>18,500</u>	
		244,770

TABLE II-A-3 (cont.)

	<u>Weight (lb)</u>	<u>Totals (lb)</u>
Miscellaneous		
Fuel tank insulation	36,000	
Oxidizer tank insulation	6,000	
Misc. weight (5% of tankage)	<u>23,230</u>	
		<u>65,230</u>
TOTAL SYSTEM WEIGHT		10,631,893
Total propellant weight	9,606,054	
Less outage (1% of total)	96,060	
Less LH ₂ cooling requirements	40,560*	
Less Stage I TVC weight	<u>42,000</u>	
TOTAL USABLE PROPELLANTS	9,427,434	
Mass Fraction = $\frac{9,427,434}{10,631,893} = 0.887$		

* Conservative allowance need not be allowed because of high specific impulse of ejected coolant.

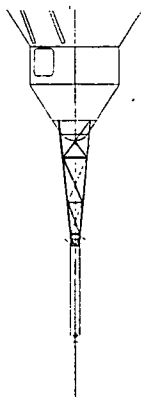


Sea Dragon Vehicle Schematic

Figure II-A-1

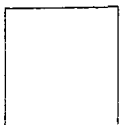
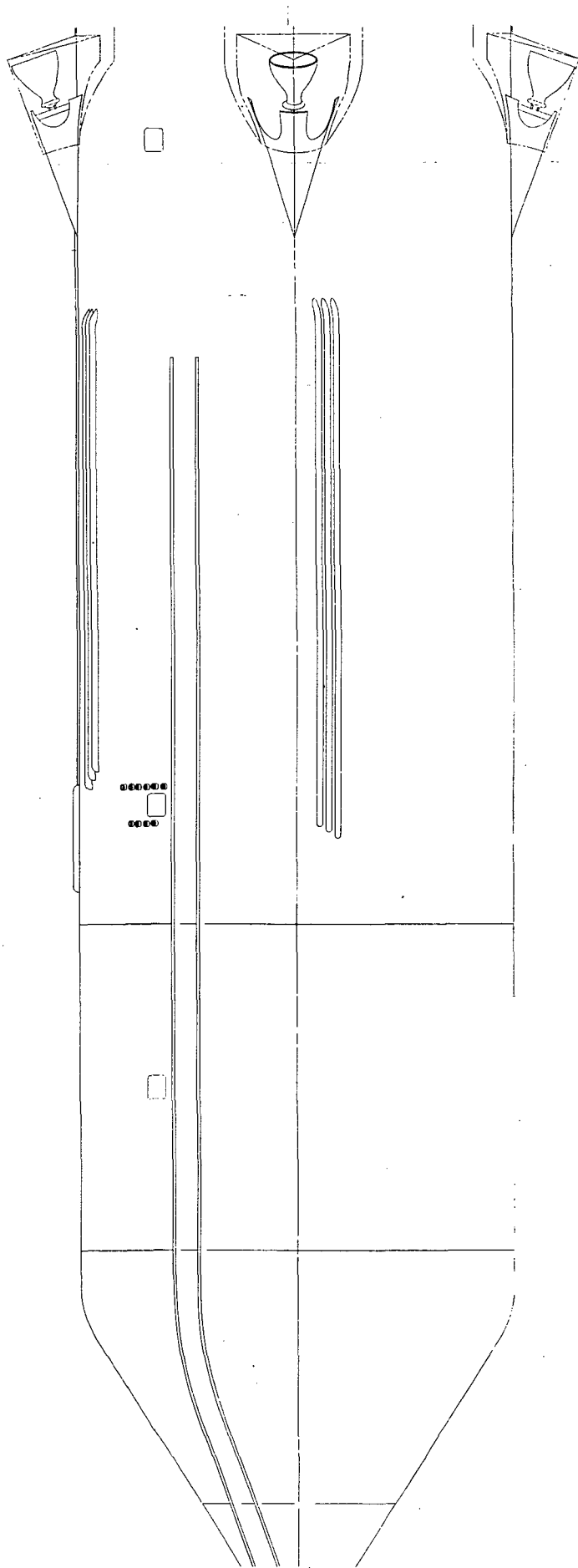
Report No. LRP 297, Volume II

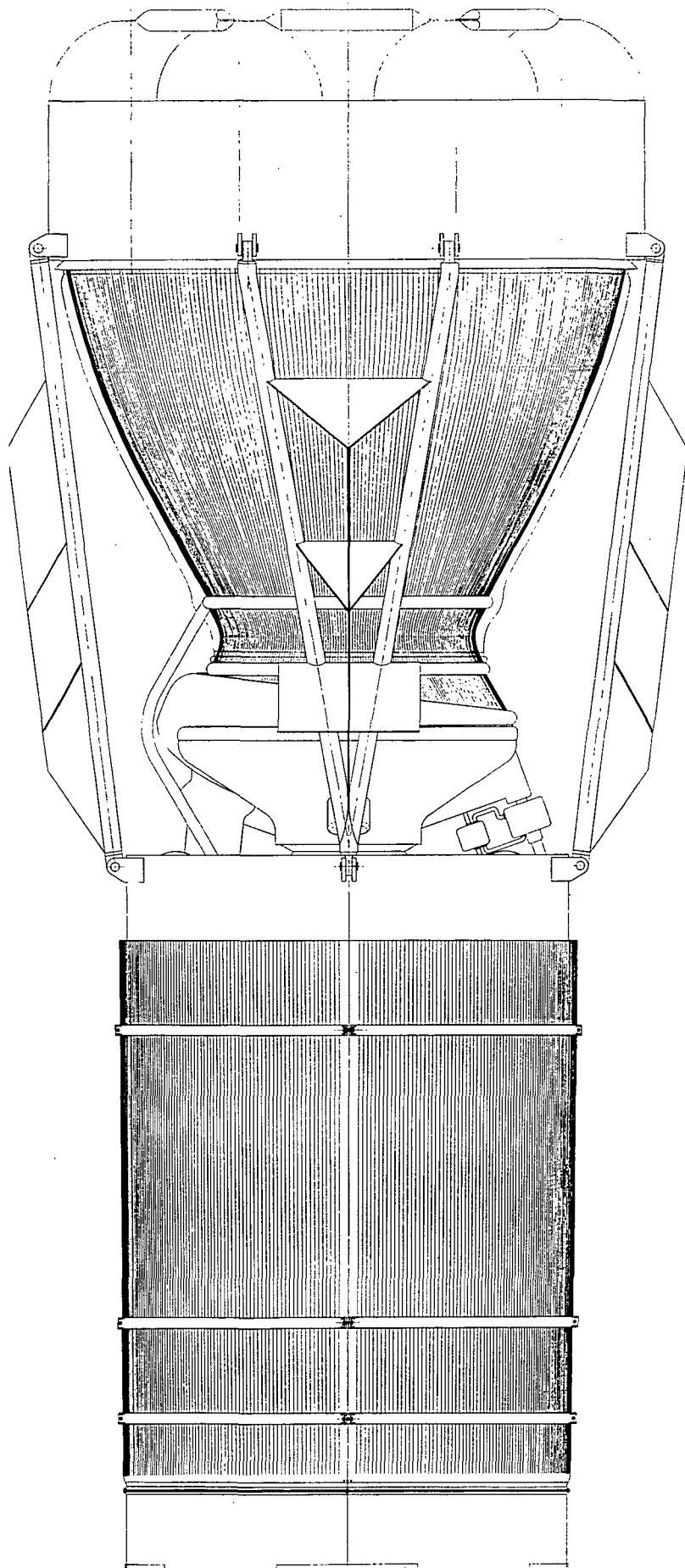
AEROJET-GENERAL CORPORATION

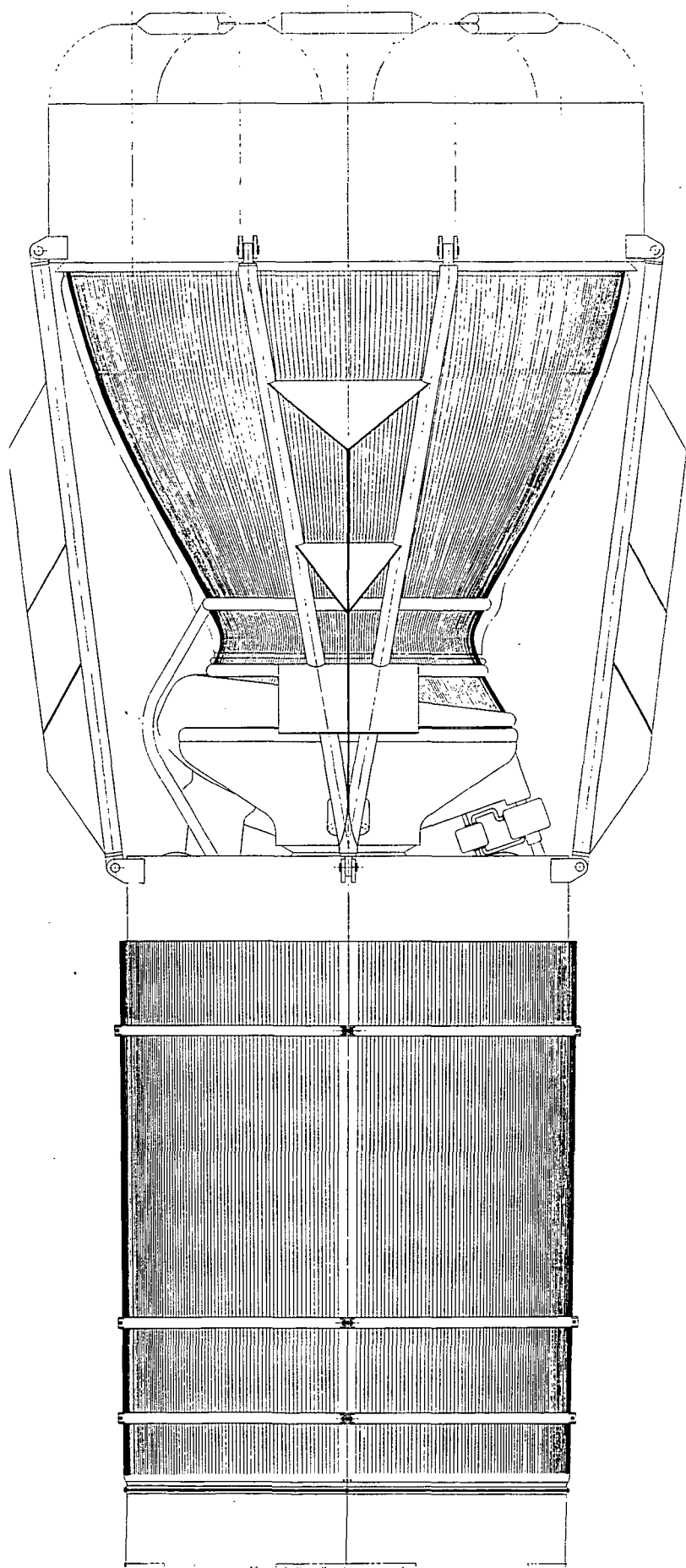


Sea Dragon Vehicle--External View

Figure II-A-2

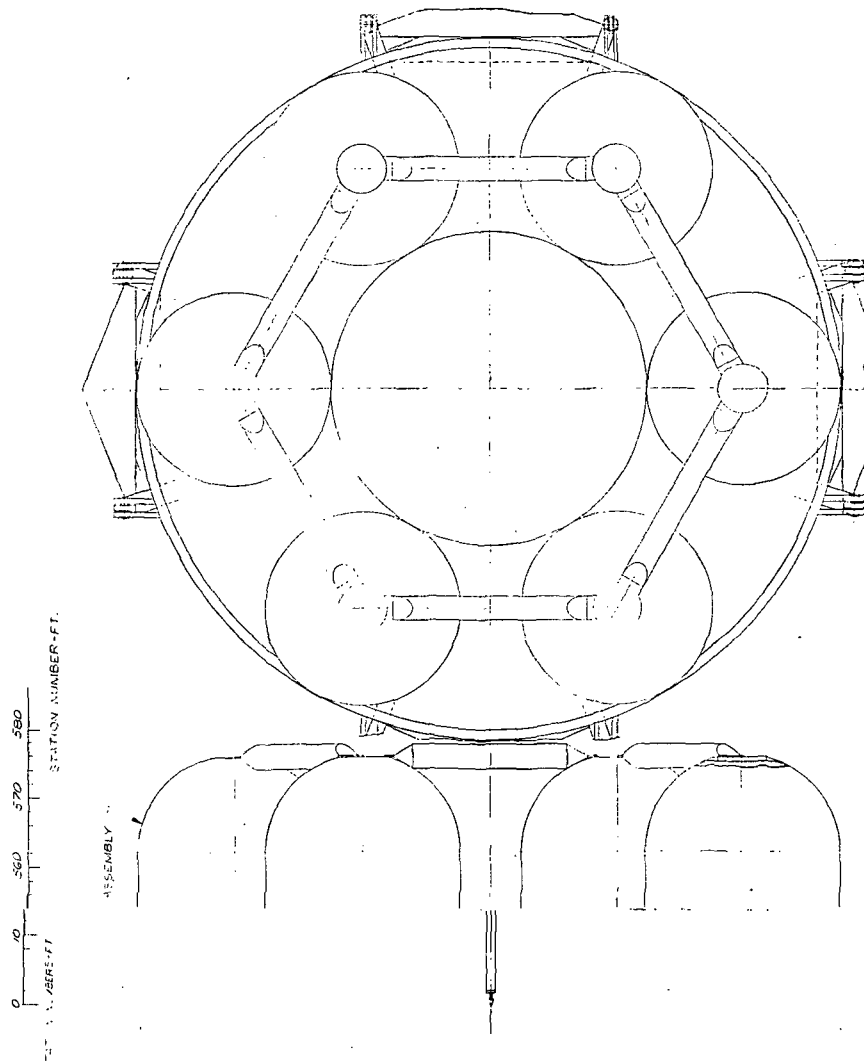






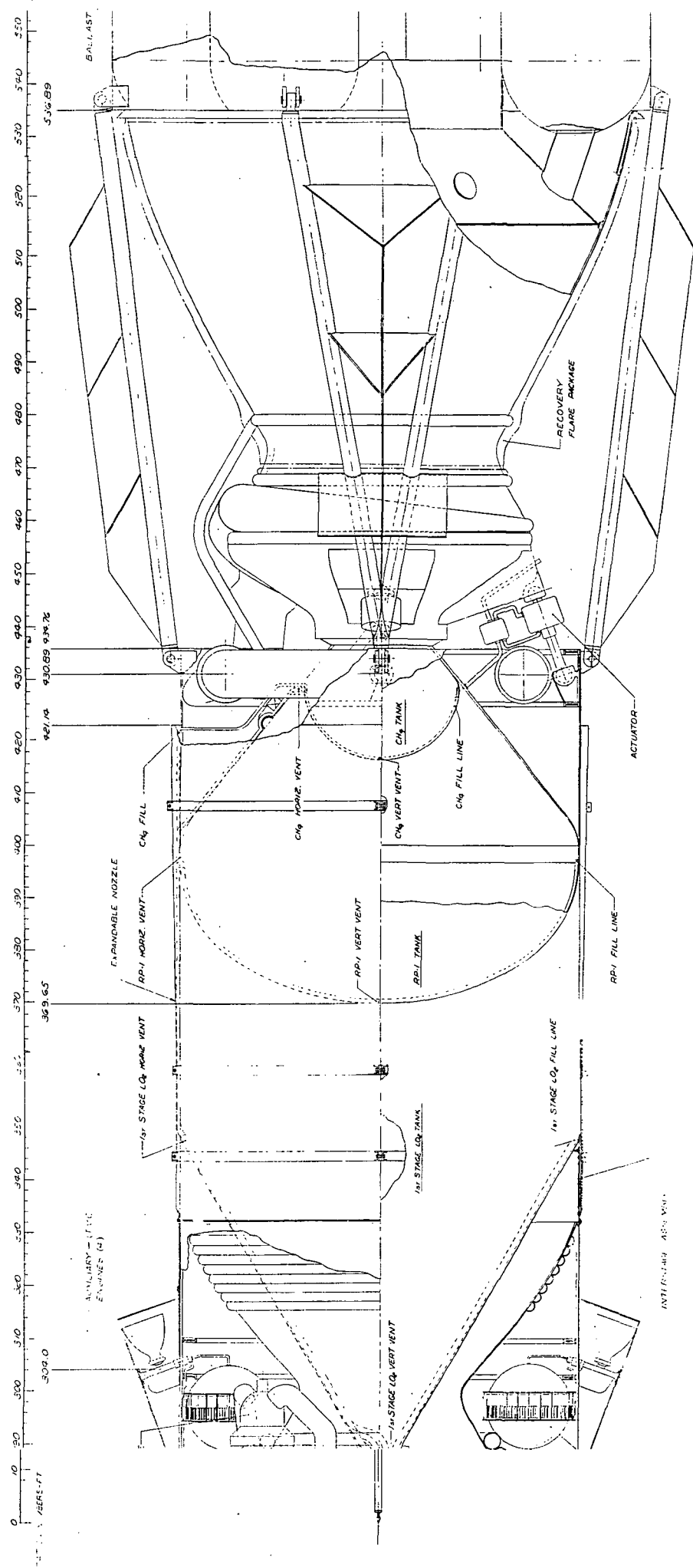
Report No. LRP 297, Volume II

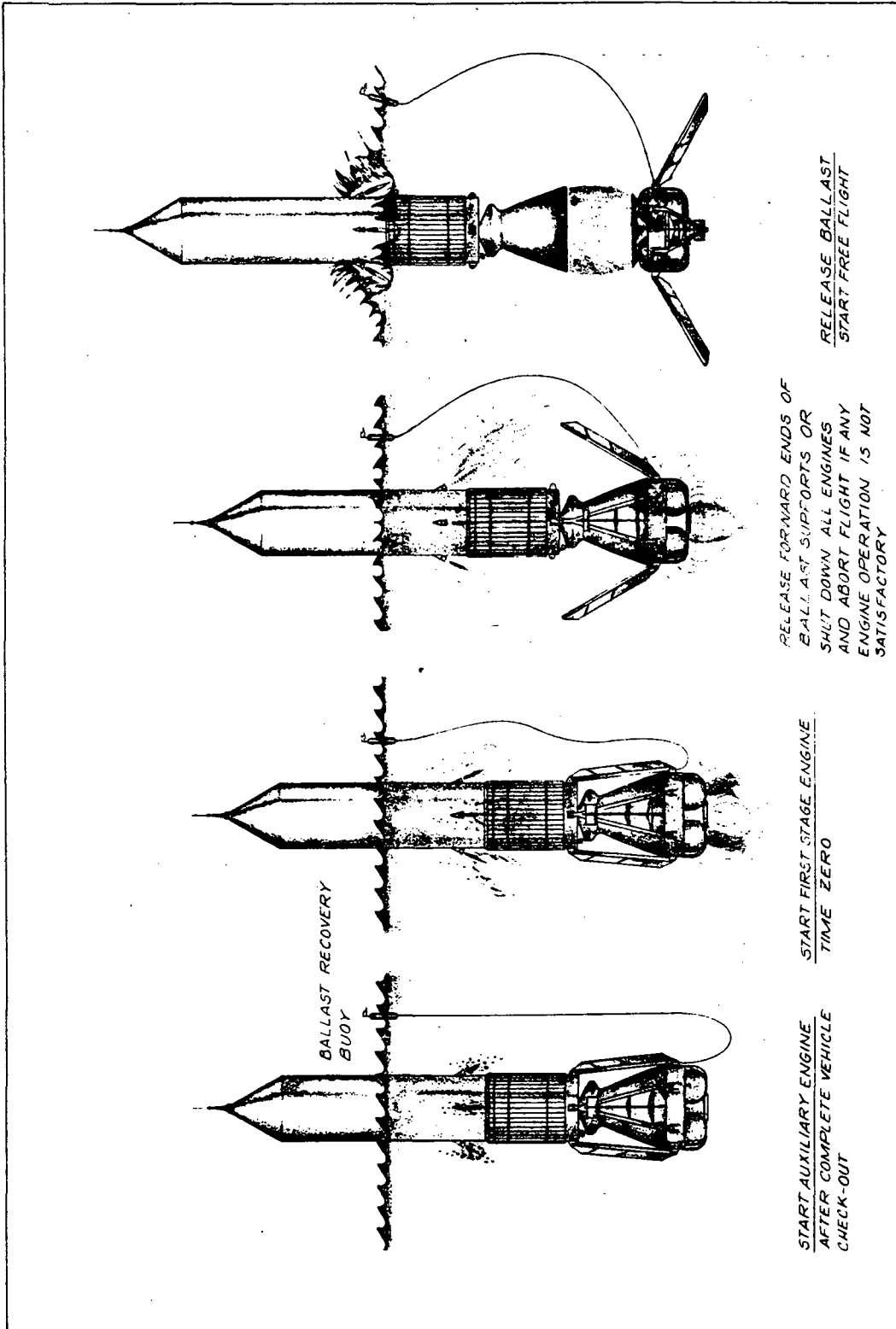
AEROMET-GENERAL CORPORATION



Sea Dragon Vehicle--Internal View

Figure II-A-3





Sea Dragon Launch Sequence

Figure II-A-4

AEROMET-GENERAL CORPORATION

TABLE II-B-1

SEQUENCE OF OPERATIONS

<u>Item</u>	<u>Operation</u>	<u>Description</u>
1.	Transportation	After satisfactory completion of vehicle check-out at the assembly point, it will be moved to the fuel service area.
2.	Chilldown and Fuel Servicing	At the fuel service area, all cryogenic tanks will be chilled down to their operating temperatures. The CH ₄ , LH ₂ and RP-1 will be loaded onto the vehicle. The ballast unit, vehicle flotation and compartment pressures will be adjusted as necessary.
3.	Transportation	The fueled vehicle will be towed to Point Bravo.
4.	Oxidizer Servicing	The vehicle will be restrained close to the oxidizer servicing barge, and oxidizer transferred.
5.	Transportation	The fully serviced vehicle will be transported to the vicinity of the launch site -- adjusted for current effects.

AEROJET-GENERAL CORPORATION

TABLE II-B-1 (cont.)

Item	Operation	Description
6.	Erection*	If all systems are in satisfactory condition upon arrival, the ballast unit will be flooded and the vehicle erected. In a normal operational sequence with no major holds, no horizontal propellant topping will be required.
7.	Final Checkout	The final system checkout and preflight calibrations will be performed, the crew loaded, and the service vessels withdrawn.
8.	Start Auxiliary Engines	The four auxiliary engines are ignited.
9.	Startup of First-Stage Engine	The first-stage engine will be ignited.
10.	Drop Ballast	The ballast will be released early in the underwater trajectory.
11.	Shutdown of First-Stage Engines	The first-stage engine will be shut down on decay of chamber pressure.

* Tank topping off will not be required unless long holds extend the time from LH₂ loading to launch to in excess of three days.

TABLE II-B-1 (cont.)

Item	Operation	Description
12.	Staging First and Second Stage	The first stage will be separated from the second stage by actuating the linear shaped charge at the forward end of the interstage structure.
13.	Recovery of First-Stage	The first stage will coast to apogee while the recovery flare is being inflated. It will return to the atmosphere, stabilize and be recovered by direct impact into the ocean.
14.	Start of Second-Stage Engine	The main engine of the second stage will be ignited, which will expand the expandable nozzle.
15.	Shutdowns of Second-Stage Engines	The second-stage engine will be shut down on command of the guidance system.

AEROJET-GENERAL CORPORATION

TABLE II-B-1 (cont.)

<u>Item</u>	<u>Operation</u>	<u>Description</u>
16.	Injection Into Orbit	The auxiliary engines will continue burning until injection into orbit.
17.	Shutdown of Auxiliary Engines	The auxiliary engines will be shut down upon command of the guidance system.
18.	Separation of the Command Module	A separation device will separate the command module and its service module from the vehicle

Report No. LRP 297, Volume II

AEROJET-GENERAL CORPORATION

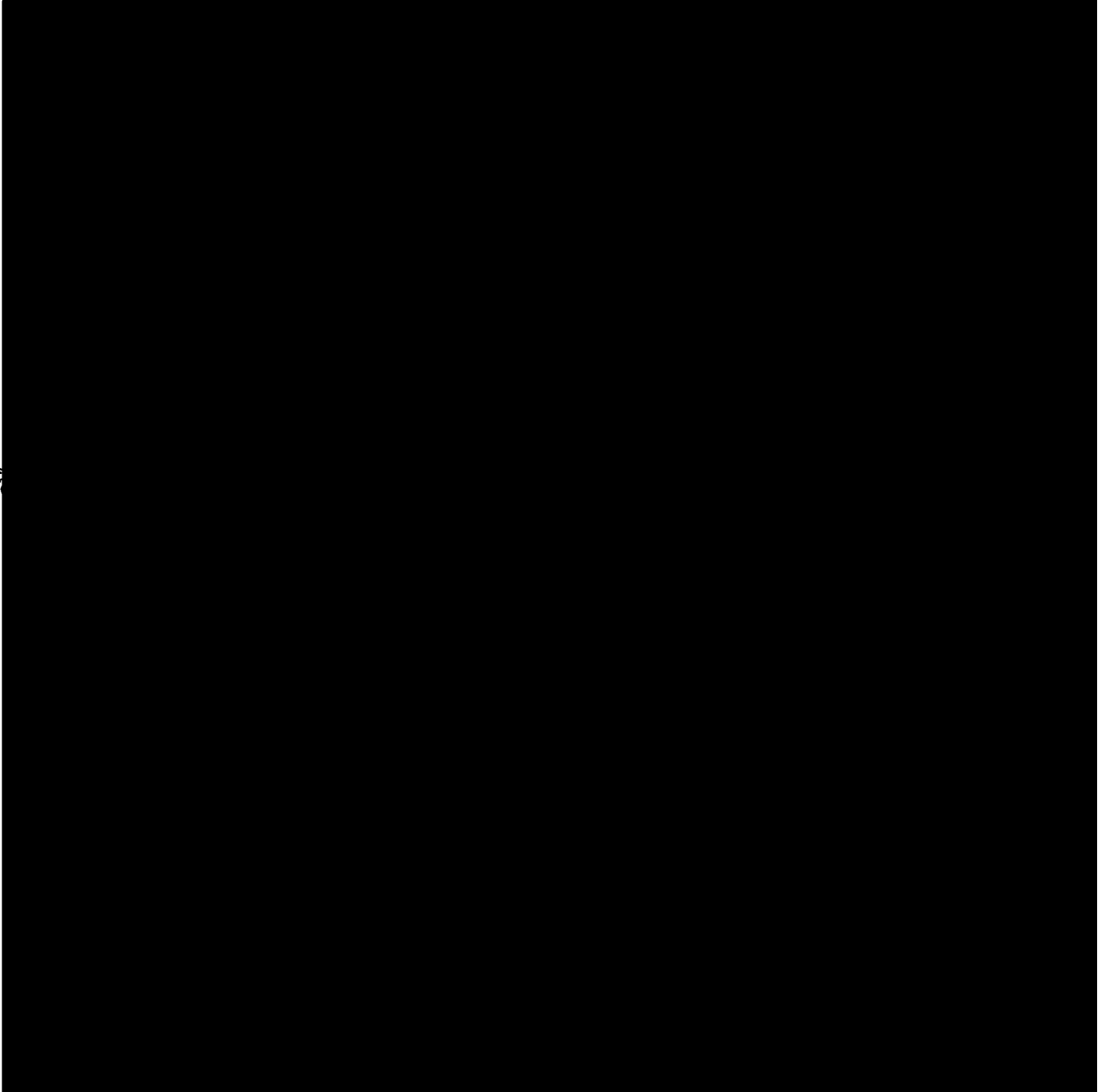


Figure II-C-1

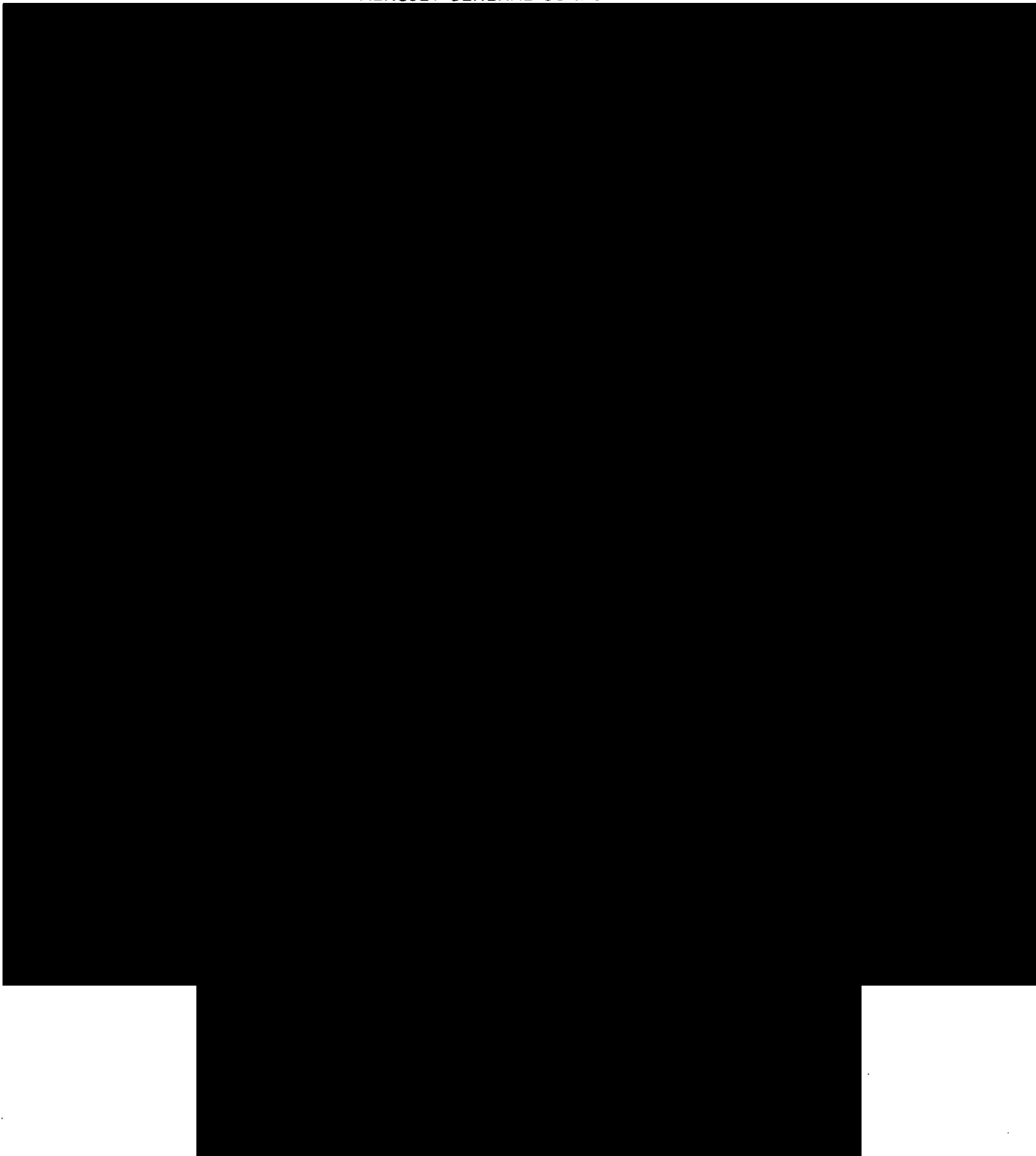


Figure II-C-2

III. VEHICLE SUBSYSTEMS

A. STAGE I PROPULSION SYSTEM

1. Description - Configuration No. 135

Stage I utilizes a liquid bipropellant, pressure-fed rocket propulsion system. The general arrangement of the stage is shown in Figure III-A-1 (Stage I Dwg.). Basic Stage I characteristics are given in the following table:

Stage Diameter	75 ft
Stage Length	262 ft
Stage Weight, Total	28×10^6 lb
Usable Propellants	25×10^6 lb
Propulsion System Mass Fraction	0.892
Propellants	LO ₂ /RP-1
Mixture Ratio	2.3
Thrust Chamber Type	DeLaval, Regeneratively Cooled
Throat Diameter	41.6 ft

III, A, Stage I Propulsion System (cont.)

Expansion Area Ratio	5
Sea Level Thrust, Nominal	80 x 10 ⁶ lb
Chamber Pressure Nominal	300 psia
Thrust Vector Control	Gimbal-roll control by Stage II Aux Engines
Propellant Tank Ullage Pressures Nominal	
LO ₂	226 psia
RP-1	425 psia

Propellants are fed from integral tankage by a combination of ullage pressurization and dynamic heads. The tankage is shaped conventionally with exception of the forward closure on the forward LO₂ tank. This closure is a 60° cone as is required to enable water entry and recovery of the stage. The forward closure for an expendable stage would utilize a 1.4 to 1 elliptical form. LO₂ is fed to the thrust chamber through a multiple line that is routed outside of the aft RP-1 tank. During expulsion of the LO₂, the difference between required injector inlet and dynamic heads is provided by ullage pressure, which is developed by heating a portion of the LO₂ flow and ducting it to the ullage space. This autogenous system is controlled by throttling the flow from the high pressure, LO₂ injector inlet manifold downstream of the main LO₂ valve to the heat exchanger that is located on the thrust chamber assembly.

III, A, Stage I Propulsion System (cont.)

The RP-1 fuel tank is located aft of and integral with the LO₂ tank; an insulated bulkhead separates the tank compartments. The RP-1 tank pressure is developed by methane, which is stored in a separate tank at equilibrium with its vapor pressure at 500 psia. The vapor pressure is used as the driving force to inject methane vapor into the bottom of the RP-1 tank where it is heated as it bubbles through to the ullage space. This secondary VāPak system maintains RP-1 feed line inlet pressure at equilibrium with the methane tank pressure. Ullage pressure is maintained at a level equal to the difference between methane tank pressure and the dynamic head. No regulating controls are therefore required.

Ignition is hypergolic. Triethylaluminum (TEA) is injected into a gaseous oxygen lead. The TEA is blown down, gas pressurized.

Main propellant valves are poppet types that are sealed in the closed position with a clamped diaphragm, which is sheared by the poppet movement. Valve actuation forces are provided

III, A, Stage I Propulsion System (cont.)

by the propellant feed line pressures controlled with mechanical detents. The gimbals actuators are low pressure hydraulic cylinders that use fuel at tank pressure as the energy source.

Propellant tanks are designed by the propellant feed requirements. The aft skirt consists of stiffened skin and frames that react with the gimbal actuator loads.

2. Propellants

a. Properties of the Propellants Selected

Propellants used for the first-stage main engine are LOX/RP-1 at a mixture ratio of 2.3:1. Considerations of the characteristics of these propellants appear in the table below:

<u>Advantages</u>	<u>Disadvantages</u>
1. Low cost (now \$0.0185/lb)	1. Cryogenic storage
2. Reasonable specific impulse (Theoretical sea level $I_s = 260$ sec at $AR = 5.0$ and $P_c = 300$ psia)	2. Icing and thermal gradients
	3. Contamination sensitive

III, A, Stage I Propulsion System (cont.)

3. High state of the art
4. Availability excellent
4. Nonhypergolic
5. High bulk density results in attractive mass fraction and favorable sea handling characteristics

Large size and reusability of the stage place greater importance on propellant costs. Current availability of the propellant is also important if propellant plant construction is not to become the pacint item.

Large size diminishes boil-off and insulation penalties associated with cryogenics. Water handling, on the other hand, adds to the icing problems associated with LO_2 and LH_2 . Although the propellant selection is not final for the conditions of this particular study, the propellants offer the greatest potential for investigation of recoverability. For a more optimistic recovery operation than assumed here, propellant cost can become the limiting item on overall operating cost. The cost of storables per pound of payload is about \$5. If one-hundred uses of each vehicle were possible, the propellant

III, A, Stage I Propulsion System (cont.)

cost would greatly exceed the hardware cost. Use of RP-1 and LO₂ also permits full-scale first-stage engine feasibility firings without commitment of large amounts of funds.

Theoretical and estimated actual performance data is shown in Figure III-A-2. The specific impulse used for vehicle performance calculations is 93% of theoretical. This is conservative (by 1%) by comparison with current practice and is in keeping with the general philosophy of the study. The acceptance of this conservative performance goal should result in reduced development program cost and increased combustion stability potential.

a. Evaluation and Recommendations

The LO₂/LH₂ combination is attractive because of its high specific impulse (theoretical sea level I_g = 342 sec at mixture ratio 5.0:1, P_c = 300 psia and area ratio = 5.0:1). Its low density makes the vehicle buoyancy characteristics undesirable and the tanks heavier. However, previous investigations have indicated

III, A, Stage I Propulsion System (cont.)

that use of an LO₂/LH₂ first stage can result in attractive vehicle geometries. These have not yet been thoroughly explored for Sea Dragon.

Both storable propellants such as N₂O₄/Aerozine-50 and the high energy cryogenics LO₂/LH₂ seem worthy of further analysis.

3. Thrust Chamber Assembly

a. Chamber and Injector

(1) A single thrust chamber assembly is used for the first stage. This assembly is of conventional DeLaval design, regeneratively-cooled with RP-1. The assembly is gimbaled. The important design and performance parameters of the first-stage TCA is given below.

III, A, Stage I Propulsion System (cont.)

DESIGN PERFORMANCE PARAMETERS

Design Sea Level Thrust (lb)	80 x 10 ⁶
Chamber Pressure, P _C (psia)	300
Chamber Contraction Area Ratio	1.8
Characteristic Length, L* (in.)	342
Converging Cone Half Angle (°)	30
Throat Diameter, D _t (ft)	41.6
Expansion Area Ratio	5
Exit Angle of Exhaust Gas (°)	13
Propellants	LO ₂ /RP-1
Mixture Ratio	2.3
Theoretical Characteristic Velocity, C* (ft/sec)	5885
C* Efficiency	0.96
Sea Level Thrust Coefficient, C _F	1.38 (97% theoretical)
Vacuum Thrust Coefficient, C _F	1.616 (97% theoretical)
Sea Level Isp (sec)	242
Vacuum Isp (sec)	283
TVC Gimbal Angle (°)	<u>+ 3</u>

III, A, Stage I Propulsion System (cont.)

(2) Nozzle Type

At the outset of this study, four different exhaust nozzle types had been investigated. These studies did not take into account all of the considerations associated with the sea launch concept. TCA design types studied were:

- Type I: Conventional DeLaval
- Type II: Plug
- Type III: Annular chamber and nozzle
- Type IV: Expansion deflection.

Figure III-A-1a illustrates these types. The conventional DeLaval thrust chamber was selected for the vehicle so that the study could concentrate on the important features of "sea" and "size," without becoming excessively involved in other new or novel concepts. Notwithstanding this consideration, the DeLaval type has some outstanding advantages that in part account for the fact that all important rocket engines in use today are of this type. Included in these advantages are:

III, A, Stage I Propulsion System (cont.)

(a) High state of art: As indicated above.

(b) Low heat flux: Less than plug or expansion-deflection types by factors of approximately 2:1.

(c) Excellent aerodynamic flow characteristics: The nozzle coefficient is high and very predictable from theory and extensive test data.

(d) Structurally efficient: The chamber is basically a pressure vessel designed with tension instead of crushing allowables. Thrust takeout structure is also usually direct.

(e) Simple valving and manifolding: Liquid propellant DeLaval thrust chambers usually utilize one fuel and one oxidizer valve.

(f) Segment of chamber can be tested: Aerojet-General has demonstrated, using the Titan LR87 first-stage engine, that a wedge can be tested and accurate data obtained on heat transfer and combustion efficiency.

III, A, Stage I Propulsion System (cont.)

(3) Number of Chambers

The thrust level required for injection of a payload in excess of a million pounds into a 300-nm circular earth orbit was found from computer trajectory studies, performed early in the study, to be 80×10^6 . This value represents a preliminary optimization and was frozen early to develop a vehicle design on which to base the other facets of the study. One thrust chamber of this size was chosen rather than a cluster of chambers. Considerations leading to this decision included reliability as indicated by the reduction of numbers of components such as chambers, valves, manifolds, igniters, gimbals, and gimbal actuators. It was believed that the structural characteristics of the system would be simplified, and therefore improved, especially for water handling and recovery conditions. A characteristic of large liquid rocket vehicles is that the diameter of the thrust chamber increases as the square root of the thrust while the tank diameter tends to increase only as the cube root. Thus, as size increases, even a single chamber exceeds the tank diametral envelope. This has happened on the vehicle studied where the

III, A, Stage I Propulsion System (cont.)

chamber exit diameter is 94 ft compared to the 75-ft tank diameter. If a cluster of chambers were used for this vehicle, their relatively inefficient packaging would result in excessive projections into the free stream.

(4) Chamber Contour

The conical combustion chamber is conical upstream of the throat with a cone half angle of 30° , which is conventional. This chamber, with a reasonable injector-to-throat area ratio, results in a chamber that is more than adequate on the basis of residence time or characteristic length, in this case, 342 in. (Titan I, burning LOX/RP-1 developing a thrust of 149,400 lb with $P_c = 584$, has an $L^* = 42$ in.). The exact contour for the diverging section of the nozzle is shown in Figure III-A-3.

(5) Injector Type

The conical chambers are advantageous in that the converging ramp tends to damp out some longitudinal

III, Stage I Propulsion System (cont.)

combustion instabilities. Even more important is the injector pattern. As a result of the large L^* and long residence time, the first-stage chamber will be able to use a stable-combustion injector such as the showerhead. This injector is very stable in engines of the current size. Its main disadvantage in short chambers is its medium rate of performance compared to other types. This selected contraction area ratio and resulting large chamber volume would provide good combustion efficiency and allow flexibility in the exact injector pattern design with virtually no performance loss. Showerhead injectors would allow the combustion to be spread out over larger volumes and thus tend to produce a combustion flow field that is less sensitive to disturbances or oscillations that might ordinarily initiate instability. A further discussion of combustion of Sea Dragon size chambers is given in Appendix II-2.

(6) Start Transient

Starting conditions resulting from large line and manifold volumes downstream of the valves can cause hard starts and initiate combustion instabilities. The Sea Dragon size and line lengths could cause considerable timing difficulties if a conventional

III, A, Stage I Propulsion System (cont.)

approach is used. To control the start timing, the fuel orifices will be sealed with unidirectional burst diaphragms. The RP-1 will be bled into the jacket up to the injector diaphragms. This arrangement allows precise RP-1 injection timing, keeps out contaminants, such as oxygen, and also provides coolant in the cooling jacket at all times. The chamber pressure buildup assumed for performance and other analytical purposes is given in Figure III-A-4.

(7) Engine Cooling

The cooling of the injector head and chamber tube walls is accomplished by regenerative cooling with RP-1. A heat transfer study has been completed on the cooling requirements of the first-stage engine in which it was found that the pressure drop necessary to cool the engine is not excessive. The study indicated a maximum heat flux of 4.72 Btu/in²sec, maximum wall temperature of 1271°F, bulk temperature increase of RP-1 of 443°F (Case 5, see Appendix II-9), total pressure drop from tank to chamber of 170 psi, tube pressure drop of 72.1 psi for Case 5, and a total coolant weight trapped in the tubes of 107,000 lb.

III, Stage I Propulsion System (cont.)

b. Flow Controls and Lines

(1) Path of the LO₂ Used in First-Stage Engine

The LO₂ feeds from the first-stage tankage through a system of 10 tubes of 2.75-ft diameter. The tubes pierce the LO₂ tank wall around the periphery of the 1.4 to 1 elliptical common bulkhead. The common bulkhead is not ported. The LO₂ flows down through the small tubes and into a horizontal collector manifold that lies in the plane of the gimbal axis. The LO₂ flows horizontally 180° around the engine before flowing into the injector. After the LO₂ turns and flows down, it passes through the main LO₂ valve. The main LO₂ valve is a poppet valve with a burst (shear) diaphragm for rapid opening and prefire sealing purposes. Once the valve is opened, the LO₂ is fed to the injector head where it is distributed to the injector orifices. The total propellant feed pressure is the sum of the ullage gas pressure in the LO₂ tank and an acceleration head. The gas pressure is the result of autogenous pressurization. This is accomplished by bleeding part of the LO₂ that normally goes to the injector and

III, A, Stage I Propulsion System (cont.)

sending it to a heat exchanger that is mounted on the exterior of the throat section of the engine. A more detailed discussion of this pressurization gas flow is given in the pressurization section of this report.

(2) Path of the RP-1 Used in First-Stage Engine

The RP-1 feeds from the tank and is collected in a manifold. The manifold runs down to the gimbal plane, then runs horizontally 180° around the head of the engine where it goes through the main RP-1 valve and into the inlet manifold of the engine. The main RP-1 valve also is a poppet valve that has a burst diaphragm to start the propellant flow. The inlet manifold is tapered in cross section around the periphery of the thrust chamber injector. The RP-1 comes into the manifold, then into every other coolant tube. For details of the exact path of RP-1, see the injector schematic diagram, Figure III-A-6. The RP-1 flows down the tubes where it goes into a turning manifold and back up to the injector. This provides two-pass

III, A, Stage I Propulsion System (cont.)

regenerative cooling of the engine. It then enters the injector face and is injected into the chamber.

Two special cases of the flow of RP-1 occur before ignition and before first-stage impact. When the vehicle is in the loaded condition, the RP-1 can be bled into the coolant tubes from an external source so that the engine start time is decreased and some cooling is provided for the tubes during the ignition period before steady operation. Before first-stage water impact recovery, the RP-1 trapped in the engine coolant tubes must be drained to eliminate excessive hydrostatic pressures caused by the 20g or greater deceleration, which could produce pressures of 550 psi or greater. The tube drainage is accomplished by a bypass line that allows the RP-1 to drain into the hemispherical concave injector head during the nose down portion of the recovery trajectory.

c. Ignition

The first stage is ignited by introducing TEA (triethylaluminum) into the chamber to react with the oxygen. The TEA

III, A, Stage I Propulsion System (cont.)

is stored in a tank that is pressurized by a high pressure bottle. The ignition sequence is as follows: (1) the main LO₂ valve is opened; (2) a pressure sensor in the head of the injector senses the pressure of the LO₂ and actuates the TEA pressurizing line valve causing the TEA to be injected into the combustion chamber of the first-stage engine. The TEA is mixed with the LO₂ at an overall mixture ratio of 20:1. Local mixture ratios will be at or near stoichiometric; and (3) the RP-1 valve is opened and main ignition occurs. This ignition system was selected for the following reasons:

- (1) TEA is hypergolic with LO₂, thus combustion is reliable and self contained.
- (2) Ignition with small ignition delays occurs over a wide range of mixture ratios.
- (3) Readily available at low cost: the details of the ignition sequence and further discussion of the ignition system and ignition sequence are given in Appendix II-7.

III, A, Stage I Propulsion System (cont.)

d. Structural Loads and Design

The TCA is subjected to many types of loading starting from towing to final recovery. The following discussion applies to the rubber gimbal pad with actuator as presented in the vehicle drawings. During towing, the TCA is subject to bending moments (approximately 62×10^6 ft-lb) and body shear forces (approximately 0.10×10^6 lb) as the result of hogging and sagging. These loads are transmitted into the tank walls by use of the gimbal actuator, shear in the rubber gimbal pad, and many large structural members connecting the ballast unit with the aft skirt of the RP-1 tank. All of the bending loads and shear loads from the ballast are taken by the large structural members. During the erection process, large moments from the ballast are transmitted into the RP-1 aft tank skirt since the ballast is flooded to allow rotation of the vehicle to the vertical position. These erection shears and moments from the ballast protect almost no loading on the TCA because the structural members are designed to react and compensate for these loads. The underwater ignition of the engine subjects the engine skirts to hydrostatic loads caused by

III, A, Stage I Propulsion System (cont.)

separation of the flow because overexpansion increases the load. The skirt loads are increased because of the hydrodynamic loads resulting from the short underwater trajectory. The nozzle wall is provided with extra structural members to accommodate these loads. This extra structural material represents a weight penalty caused by underwater launch.

During first-stage burning, the loads on the TCA are: thrust loads that result from the pressure distribution in the engine; aerodynamic loads on the skirt resulting from various angles of attack; and gimbal actuator loads. The engine structural design enables accommodation of these loads with very little difficulty. Wherever possible, pressure forces have been reacted with pressure forces and concentrated loads have been transmitted as pressure loads. The various TCA loadings that are inherent to sea launch and recovery techniques are given in the following:

- (1) Shear and bending loads resulting from hogging and sagging during towing operations before launch and after recovery

III, A, Stage I Propulsion System (cont.)

- (2) Shear and bending loads resulting from erection during prelaunch operations
- (3) Hydrostatic and hydrodynamic compressive loads on the DeLaval nozzle skirt caused by underwater trajectory
- (4) Amplification of gimbal actuator loads if thrust vectoring is required while the TCA is underwater
- (5) Gimbal has to transmit tension loads from the recovery drag flare to the tankage. This load represents approximately 23×10^6 lb
- (6) The impact deceleration "g loading" (approximately 20g) requires that the coolant be bled from the cooling tubes to prevent tube rupture, because hydrodynamic pressures of 550 psi or greater are produced.
- (7) The gimbal region has to be designed to transmit the impact loading of the TCA and the tankage during water entry (approximately 20g gives loading of 16×10^6 lb or 400 psi over the area of the gimbal bearing).

III, A, Stage I Propulsion System (cont.)

e. Evaluation and Recommendations

Load reaction and transmission associated with sea launch and recovery is practical. The incremental weight of the necessary structure is compatible with the Sea Dragon concept and does not represent a significant performance penalty.

Certain problems concerned with the first-stage TCA need more investigation, as follows:

- (1) Better definition of loading because of underwater TCA vectoring requirements
- (2) Engine start transients chamber pressure buildup and emptying of water slug from the engine
- (3) More effective method of ballast arrangement regarding the TCA

III, A, Stage I Propulsion System (cont.)

(4) Optimization of first-stage engine cooling.

Several methods of heat protection are given in Figure III-A-6, such as film cooling, ablative cooling, and alternate plumbing configurations for regenerative cooling

(5) Better definition of recovery loading on TCA from drag flare and impact loading on gimbal

4. Thrust Vector Control (TVC)

a. Gimbal

A gimbal thrust chamber was selected for TVC with a capability of $\pm 30^\circ$ gimbal angle deflection. The factors that lead to this selection are: potential reliability, relative simplicity, and efficiency. The gimbal concept fits into a Sea Dragon development program in that much component development and system functional testing can be done without operation of the propulsion system.

III, A, Stage I Propulsion System (cont.)

The first-stage TCA is gimbaled by mounting the assembly on the spherical aft end of the methane tank, which is part of the aft closure of the RP-1 tank. After considering more conventional configurations, such as a spherical bearing, a slightly less conventional design was chosen, which is a rubber pad bonded to the tank and TCA and provides movement of the TCA by elastic shearing of the rubber. The latex rubber is cured to contain a central core of fluid that can take pressure, but does not offer the shear restraint of the rubber itself. The pad edges are restrained with a fabric material capable of allowing rubber shear deflections but not radial expansion.

b. Actuators and Controls

The actuator used is a hydraulic actuator using RP-1 as an actuator fluid. The rubber pad allows efficient conversion of the thrust force into a pressure force distributed over the face of the pressurized spherical methane tank. The design of the actuator system required an analysis of the chamber moment of inertia,

III, A, Stage I Propulsion System (cont.)

shear of the rubber pad, movement of the flexible joints in the propellant lines, external aerodynamic loads on skirt, lateral and axial accelerations, and jet damping. An analysis of the torque requirement of the actuation system is given below:

	<u>Maximum Torque (ft-lb)</u>
1. Angular Acceleration Torque $\theta = 3^\circ \dot{\theta} = 0.26^\circ/\text{sec}^2$, I (gimbal) = $3 \times 10^9 \text{ lb ft}^2$	504,000
2. Gimbal Bearing Torque (latex center)	50,000,000
3. Actuator and Flexible Lines (estimate)	30,000
4. External Aerodynamic (approximately) for $\theta = 3^\circ$	12,000,000
5. Lateral Acceleration (0.1g)	140,000
6. Axial Acceleration (5g)	250,000
7. Jet Damping (approximately)	655,000
TOTAL (These may not be acting simultaneously)	<hr/> 63,079,000

III, A, Stage I Propulsion System (cont.)

This total moment is supplied by a hydraulic actuator having a moment arm of 32.5 ft and using RP-1 at 400 psi, which is fed to a 6-ft diameter piston. The amount of RP-1 dumped overboard based on an estimated duty cycle for the trajectory is 40,000 lb. The flow control to the actuator piston is achieved by a two-way valve which has a feedback system allowing maximum RP-1 utilization efficiency. The schematic showing the actuator and valve system is given in Figure III-A-8.

c. Structural Loads and Design

The thrust load is reacted by the rubber gimbal pad at 1,800 psi in compression and the drag load during recovery will reach as high as 400 psi in tension. Both of these loadings are the most extreme conditions that the gimbal pad will experience. The actuator torque developed is 63×10^6 ft-lb, which gives an actuator force of approximately 2×10^6 lb. This load is transmitted into the TCA by shear on the periphery of the injector and into the RP-1 tank

III, A, Stage I Propulsion System (cont.)

by the aft tank closure skirt, which has additional structural members at the actuator attachment point. During flight, when the first-stage TCA is not gimbaleed, there is symmetric aerodynamic loading on the nozzle skirt because the exit diameter of the skirt is 94 ft as compared to the vehicle diameter of 75 ft. The most severe aerodynamic loading incurred in flight occurs when the engine is gimbaleed the full 30° at low altitude. The moment produced on the skirt is less than 12×10^6 ft-lb, which results in a tube stress at the throat of 6,600 psi. This is well below the yield strength of the tube metal at the elevated temperature.

d. Evaluation and Recommendations

The gimbal system studied can be developed; however, several potentially serious problems have been revealed by the study. The main problems are associated with sea handling loads and these make a rigid chamber installation using secondary injection or other alternative TVC system appear worthy of further study.

III, A, Stage I Propulsion System (cont.)

From the table of torques, it is clear that the largest torque required is used to overcome the shear in the rubber. This is one area that could be improved considerably by selection of a softer, low shear rubber.

The total weight penalty of the gimbal system is 84,000 lb, which includes actuator weights and the RP-1 dumped. The system could be improved if the dumped RP-1 could be used effectively for engine cooling or combustion. If the dump pressure of the RP-1 is greater than the pressure in the injector head, the fluid could be fed back into the injector and used for combustion. It could also be fed into the throat region for cooling but would be too undependable for design cooling. The present design calls for dumping the RP-1 overboard during flight.

An alternative approach to the first stage engine TVC is proposed in Appendix II-10. "An Alternate First-Stage TVC System," where a secondary injection system is discussed and a schematic is given showing part of the combustion gases being bled

III, A, Stage I Propulsion System (cont.)

from the injector region and dumped back into the nozzle downstream of the throat. The gases are bled out at an off-optimum mixture ratio so that the combustion gases are relatively cool. The prime advantage of this system is that the combustion chamber can be mounted rigidly to the vehicle structure.

5. Tankage

a. General

Propellants for the Stage I Sea Dragon engine are pressure fed from two main tanks. Accessory tankage is provided on the first stage for methane, which is used for the pressurization of the RP-1 fuel tank and to pressurize the inflatable recovery flare. The methane tank also provides gimbal bearing structure that reacts against the thrust of the first-stage nozzle.

Vehicle tankage arrangement is shown in the stage layout drawings (Figure III-A-1 and Figure III-B-1). A weight breakdown is given in Table III-A-1.

III, A, Stage I Propulsion System (cont.)

Table III-A-2 provides tankage parameters to afford a general understanding of the structure. Tabulated are the material thicknesses and weights for 2014-T6 aluminum alloy, an alloy showing some promise for the application. This alloy was used for study purposes. Material studies resulted in the final conclusion that a more optimistic selection would have been 18% maraging steel for all but the LH₂ tank where a titanium alloy would be applicable. (See Appendix II-1 "Tankage Materials" and the remarks at the end of this section under Evaluation and Recommendations.)

Figure III-A-9 compares mass fraction with tank material and indicates the relative structural performance of the material selected for the Sea Dragon.

All tankage is designed on the properties of the material at working temperature. All tanks are proof tested at a pressure level calculated for the proof test temperature at yield in the material. The proof test pressure is calculated from maximum expected operating pressure at temperature, increased by a factor of 1.15. The nominal ultimate design load factor is 1.28.

III, A, Stage I Propulsion System (cont.)

All cryogenic tankage is insulated to control boiloff and to prevent the general formation of ice. The insulation material and analytical considerations are presented in Appendix II-4.

The main propellant tanks are cylindrical in form at a diameter of 75 ft with end closures selected to best counteract the structural loading imposed. All main tankage is integral; an insulated bulkhead is common to the two main tanks of each stage.

b. Stage I Tankage

The first-stage tankage assembly consists of a forward LO₂ tank, an aft RP-1 tank divided by a bulkhead, and a CH₄ tank located in the aft center of the RP-1 tank aft closure. The first-stage tankage is completely enclosed in the second-stage expandable nozzle when the vehicle is assembled; the entire first stage is submerged when the vehicle is in the sea launch configuration. Thrust reaction is through the RP-1 tank aft closure.

III, A, Stage I Propulsion System (cont.)

(1) RP-1 Fuel Tank

RP-1 fuel tank is located at the aft end of the first stage. This tank serves as the main load reacting element of the gimballed first-stage engine, loads input at the aft skirt, and body forces along its short cylindrical tank length.

(a) Forward Closure, RP-1 Tank

The forward closure is a 1.4:1 ellipse, which is insulated to control LO₂ boiloff and RP-1 ullage pressurizing gas (CH₄) cooling. The four inches of insulation is encapsulated in the space between the membrane and a 1/8 in. thick aluminum skin on the RP-1 side of the bulkhead. The bulkhead (RP-1 tank forward closure) is unported.

The bulkhead is designed to withstand an internal pressure of 162 psi. Relative tank pressures between the LO₂ and RP-1 are so controlled that crippling pressure loading on

III, A, Stage I Propulsion System (cont.)

the bulkhead is not probable. With the exception of the insulation and the encapsulating shell, the bulkhead is an unreinforced membrane of 1.58 in. uniform thickness.

(b) Cylindrical Section, RP-1 Tank

The length of the cylindrical section of the RP-1 tank is 6 ft. This structure is unreinforced and 4.17 in. thick. The cylindrical section is ported for RP-1 vent and fill lines and provides for attachment of the aft cylindrical skirt and the cylindrical section of the LO₂ tank.

(c) Aft Closure, RP-1 Tank

The RP-1 tank aft closure is a 90° cone. This closure shape is chosen as it best counteracts, rigidly, the tank pressure with a concentrated load at the center. The closure supports the methane tank through which the engine loads are input.

III, A, Stage I Propulsion System (Cont.)

The conical aft closure is reinforced at the intersection of the aft spherical element of the CH₄ tank (gimbal base) as is required to distribute the concentrated load over the area necessary to provide RP-1 tank pressure reaction of the thrust (first-stage engine). The conical portion of the closure is uninsulated.

The closure is ported, for main propellant feed, near the intersection between the closure and the CH₄ tank. The port is made of a number of small holes as is required to minimize discontinuities in the structure.

(d) Antislosh Baffles

Antislosh baffles are mounted on the cylindrical and conical portions of the RP-1 tank. The slosh baffles are a highly discontinuous structure providing no hoop or circular stability to the tank. The baffles are designed to eliminate sloshing and to counteract impact loads developed by relative fluid motion.

III, A, Stage I Propulsion System (cont.)

(2) Methane (CH_4) Tank

The methane tank is an elongated spherical structure. The forward and aft closures are hemispherical with a conical connecting element; the forward closure is common to the RP-1 tank, insulated, unported, and designed to withstand full CH_4 tank pressure.

The conical connecting element provides structural reinforcement for the RP-1 aft closure at the joint between the two tanks, provides CH_4 tank pressure holding structure, and provides distribution of the gimbal loads to the RP-1 aft closure. The conical element is ported for CH_4 fill and vent and CH_4 feed to the RP-1 tank.

The CH_4 tank aft closure is spherical, insulated, and unported. This element serves as the base for a bonded rubber gimbal bearing. The insulation is designed to keep the rubber at proper working temperatures as well as minimizing the change in condition of the CH_4 charge.

III, A, Stage I Propulsion System (cont.)

(3) LO₂ Tank

(a) Forward Closure, LO₂ Tank

The forward closure of the first-stage LO₂ tank is a 60° included angle cone. This shape has been determined to be best able to counteract the water entry loads during recovery of the first stage. The closure is insulated internally with a 1.25-in. insulation thickness and is ported for vent and fill line access of all lines from all first-stage tankage to the stage umbilical connection. The closure is designed by the water impact loading; analysis indicates that by maintaining a high final LO₂ tank pressure (130 psia minimum) a forward closure of 2.6-in. constant thickness is required. An expendable vehicle would be able to utilize an elliptical forward tank closure with some weight saving.

(b) Cylindrical Section, LO₂ Tank

The LO₂ cylindrical tank wall is the primary body load reacting member and is continuous with the RP-1

III, A, Stage I Propulsion System (cont.)

tank cylindrical section. The LO₂ cylindrical section is 2.26 in. thick, has 1.25 in. of insulation, and is ported for fill and vent line access and for main propellant feed. The main feed line ports are multiple and of small size located just forward of the aft closure (bulkhead). The porting is designed to minimize structural discontinuity and optimize propellant feed from outage and swirl aspects.

The cylindrical portion of the LO₂ tank provides structural support for and counteracts loads input from antislosh baffle plates. The slosh baffle plates are highly discontinuous structures, providing no hoop or circular stability to the tankage.

c. Structural Loads

(1) Summary

The sea handling concept is developed from a consideration of the weight of structure required to distribute

III, A, Stage I Propulsion System (cont.)

concentrated loads over large pressure holding vehicles. To reduce the weight of the vehicle and its support equipment, hence its cost, it has been practice to avoid the generation of concentrated loads by reacting pressure with pressure.

The self-generated loads developed during handling and operation are pressures, shears, and moments. It has been found that these loads can be reacted by maintaining pressure in the compartments of the vehicle that have pressure holding as a primary function.

(2) Pressures

The structure must counteract externally applied pressures resulting from the sea and atmospheric environment and those that are self-generated and result from the pressure fed propellant feed system. In the system that has been defined for the study purpose, it has been found that internal pressure provides the designing criterion and very little stiffening is necessary anywhere

III, A, Stage I Propulsion System (cont.)

on the vehicle; it has been possible to counteract pressures with pressure in most areas by use of unreinforced membrane structure. All handling loading is reacted with pressure, as is all flight loading.

Stiffening is required in four locations:

The RP-1 tank aft closure is stiffened to react the thrust chamber loads; the LO₂ forward closure is of a thickness greater than that required to react the internal tank pressure as a result of concentrated high pressure forces that exist during water entry; the aft skirt on the RP-1 tank is structure that distributes concentrated forces from the ballast stabilizing struts; and the gimbal TCA (engine) actuators.

(3) Bending Moments

Body bending moments are reacted by the cylindrical elements of the tankage structure. Pressure charges are maintained in all tanks so that no compressive or crippling forces are present. During flight and during erection of the floating loaded vehicle, large body bending moments, similar in magnitude, are developed. These moments are counteracted by the tankage designed by pressures

III, A, Stage I Propulsion System (cont.)

required by the propellant feed system. Table III-A-2 shows the pressure level in tanks required to counteract maximum compressive loads developed as a result of bending and other environments.

(4) Mechanical Loading

Concentrated or mechanical loads are distributed to and counteracted by the cylindrical structure. This approach enables development of rigid points for counteracting concentrated loads and reduces interactions between those hard points and the flexible pressure holding structure.

(a) Ballast Support

All forces applied by the ballast to the vehicle are delivered by struts attached to the ballast and to the vehicle at the aft thrust chamber skirt. An axial force reacting capability exists through an attachment between the ballast and the aft end of the first-stage thrust chamber assembly. The structure

III, A, Stage I Propulsion System (cont.)

staging joint provided at that location is for retention of the ballast during powered operation of the first stage and provides for separation of the ballast upon command.

(b) Force Reaction, Thrust Chamber Assembly

The thrust of the first-stage engine is counteracted by the gimbal bearing. This bearing can react to both positive and negative thrusts of the same magnitude for appropriate RP-1 tank pressures. The gimbal bearing reacts side and torsional loads through shear in the flexible element.

(c) Force Reaction, Gimbal Actuator

The gimbal actuator reactions are near the aft skirt extension of the RP-1 tank. Radial components of the reactions are through the RP-1 tank conical aft closure, axial reactions are directly distributed in shear to the aft strut.

III, A, Stage I Propulsion System (cont.,)

(d) Stage I Thrust Structure

The first-stage thrust is transmitted structurally from the TCA through the gimbal bearing and RP-1 tank aft closure to the cylindrical tank elements. The stage thrust is delivered to the second stage by a cylindrical forward section of a staging joint located on the inside contour of the second-stage nozzle at the major body diameter.

(e) Atmospheric Entry

During atmospheric entry, a large drag area will be provided by an inflatable flare, which is attached to the first-stage TCA. All loads generated by the flare will be counteracted by the TCA.

(f) Water Entry

With the exception of a small forward portion of the 60° conical forward closure of the LO₂ tank,

III, A, Stage I Propulsion System (cont.)

the first-stage water entry loads are counteracted by the retained tank gas pressure. Concentrated loads resulting from the 22g deceleration develop on components such as the TCA and accessory lines and valves, which must be counteracted as concentrated loads.

d. Evaluation and Recommendations

The tankage design described is believed to be adequate for the study purposes and feasible in an environment of an advancing state of the art. An evaluation of the design described is presented below from the aspects of the alternates considered in the development of the design.

(1) Tankage Geometry

Integral and separate tankage configurations were studied preliminarily. An analysis was made comparing the weight of integral (common bulkhead) versus separate bulkheads between propellant tanks, considering propellant feed lines, distribution manifolds, insulating requirements, and intertank structure. The

III, A, Stage I Propulsion System (cont.)

results indicated a significant weight penalty for the separate tankage. The weight penalty was approximately equal to the weight of one of the closures on the separate tanks. Other factors, such as maintaining the integrity of the insulation, leaks between tanks, vehicle rigidity, manufacturing sequence, and costs have been evaluated only qualitatively. Consideration of these factors develops arguments for either approach. As an example, separate tankage that appears to afford simpler manufacturing and proof test procedures necessitates, in application to the vehicle, an additional compartment that would not normally be pressurized. During sea handling operations this compartment must be either (1) flooded to equalize pressure differences, (2) must be sealed and the intertank structure made capable of taking significant crushing pressure, or (3) must be pressurized to offset the high crushing pressure level.

If the compartment is flooded, the requirements on the amount of and integrity of the insulation are probably more severe than that for the integral tankage configuration. This results from the fact that the flooded compartment will be quiescent and regardless of the amount of insulation applied, the water will

III, A, Stage I Propulsion System (cont.)

freeze in time. Buildup of ice in compartments is an obvious hazard. Furthermore venting of the water from the flooded compartment during the first portion of flight produces unusual structural requirements.

If the compartment is sealed, a structure required to counteract high crushing pressure loads developed during sea handling modes becomes unreasonable from weight aspects.

If the compartment is pressurized, the management of pressure in the compartment becomes of extreme importance to the success of the mission. Loss of pressure in the compartment while submerged would result in structural failure; failure to vent pressure in an intertank compartment could result in collapsing pressures on a closure of one of the propellant tanks, which would produce structural failure.

The conclusions drawn at this time are: (1) That separate tankage does not avoid the inadvertent occurrence of a collapsing pressure on a bulkhead and does not avoid or

III, A, Stage I Propulsion System (cont.)

minimize the requirements for the integrity of a propellant tank insulation, (2) the weight penalty for separate tankage as compared to integral tankage is approximately equal to the weight of one of the tank bulkheads. For these reasons, the Sea Dragon design utilized integral tankage.

Single versus cluster tanks was also considered. Reduced wall thicknesses, simplified pressure vessel design, and the greater number of units produced tend to reduce development time and fabrication cost and improve reliability and transportability for clustered tanks. These factors are felt to be offset by the very complex clustering structure and the probable vehicle weight penalty as compared to single integral tanks. For these reasons, the Sea Dragon vehicle design was based on the use of single tanks.

The locations selected for the propellant constituents include consideration of vehicle performance and tend to optimize propellant feed systems. The forward location of the LO₂ tankage provides the most forward vehicle center of gravity

III, A, Stage I Propulsion System (cont.)

position. In addition, the long stand pipe length for the LO₂ feed line provides a large portion of the required LO₂ injector inlet pressure. This factor is important because the required final LO₂ ullage pressure is low affording a significant pressurant gas weight saving. Higher required ullage pressures for the aft located fuel tankage does not compensate because the pressurant gases available for fuel are less dense. The arrangement chosen provides maximum vehicle stability resulting from the forward center of gravity location and the inert weight advantage mentioned above.

The methane tank was located integral with the Stage I RP-1 tank because the higher working pressure of that compartment would counteract the pressures generated in the gimbal bearing. The low temperature of the methane, -128°F, must be isolated from the rubber bearing. Insulation provided for that purpose is internal to the methane tank. The methane tank is designed to withstand full tank pressure at room temperature with no reinforcement by RP-1 tank pressure.

III, A, Stage I Propulsion System (cont.)

(3) Tankage Material

(a) Sea and size effects are strong factors affecting selection of tank materials. Galvanic corrosion will be an important consideration in operation of the system. The tank size will advance the state of the art of flight tankage, especially in joining techniques. For purposes of the study, a material was chosen that has better known properties, is cheaper, and more available than other types that might be used. This was 2014-T6 aluminum. Its use results in weight estimates that are conservative. However, a difficulty arose in certain phases of the study as a result of the specification of this material. This was concerned with the welding of the resultant thick walls.

Appendix II-1, Tankage Materials, summarizes some of the data accumulated in the study. The final result indicated that 18% maraging steel and some titanium alloys were potentially more attractive than the aluminum. Sufficient unknown

III, A, Stage I Propulsion System (cont.)

areas exist in the selection of large rocket tank materials to warrant a considerable materials program especially directed towards such large tankage.

6. Pressurization and Feed Systems

a. General Concepts and Advantages

The propellant feed systems for both stages of the Sea Dragon will consist of pressure-fed systems rather than pump-fed systems. Three separate concepts are being used in the proposed pressure feed systems. These concepts include: (1) Autogenous pressurization, i.e., the utilization of a vaporized and superheater propellant for self-pressurization, (2) vapor pressurization, i.e., the utilization of a liquid propellant's vapor pressure for self-pressurization, and (3) acceleration head effects that become as large as 270 psi because of the large heights of the propellant tanks.

III, A, Stage I Propulsion System (cont.)

A list of the more pertinent advantages and disadvantages of a pressure-fed propulsion system for the Sea Dragon first stage includes:

Advantages

- (1) Simplicity
- (2) Rugged tanks for sea handling and recovery.
- (3) Because of size, the tanks must be designed for moderately-high pressures even with turbopumps.
- (4) Eliminates the high cost of pump development, fabrication, and refurbishment.

Disadvantages

- (1) Higher tank weights, thicker walls and lower mass fractions.
- (2) Tanks may be more expensive.

III, A, Stage I Propulsion System (cont.)

b. Oxidizer System

Figure III-A-10 illustrates the Stage I pressurization system. The first-stage oxidizer tank uses an autogenous pressurization system. A small amount of LO_2 is taken from the bottom of the LO_2 tank, sent through a heat exchanger where it is vaporized and superheated, and fed back to the top of the LO_2 tank to supply the necessary ullage pressure. The driving force for the pressurization process is provided by the acceleration head in the LO_2 tank and propellant line. The acceleration head effects account for 161 psi at first-stage ignition (2.0 g) and 117 psi at first-stage burnout (4.6 g). The various ullage pressures in the LO_2 tank plus the acceleration head effects results in the required injector manifold pressures.

A summary of the design criteria for the first-stage oxidizer pressurization system is listed as follows:

III, A, Stage I Propulsion System (cont.)

Initial gaseous oxygen pressure	226 psi
Final gaseous oxygen pressure	130 psi
Final gaseous oxygen temperature	0°F
Final gaseous oxygen pressurant weight	213,000 lb

The amount of gaseous oxygen that flows through the heat exchanger is 236,000 lb (Accounts for condensation).

c. Fuel System

Liquid methane is used as the pressurizing fluid for the RP-1 tank. The liquid methane is stored at a temperature of -128°F, with a corresponding vapor pressure of 500 psi. The liquid methane is forced, because of its own vapor pressure, into the RP-1 tank. The methane then vaporizes and superheats as it bubbles up through the RP-1. This process provides the ullage pressure. A methand weight of 178,000 lb is required for a final ullage gas pressure of 293 lbs/in.² (final gas temperature of 0°F. The methane, stored as a liquid, occupies a volume of 10,500 ft³. It is proposed

III, A, Stage I Propulsion System (cont.)

that the methane be stored inside the first-stage gimbal ball, which can use internal pressurization to react engine thrust loads.

A more detailed description of the first-stage fuel pressurization system includes:

Pressurant	Liquid methane
Storage Temperature	-128°F
Storage Pressure	500 psi
Density of liquid methane	17 lbs/ft ³
Weight of methane required for pressurization	178,000 lbs
Volume of methane	10,500 ft ³
Initial methane vapor pressure	500 psi
Final Methane vapor pressure	320 psi
Initial ullage pressure in RP-1 tank	425 psi
Final ullage pressure in RP-1 tank (first stage burnout)	290 psi
Final ullage pressure in RP-1 tank (After drag flare is pressurized)	130 psi

III, A, Stage I Propulsion System (cont.)

Final temperature of methane in RP-1 tank	0°F
Temperature drop in RP-1 caused by heating up the methane	15°F

d. Ullages

Both first-stage propellant tanks have initial ullages volume of three percent. The gimbal ball that stores the methane has zero ullage. Initial and final ullage pressures have been previously discussed. Figure III-A-11 illustrates the profile of pressure drops incurred during first-stage operation.

e. Ignition

A hypergolic type start using the reaction of triethylaluminum (TEA) with LO_2 was selected. Appendix II-7, "Ignition," presents further details.

III, A, Stage I Propulsion System (cont.)

f. Overall Operational Characteristics

Liquid oxygen flow is ducted from the bottom of the LO₂ tank near the intersection of the common bulkhead of the cylindrical outer tank wall. The cylindrical wall is ported with a number of small diameter holes (10 tubes of 2.75 ft dia) to which lines are attached to pass the flow outside of the RP-1 tank. The small lines are manifolded to a single line that is provided with flexible joints enabling gimbaling of the first-stage manifold. The main LO₂ propellant valve is mounted structurally on the forward side of the first-stage injector. The main propellant valve in its shut-off condition is hermetically-sealed by a diaphragm between the body of the valve and its movable element. The valve in its shut off position is retained mechanically. The mechanical retention can be released by application of pressure or by an explosive device. Propellant flow is initiated when the mechanical device is released that permits controlled travel of the poppet to an intermediate position where it engages another mechanical stop. The sealing diaphragm is designed to fail in shear when the poppet moves and not because of the direct

III, A, Stage I Propulsion System (Cont.)

action of LO₂ pressure. The valve is actuated by pressure in the propellant line. The main propellant valve is shut off by release of the intermediate mechanical stop by mechanical or explosive device and moves under control to engage a conical seat at the aft extent of travel. The valve is moved to the shutoff position by the pressure drop across the valve during propellant flow. The valve is retained in the closed position by a mechanical device which tightens as the acceleration increases. This device eliminates the possibility of propellant flow or tank pressure loss during recovery.

When the main LO₂ propellant valve is open, a line is provided to a component which regulates liquid oxygen flow to the heat exchanger located in the throat region of the first-stage thrust chamber assembly. This controller responds to sensed pressures at the RP-1 injector manifold. Hence, oxidizer flow is controlled to match the fuel flow and maintain a constant mixture ratio.

The RP-1 main propellant feed is ducted from the bottom of the RP-1 tank at Station 425 through a number of small

III, A, Stage I Propulsion System (Cont.)

ports. Flow from the ports is manifolded to a main propellant feed line that is provided with flexible joints to enable gimbaling of the first-stage thrust chamber assembly.

The characteristics of the fuel thrust chamber valve are similar to the oxidizer valve and permit the valve to take one of three positions. There is no necessity for a high pressure actuation system in the valve, and therefore, a weight saving results. The fuel valve is normally closed. An annular ring serves as a shear diaphragm. This ring is attached between the valve pintle and the valve housing, thus restricting any flow from entering the injector. Upon receiving the proper signal, an explosive charge blows a pin that causes the annular ring to shear and thus gradually opens the propellant valve. A second pin is sheared at first-stage burnout. This operation causes the valve pintle to drop and seat against the lower portion of the valve housing. The valve is completely closed in this final position. A mechanical device will lock the valve in the closed position to eliminate any leakage during the recovery process.

III, A, Stage I Propulsion System (cont.)

g. Evaluation and Recommendations

One problem exists in the above described first-stage pressurization system. The problem concerns the maintenance of sufficient ullage pressures during first-stage ignition. Preliminary analysis indicates a decay in LO₂ ullage tank pressure from 266 psia to 21 psia in ten sec, assuming full propellant flow and no gaseous pressurization addition (refer to Figure III-A-12). Similarly, the RP-1 ullage tank pressure will decay from 425 psia to 45 psia in ten sec assuming full propellant flow if the methane gas pressure does not supplement the initial ullage pressure (refer to Figure III-A-13). Naturally, the vehicle would never get out of the water if the tank pressures were as low as the above analysis would seem to indicate. However, the analysis is somewhat misleading in that it assumes continuous full flow, a condition that cannot exist under reduced tank pressures.

The immediate solution to the problem is to be certain that both first-stage propellant tanks are given supplementary gas pressures as soon as possible once the expulsion of the

III, A, Stage I Propulsion System (cont.)

propellants has been initiated. For this reason, it is recommended that additional analysis be conducted. In the case of the fuel circuit, the time required for the methane to bubble up through the RP-1 tank must be determined so that the valve that admits the flow from the methane tank (gimbal ball) to the RP-1 tank is properly sequenced. In the case of the oxidizer circuit, it is suggested that the propellant utilization valve illustrated in Figure III-A-10 be located immediately upstream of the heat exchanger. Therefore, as soon as the valve is opened, additional LO₂ gas pressure becomes available to supplement the initial ullage pressure. The pressure differential that pumps the pressurization gases from the heat exchanger to the LO₂ tank is the result of the difference of acceleration head of the liquid and gaseous oxygen.

7. Aft Skirt

a. Description

The aft skirt on Stage I consists of a cylindrical extension on the aft RP-1 tank. It extends from vehicle

III, A, Stage I Propulsion System (cont.)

Station 414 to 436 and provides nesting support for the expandable nozzle, which has its trailing edge at Station 421. The aft skirt is designed to provide hard points or fittings for actuator and ballast strut reactions.

The skirt structure is stiffened skin, 0.5-in. total equivalent thickness, that attaches to a cylindrical extension on the RP-1 tank. The skirt is stiffened at its trailing edge with two deep frames designed to provide local circular stability. Gimbal actuator and ballast strut reactions are input to these circular frames through fittings.

b. Evaluation of Problems and Potential Improvements

The aft skirt distributes concentrated loads from the gimbal actuators and from the ballast struts to the tank structure. The skirt provides a surface against which the expandable nozzle is stowed. These structural functions could be provided by a

III, A, Stage I Propulsion System (cont.)

truss-type structure for lower weight by additional design development. Concentrated loads from the truss structure could be distributed in a very short cylindrical structure at the aft end of the RP-1 tank. Expandable nozzle stowage could be provided at its trailing edge with a ring channel section with its open end forward. Upon staging separation, the convolutions of the trailing edge of the expandable nozzle are released by the relative motion of the stages.

Alternate thrust chamber design types and approaches to thrust vector control applicable to the Sea Dragon would not require an aft skirt extension. Where the thrust chamber is not articulated (such as a rigid chamber using secondary injection), the expansion section of the nozzle can be made to counteract ballast loads that are input in a circularly continuous manner. The incremental weight of the thrust chamber for this additional structural function probably would be less than that for the separate skirt extension. If a plug nozzle were to be used, separate skirts would not be required. In this case, the ballast loads would be input to a truncated isentropic spike in a circularly continuous manner.

III, A, Stage I Propulsion System (cont.)

The aft skirt structure shown on the Stage I drawing is considered to be adequate to provide the structural functions defined above. A detailed analysis has not been attempted. Applicable thrust chamber design types of other designs could remove the requirement for a separate skirt.

8. Fill, Vent, and Dump System

a. Description

The LO₂ tank, the RP-1 tank, and the CH₄ tank have filling, venting, and dumping capabilities. Each has one fill line, one horizontal vent line, and one vertical vent line. These lines are all routed from the second stage forward compartment to the internal umbilical or disconnect assembly and to the respective tanks. The Stage I and Stage II layout drawings illustrate the location and routing of all Stage I fill and vent lines. Additionally, Appendix II-8 provides a flow schematic of the first-stage fill and vent system, a functional description of all hardware used in filling a venting,

III, A, Stage I Propulsion System (cont.)

minimum pressures required during filling operations, and the positions that each component assumes during loading, towing erection, launch, staging, recovery, and dumping.

b. Evaluation

The proposed vent system is flexible with many redundant features. Additionally, all filling and venting is conducted in a region that is accessible to the ground support equipment.

9. Internal Umbilical Provisions

a. General Configuration

The internal umbilical interface is located in the center of the Stage II injector. Physically, it consists of a 6 ft dia recessed hold into which the male portion of the connector (located on the Stage I nose cone) will slide and engage. Directly behind this recess is a tunnel that provides routing of the instrumentation and control lines from Stage I to the outer periphery of the

III, A, Stage I Propulsion System (cont.)

Stage II injector from which the various lines are rerouted to the vehicle GSE interfaces.

b. Hydraulic Disconnect Couplings

All the hydraulic couplings are identical in basic design and consist of two specially-designed check valves, back to back, which are held open by a compression rod that actuates the valves through a linkage system and provides an open circuit on all lines when Stage I and Stage II are coupled.

Upon separation, the compression rods automatically are released allowing the check valves to resume a closed position isolating all systems from external contaminants.

c. Electrical Disconnect Couplings

All control and instrumentation lines will be connected by use of common-type bulkhead connectors and arranged by

III, A, Stage I Propulsion System (cont.)

function into various banks. Separation is simplified by use of this pin and socket combination.

d. Disconnects (number and relative sizes)

Hydraulic

Oxid. Fill Line	-	1.35 ft dia
Oxid. Horiz. Vent	-	.828 ft
Oxid. Vert. Vent	-	.828 ft
Fuel Fill Line	-	1.10 ft dia
Fuel Horiz. Vent	-	.75 ft
Fuel Vert. Vent	-	.75 ft
CH ₄ Fill Line	-	1.00 ft dia
CH ₄ Horiz. Vent	-	.50 ft dia
CH ₄ Vert. Vent	-	.50 ft dia

III, A, Stage I Propulsion System (cont.)

Electrical

Pressure transducer, thermocouple, and sensor input, output and test cables, micro-switch, potentiometer, input and output cables. Electrical impulse for explosive bolts, valve control, and actuator control.

10. Propulsion System Performance

a. Summary

The thermochemical properties of the LOX/RP-1 propellants for the first-stage vehicle were given in Figure III-A-2 where the I_{sp} versus mixture ratio curve is found to be very flat at the design mixture ratio. Because the engine is regeneratively-cooled with the propellant, the heat loss in the combustion chamber represents virtually no net loss. For the first stage vehicle, Figure III-A-14 gives a plot of chamber pressure versus specific impulse at sea level for various mixture ratios showing the small performance advantage when using chamber pressures much greater than 300.

III, A, Stage I Propulsion System (cont.)

b. Evaluation and Recommendations

The conservative value of 93% of theoretical specific impulse assumed should be readily achievable. It is expected that the chamber can be cooled by convection techniques only and therefore no loss because of film cooling need be considered. The large chamber volume will allow the reaction to attain a high degree of completion while using stable injector designs.

11. Propulsion System Weights, Stage I

a. Summary

The weights of the first-stage propulsion system are given in a weight breakdown accompanying this section. The results are given in Table III-A-3.

The weights of all components have been calculated on the basis of the configurations defined. Component definition

III, A, Stage I Propulsion System (cont.)

has been on the basis of estimates, where necessary, as is discussed in other sections.

b. Evaluation and Recommendations

The total propulsion stage weight is felt to be conservative in terms of stage performance. It appears that through application of alternate component design concepts and materials significant stage performance improvement could be achieved. Utilization of higher strength structural materials for tankage and other components will provide an improvement in stage mass fraction. Application of alternate thrust chamber design types may offer weight advantages.

The weight breakdown, Table III-A-3, indicates a miscellaneous weight of 5% of the tankage weight. This allowance is made for weld joint reinforcement. This allowance accounts for thickening at the weld joints to allow for approximately 50% reduction in the strength of the as-welded joint. The reinforcement will be

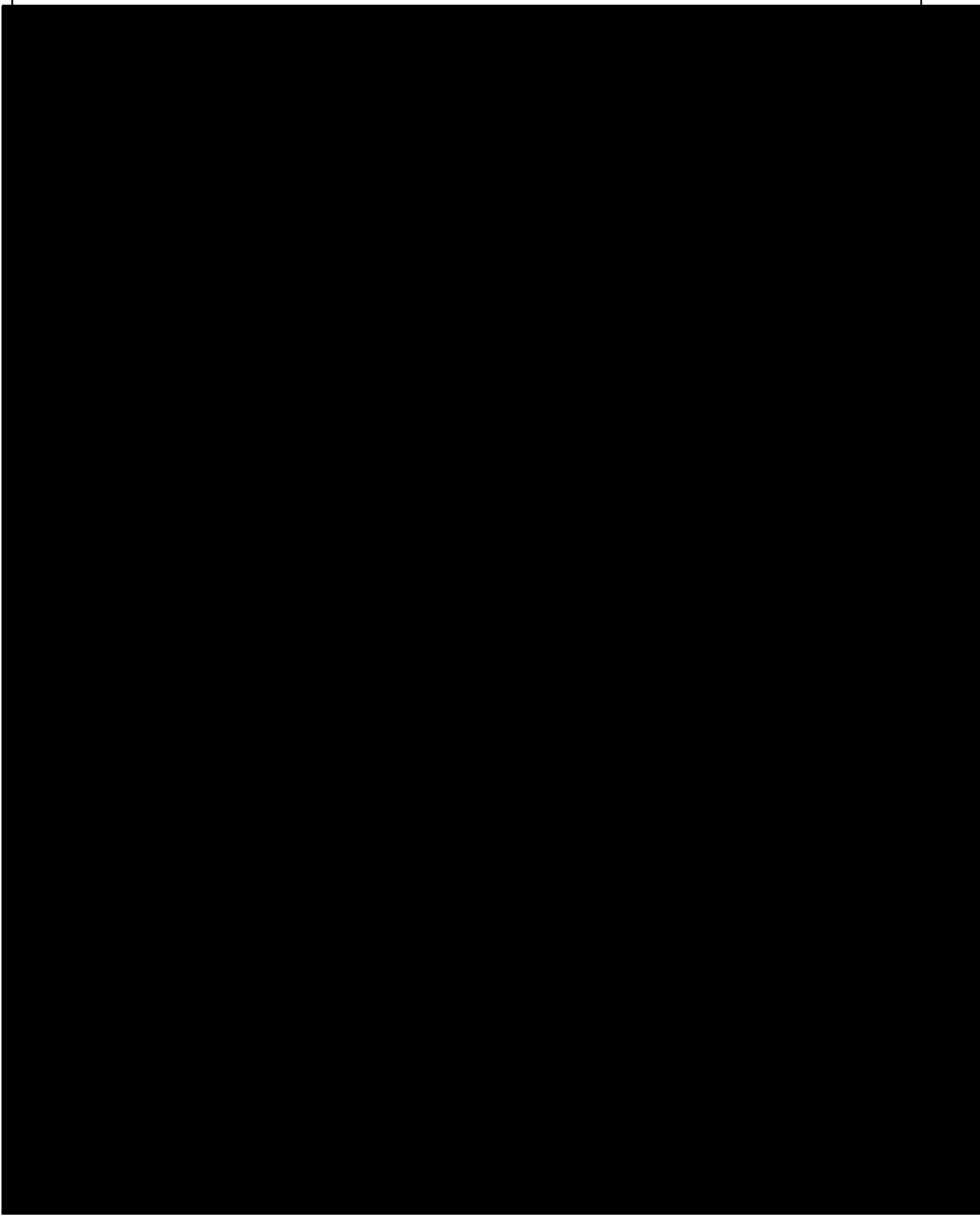
III, A, Stage I Propulsion System (cont.)

applied to longitudinal welds. The 5% will account for this reinforcement in the thinner sheets; a separate allowance is made for the thicker tankage elements. The RP-1 tank weight includes 70,000 lb for integral stiffening of the conical aft closure to counteract the concentrated loads input by the gimbal bearing. Weld joints thickening will form the integral frame and stringer reinforcing element.

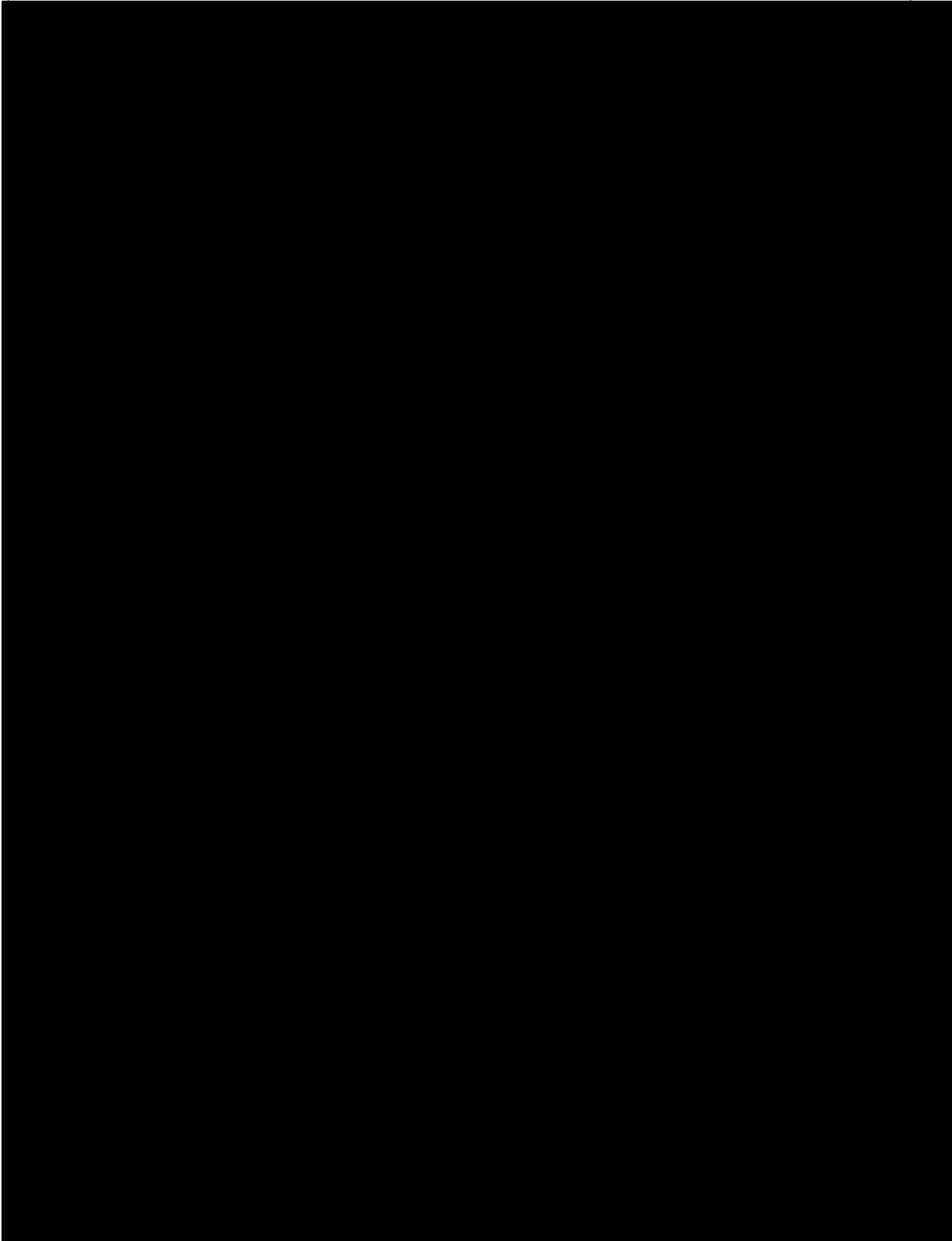
Bulkhead insulation weights are on the basis of estimated thickness requirements of 4 in. Subsequent analysis has shown this to be very conservative.

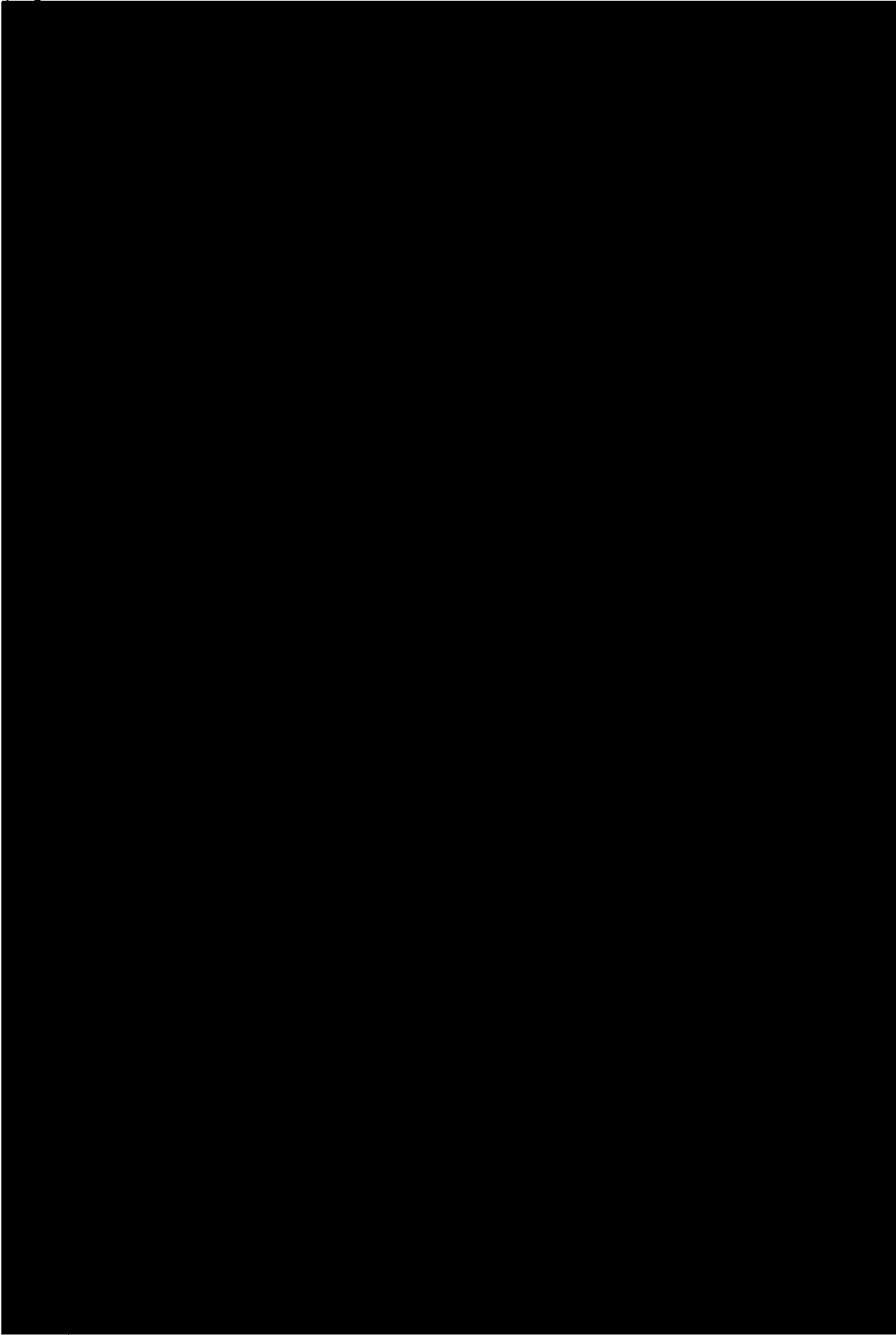
The weight savings achievable for an expandable vehicle are shown in Table II-A-2.

Report No. LRP 297, Volume II



Report No. LRP 297, Volume II





Report No. LRP 297, Volume II

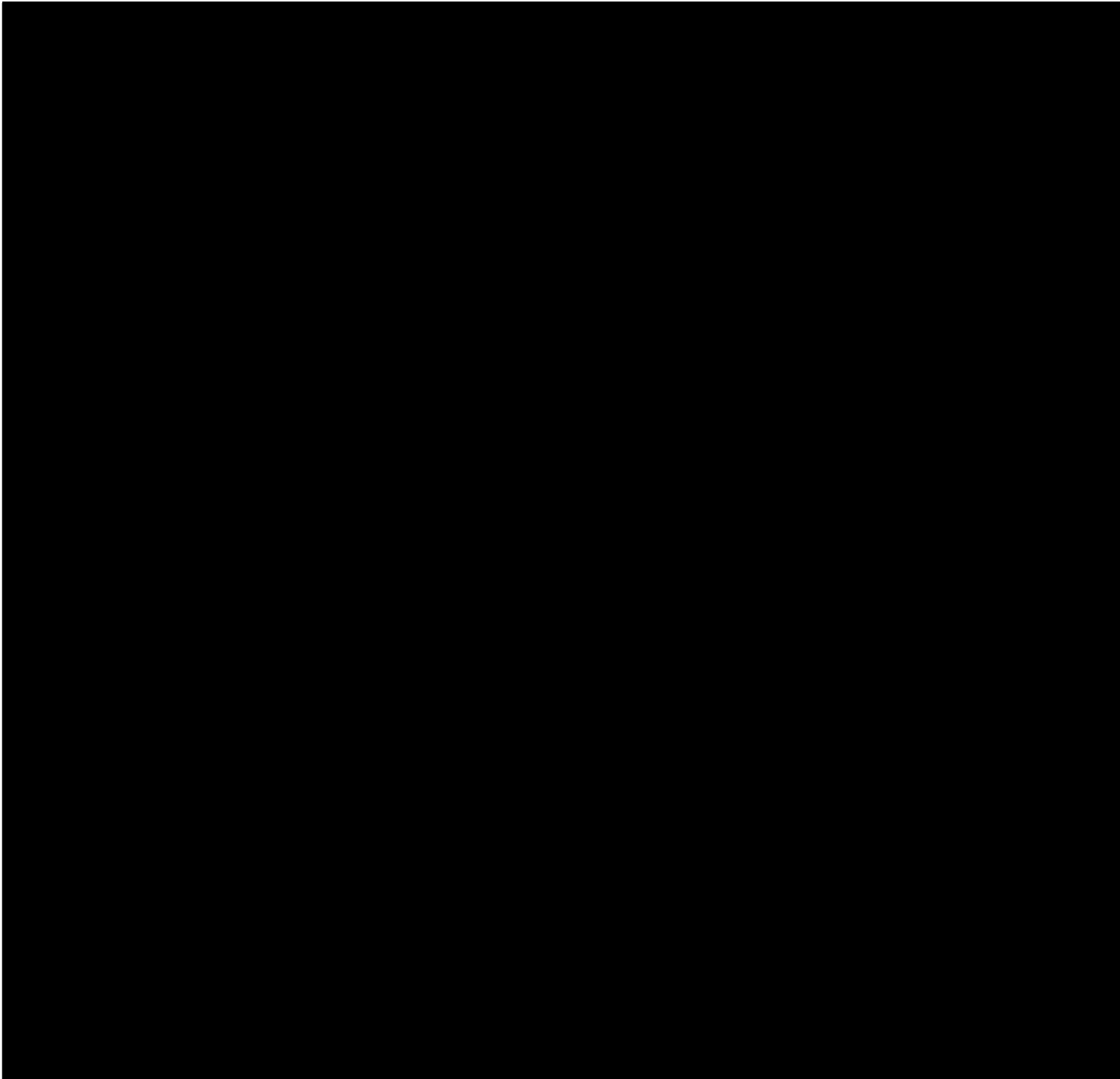
AEROJET-GENERAL CORPORATION

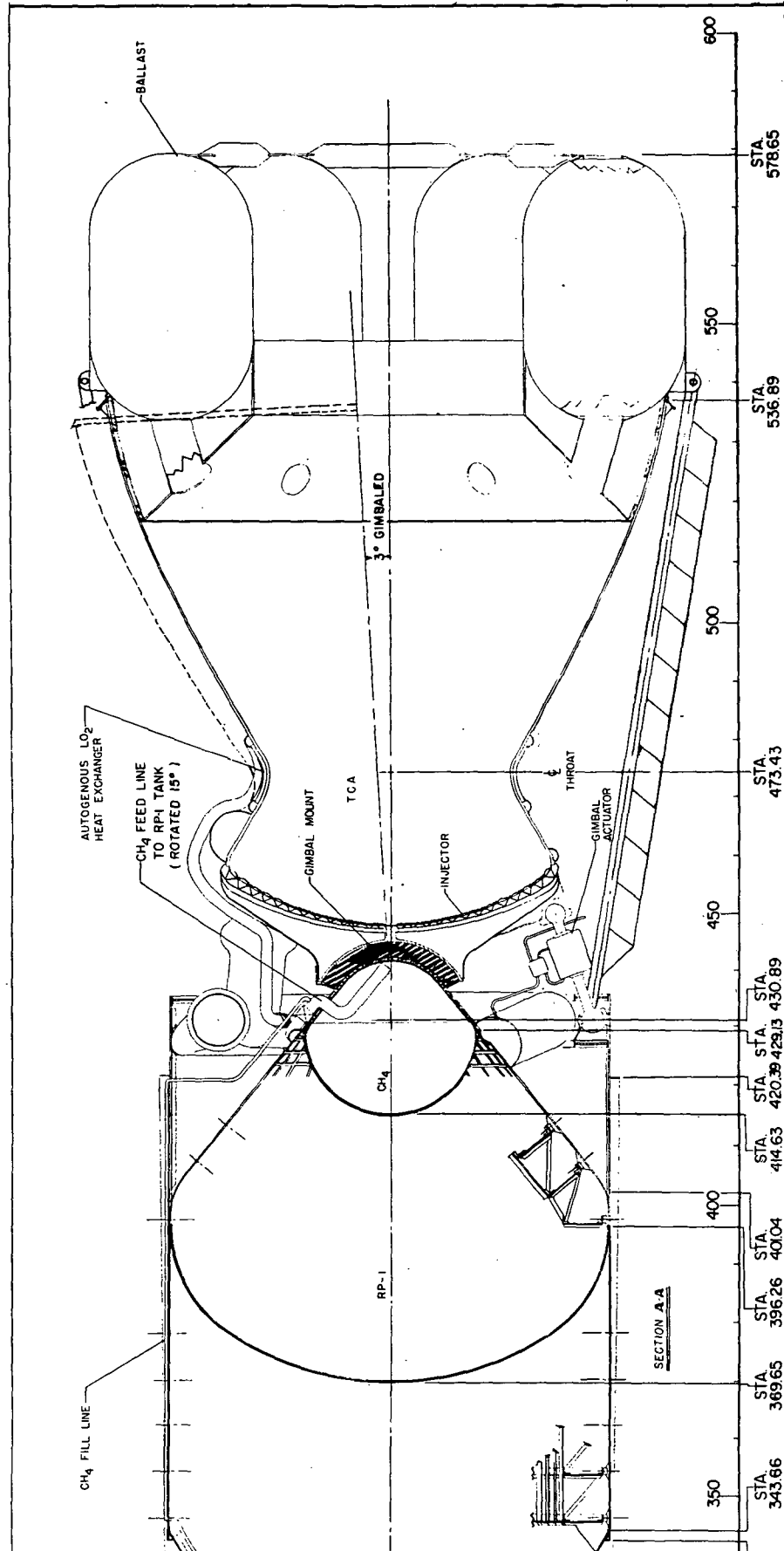


Report No. LRP 297, Volume II

AEROJET-GENERAL CORPORATION

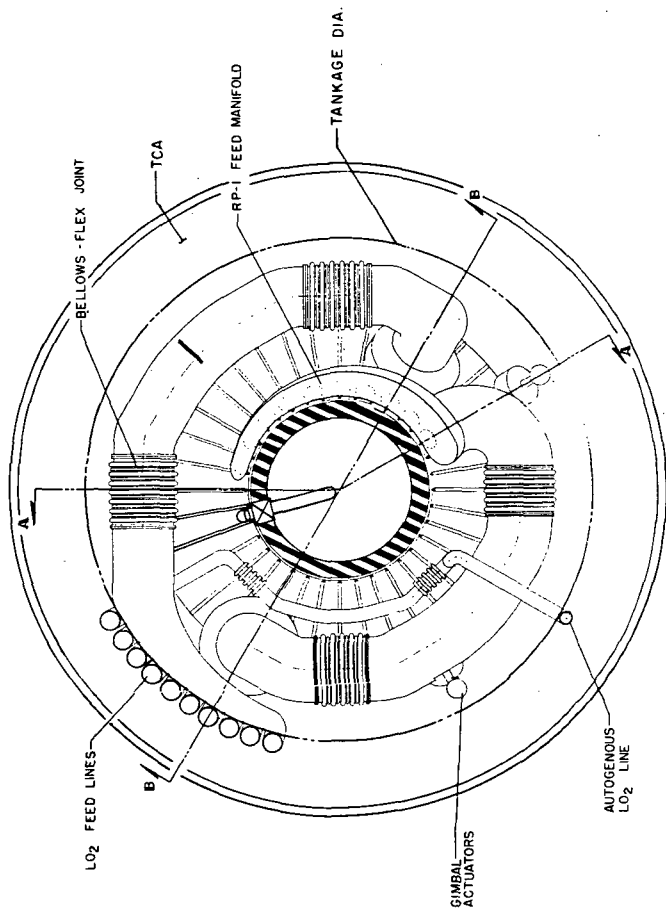




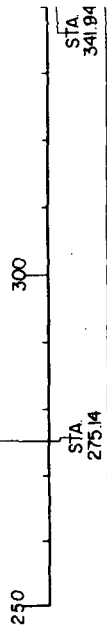
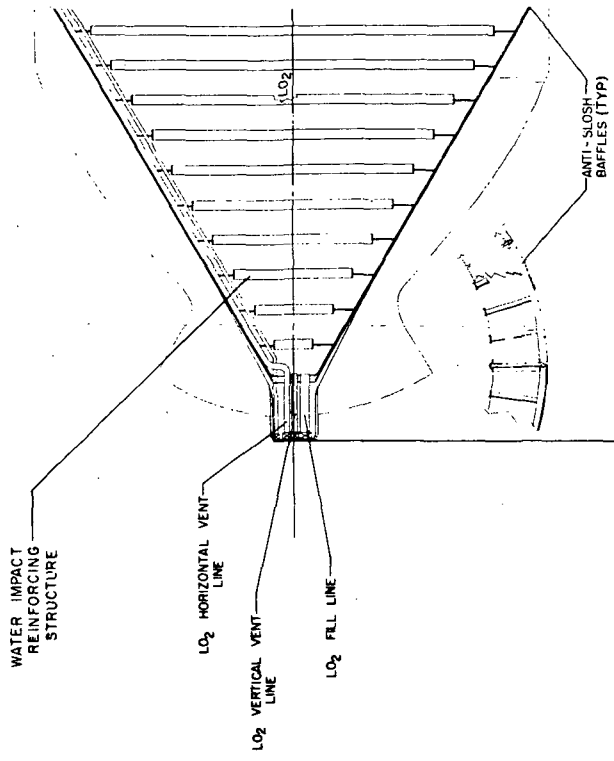


Stage I Propulsion System Layout Drawing

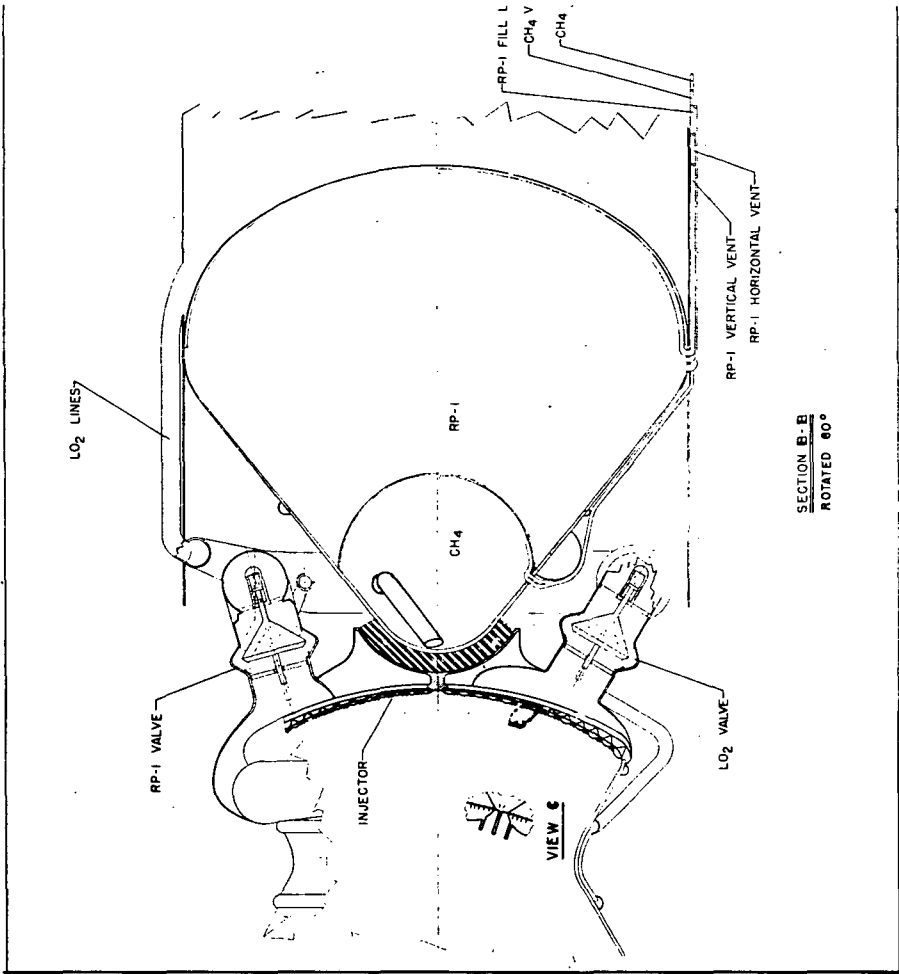
Figure III-A-1



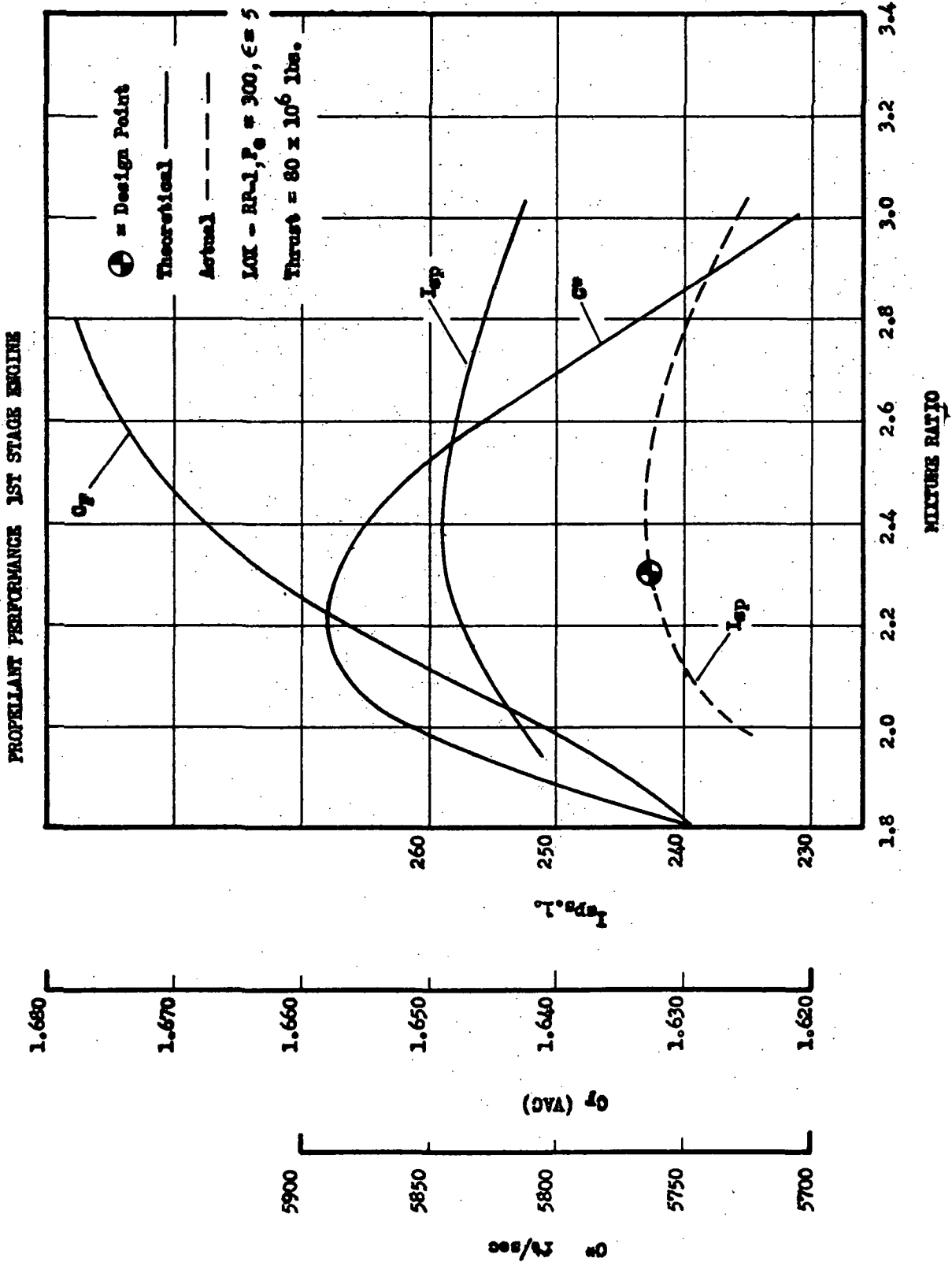
VIEW LOOKING AFT WITH TANKAGE REMOVED FOR PURPOSES OF CLARITY



VERTICAL VENT
 HORIZONTAL VENT



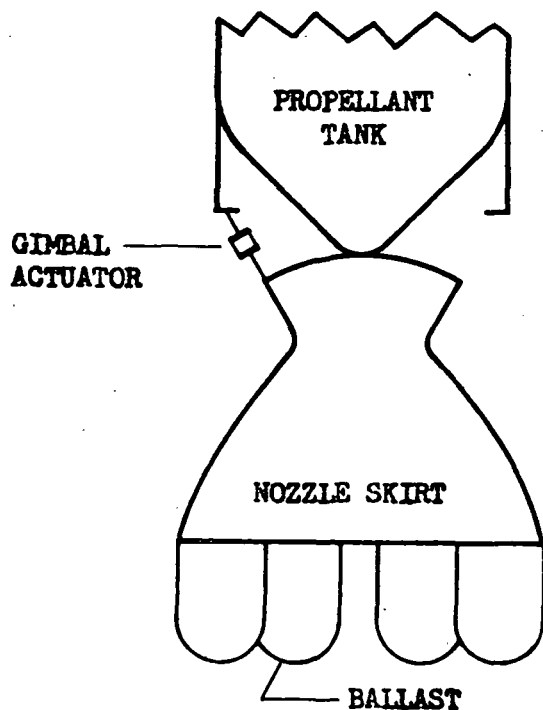
SECTION B-B
ROTATED 90°



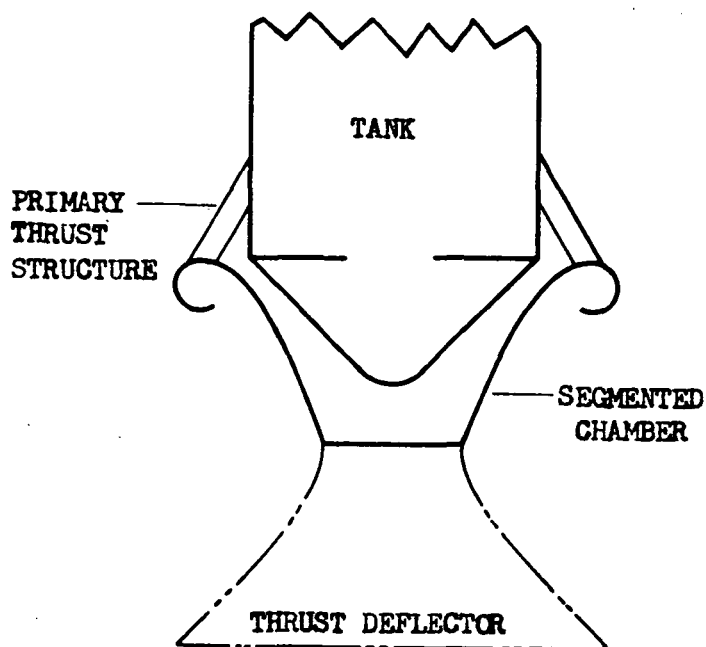
Stage I Propellant Performance

Figure III-A-2.

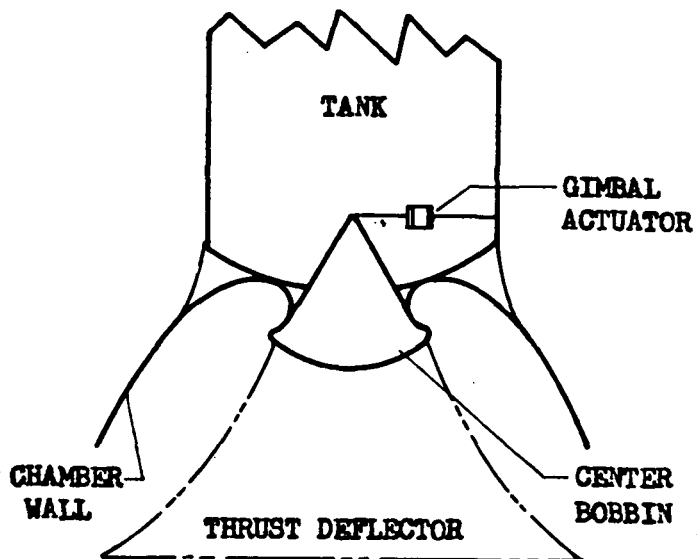
TYPE I - DELAVAL



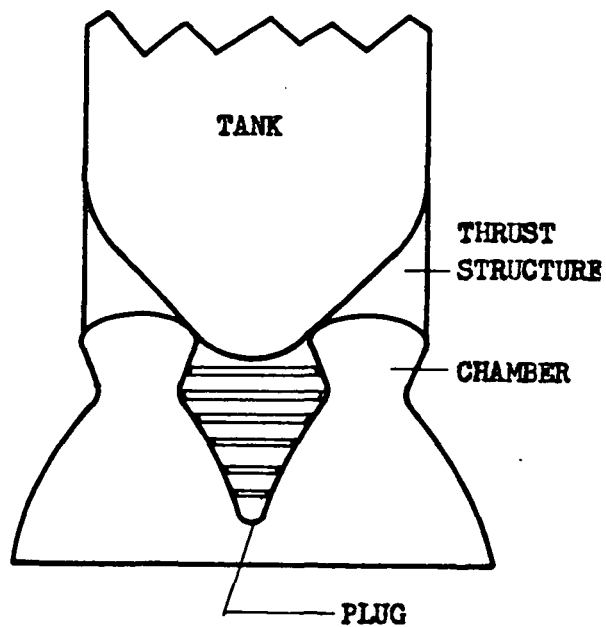
TYPE II - PLUG



**TYPE III
EXPANSION DEFLECTION (E-D)**

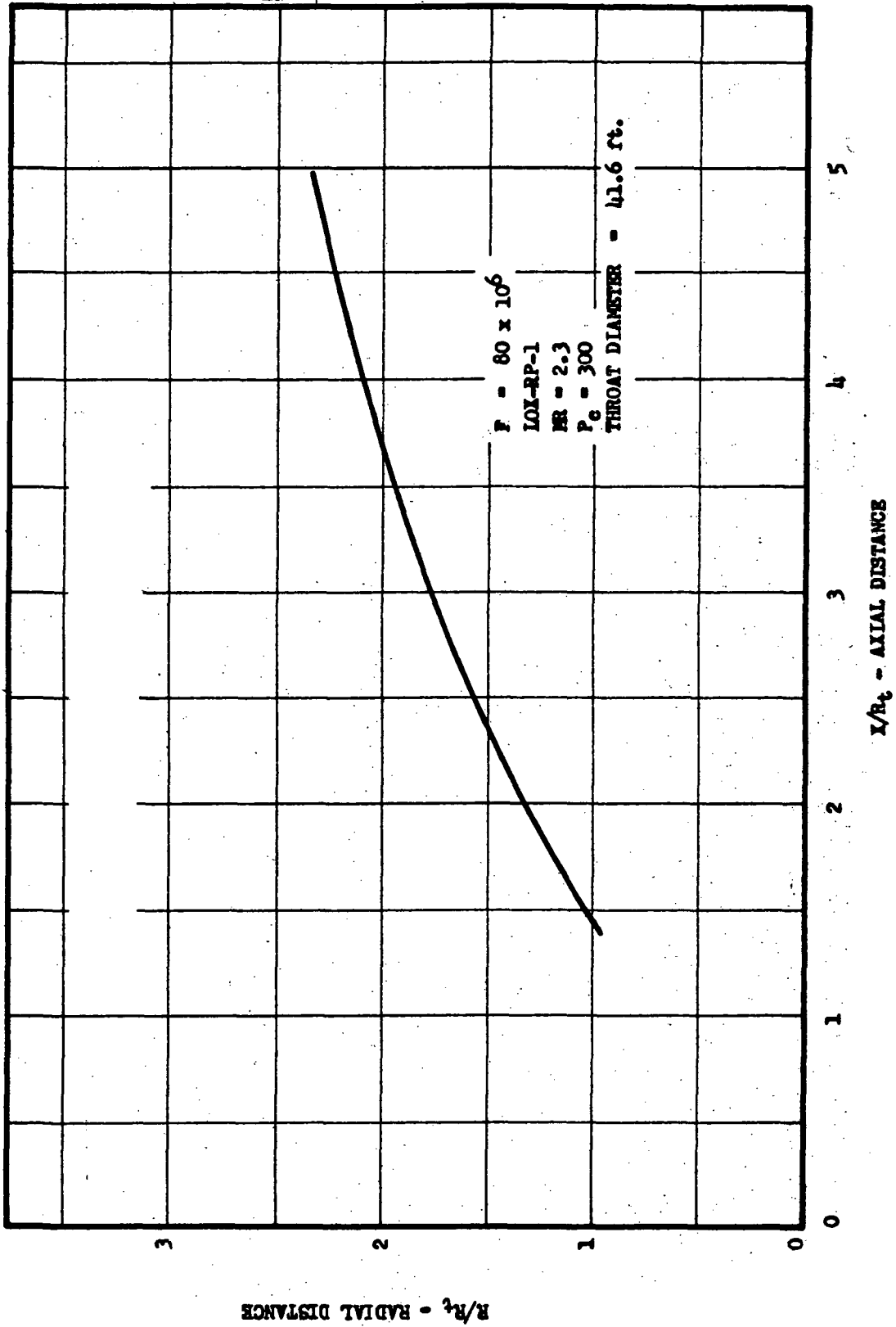


TYPE IV ANNULAR NOZZLE



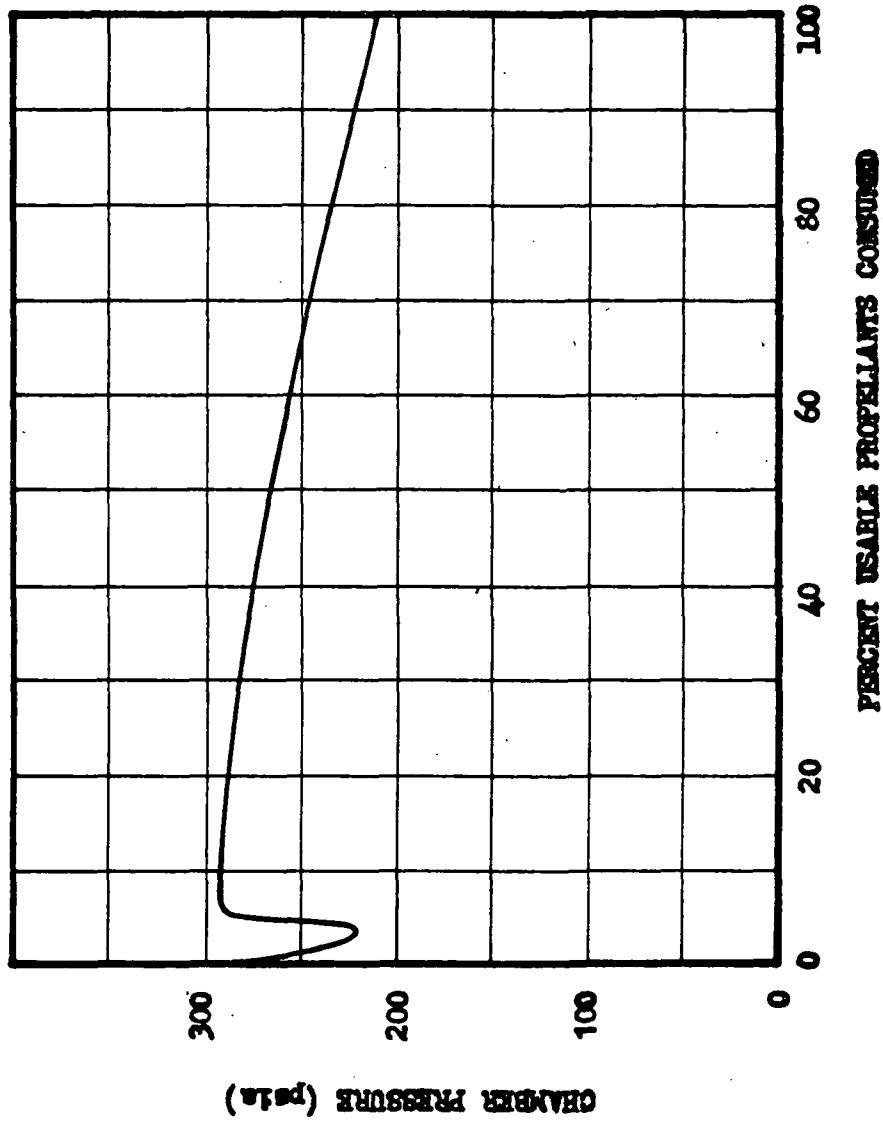
Stage I Nozzle Types

Figure III-A-3



Stage I Engine Contour

Figure III-A-4



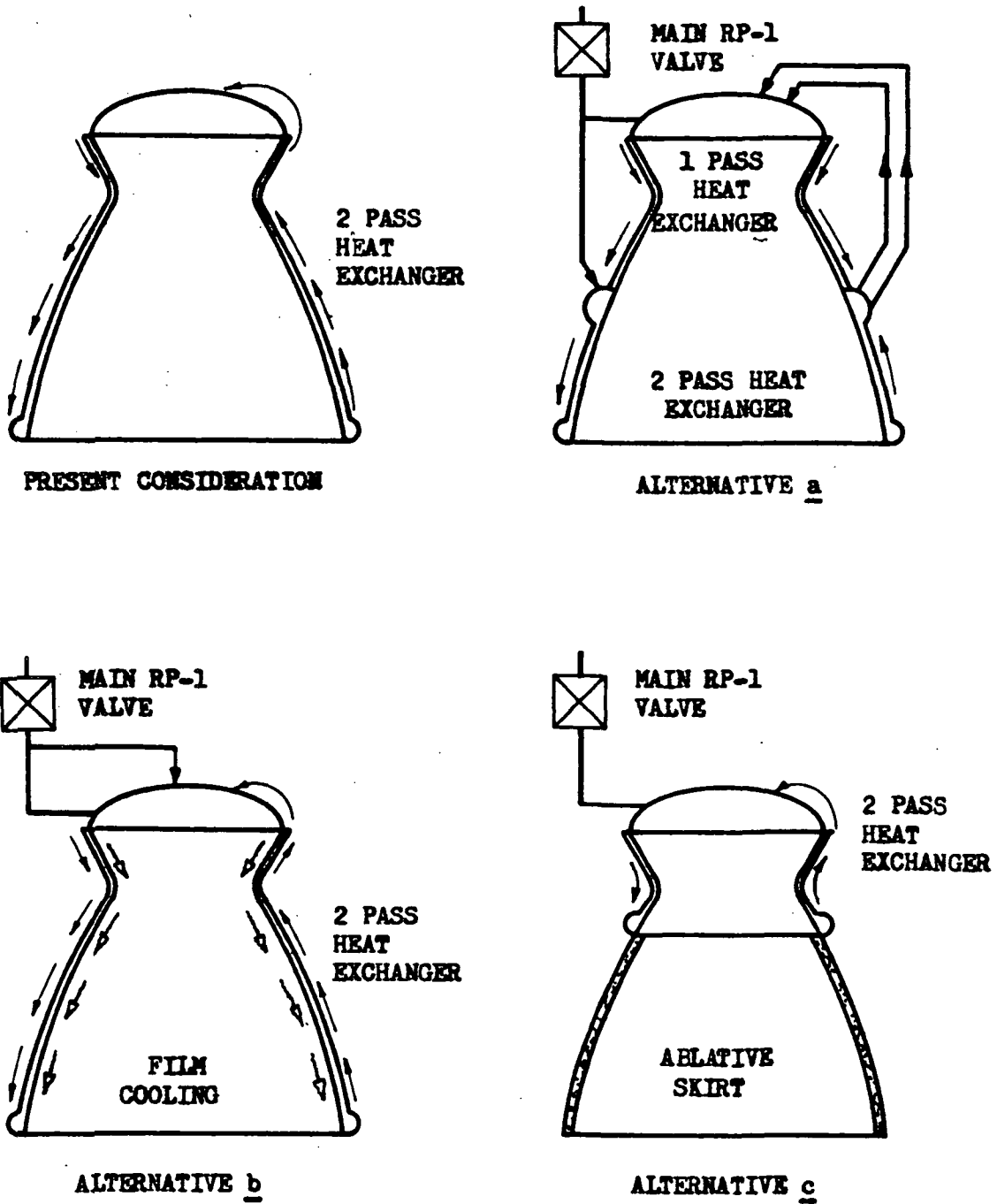
Chamber Pressure versus Propellant Consumption
(Stage I)

Figure III-A-5

Report No. LRP 297, Volume II

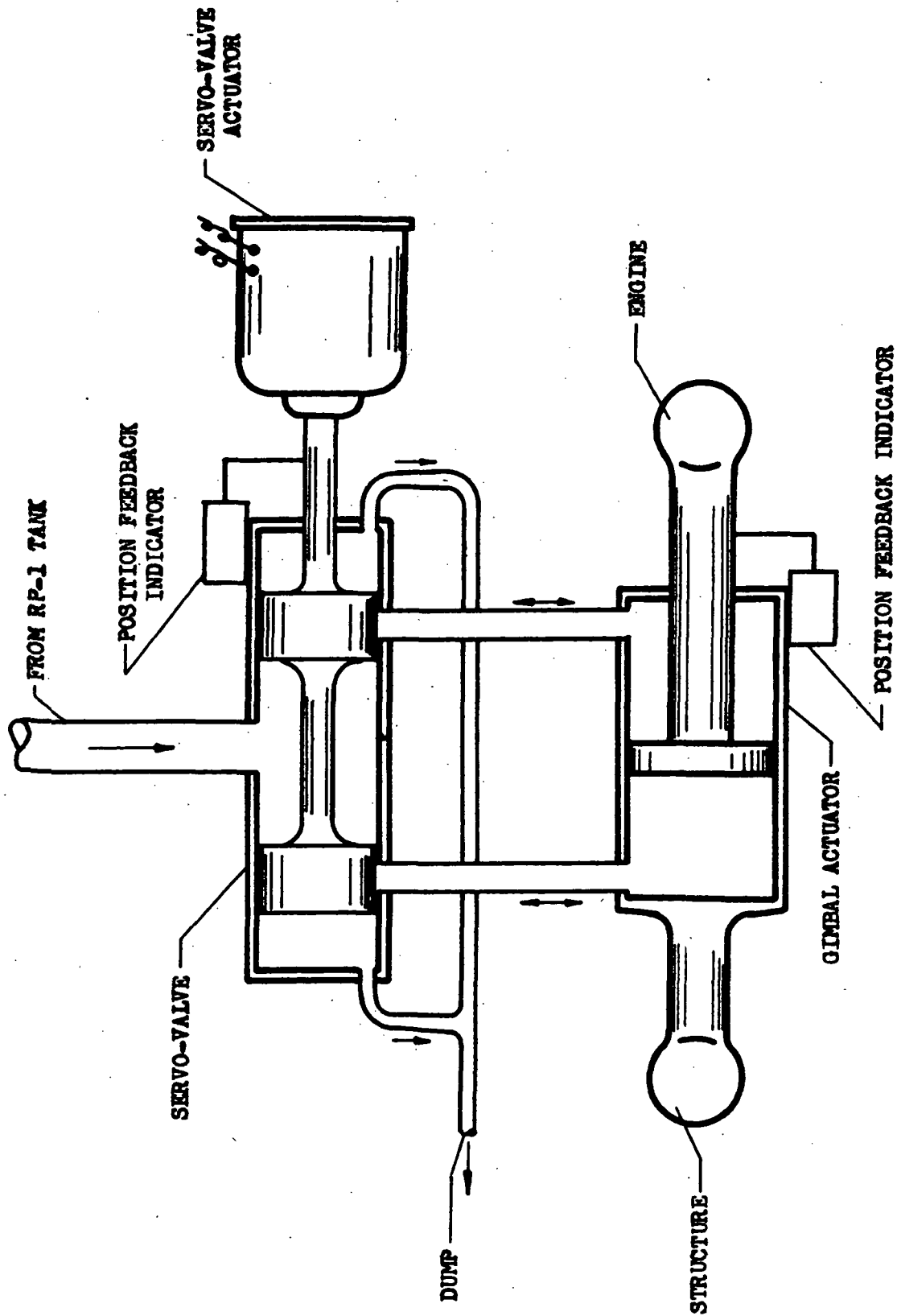
AEROJET-GENERAL CORPORATION





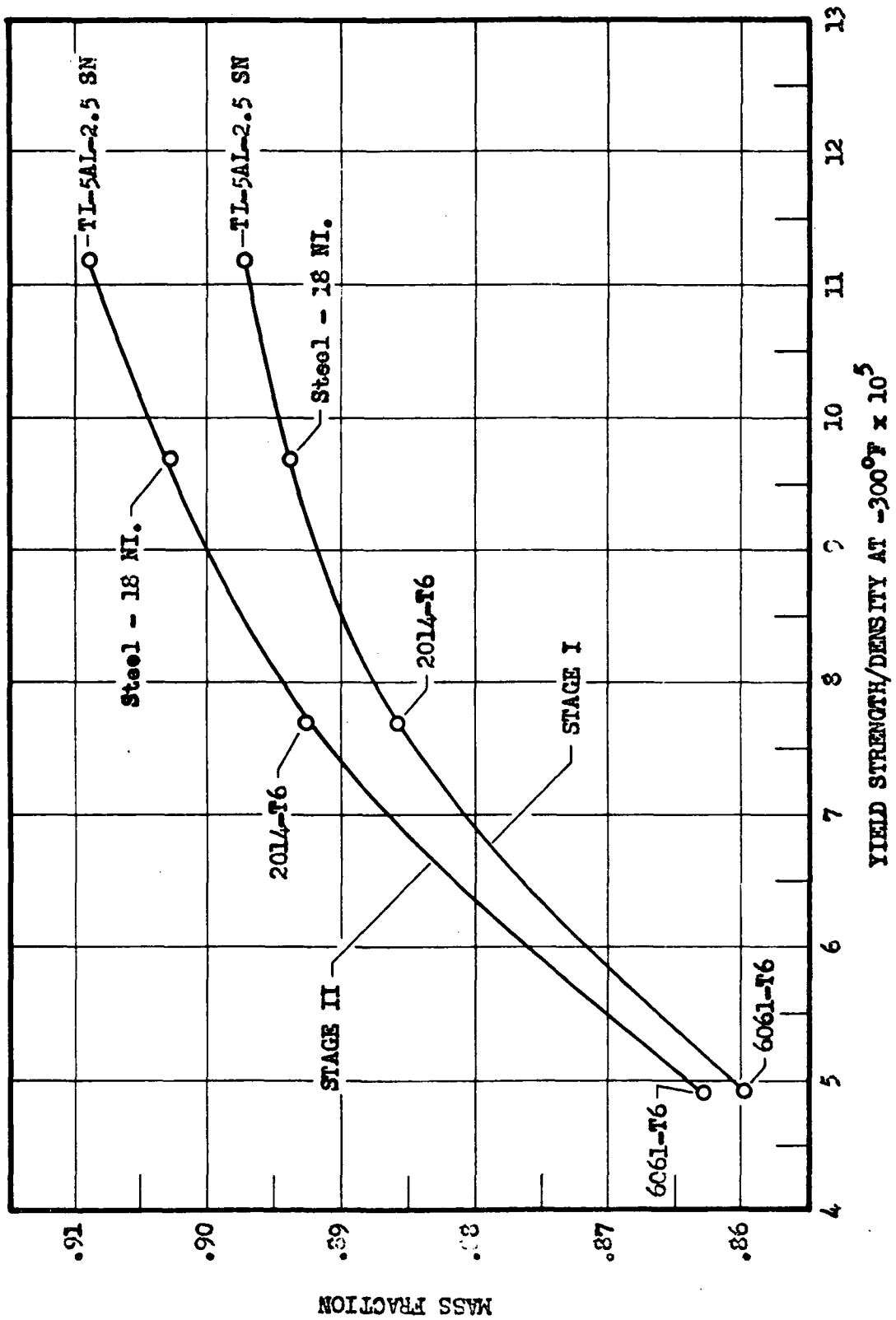
Alternate Thrust Chamber Coolant Designs

Figure III-A-7



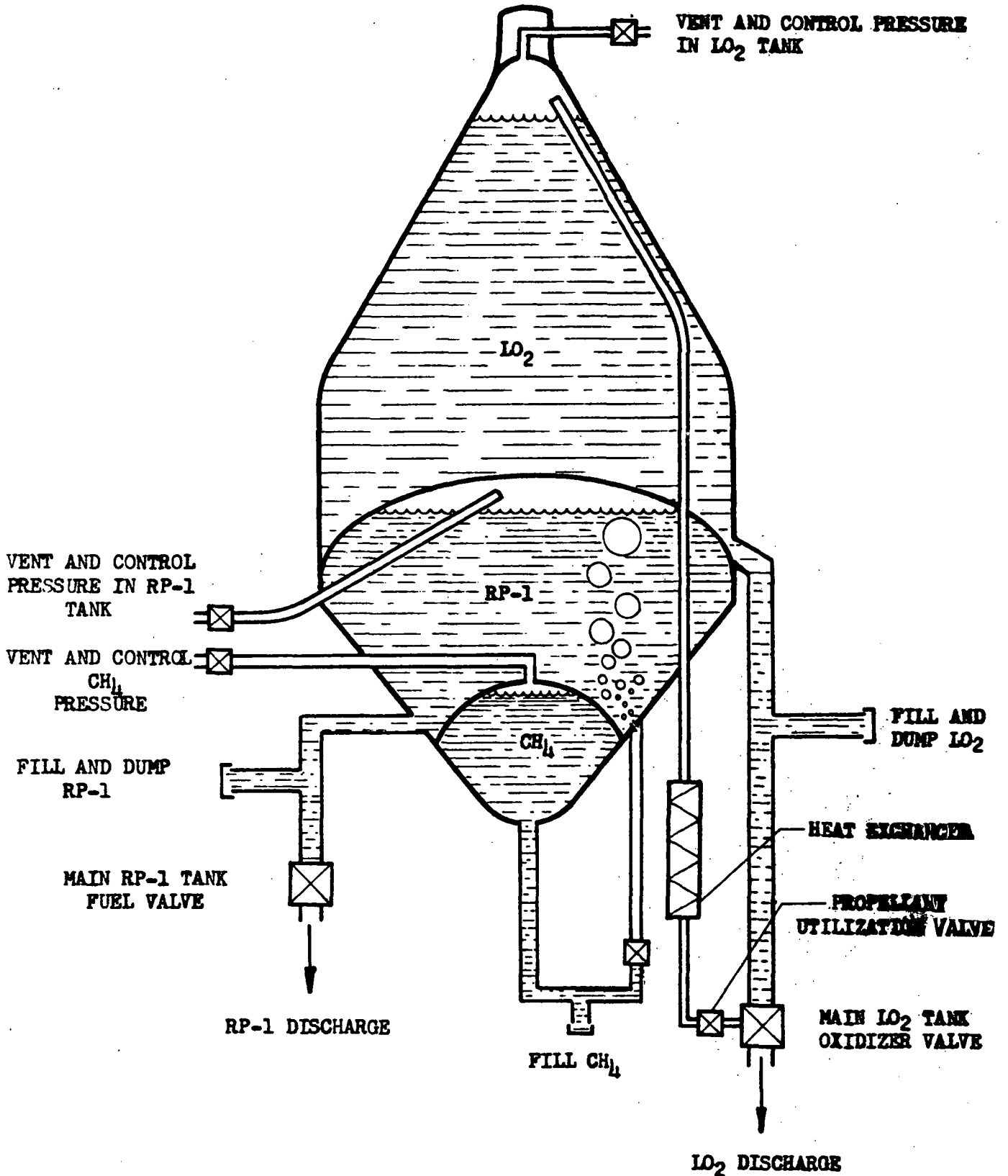
Gimbal Actuator Flow System

Figure III-A-8



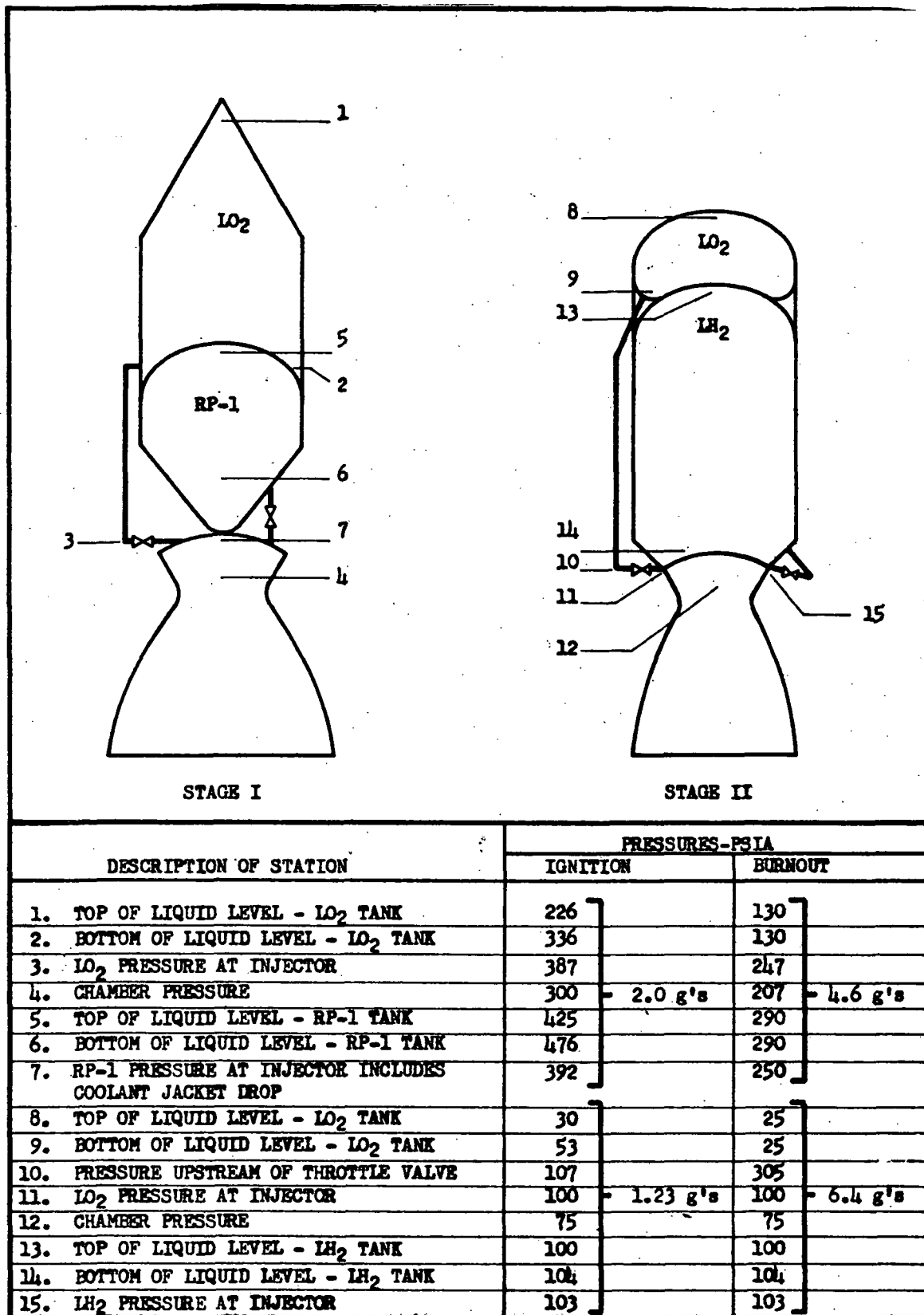
Mass Fraction versus Tank Material

Figure III-A-9



Stage I Pressurization System

Figure III-A-10



Profile of Pressure Drops

Figure III-A-11

Report No. LRP 297, Volume II

AEROJET-GENERAL CORPORATION



Report No. LRP 297, Volume II

AEROJET-GENERAL CORPORATION



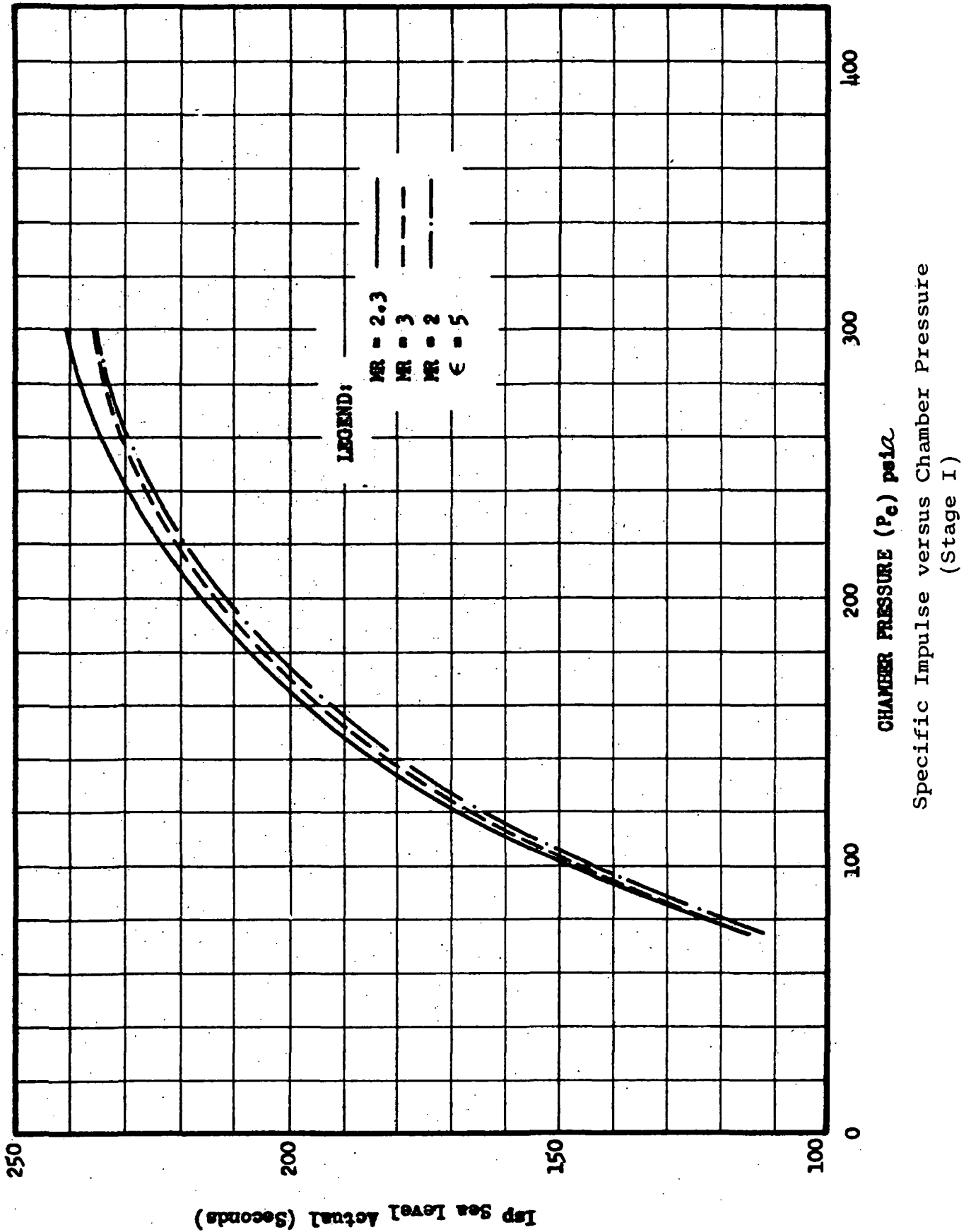


Figure III-A-14

III, Vehicle Subsystem (cont.)

B. STAGE II PROPULSION SYSTEM

1. Summary

The Stage II vehicle utilizes a bi-propellant pressure-fed rocket propulsion system. The general arrangement is shown in Figure III-B-1: Basic Stage II characteristics are given in the following table:

Stage Diameter	75 ft
Stage Length to Separation Joint	188 ft
Stage Weight, Total	10.6×10^6 lb
Usable Propellants	9.5×10^6 lb
Propulsion System Mass Fraction	0.8905
Propellants	LO ₂ /LH ₂
Mixture Ratio	5
Thrust Chamber Type	DeLaval, Fixed Expandable Nozzle
Throat Diameter	31 ft
Expansion Area Ratio	20
Thrust, Nominal	14×10^6 lb

III, B, Stage II Propulsion System (cont.)

Chamber Pressure, Nominal	75 psia
Thrust Vector Control	4 aux engines
Propellant Tank Pressures, Nominal	
LO ₂	30 psia
LH ₂	100 psia

Propellants are pressure fed from integral tankage. Injector inlet pressure is developed by a combination of ullage pressurization and acceleration head. The forward LO₂ tank is self-pressurized and loaded at temperature equilibrium with vapor pressure at 30 psia. The required injector inlet pressure of 100 psia results from the additive acceleration head. The aft located LH₂ tank is separated from the LO₂ tank by an insulated bulkhead. Pressurization of the LH₂ tank is autogenous; liquid hydrogen is admitted to a heat exchanger on the cooled section of the thrust chamber where it is vaporized. Vapor is ducted to the propellant tank ullage through a low pressure drop line.

III, B, Stage II Propulsion System (cont.)

Auxiliary thrust vector control engines use propellant from the main LH_2 tank; LO_2 is provided from separate spherical tanks that are pressurized from a regulated high pressure gas source.

Main stage and auxiliary engines are ignited by injection of blowdown gas pressurized TEA.

The main propellant valves are poppet types that are sealed in the closed position with clamped diaphragms. The valves are actuated by propellant-fed line pressure controlled with mechanical detents. The diaphragms are sheared by poppet motion.

Propellant tanks are designed by the propellant feed requirements and are stabilized by pressure for all handling and flight loads. Skirts are made of stiffened skin.

III, B, Stage II Propulsion System (cont.)

2. Propellants

a. Selection

A comparison and evaluation of several propellant combinations is given in Section III-A-2. A decision to use $\text{LO}_2/\text{RP-1}$ in the first stage resulted. On a similar basis, LO_2/LH_2 was selected as the propellant combination for Stage II. Previous studies at Aerojet-General on other sea-launched vehicles similar to Sea Dragon indicated that high performance coupled with reasonable cost and the ability to operate at low chamber pressures in upper-stage applications led to selection of LO_2/LH_2 . The performance of this propellant combination is given in Figures III-B-2, -3, -4, and -5.

b. Evaluation and Recommendations

Further optimization of propellant selection on a cost effectiveness basis was not incorporated in this study but is recommended for future effort.

III, B, Stage II Propulsion System (cont.)

3. Thrust Chamber Assembly

a. General

One rigidly mounted thrust chamber assembly is used in the second-stage propulsion system. The configuration is conventional (DeLaval nozzle, single combustion chamber, injector at forward end of combustion chamber, and one fuel and one oxidizer valve). The nozzle subsystem incorporates an expandable nozzle. The nozzle expansion section is a cooled, conventional rigid section with an expansion area ratio slightly greater than 6.0:1. Downstream of this point the nozzle is radiation-cooled, expandable, and is stowed in a contracted position on the Stage I tanks until second-stage firing.

The following table gives the important engine parameters:

Design and Performance Parameters

Design thrust, vac	= 14.12×10^6 lb
Chamber pressure, P_c	= 75 psia

III, B, Stage II Propulsion System (cont.)

Contraction area ratio	= 1.8:1
Characteristic length, L^*	= 235 in.
Converging cone half angle	= 30°
Throat diameter, D_t	= 30.6 ft
Expansion area ratio	= 20:1 (including expandable nozzle)
Exit section half angle	= 20°
Propellants	= LO_2/LH_2
Mixture ratio	= 5:1
Characteristic velocity, C^* , theor	= 7,640 ft/sec
C^* efficiency	= 0.97
Vacuum Thrust Coefficient, C_F	= 1.841 (theor.)
C_F efficiency	= 0.96
I_s , vac (sec)	= 440 (theor.)
I_s , actual	= 409 sec
Pitch and yaw thrusts provided by 4 auxiliary engines	= 0.435° equivalent main jet deflection

III, B, Stage II Propulsion System (cont.)

b. Design Basis

A single thrust chamber was chosen because (1) the second-stage feed system is pressure-fed for system simplicity, which is expected to result in ease of development and flight reliability, (2) to realize a high stage mass fraction, especially for the low bulk density propellants, the system pressure levels must be kept low, and (3) to realize a high specific impulse, an expansion area ratio of 20 or higher is necessary. The scale effect (chamber and tank diameter vary as square and cube root respectively) was already mentioned in the discussion of the first-stage chamber. The net effect of the above factors is that a conventional clustered arrangement of chambers cannot be installed within the envelope above the first stage. The expandable nozzle in combination with the single chamber provides the necessary expansion area ratio without the drag and weight penalty of a conventionally cooled expansion section.

The single chamber is mounted rigidly to the second-stage tankage and thrust chamber compartment skirt. The first-stage tanks rest within the second-stage thrust chamber, thereby minimizing interstage length.

III, B; Stage II Propulsion System (cont.)

c. Chamber and Injector

The combustion chamber is of conventional design. The 30° cone half angle and contraction area ratio of 1.8:1 allows more than enough combustion chamber volume. The conical chamber tends to inhibit longitudinal pressure fluctuations. The large chamber volume provides efficient combustion and flexibility in injector design. A possible injector configuration utilizes a shower head pattern which produces a combustion flow field over a relatively large portion of the chamber volume. Thus, the combustion reactions would not be as concentrated as for other injector types, and large perturbations that trigger combustion instability are less likely to occur. A discussion of combustion stability is included in Appendix II-2 for a Sea Dragon engine.

Flow turning in the subsonic region upstream of the throat is gradual; turning of a supersonic gas stream can be made at a sharper angle. The chamber contour upstream of the throat is $0.5R_t$ (throat radius); the downstream radius of curvature is $0.2R_t$. The gases are expanded around this downstream throat radius until a

III, B, Stage II Propulsion System (cont.)

half angle of 40° is reached at which point a contoured shape is attached. The expansion section contour is tangent to a half angle of 20° at an area ratio of 6.17:1. At this point the radiation cooled expandable metal nozzle section is attached. A 20° half angle was selected for the expandable nozzle. Appendix II-6 gives the results of the study performed to choose this expansion angle.

The second-stage engine is cooled (nonregeneratively) with hydrogen. Results of a computer heat transfer analysis indicate that hydrogen coolant flow rates of 260 lb/sec or 4% of the total hydrogen flow can cool the chamber to the $A = 6.17$ station. The maximum flux is 1.91 Btu/in.²sec; maximum wall temperature is 1,510°F, coolant bulk temperature increase is 1,520°F and total pressure drop is 93 psi. No loss in engine I_s need be considered because the coolant is exhausted supersonically from the end of each tube with high I_s because of the low molecular weight of the gas. A more detailed discussion of engine cooling is given in Appendix II-3.

III, B, Stage II Propulsion System (cont.)

A large volume, circumferential, low pressure drop heat exchanger is applied to the exterior of the hydrogen coolant passages of the thrust chamber near the aft end of the rigid portion of the nozzle. The heat exchanger provides structural reinforcement for the thrust chamber and a heat source for pressurization of the second-stage LH₂ tank during second-stage operation. A heat transfer analysis was made that proved the feasibility of the autogenous hydrogen pressurization system. The results of this investigation are given in Appendix II-5.

The expandable nozzle is radiation cooled. Basically, the nozzle section is a thin wall, conical section in which convolutions or corrugations are formed. The depth of corrugations increases from the attachment point at Station 328 to the trailing edge, Station 420. A large nozzle currently undergoing altitude firing tests is shown in Figure III-B-10. The expandable element is nested on foam material and retained by several external straps. These straps provide mechanical retention of the expandable nozzle for prelaunch handling and first-stage flight modes. During the staging sequence, the straps

III, B, Stage II Propulsion System (cont.)

counteract pressure forces from an expanding gas charge that expels the expended first stage from the breach formed by the expandable nozzle. When adequate relative velocities of first and second stage have been achieved, the straps are separated by shaped explosive devices, and the expandable nozzle is free to inflate at second-stage ignition. The straps and nesting materials provide mechanical protection of the expandable element, which varies in metal thickness from approximately 0.2 in. at its attachment point at Station 328 to approximately 0.02 in. at its trailing edge.

d. Flow Control and Lines

(1) Flow of LO_2

Once the second stage is clear of the first stage, the main LO_2 valve can be opened. This valve is a poppet valve that has a shear diaphragm for a positive storage seal. An LO_2 flow control throttle is installed downstream of the poppet valve. The throttling feature allows slaving of the LO_2 flow to the LH_2 flow to maintain mixture ratio and propellant utilization control. One insulated

III, B, Stage II Propulsion System (cont.)

LO₂ propellant line is installed on the outside of the fuel tank. The LO₂ valve is located close to the injector head to minimize shutdown volume downstream of the valve. The pressure forcing the LO₂ out of the tank is the sum of the ullage gas pressure in the tank and the acceleration head pressure of the LO₂. The gas pressure in the tank is the result of pressurizing the LO₂ with its own vapor pressure.

(2) Flow of Ignition Fluid

A pressure transducer in the head of the injector or timer senses the presence of the LO₂ in the chamber and initiates an injection of hypergolic ignition fluid, triethylaluminum (see Appendix II-7). The TEA (triethylaluminum) is stored in a tank and is pressure fed by N₂ gas stored in a high pressure tank nearby. The high pressure gas is simply allowed to blow down without use of a pressure regulator. This mechanical simplification is possible since the TEA can react with LO₂ over a wide mixture ratio range with very small ignition delays.

III, B, Stage II Propulsion System (cont.)

(3) Main LH₂ Flow

After the LO₂/TEA sequence, the LH₂ valve is opened. The flow leaves the LH₂ tank through a line running from the tank to the plane of the injector. The flow goes through a valve that is mounted in this line and then proceeds to the injector. The main LH₂ valve is of the poppet type, having a shear diaphragm for sealing purposes as does the LO₂ valve. The LH₂ main feed line standpipe (in the tank) allows a small amount of LH₂ to be trapped in the tank when the main engine burns out. This propellant is used by the thrust vector control engines for orbital injection of the second stage and payload. The LH₂, after flowing through the valve, goes into a split manifold where approximately 4% of the total hydrogen flow is used for non-regenerative cooling of the engine. The engine walls are small tubes having openings at the top. These holes are sized so that they act as orifices and meter the flow into the cooling jacket. The main part of the hydrogen flow goes into the tapered manifold around the top of the engine. The flow is fed into the injector head by radial tubes that run from the manifold to the umbilical tunnel in the center

III, B, Stage II Propulsion System (cont.)

of the injector. These radial tubes are tapered toward the center of the injector. Every other tube is used for the LO_2 and the remaining tubes are used for LH_2 . A schematic diagram of the flow in the injector head is given in Figure III-B-3.

The pressure forcing the LH_2 from the tank is the sum of the ullage gas pressure and the acceleration head of the fluid. The ullage pressure in the tank is the result of autogenous pressurization. Part of the flow that goes through the main LH_2 valve goes into a line that carries it to the heat exchanger located on the diverging section of the engine. The poppet valve stem actuates a valve that opens this line at the time the main LH_2 valve is opened. The flow entering this line goes to the heat exchanger on the diverging part of the nozzle where the hydrogen is superheated. A line located on the outside of the LH_2 tank carries this gas back to the forward end of the LH_2 tank. As long as the hydrogen valve is open a continuous flow of pressurization gas is available. This system is stable. The ullage pressure in the tank will tend to match the propellant feed line pressure minus the pressure drop in the heat exchanger and vapor feed lines.

III, B, Stage II Propulsion System (cont.)

(4) Coolant H₂ Flow

The expandable nozzle is radiation cooled during flight. The chamber coolant hydrogen gas flows longitudinally down the cooling tubes. At the point of attachment of the expandable nozzle ($\xi = 6.17$), the hydrogen gas is injected at supersonic velocity into the hot-gas stream close to the wall. The dumping of the relatively cool hydrogen gas into the boundary layer at the point of attachment will provide a small amount of thermal protection for the upstream portion of the expandable nozzle.

e. Ignition

The ignition is accomplished using triethylaluminum (TEA) that is hypergolic with LO₂. The ignition systems are discussed in detail in Appendix II-7.

III, B, Stage II Propulsion System (cont.)

f. Structural Loads

The second-stage thrust chamber assembly is rigidly mounted to the vehicle structure. The injector is integral with the LH₂ tank. The injector is a double wall semisandwich structure as necessary to withstand tank pressure. Radial ribs and stressed skin construction will be used to integrate the tank and injector walls. The trailing edge of the cooled portion is rigidly supported by the transition skirt that extends from the aft end of the pressurized tank and that counteracts loads from the expandable section of the nozzle. The heat exchanger located on the diverging section of the chamber gives added hoop strength to the nozzle. This structure will counteract the engine compartment pressure of 45 psia. This compartment is pressurized prior to ignition to counteract submersion loads and to provide staging by expelling the burned out Stage I booster from the second stage. A design chamber pressure of 1.25 x 75 psia (nominal) was used to allow for unpredictable pressure surges. The materials used for the various parts of the TCA are given in the following table:

III, B, Stage II Propulsion System (cont.)

<u>Component</u>	<u>Material</u>
Coolant tubes	347 stainless steel
Injector	Aluminum alloy
Hoop tension shell and bands on chamber	Steel
Heat exchanger	347 stainless steel
Manifolds for Fuel and LO ₂	Aluminum alloy
Expandable metal nozzle	310 stainless steel

A complete weight breakdown for the second-stage vehicle is given in "Weights and Performance," Section III, B, 9. The dry weight of the thrust chamber is 82,920 lb; the wet weight increment is negligible. The expandable nozzle section weighs 71,500 lb.

g. Evaluation and Recommendations

The cooled elements of the Stage II thrust chamber assembly are considered to be of conventional design, which in application to Sea Dragon does not introduce problems because of large

III, B, Stage II Propulsion System (cont.)

size. The chamber is conventionally shaped and advantages in combustion efficiency and stability may result from scaling. When requirements for contraction ratios (injector to throat area) and contraction angles are met, the resulting characteristic length is large. This factor is of importance because stable injector patterns, which produce performance loss in short chambers, can be used in Sea Dragon.

An interaction between the expandable nozzle and flow from the auxiliary thrust vector control engines may be important. The interaction involves all propulsive operational modes. This interaction will require additional study to define severity and establish design requirements for affected components. The influence of flow from the auxiliary engines on the expandable nozzle can be modified by changing the mounting location or exhaust angle of the auxiliary engines.

The effect of the sea on the second stage is in water handling and erection loadings and the ability of the tanks to sustain asymmetric loading. Corrosion of the components is

III, B, Stage II Propulsion System (cont.)

minimized by the sealed interstage compartment. Most of the exposed surface of the second stage will be covered with sealed layers of insulation for cryogenic storage.

4. Stage II Tankage

a. Summary

(1) Propellants for Stage II are pressure fed from two main tanks; accessory tankage is provided in the engine compartment at Station 295 for LO_2 that is expended in the auxiliary thrust vector control engines. High pressure nitrogen tanks for the pressurization of the accessory LO_2 tanks is provided in the Stage II forward compartment at Station 180. A weight breakdown is given in Table III-B-1. Tankage arrangement is shown on the stage layout drawing.

(2) As already discussed in Section III,A,5, Tankage, the material used in the study was 2014-T6 aluminum. All weights and wall thicknesses given in the following text refer to

III, B, Stage II Propulsion System (cont.)

this material.. This was considered a conservative approach for the study objectives. Appendix II-1, Materials, presents data summaries and recommendations where 18% maraging steel and titanium are recommended for the LO_2 and LH_2 tanks, respectively.

(3) Tank insulation is briefly described in the following text. For more detailed discussion on its design, installation, and characteristics, see Appendix II-4, Insulation.

b. Stage II Tankage

(1) LH_2 Tank

(a) Forward Closure-- LH_2 Tank

The forward closure of the second-stage hydrogen propellant tank is a 1.4 to 1 ellipse. It is insulated with 4 in. of polyurethane encapsulated on the LH_2 side of the bulkhead between the 0.72 in. thick metal membrane and 1/8 in. thick skin.

III, B, Stage II Propulsion System (cont.)

The bulkhead is reinforced to allow reaction of a crushing pressure differential of 50 psi and is designed to withstand full LH₂ tank pressure. The bulkhead is ported for vent line access.

(b) Cylindrical Section--LH₂ Tank

The cylindrical section is an unreinforced membrane 0.72 in. thick; it is externally insulated with 3 in. of urethane and is ported for fill, vent, and pressurizing line access.

(c) Aft Closure--LH₂ Tank

The aft closure is a 90° cone having a curved cone-cylinder transition section and is integral with the second-stage thrust chamber assembly. The closure is insulated with 3 in. of material and is 0.80 in. (nominal metal thickness). The aft LH₂ tank closure is ported for main propellant feed near the joint between the closure and the second-stage thrust chamber assembly. A structural joint is made at the intersection between the aft closure

III, B, Stage II Propulsion System (cont.)

and cylindrical section with the second-stage engine skirt. This second-stage aft skirt serves as the primary body, load carrying element through the second-stage engine compartment. This skirt counteracts the mounting loads of the spherical LO₂ tanks and second-stage auxiliary engines.

(2) LO₂ Main Tank

(a) Forward Closure--LO₂ Tank

The forward closure of the LO₂ main tank is a 1.4 ellipse. It is insulated with 1.5 in. of material on its forward external surface, and it is an unreinforced membrane, 0.72 in. thick. It is ported for fill and vent line access.

(b) Cylindrical Section--LO₂ Tank

The short cylindrical section is an unreinforced membrane 0.72 in. thick; it uses 1.25 in. of insulation.

III, B, Stage II Propulsion System (cont.)

(c) Aft Closure--LO₂ Tank

The aft closure of the second-stage LO₂ main tank is a hybrid bulkhead; a center portion is common to the LH₂ tank and an outer portion is separate. A compartment is formed between the two main tanks, which remains above the water when the vehicle is in the launch position. The compartment is used for umbilical access as well as for structural mounting of many components that may require access for checkout or servicing. For example, a gas pressurizing source for the second-stage auxiliary engines is located in this compartment.

The separated portion of the LO₂ aft closure is designed to withstand full LO₂ tank pressure and is a membrane 0.72 in. thick; insulation 1.25 in. thick is used. The closure is ported for main propellant feed line access.

The closure was designed to preclude generation of high pressures in the LO₂ tank resulting from

III, B, Stage II Propulsion System (cont.)

hydrodynamic heads, generated during firing, that must be counteracted by the LH_2 tank closure as a crushing pressure and that are not useful for propellant feed.

(d) Spherical LO_2 Tanks

The thrust vector control engines burn LO_2/LH_2 that is supplied from 4 spherical LO_2 tank. The 4 spherical LO_2 tanks have 1.5 in. of insulation and are mounted in the second-stage engine compartment on a spherical ring. This ring is, in turn, suspended by a tripod truss structure from the aft tank skirt ribs and the manifold region. The LO_2 tanks are pressurized with nitrogen gas that is stored in high pressure nitrogen tanks between the LO_2 and LH_2 tanks of the second stage. Data on the LO_2 tanks and pressurization system are as follows:

Thrust Vector Control--Oxygen Pressurization System

LO_2 Weight required for TVC operation: 583,000 lb

LO_2 TVC storage tanks: 4 required, 16.0-ft dia each

III, B, Stage II Propulsion System (cont.)

LO₂ Tankage weight (with supports and safety factor of 1.2):
8,000 lb (total of all 4 spheres made from aluminum alloy)

LO₂ Feed pressures: 100 psi

GN₂ Storage pressure: 3,000 psi

GN₂ Weight: 3,280 lb (with supports and safety factor of 2.0)

GN₂ Storage temp: 60°F

Diameter of GN₂ storage bottle: 10.7 ft

c. Skirts and Transition Sections

(1) Stage II Transition Structure (Aft Tank Skirt)

The Stage II transition section is the primary body, load carrying element through the axial length occupies by the fixed portion of the second-stage TCA. This cylindrical structure is a skin of 0.375 in. thickness reinforced with hat sections. Aluminum is used except at the extreme aft end where steel or titanium would be used because of the nozzle heating effects. The total equivalent thickness of aluminum required is 0.75 in. The

III, B, Stage II Propulsion System (cont.)

structure is ported for manned and line access from the stage umbilical connector to the forward second-stage inter-tank compartment.

(2) Forward Compartment Transition Structure

The Stage II forward compartment formed at Station 180 between the separated portions of the LH_2 tank forward closure is similar in design to the Stage II engine skirt. The 0.19 in. thick skin is stiffened with hat section stringers for a total equivalent thickness of 0.38 in. The forward compartment skirt structure is ported for line and man access.

(3) Forward Tank Skirt

A short skirt section is provided at the forward end of the cylinder section of the LO_2 tank. This will be only large enough to allow attachment of the vehicle payload.

III, B, Stage II Propulsion System (cont.)

d. Stage II Structural Loading

Pressure and body bending moments developed as a result of handling and flight environments are reacted by the pressurized propellant tank structure as for the first stage. The second-stage transition section and bulkhead section react flight body axial and bending loads as an unpressurized stiffened shell. During water handling operations, the compartments are pressurized to balance the external pressures encountered in the floating or submerged sea handling operation.

The mechanical or concentrated loads applied to the second stage are the following:

The first-stage thrust is reacted by the second stage at a structural (staging) separation joint located on the 75 ft cylindrical diameter at the aft end of the second-stage transition section at Station 328. The load path is along the cylinder; second-stage thrust chamber and expandable nozzle support loads are added at the same point.

III, B, Stage II Propulsion System (cont.)

The second-stage thrust chamber is supported by the aft closure of the LH₂ tank. Concentrated loads are not developed as the thrust chamber is primarily pressure supported. The cooled expansion portion of the nozzle (inside the 75 ft dia) and expandable section of the second-stage thrust chamber assembly are supported at attachments provided at the aft end of the second-stage structural transition section.

Auxiliary engines (TVC) are mounted on the second-stage transition section. All longitudinal components of force reactions are distributed in the skin; all radial components are taken by circular frames.

All structural load inputs to the payload are through the forward cylindrical skin. The payload is assumed to be designed to interface with a short cylindrical extension on the forward end of the second-stage LO₂ tank.

III, B, Stage II Propulsion System (cont.)

e. Evaluation and Recommendations

A general evaluation and description of alternate approaches applicable to Sea Dragon tankage is given in Section III, A. Items of specific applicability to Stage II are shown in the stage layout drawing. Special loading effects are discussed as follows:

(1) Hydrodynamic Effects

The arrangement of Stage II tankage is favorable from vehicle center of gravity and pressurant gas weight aspects. The arrangement produces, in the light, pressure-stabilized structure, some effects resulting from hydrodynamic loading that are not well understood. As an example, for a one-gravity transverse acceleration, the LO_2 pressure on the cylindrical tank wall will be 37 psi higher than on the opposite side. This pressure difference distributed around the surfaces of the pressure vessel may produce a general distortion of the structure. If the effect is dominant, bulkhead or closure failure may result. The analytical prediction of

III, B, Stage II Propulsion System (cont.)

this behavior is very complex and has not been attempted. Differential pressure loading on the pressure stabilized tank structure results from other environmental factors such as the variable depths of submergence at vehicle erection.

During Stage II operation for a vehicle acceleration of 5g, the LO₂ feed line pressure at the throttle valve is 3.5 times the required pressure. This results from the hydrodynamic head in the long feed line and must be throttled to required levels for injection.

Both hydrodynamic effects could be minimized by alteration of the tankage arrangement. Preliminary evaluation of a concentric tankage arrangement has been made, indicating that for a central LO₂ tank the enclosing surface area is the same as the insulated common bulkhead. Differential pressure resulting from transverse accelerations would be reduced by a factor of 2.9; excess feed line pressure would be reduced because the stand pipe height decreases as a function of burn time. Final ullage pressures would

III, B, Stage II Propulsion System (cont.)

be higher with resultant higher outage gas weights; the transverse structural support of the central tank at its forward end would probably cause an inert weight penalty as compared to the present design.

(2) SLOSH Baffles

No slosh baffling is shown for the Stage II tankage. It is expected that during Stage II operation the external perturbing influences will be small. Additional analysis will be required to confirm this conclusion.

5. Pressurization and Feed Systems

a. General Concept

The general pressurization concepts used on Stage I are also used on Stage II. These concepts include autogenous pressurization, vapor pressurization, and acceleration head effects.

III, B, Stage II Propulsion System (cont.)

b. LO_2 Tank Pressurization System

Pressurization of the Stage II LO_2 tank is accomplished by a combination of the acceleration head effect and the oxygen vapor pressure (see Figure III-B-4). The liquid oxygen is stored at a temperature of -283°F with a corresponding vapor pressure of 30 psia. The final oxygen vapor pressure is 25 psia.

The total pressure felt at the throttle valve varies from 107 psia at second-stage ignition (1.23g) to 305 psia at second-stage burnout (6.4g). The pressures are throttled down to the desired 100 psia injector inlet pressure. The ullage pressure of the gaseous oxygen at shutdown is 25 psi with a corresponding vapor density of 0.44 lb/ft^3 . The residual gaseous pressurant weight is 52,000 lb.

c. LH_2 Tank Pressurization System

The second-stage fuel tank is autogenously pressurized in a manner similar to the first-stage oxidizer tank. A complete flow schematic illustrating the second-stage pressurization

III, B, Stage II Propulsion System (cont.)

system is included as Figure III-B-4. Liquid hydrogen is taken from the bottom of the tank, sent through a heat exchanger where it is vaporized and superheated, and fed back to the top of the LH₂ tank to supply its ullage pressure. The driving force needed for this pressurization process is provided by the acceleration head of the LH₂. An analysis of the system is included in Appendix II-5.

The gaseous hydrogen pressure at shutdown is considered to be 100 lb/in.² at a temperature of 300°R. A very detailed analysis would be required to obtain the exact pressure at the time of shutdown. No serious difficulty is anticipated in regard to the final tank pressure. The weight of the pressurizing gas at Stage II burnout is 18,500 lb. The heat exchanger consists of large diameter tubes wrapped around the coolant tubes of the second-stage thrust chamber assembly. The nearly constant ullage pressure ensures a constant chamber pressure because the liquid acceleration head only contributes a maximum of 4 psi to the total pressure available.

III, B, Stage II Propulsion System (cont.)

Design criteria for the second-stage fuel

system include:

Initial gaseous hydrogen tank pressure	100 psi
Final gaseous hydrogen tank pressure	100 psi (approx)
Final gaseous hydrogen tank temperature	-160°F
Weight of gaseous hydrogen flowing through the heat exchanger (accounts for condensation)	22,200 lb

d. Ullage Pressure Characteristics

Initial tank ullages are 3% and zero for the second-stage fuel and oxidizer tanks respectively. The tank volume, and hence, the total tank weight of the second-stage oxidizer tank is reduced because of the condition of zero ullage. An initial condition of zero ullage in the LO₂ tank is possible because of the VāPak (vapor pressurization) system.

No initial decay in LO₂ ullage pressure is expected during liquid expulsion. As the liquid propellant is expelled, flashing occurs, creating an equilibrium condition between the liquid

III, B, Stage II Propulsion System (cont.)

and the gas. The gas then maintains the ullage pressure. Tests have been conducted on the vapor pressurization concept using many laboratory models with initial tank ullages varying from 0 to 30%. The tank pressure versus time curves are very similar in all cases thus establishing the fact that the initial pressure drop is independent of ullage. Figure III-A-11 illustrates the initial ullage conditions and the pressure drop profile for the second stage at ignition and burnout for that stage.

e. Ignition

Ignition will be accomplished through use of a triethylaluminum (TEA) reaction with LO_2 . See Appendix II-7 for further details.

f. Overall Operational Characteristics

Hydrogen propellant is ducted from short stand pipes near the bottom of the hydrogen tank to the main propellant valve. The stand pipes limit the thrust chamber propellant utilization to

III, B, Stage II Propulsion System (cont.)

the liquid level adjacent to the stand pipes. Liquid below the stand pipes permits continuous flow to the TVC engines.

With the main propellant valve in the open position, flow is admitted to a line leading to the heat exchanger located near the aft of the cooled portion of the second-stage thrust chamber assembly. Heated hydrogen from the exchanger is ducted to the ullage space by a large line that is routed external to the second-stage tankage. The coolant tubes are orificed at the top so that a small portion of the main hydrogen flow is admitted into the tubes. The bulk hydrogen flow goes directly into the injector.

The second-stage fuel thrust chamber valve is very similar to the first-stage thrust chamber valves that have been previously discussed. This valve is also a three position valve (normally closed, fully open, and closed). Two pins allow the valve to attain positions two and three. The pintle is in the bottom of the valve housing in position three.

III, B, Stage II Propulsion System (cont.)

The second stage LO_2 flow is ducted from the aft end of the oxygen tank to the main propellant valve through a line supported on the outside of the LH_2 tank. The main propellant valve is similar to the other propellant valves except for the throttling device that is located downstream of the main valve housing. The throttling device consists of a half hemisphere which is fully open prior to second-stage ignition. The half hemisphere gradually closes during second-stage operation in order to maintain a constant oxidizer injector manifold pressure compatible with LH_2 injector inlet pressure.

g. Evaluations and Recommendations

Liquid hydrogen, necessary to feed the TVC engines, is expelled from the fuel tank during first-stage operation. A loss of ullage pressure will result from expansion of the ullage gas or possibly from sloshing during Stage I burning since the Stage II pressurizing system is not operative at this time. Therefore, some method of maintaining or supplementing the ullage pressure is required.

III, B, Stage II Prooulsion System (cont.)

Several methods are available. One method would be to allow the LH₂ tank to decay in pressure. If bulk temperature of the LH₂ is controlled to -413°F at liftoff the pressure cannot be dropped below 56 psia, its equilibrium vapor pressure. Therefore, the LH₂ flow rate at ignition will be less than full flow; however, it will increase to full flow once the heat exchanger supplies the heated hydrogen to increase the ullage pressure to 100 psia.

Helium could be used as the initial pressurization fluid if condensation of the gaseous hydrogen becomes a problem. Therefore, a helium charge could be inserted into the tank prior to launch. A floating barrier between the gaseous hydrogen and the liquid hydrogen would minimize condensation.

Approximately one third of the total ullage volume is enclosed in the LH₂ heat exchanger and is not in contact with the LH₂ liquid surface. It is expected that this isolation will enable adequate control of ullage pressure prior to Stage II main engine operation. Additional study of this area is required to establish system adequacy.

III, B, Stage II Propulsion System (cont.)

6. Fill, Vent, and Dump System

a. Description

Both fuel and oxidizer systems contain a fill line, a horizontal vent line, and a vertical vent line. Dumping is achieved by reversing the flow in the fill line and in the vertical vent line. All external fill and vent line connection points are located around the periphery of the forward compartment of the second-stage tankage, Station 180. The second-stage layout drawing illustrates the line routing of all fill and vent lines from the forward compartment to various tanks. Appendix II-8 provides a more complete functional description of the second-stage fill and vent system. Included in this appendix is a flow schematic and the operational features of the system.

b. Evaluation

The components installed for management of pressurized compartments are felt to afford adequate flexibility for

III, B, Stage II Propulsion System (cont.)

operation of the Sea Dragon vehicle. In all functions it appears possible to provide adequate functional checkout of components and redundancy.

7. Auxiliary Thrust Chambers

a. Description

The TVC function for the second-stage vehicle is accomplished by use of four auxiliary LO_2/LH_2 engines located on the exterior of the vehicle, Station 299. These four engines are located 90 degrees apart on the exterior of the vehicle and can be actuated to rotate around an axis which is at 20° to a Station plane. The actuation stroke is 170 degrees. The propellant feed for the TVC engines is shown in schematic on Figure III-B-9-1; gimbal angle is half of this angle. The design performance data is given below:

TVC Design Performance Parameters

Design Thrust: 212,800 lb, 4 engines at 53,200 lb per engine

Thrust at Sea Level: 26,700 lb per engine

III, B, Stage II Propulsion System (cont.)

Chamber Pressure: 75 psia

Contraction Area Ratio: 1.80

Characteristic Length: 37 in.

Converging Half Angle: 30°

Throat Diameter: 1.91 ft

Expansion Area Ratio: 20:1

Exit Angle of Exhaust Gas: 13°

Propellants: LO_2/LH_2

Mixture Ratio: 4:1

Characteristic Velocity: 7,921 ft/sec (Theoretical)

C* Efficiency: 0.96

Thrust Coefficient (vac): 1.796

C_f Efficiency: 0.97

I_s vacuum: 442 sec (Theoretical)

I_s vacuum: 411 sec (Actual)

I_s S.L.: 206 sec (Actual)

III, B, Stage II Propulsion System (cont.)

The proposed auxiliary chambers can meet all vehicle control force requirements except pitch and yaw of the first stage. They provide:

- (1) Roll control for first stage
- (2) Propellant settling acceleration during staging
- (3) Pitch, yaw, and roll for second stage
- (4) Pitch, yaw and roll coast period
- (5) Orbital injection of Stage II and spacecraft
- (6) Other Possibilities:
 - (a) Retrothrust
 - (b) Rendezvous maneuvers

The chambers are of conventional De Laval design either ablatively cooled or nonregeneratively cooled with hydrogen. Ignition of the small engines occurs underwater at a depth of about 70 ft. The ignition sequence consists of the following: LO_2 flow is admitted to the chamber and the ignition fluid (TEA) is fed directly

III, B, Stage II Propulsion System (cont.)

into the chamber a fraction of a second after the LO_2 , and combustion is initiated. LH_2 flow is admitted when chamber conditions are satisfactory. A more detailed discussion of the ignition system is given in Appendix II-7.

b. Actuation System, TVC Engines

Vectoring of the engines is accomplished by use of electrical actuators. The actuators can rotate the engines to various angles so that in combination the four engines provide pitch, yaw, and roll control throughout the vehicle flight operations.

c. Evaluation and Recommendations

It appears that the overall vehicle simplicity and reliability is enhanced by the auxiliary system because rigid mounting of the Stage II main chamber is made possible. Propellant used during first-stage burning penalizes second-stage mass fraction. Also, the injection of the expended second stage into orbit requires greater energy than for the spacecraft and payload alone. These penalties are relatively minor and are offset by the operational simplicity obtainable.

III, B, Stage II Propulsion System (cont.)

There are certain flow interaction problems which arise when an external gas source is mounted on the exterior of the vehicle. When the gas stream is directed away from the axis of the vehicle, the skin heating due to hot-gas impingement is minimized, but the axial thrust is decreased. One inherent disadvantage of having the TVC engines mounted on the exterior of the vehicle upstream of the expandable nozzle is that the structure to support the engines and the gas stream, directed into the external flow field, produces shocks which alter the flow field around the expandable nozzle. This has the effect of causing the expandable nozzle to distort, depending on the strength of the shock. These are possible problems which have not been investigated. Future work on this vehicle should determine the importance of these interactions. It may be possible to move the engines forward on the vehicle and alleviate the situation. Heating on the missile skin may be controlled by addition of a small patch of ablative insulation. It is felt that additional analysis of these areas is required to fully define the system.

III, B, Stage II Propulsion System (cont.)

8. Performance of Second-Stage Propulsion System

a. Summary of Characteristics

The second-stage propulsion system consists of the main engine and the 4 auxiliary thrust chambers. The design performance of these engines can be found in Sections III, B, 3 and III, B, 7. Heat transfer studies of the second-stage engine indicate that the coolant flow rate required to cool the engine (260 lb/sec of hydrogen) results in conditions at the end of the tubes as follows: pressure of 20.78 psia, temperature of 1,092°F, and velocity of 1,525 ft/sec. The conditions in the main exhaust stream are as follows: velocity of 11,773 ft/sec, pressure of 2.01 psia, and temperature of 3,460°R. The conditions of the coolant gas flow in the tubes is different in addition to a molecular weight difference. If the tips of the tubes are pinched to form a converging diverging nozzle, then the expansion of the coolant gases will produce a velocity of 11,663 ft/sec. It is concluded that the theoretical I_s will not be penalized by non-regenerative cooling when the coolant is dumped into the main gas stream. The resulting propulsion

III, B, Stage II Propulsion System (cont.)

system mass fraction is 0.8905. The specific impulse of the main gas stream is given in Figure III-B-9. The performance of the TVC engines with altitude are given in Figure III-B-6, -7, and -8. The I_s of the TVC engines is virtually constant after first-stage burnout. The I_s and thrust are given as they vary with altitude for different mixture ratios.

b. Evaluation and Recommendations

The performance assumed in the study is conservative. Another 1% in specific impulse might easily be claimed.

9. Weights, Stage II

a. Summary

The weights of Stage II are given in tabular form in Table III-B-1.

III, B, Stage II Propulsion System (cont.)

The weights of all components have been calculated based on the configurations defined. Component definition has been based on estimates, where necessary, as is discussed other sections.

b. Evaluation and Recommendations

The total stage weight is felt to be conservative in terms of stage performance. Higher strength to density ratio materials such as 18% maraging steel for the LO_2 tank and titanium for LH_2 tank will improve mass fraction. Such a material combination would increase the stage mass fraction to 0.90 from its present value of 0.89:

The common bulkheads and intertank structure should be reviewed for possible weight saving. A substantial portion of the Stage II weight exists in the transition skirt on the aft end of the LH_2 tank. It is possible that incorporation of pressurized tanks in this area, serving the double purpose of taking first-stage thrust and storing propellant, would save weight. The low density for the LH_2 used for design should be reviewed operationally to determine if a higher value could be used.

(End III, B)

TABLE III-B-1

STAGE II PROPULSION SYSTEM WEIGHT BREAKDOWN

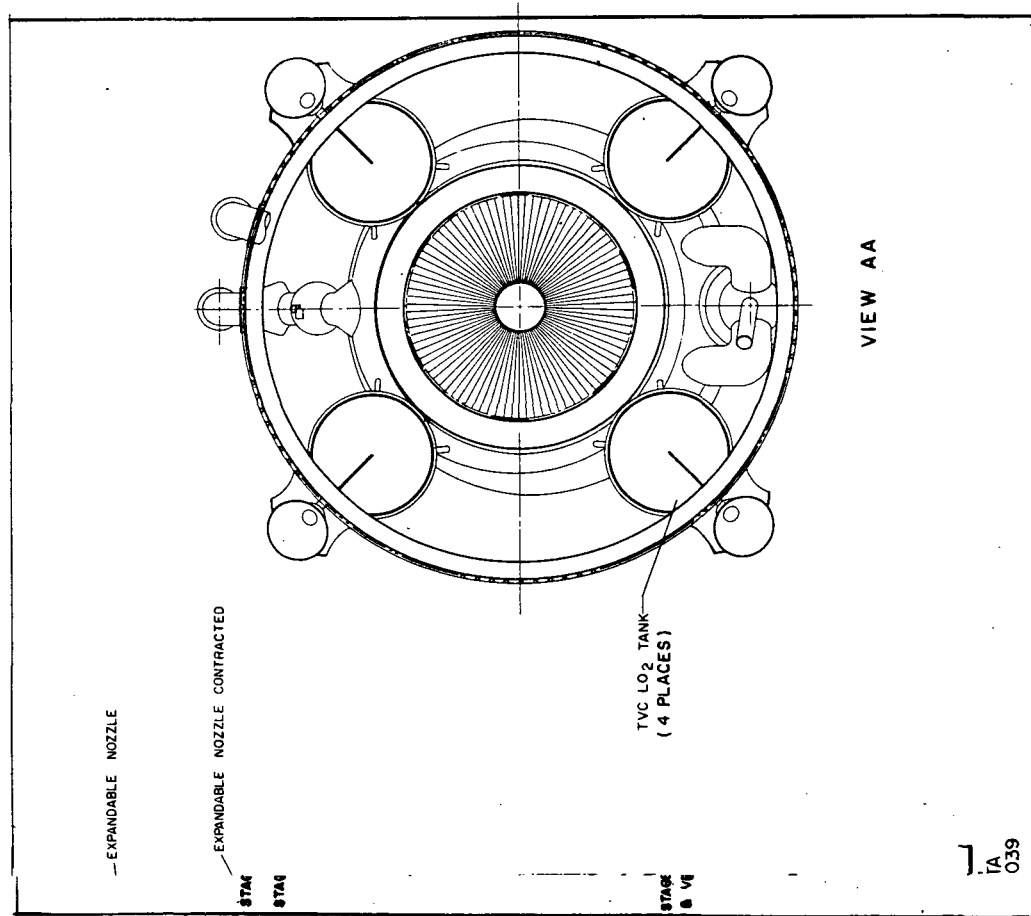
<u>Components</u>	<u>Weight (lb)</u>	<u>Subtotal (lb)</u>	<u>Subtotal (lb)</u>
Propellants			
Oxidizer, LO ₂	8,005,045		
Fuel, LH ₂	<u>1,601,009</u>		9,606,054
Thrust Chamber Assembly			
Injector Assembly (includes Ignition system)	10,000		
Chamber	51,400		
Expandable Nozzle	<u>71,500</u>		132,900
Thrust Vector Control System			5,300
Tankage			
LO ₂ Tank			
Forward closure	77,471		
Cylindrical Section	8,875		
Aft Closure Spherical Torus	36,964		
Tank Insulation	<u>6,000</u>		129,310
LH ₂ Tank			
Forward closure	77,471		
Cylindrical Section	181,323		
Aft Frustrum Closure	49,497		
Aft Spherical Segment	10,105		
Bulkhead Insulation	9,479		
Encapsulation Skin	13,428		
Vortex Structure	2,700		
Tank Insulation	<u>36,000</u>		380,003
			509,313

TABLE III-B-1 (cont.)

<u>Components</u>	<u>Weight (lb)</u>	<u>Subtotal (lb)</u>	<u>Subtotal (lb)</u>
Feed System			
Oxidizer			
LO ₂ Valve	3,640		
Line from Tank to Chamber	<u>4,700</u>		
		8,340	
Fuel			
LH ₂ Valve	4,480		
Line from Tank to Chamber	<u>1,360</u>		
		5,840	
			14,180
Pressurization System			
Oxidizer Pressurant		52,000	
Fuel			
Pressurant	18,500		
Heat Exchange	13,400		
Pressurizing Equipment	<u>1,820</u>		
		33,720	
Thrust Vector Control System			
Bottle Weight (4 req'd)	8,340		
N ₂ Weight	2,000		
N ₂ Bottle Weight	3,300		
Valves and Support Structure	<u>910</u>		
		14,550	
			100,270

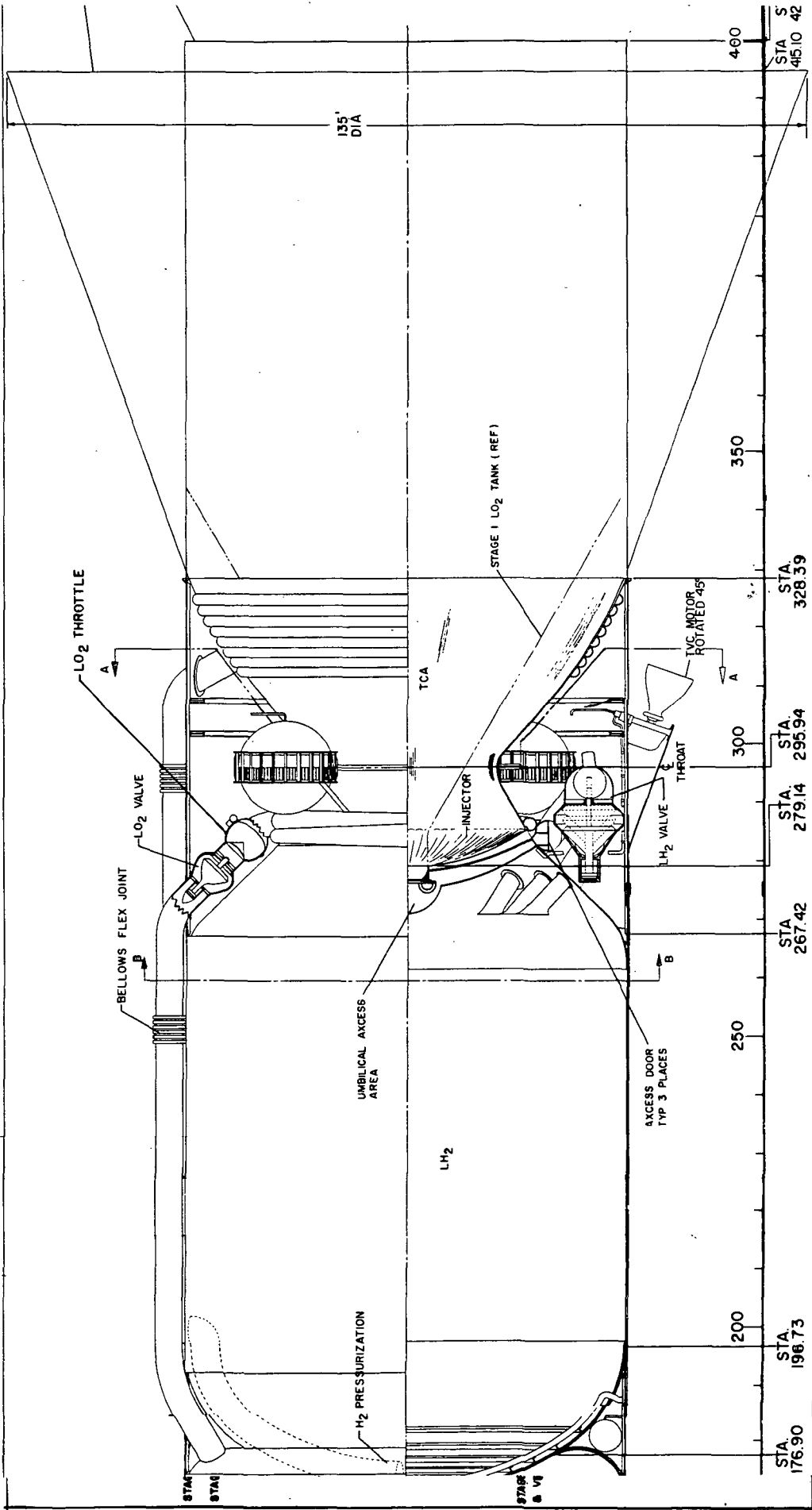
TABLE III-B-1 (cont.)

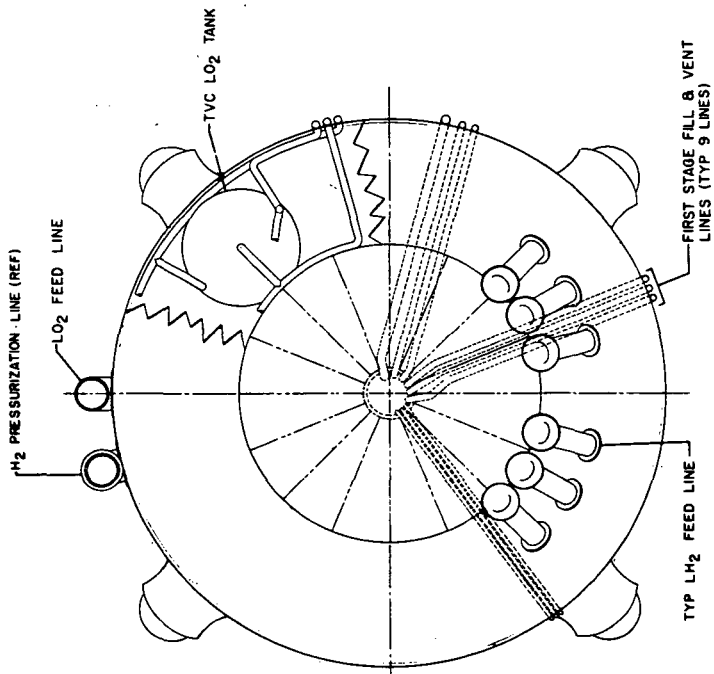
<u>Components</u>	<u>Weight (lb)</u>	<u>Subtotal (lb)</u>	<u>Subtotal (lb)</u>
Fill and Vent System			1,525
Miscellaneous			
Aft Tank Skirt	211,984		
Skirt Between LO ₂ LH ₂ Tanks	27,137		
Misc. Weight (5% of Tankage)	<u>23,230</u>		
			262,351
TOTAL WEIGHT OF PROPULSION SYSTEM			10,631,893



Stage II Propulsion System Layout Drawing

Figure III-B-1



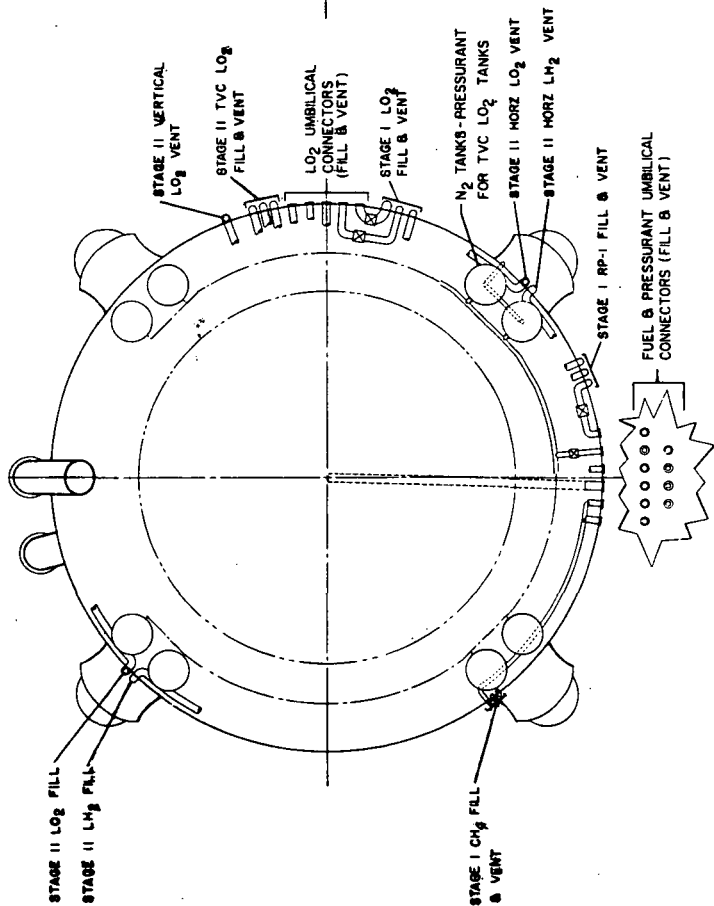


VIEW BB

150

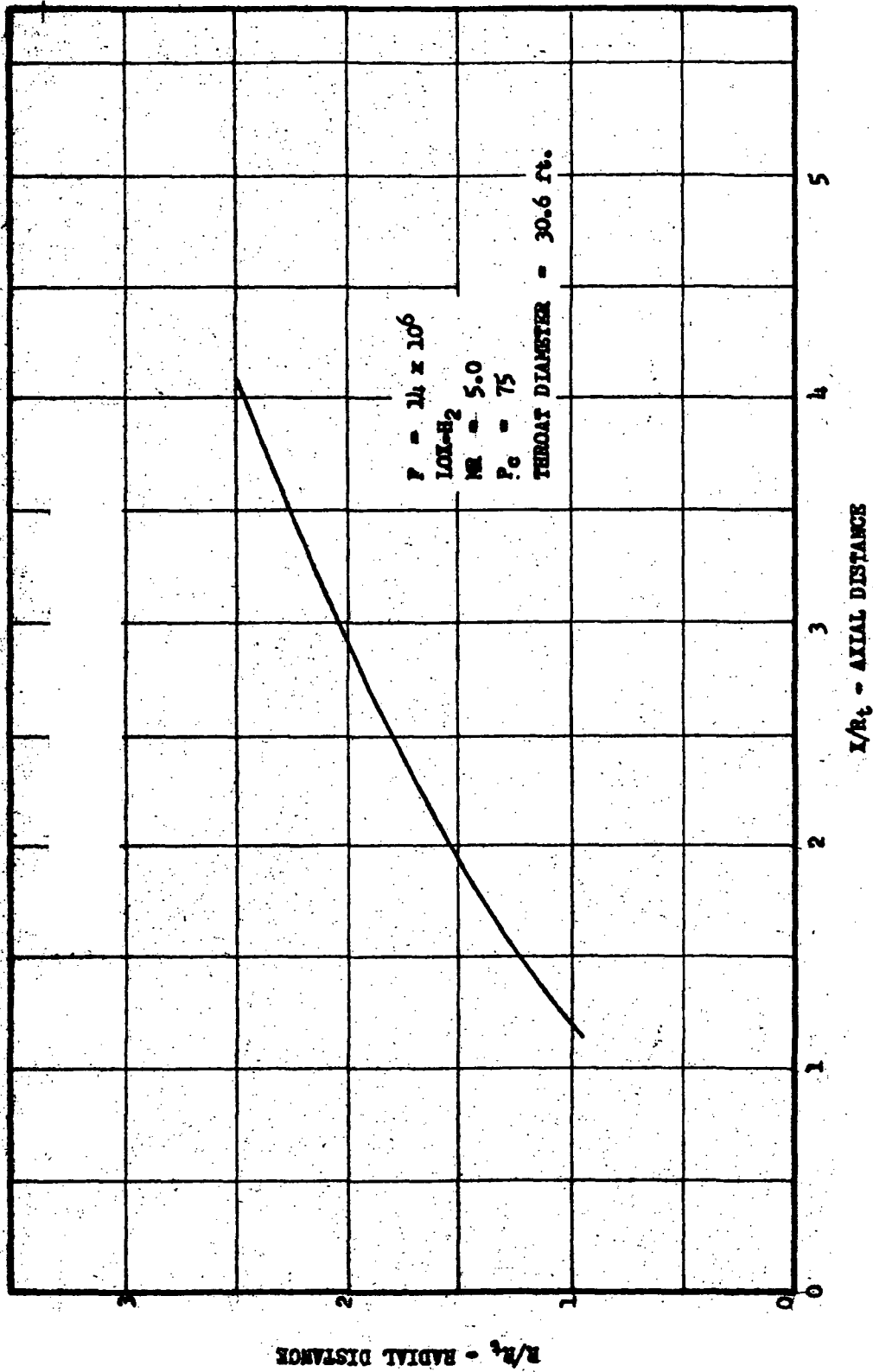
100

STA. 140.0 STA. 166.61 STA. 170.55



VIEW CC

AFT CLOSURE OF LO_2 TANK REMOVED FOR CLARITY



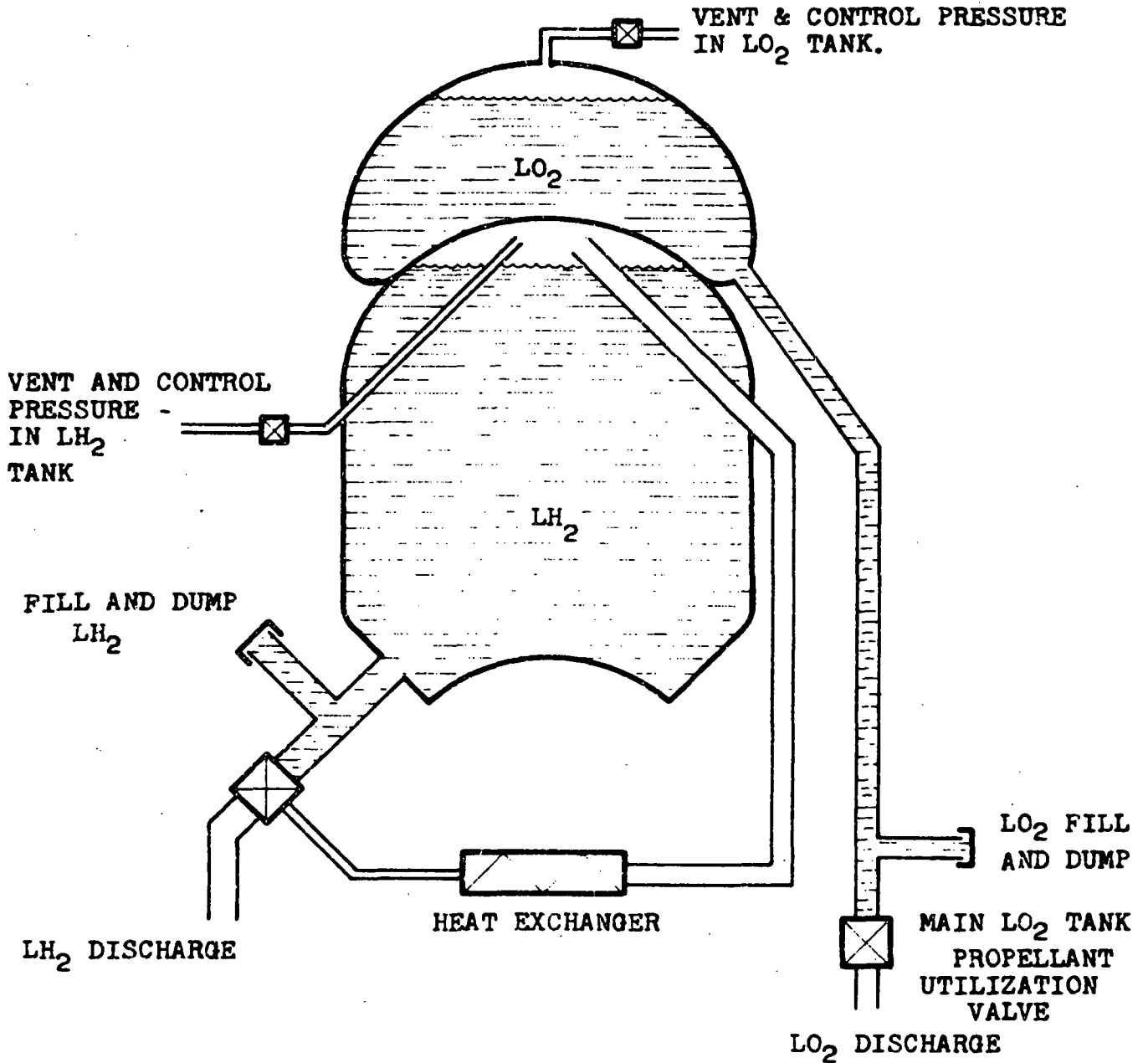
Stage II Engine Contour

Figure III-B-2

Report No. LRP 297, Volume II

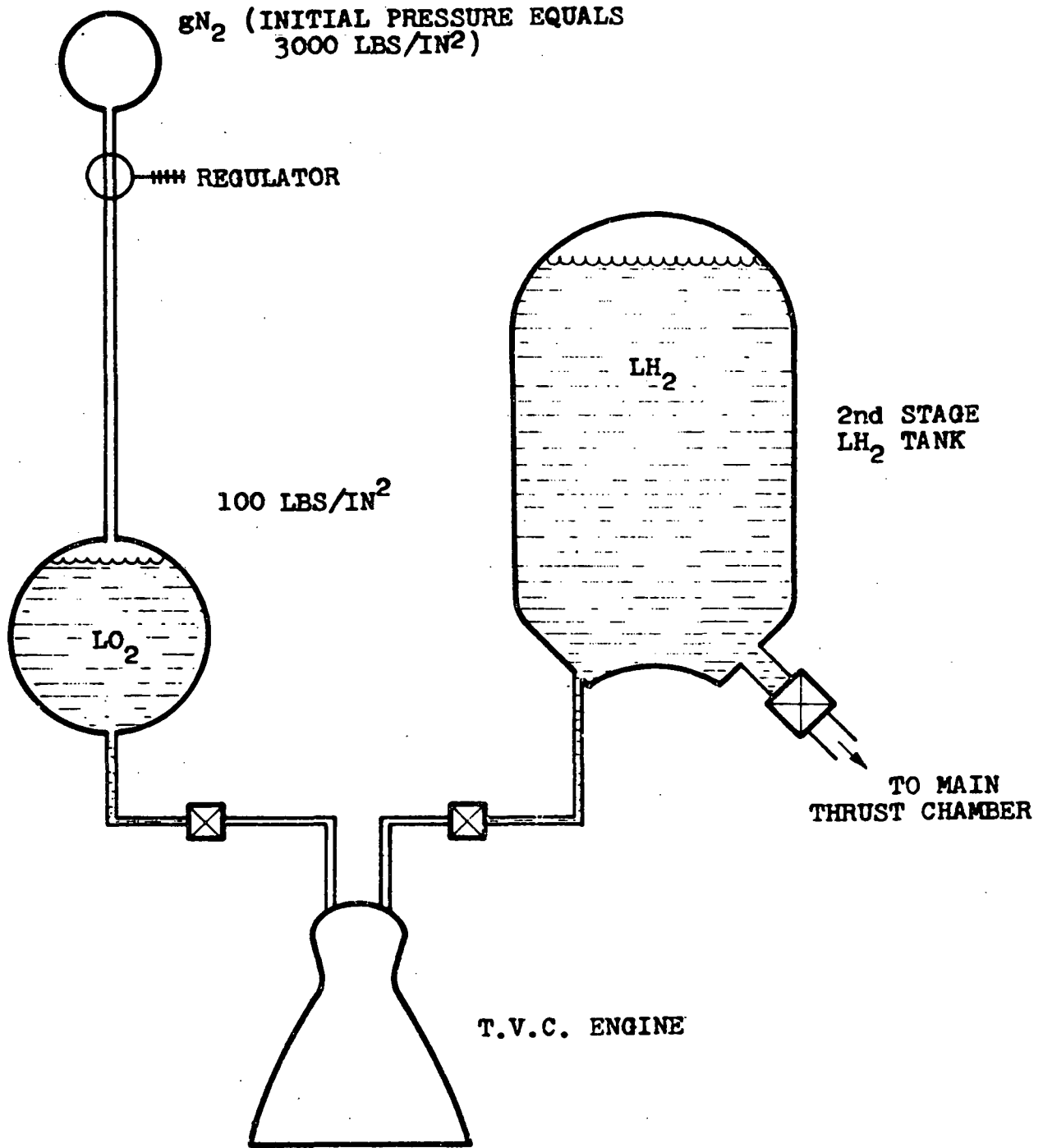
AEROJET-GENERAL CORPORATION





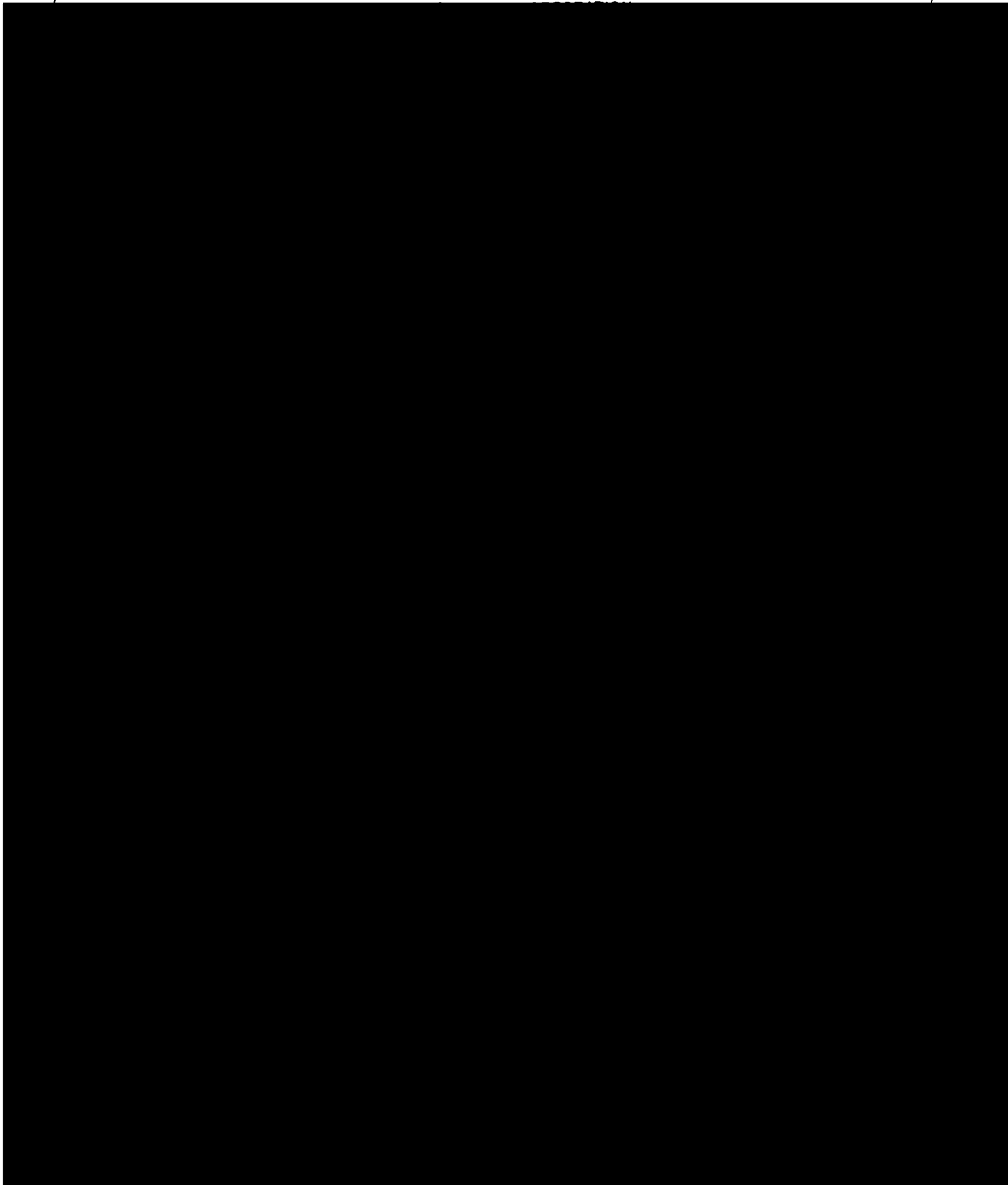
Stage II Pressurization System

Figure III-B-4



TVC Engine Pressurization System

Figure III-B-5



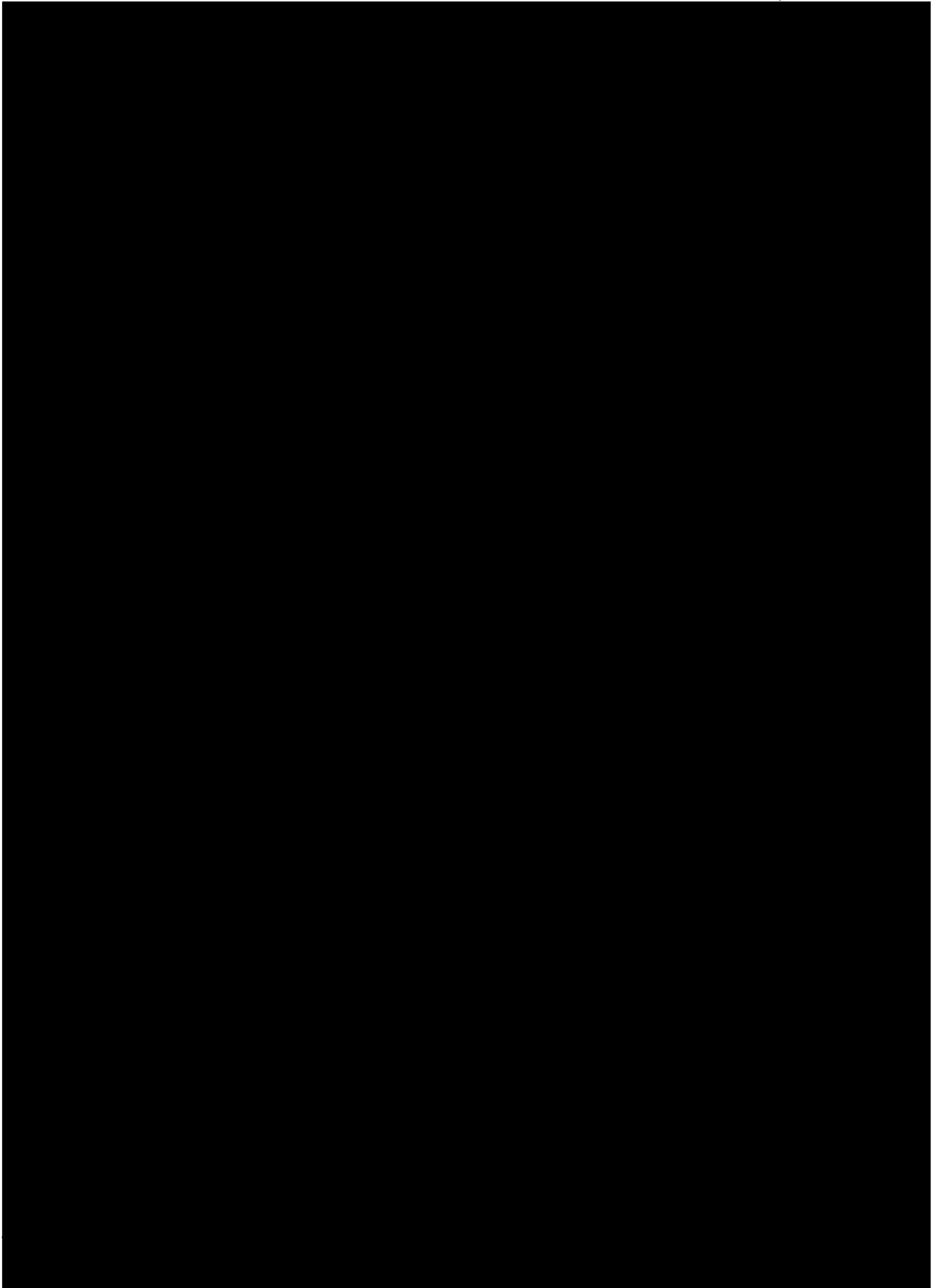
Report No. LRP 297, Volume II

AEROJET-GENERAL CORPORATION



Report No. LRP 297, Volume II

AEROJET-GENERAL CORPORATION



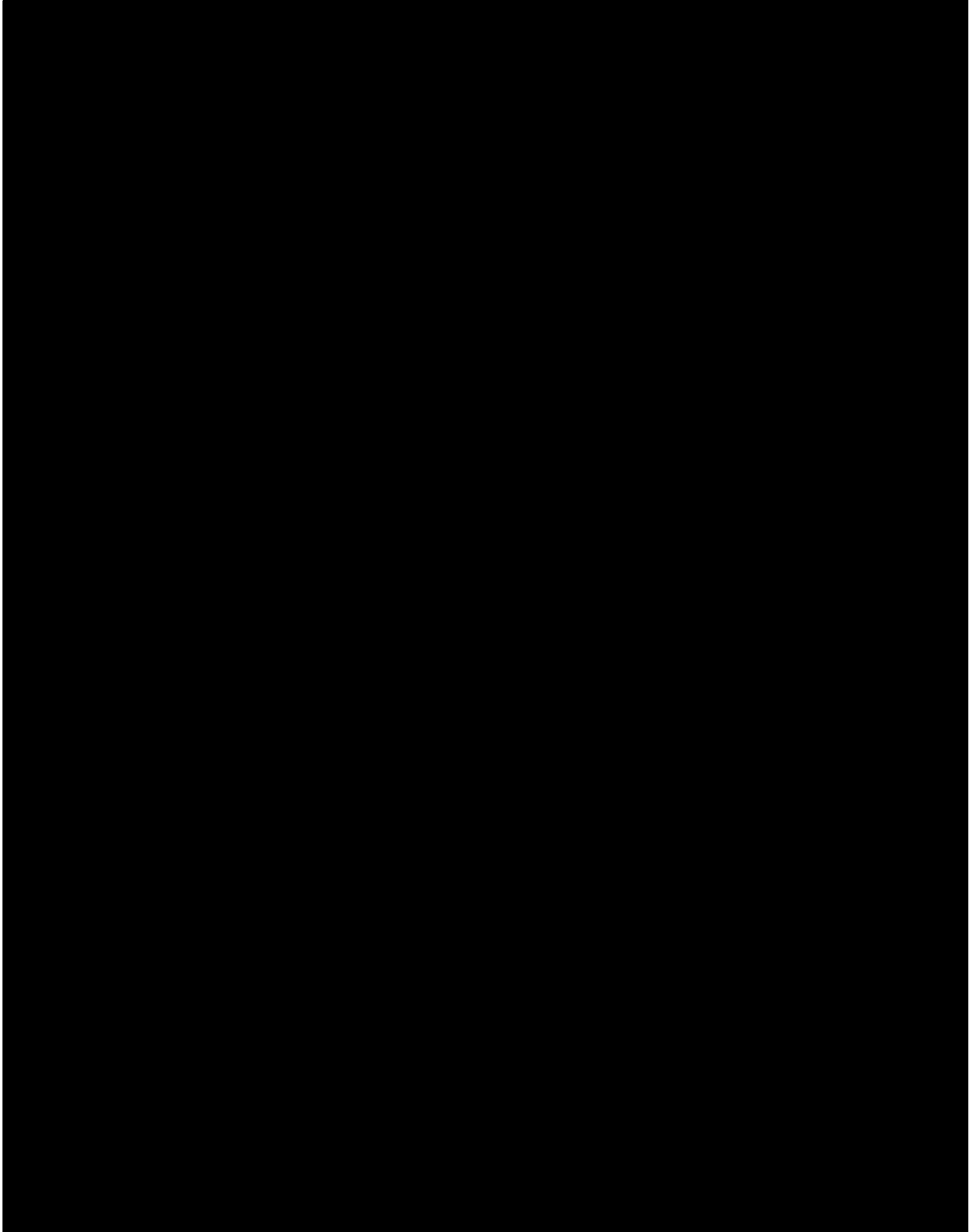
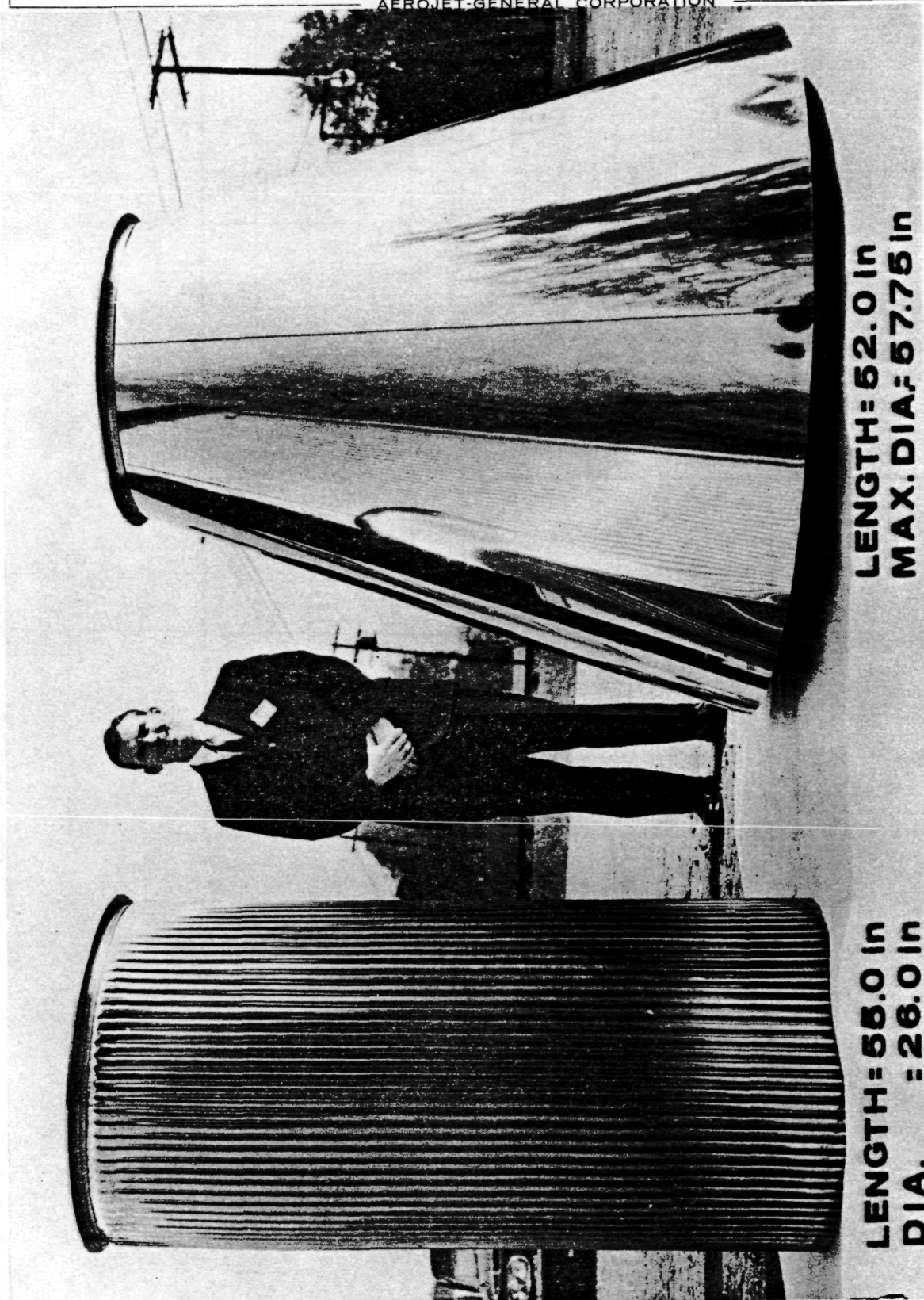


Figure III-B-9

AEROJET-GENERAL CORPORATION



Large Expandable Nozzle Currently Undergoing
Altitude Tests

Figure III-B-10

III, Vehicle Subsystem (cont.)

C. INTERSTAGE STRUCTURE ASSEMBLIES

1. Summary

The interstage structure assemblies of the vehicle are the interconnecting structures that transmit the loads between the major sections of the vehicle. These structures are:

- a. The cylindrical structure supporting the command module and enclosing the service module
- b. The conical structure at the forward end of the payload that encloses the payload service module
- c. The cylindrical structure between the payload and second stage
- d. The cylindrical structure between the first and second stages

The latter structure, between the first and second stages, incorporates provisions for the separation or staging operation between the stages as shown in Figures III-C-1 and III-C-2. A more

III, C, Interstage Structure Assemblies (cont.)

detailed presentation of the structural assembly and staging provisions is given later in this section and is representative of the other interstage structures and separation provisions.

Except in the case discussed above, the interstage structures do not contain staging provisions because the entire vehicle forward of the first stage remains connected through orbit attainment. However, there are separation devices for the command module for abort and re-entry operations. All interstage structures will be designed to provide access as required for assembly and maintenance operations. When these structures are pressurized, and emergency access is required, airlock provisions will be made for manned entry and operations using a pressurized suit.

2. Interstage Assembly (Stage 1 to Stage 2)

a. Description and Operation

This assembly is shown in Figure III-C-1 and its basic function is to connect the two stages and to provide for the

III, C, Interstage Structure Assemblies (cont.)

staging function. It is pressurized up to 40 psi for structural stability and to provide a positive separation force during staging. A linear shaped charge assembly is located slightly aft of the second-stage joint to effect separation of the structure upon command. Additional shaped charge assemblies will be used to jettison the remaining structure after complete separation to leave a nose configuration suited to recovery. The sequence of staging operations is shown on Figure III-C-2 and these operations are described in more detail later in this section.

b. Structural Configuration and Material

The main interstage structure will be made of 18% nickel, maraging steel. Longitudinal stiffeners are provided to resist buckling in the unpressurized condition and to assist in maintaining structural stability under maximum loading conditions when pressurized. This structure, although expendable, will be coated to resist salt water corrosion. The expandable nozzle is attached to the forward end of this structure that will continue to support the nozzle after the staging operation and during the second-stage main

III, C, Interstage Structure Assemblies (cont.)

engine firing. Therefore, this forward section will be subjected to temperatures of 1,000°F from the gas injected just upstream of the joint. The use of aluminum was considered, but was dropped because of the temperature environment.

c. Structural Load Path and Pressurization

The load path is directly along the cylindrical structure between the first and second stages. The flanges provide full development of the compressive strength and nearly full development of the tensile strength.

The main second-stage engine and the space enclosed in the interstage structure will be pressurized to approximately 10 psig at the conclusion of the vehicle assembly operation. This pressure will stabilize the interstage structure and will prevent water entry during the towing to the launch point. The pressure will be controllable and may be increased to as much as 40 psia prior to launch. This pressure is held by seals at the joints and the flexible seal and nozzle support at the aft end of the second-stage nozzle.

III, C, Interstage Structure Assemblies (cont.)

d. Assembly

The main interstage structure is bolted to the stub skirt at the forward end of the first stage. This structure will be fabricated at the manufacturing plant and attached to the first stage before it is towed to the vehicle assembly site. The remainder of the interstage assembly will be assembled at the assembly site when the first and second stages are mated. The bolted joints provide flexibility of operations and ease of replacement of this structure after recovery of the first stage.

The linear shaped charge assemblies are located within the structure and, therefore, will be installed before mating of the stages. Safety will be provided by remotely-monitored safe and arm mechanisms with positive mechanical shutters that are reversible to arm or safe the ordnance items by remote control. The linear shaped charge assemblies and safe and arm mechanisms are enclosed in housings pressurized with dry nitrogen gas, and can withstand submersion during operations.

III, C, Interstage Structure Assemblies (cont.)

The last stages of assembly will be the mating of the first and second stages followed by the assembly of the expandable nozzle and the segmented straps holding the expandable nozzle. These steps are shown in detail in the Operational Plan Section.

e. Staging Sequence

The staging sequence between Stages I and II, is started by command of the guidance system after the first-stage engine has been shut down Figure III-C-2 illustrates the operation.

The first step is the cutting of the interstage structure circumferentially with the forward linear shaped charge assembly. Because of the air pressure in the interstage structure, separation forces exist between the stages that are immediately released when the interstage structure is cut. Because the gas pressure acts on the entire cross-sectional area of both stages there are equal and opposite forces of large magnitude developed that give relative separation accelerations between the stages. A gas

III, C, Interstage Structure Assemblies (cont.)

obturating seal between the interstage structure and the expandable nozzle provides capability to the expandable nozzle to withstand this pressure. Thirdly, after the first stage has moved aft relative to the second stage about 5 - 10 ft, the segmented straps on the expandable nozzle will be jettisoned by means of explosive bolts at each joint. These bolts incorporate a piston and cylinder arrangement that provides positive outward impulse to the segments so they will move away from the nozzle. The nozzle is then free to expand because of the remaining gas pressure, and hard contract with the first stage is prevented.

After the first stage has moved aft, so there is considerable space between stages, the fourth operation is accomplished, which is the jettisoning of the remaining portion of the interstage structure forward of the joint connecting it to the first stage. This is accomplished by simultaneously firing the aft linear charge assembly and 16 longitudinal linear charge assemblies so that the structure is cut into 16 pieces without damaging the joint of the recoverable first stage. This operation removes the greatest portion of the structure for improved aerodynamic stability

III, C, Interstage Structure Assemblies (cont.)

and reduced water impact loading during the subsequent recovery phase. The first-stage recovery system includes the sequencing and power systems required for this and subsequent operations.

3. Other Interstage Assemblies

The other interstage assemblies are less complex than the one described above. Their main function is to provide structural interconnections as described below.

The interstage structure that supports the command module is cylindrical and reinforced to provide adequate strength as well as sea handling. At the forward end of the interstage structure, there is a separation device that is capable of separating the command module from the service module upon abort of the flight so the abort propulsion system will carry the command module away from the vehicle. At the aft end of the interstage structure, there is a similar separation device that operates to separate the command module for re-entry under normal operating conditions. Simultaneously, the posigrade rocket propulsion system will accelerate the command module away from the vehicle.

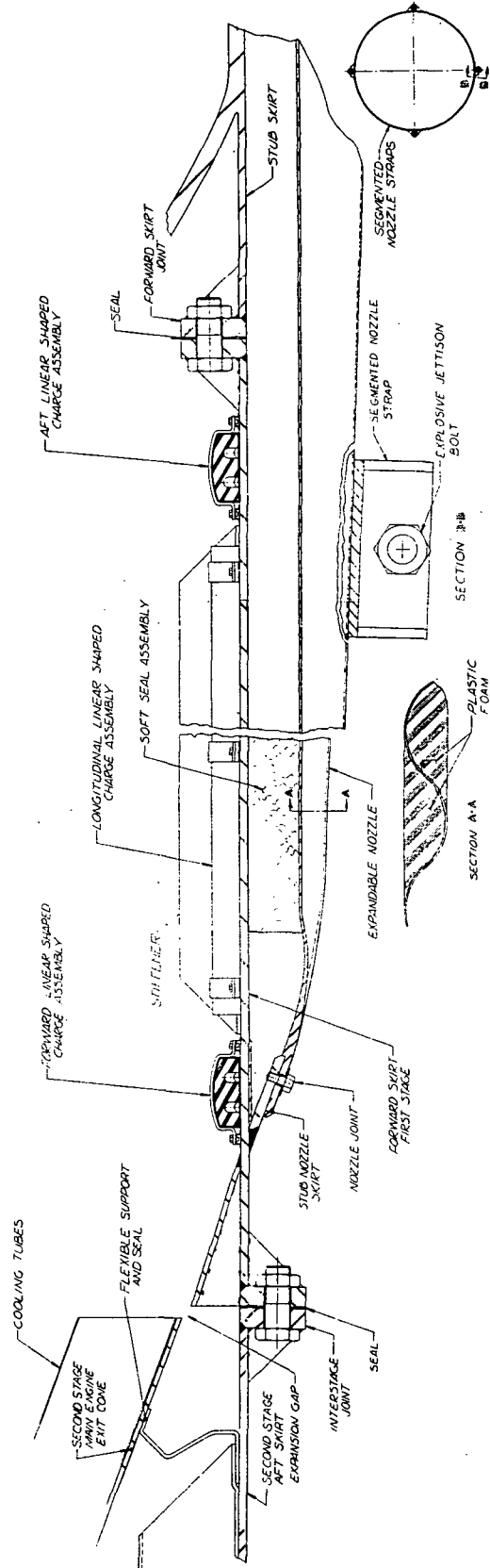
III, C, Interstage Structure Assemblies (cont.)

The second assembly is the interstage structure between the payload and the command module. This is a continuation of the forward conical section of the payload. Thus, the interstage structure of the payload supports the command module and the interstage and service module for the command module.

The interstage structure is between the payload and the second stage and is a stiffened aluminum cylinder. This section contains the battery power supply and other equipment for the vehicle that requires service access. There will be access manholes in this portion of the structure so that the servicing and assembly can be accomplished. This interstage structure is bolted to the payload and to the second stage.

SECOND STAGE

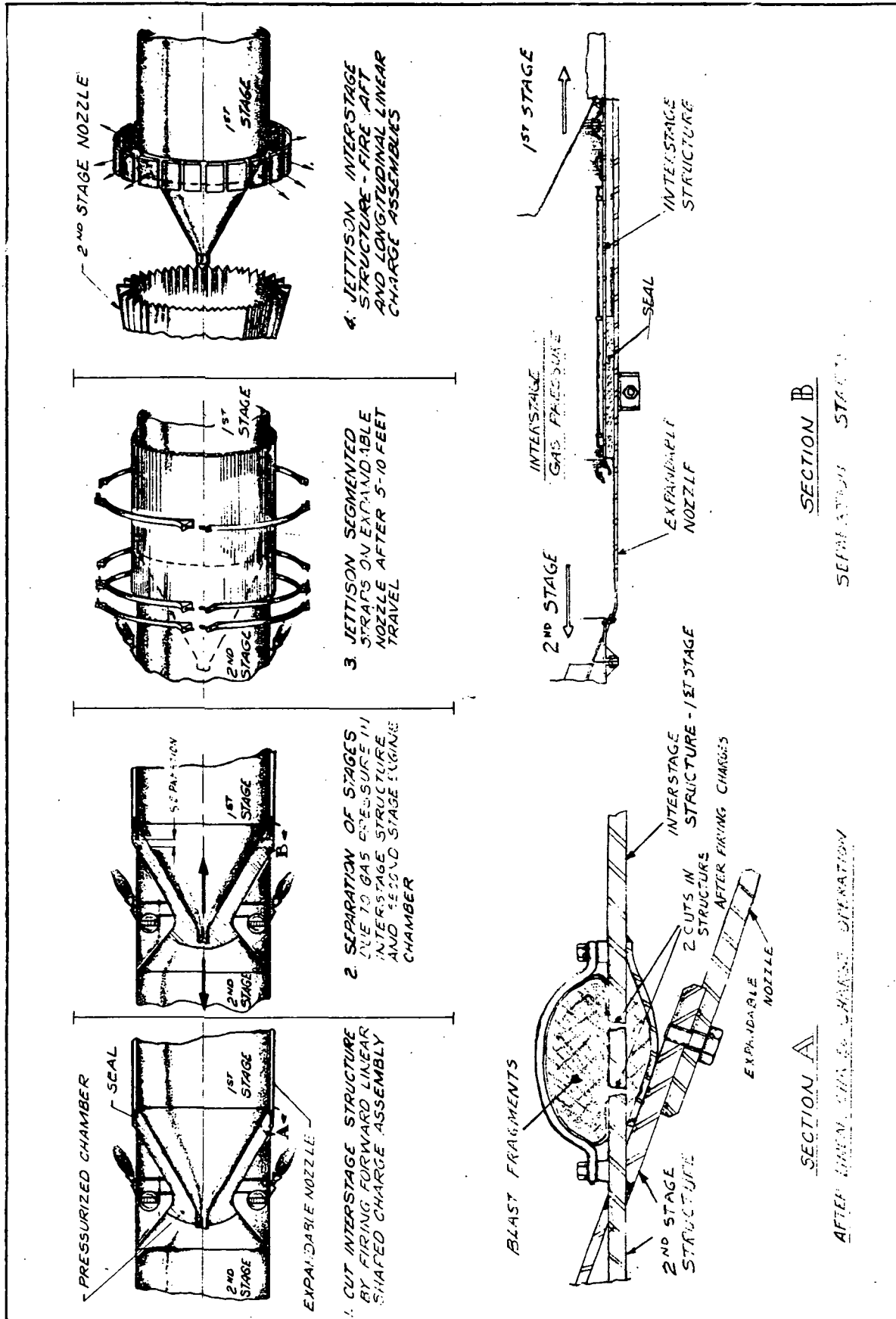
FIRST STAGE



Interstage Assembly

Figure III-C-1

AEROJET-GENERAL CORPORATION



Staging Sequence Schematic

Figure III-C-2

III, Vehicle Subsystem (cont.)

D. PAYLOAD

1. Summary

The basic payload is assumed to be a tank containing one million pounds of liquid hydrogen with a service module attached to provide those functions that must be performed by the payload after orbit has been achieved and the command module has separated to return to earth. Because the second stage and command module are attached to this payload, the payload that is placed in circular orbit includes the entire vehicle forward of the second stage as show in the Flight Sequence illustration, Figure II-3. Details of the vehicle are shown in Figure II-1.

The payload could be varied for other missions to provide additional propulsion stages or to provide variations in configuration, density and function.

III, D, Payload (cont.)

The command module is a manned Apollo spacecraft that provides the basic guidance, control, and communications functions during flight. The module will return to earth using its service module to provide separation and recovery functions. An abort propulsion system is also provided. If the only function of the command module is to ensure attainment of orbit by the LH_2 payload, a considerably smaller and simpler module similar to Mercury or Gemini could be utilized.

The payload fuel tank will be constructed of aluminum. Provisions are made for fueling and venting in the same manner as the liquid hydrogen tank in the second stage. The tank will be insulated as necessary to limit heat transfer during transportation, flight, and the orbital environment.

After orbit has been attained and the command module has separated and returned to earth, the remaining payload will continue to orbit until rendezvous with a spacecraft. The service module of the payload will provide communications and attitude control functions to assist in location, identification and docking. Fuel transfer functions will also be provided.

III, D, Payload (cont.)

2. Tankage

The payload tankage for the liquid hydrogen will be a welded aluminum structure with features similar to those of the second-stage liquid hydrogen fuel tank. The tank is supported at both ends by the respective interstage structures. Provisions will be made for loading the payload in a horizontal position and for topping in both a horizontal and vertical position.

The forward end of the payload will be conical to provide efficient aerodynamic performance and strength for supporting the command module at the forward end. The aft portion of the pressure vessel will be hemispherical in shape with a transition section at the outer diameter between the spherical and conical sections.

This configuration has not been optimized for the liquid hydrogen payload.

III, D, Payload (cont.)

The insulation of the tank will be external and of the same type provided for the second-stage liquid hydrogen tank. The exact thickness used depends on the mission profile, time in orbit, and other parameters not investigated in this study.

3. Service Module for Payload

The payload service module will contain those functions essential to orbit, rendezvous, and fuel transfer of the payload. These are:

- a. Command receiving and transmission functions
for rendezvous
- b. Radio transmission for location and identification
- c. Telemetry system for payload
- d. Attitude control system
- e. Fuel transfer system

III, D, Payload (cont.)

The attitude control system will be controlled by command instructions from the vehicle that is attempting to rendezvous with the payload. It is considered feasible to use the ullage pressure of hydrogen in the payload to orient the payload on command by the use of payload attitude control rockets. The hydrogen will provide considerable specific impulse because of its low molecular weight, even though it is quite cold.

The power supply for the payload service module will be the main power supply for the vehicle. It is located between the second stage and the payload, because the second stage will remain with the payload in this version of the vehicle mission.

The design of the attitude control system and the fuel transfer system for rendezvous operation involves equipment and techniques that are considered beyond the scope of this study.

III, D, Payload (cont.)

4. Command Module

The command module contains the main vehicle guidance and control systems as well as the communications system for communicating with ground control stations. The command module is located at the forward end of the vehicle and will be attached at the assembly site before towing to the launching site. All checkout of the equipment will be made prior to this towing operation.

For the purposes of the present study, it was assumed that the command module is a manned module of the Apollo type. Depending on further mission definition, a considerably simpler spacecraft such as Mercury or Gemini may be adequate. All of the applicable equipment and operational techniques for the Apollo program are assumed to be developed and available, including the life support system, at the time of the first flight. The manned concept does not preclude the use of an unmanned command module that would be physically interchangeable with the manned module.

III, D, Payload (cont.)

Primary equipment that will be in the command module for vehicle operations will be as follows:

a. Main Vehicle Guidance and Control System

The main vehicle guidance and control system including all computers, autopilots, sequencing equipment, and related checkout equipment will be in the command module. This system will also provide for the separation, propulsion, and control and guidance functions necessary for recovery of the module. A further description of the main vehicle guidance and control system is contained in another part of this report.

b. Electrical Power Supply

The electrical power supply for the command module will be a battery pack that is activated after the vehicle has been erected, or it will be the type of power supply available from the Apollo program if applicable.

III, D, Payload (cont.)

It will have the capability for operating the essential functions for the command module throughout the flight and recovery operations. Additional power will be provided by the main vehicle electrical power supply system where command module weight can be saved.

c. Communications Receivers and Transmitters

Provisions for two-way communications will be made. The total extent of the communications will depend on further studies of the operational requirements for the mission and will include all aspects of voice, command functions, telemetry, and tracking. Additional telemetry transmitters may be used in the vehicle outside of the command module to save weight and complexity of this module.

d. Instrumentation and Observation Equipment

Instrumentation and observation equipment will be provided in the module as required to provide maximum safety

III, D, Payload (cont.)

for the crew and monitoring for the entire operation so that information can be transmitted to the command ship or action taken aboard the command module to correct performance or to abort the mission. Automatic recording and telemetry will be provided for all critical data as an integral part of the checkout and operation of the vehicle.

e. Abort System

For the manned command module, an abort system will provide automatic abort with manual override under some situations to provide as a whole maximum manned safety and maximum probability of mission success.

Abort provisions will be made for the entire vehicle at launch during an initial period of a few seconds after the start of the first-stage engines and before the flight is committed. That is, if it is evident that the first-stage engine firing or other critical operations are not satisfactory, it is possible to shut down the engines and abort the mission without destroying the vehicle.

III, D, Payload (cont.)

This is possible at this time because the vehicle will not be seriously damaged by allowing it to settle back into the sea.

5. Service Module for Command Module

The service module for the command module will be essentially the same type that will be provided for the Apollo earth orbit mission command module. The propulsion systems for earth re-entry are the major elements of this service module. In addition, however, there will be included any support equipment that will reduce the total weight and complexity of the command module.

The service module will contain:

- a. Posigrade rocket system for separation
- b. Retrograde rocket system for de-orbit
- c. Stage separation systems for abort and for re-entry operations
- d. Support equipment for the command and service modules.

III, Vehicle Subsystem (cont.)

E. CONTROL SYSTEM

1. Summary

In the present design, all of Sea Dragon attitude control is achieved by jet forces; neither moveable nor fixed fins are employed. Directional control moments for the vehicle during first-stage operation are developed by rotation of the entire first-stage engine, which is gimbaleed. Movement of the system is obtained by means of piston-type actuators and an open-loop hydraulic system fed by the main fuel tank at 400 psi. An estimated 40,000 lb of RP-1 is dumped after use by the control system. Second-stage directional control is accomplished by four auxiliary LO₂-hydrogen engines, each pivoted and electrically actuated to provide a maximum side thrust component of \pm 53,200 lb - or an equivalent deflection of the main engine thrust equal to 0.43 degrees. These engines provide roll control throughout all stages of flight in addition to directional control after completion of first-stage operation.

III, E, Control System (cont.)

Analyses of the control system have consisted mainly of evaluating performance capabilities of the preliminary design, which was based on estimates, while also defining a more complete set of requirements for the final design. In this process, consideration was given to the effects of imperfections in the vehicle itself and of perturbations caused by its environment and its program. Wind and sea conditions, thrust and aerodynamic misalignments, maneuver programs, propellant sloshing, and body bending, therefore, were analyzed. Excepting the two latter effects, it was found that the original estimated $\pm 3^\circ$ rotation of the first-stage main engine provides more than adequate control capability. Propellant sloshing and body bending influence mainly the control loop stability, which was not completely analyzed. Preliminary results indicated that sloshing will not be particularly troublesome because the first body bending mode frequency is at least three times the first slosh mode frequency. However, body bending coupling possibilities will require careful selection of loop gain, instrument location, and actuation system lag. For this evaluation, a simplified autopilot design was selected on the basis of a single-plane, rigid-body analysis of first-stage attitude control.

III, E, Control System (cont.)

The second-stage system requirement is determined primarily by the effects of thrust misalignment, although staging, propellant sloshing, wind and maneuver program conditions were also examined. It was found that the combined effects of thrust misalignment and wind require a directional trimming moment corresponding to 0.37° main thrust deflection. To obtain some performance margin above the 0.43° present design capability, the auxiliary engine size will be increased; however, a more complete analysis of the system requirements will be made first. In particular, the effect and likelihood of control system saturation because of propellant sloshing must be considered when specifying the required performance margin. The auxiliary engines provide the vehicle roll correction. In addition, they provide orbital injection without a restart requirement, a retrothrust capability if second-stage recovery is considered, and a capability that is difficult to achieve with the single first-stage gimbaled engine. For both stages, alternate TVC concepts have been studied and will be reviewed in follow-on vehicle design phases.

III, E, Control System (cont.)

2. TVC Requirements

Of the many considerations that determine control system requirements, those that are discussed in this section pertain primarily to the thrust vector deflection characteristics. The most important considerations of physical properties, such as simplicity, reliability, state of development, adaptability for packaging, and suitability for use in the water environment are discussed briefly. A full description of the TVC system selected is given in Section III,A.

a. First Stage

At the outset of this study, it was estimated that the first-stage TVC requirement would be for 3° maximum deflection of the main engine thrust. Subsequent analyses have shown that a lesser requirement (closer to $1\ 1/2^{\circ}$) probably will suffice; however, many aspects of the control system analysis remain to be done. Some influences on the control loop stability have been analyzed, and are

III, E, Control System (cont.)

discussed later in this section; however, most of these results are on the basis of uncoupled operation of the system under quasi-steady-state conditions. Discussion of first-stage control is confined to directional control requirements; roll control is included as part of the second-stage discussion because it is effected by second-stage engines.

The principal factors that determine the directional TVC requirements for first-stage operation are thrust misalignment, aerodynamic misalignment, launch transients (wind and sea affects), pitch maneuver program, upper atmosphere wind and propellant sloshing. Their effects are discussed separately below:

Thrust misalignment - Although it is not known with certainty what degree of mechanical alignment can be maintained in a structure of Sea Dragon dimensions, it is estimated that the equivalent of $1/4^{\circ}$ thrust alignment accuracy can be achieved, and this value has been used in all analyses to date. In reality, thrust misalignment is made up of many components such as flow misalignment

III, E, Control System (cont.)

of the mechanical assemblies, bias in the actuation system, and lateral displacements of the combined center of gravity with respect to the reference center line of the vehicle. Most of these components vary with time as the propellant in the system is used and the structures are exposed to changing loading and heating conditions. Also, these components are randomly distributed and a statistical analysis of their combined effect eventually is required to completely define the characteristic. Although the Sea Dragon scale difference is recognized, experience with the largest rocket motors to date would indicate that the value of $1/4^\circ$ thrust misalignment is a reasonable assumption.

Aerodynamic misalignment - An analysis has not been made to determine the magnitude of aerodynamic misalignment; however, because the vehicle is not equipped with predominant aerodynamic surfaces, such as wings or fins, it is believed that the overall aerodynamic misalignment effectiveness will be almost negligible. To further assure that it is minimized, every effort is made in the

III, E, Control System (cont.)

vehicle configuration to retain features of symmetry. This is done not only to minimize aerodynamic contributions to directional moments, but also to avoid coupling with the roll characteristics.

Launch transients - Associated with underwater launch are certain unique requirements for control. These are derived from the fact that the vehicle is in motion prior to ignition and "flies" through a high density medium wherein it can develop high q effects at low velocity. The vehicle's emergence into surface winds while its aft end is still immersed and somewhat constrained creates another unusual effect. In addition, the water environment restricts the control surface (nozzle) motions; however, as velocity is reached, it also increases the gain of the system; that is, less deflection is needed to achieve a given moment.

There are certain advantages in leaving the first-stage control system "locked-out" until the vehicle has cleared the water. These advantages relate primarily to ballast staging considerations. Because the locked control case would result in the

III, E, Control System (cont.)

largest vehicle dispersion during launch, it was analyzed. The result showed that vehicle motion characterized by 5.8° pitch and 1.7 degree/sec pitch rate could be developed by the combined effects, considering wind, sea condition, and thrust misalignment. This analysis, and others, are presented in Section V,B. Subsequently, it was determined that the control system can overcome these effects by $1 \frac{1}{2}^{\circ}$ deflection for 5 sec.

Kick maneuver - The vehicle pitch maneuver required to program into the gravity turn has been estimated to require thrust deflection of 0.75° for approximately 8 sec, which in turn achieves a pitch rotation of six to eight degrees, as discussed in Section III, F, 3. Further trajectory studies will determine a definite command pitch rate program for trajectory optimization.

Wind - The influence of surface winds was included in the analysis of launch transients as discussed previously. Subsequently, in the atmospheric flight, wind effects continue throughout most of the first-phase flight. A discussion of the wind-produced angle of attack is given in Appendix VI-Q. A typical expected TVC

III, E, Control System (cont.)

deflection history because of wind conditions is included in this appendix. The wind condition that exists at the time when the vehicle reaches its peak value is of most interest. It was found that the most severe requirement because of wind occurs 25 sec after launch and leads to a TVC requirement of 0.95° . This was on the basis of conditions produced by zero drift.

For the Sea Dragon vehicle wind conditions may not have to be treated as having completely random direction; for a particular launch location, such as Cape Canaveral, prevailing winds can be assumed to pertain since the launch direction is always the same.

Sloshing - Propellant sloshing affects the control system as more of a transient influence than the factors cited above; however, it is not expected to have a strong effect on the required thrust vector deflection. In Section V,B,11, sloshing considerations are further discussed.

III, E, Control System (cont.)

Conclusion - Although further work must be done to fully define the combinations of effects on TVC requirements during first stage, indications at present are that a thrust vector deflection of less than 3° will be sufficient. Because the present system is designed to provide the 3° requirement, it is believed to be conservative in this regard.

b. Second Stage

For auxiliary engines suitably pivoted are used for deriving the control moments necessary for second-stage steering. In addition, these auxiliary motors, operating in a mode of differential deflection, provide the roll control capability of the vehicle throughout the first stage of flight. At the time of staging, the auxiliary motors are switched to a mode of operation in which they can provide combined directional and roll control, which continues to the point where orbit injection is achieved for the entire upper-stage system. An evaluation of roll moment requirements has not been made;

III, E, Control System (cont.)

however, it is conservatively estimated that auxiliary engines suitably sized for directional control of the second stage will have ample capability for roll stabilization and maneuver of the entire vehicle during its first stage of flight.

During second-stage operation, the principal considerations in deriving thrust vector control requirements are the influences of the staging process, thrust misalignment, propellant sloshing, and the pitch program requirement. Because the system is designed for staging at low-q condition (100 psf maximum), the aerodynamic effects will be negligibly small. A staging altitude of more than 125,000 ft also precludes the encounter of any seriously high-q wind effects. If it is conservatively assumed, however, that an angle of attack as high as 1° occurs because of any effects at the time of staging, the corresponding aerodynamic moment will require a thrust vector deflection of 0.12° . (As in subsequent discussion, the quoted figures are equivalent deflections of the main engine thrust, not deflection of auxiliary engine thrust.) As discussed previously,

III, E, Control System (cont.)

it is estimated that the Sea Dragon engines will be characterized by a thrust misalignment of no more than $\frac{1}{4}^{\circ}$. Using this value, the combined aerodynamic and thrust misalignment effects call for a thrust vector deflection of 0.37° . As in the first-stage case, the control requirements uniquely associated with propellant sloshing in the second-stage system have not been determined, but it is believed that they will be of a transient nature. The second-stage TVC auxiliary engines as presently designed will provide 0.43° equivalent deflection in the plane of one pair of engines or 0.6° in a plane half-way between the pairs of engines, which is the combined plane. It is evident from these considerations that additional capability must be added to the second-stage TVC system because little margin exists above presently known demands. The most straightforward way of doing this is to increase the size; however, this and other alternatives, such as Canard systems will be examined in the next study phase.

III, E, Control System (cont.)

3. Selection of TVC System Type

The selection of a gimbale engine system for the first-stage TVC was made primarily because of its simplicity and successful use in other applications. Historically, its use imposes the least propulsion penalty of all candidate systems. The concept is well understood and thoroughly proven and may be regarded as being within current state-of-the-art. For these reasons, its reliability is considered to be excellent; however, it imposes problems in actuation, flex line requirements, and in transmitting large loads through a relatively restricted structure. The latter consideration is particularly important in Sea Dragon as regards the load conditions at water re-entry. Also, the use of the gimbale single engine requires an auxiliary system to provide roll control capability.

Other systems under consideration are those involving secondary injection, which is attractive from a structural standpoint, but which has greater complexity and perhaps greater limitation for underwater operations. By comparison to the gimbale system, however, its most attractive feature is in the simplicity of actuation requirements.

III, E, Control System (cont.)

Another applicable concept that has been given limited study employs auxiliary engines. Aside from the additional complexity of having four engines instead of one, the auxiliary engine system has many of the attractive features of the simple gimballed engine. In addition, and perhaps the most outstanding attraction of this concept, is the fact that it can be developed and checked out independently of the main engine.

For the second-stage TVC system, improved auxiliary engines are being given attention as previously indicated. This initial selection was on the basis of consideration of the expandable nozzle, which tends to preclude the use of secondary injection and gimbaling.

In Section III,A, the physical and mechanical characteristics of the TVC systems and alternates under consideration are discussed in detail.

III, E, Control System (cont.)

4. Closed Loop Autopilot Design

a. Rigid Body Dynamics

A simplified single-plane, rigid-body analysis for the attitude control of the first stage is presented to determine the approximate values of position and rate attitude gains and the autopilot bandpass.

The variables of interest are defined in Figure III E-1.

Because the airframe center of pressure is forward of the center of gravity, the most critical case for the assumed model occurs for cases of near maximum dynamic pressure.

III, E, Control System (cont.)

Parameter values selected for this analysis are listed below.

$$\begin{aligned}
 C_N &= 0.075^{o-1} & T &= 80 \times 10^6 \text{ lb} \\
 L_P &= 87 \text{ ft} & L_C &= 140 \text{ ft} \\
 I &= 7.6 \times 10^9 \frac{\text{slug}}{\text{ft}^2} & A &= 4421 \text{ ft}^2 \\
 M &= 28 \times 10^6 \text{ lb} & q &= 2200 \text{ lb/ft}^2
 \end{aligned}$$

A block diagram of the simplified autopilot is shown in Figure III-E-2. A first estimate of the hydraulic actuation system is approximated by a first-order lag with a time constant (τ) of 0.2 sec.

The torques that act on the rigid body may be derived from Figure III-E-1. Summing up torques

$$I \ddot{\theta} = T L_C - 57.3 C_N \alpha A q L_P$$

or

$$\ddot{\theta} = \mu_c \delta - \mu_\alpha \alpha$$

III, E, Control System (cont.)

Because γ measures only an arbitrary reference for stability analysis, we can make this reference the trimmed condition of the vehicle or

$$\gamma = 0$$

so

$$\alpha = -\theta$$

Therefore:

$$s^2 \theta = \mu_c \delta + \mu_\alpha \theta$$

$$\text{or } \frac{\theta}{\delta} = \left(\frac{\mu_c}{s^2 - \mu_\alpha} \right)$$

Using the control system shown in Figure III-E-2, the engine angle is given by

$$(K_R S + K_P) \theta + (1 + \tau S) = K_P \theta_c$$

Written as matrix equation

$$\begin{bmatrix} s^2 & -\mu_\alpha \\ K_R S & + K_P \end{bmatrix} \begin{bmatrix} \theta \\ \delta \end{bmatrix} + \begin{bmatrix} \mu_c \\ 1 + \tau_s \end{bmatrix} = \begin{bmatrix} 0 \\ K_P \theta_c \end{bmatrix}$$

III, E, Control System (cont.)

The characteristic equation is

$$(s^2 - \mu_\alpha) (1 + \tau s) + \mu_c (K_R s + K_P) = 0$$

or
$$\tau s^3 + s^2 + (\mu_c K_R - \mu_c \tau) s + (\mu_c K_P - \mu_\alpha) = 0$$

For stability

$$\frac{K_R}{\tau} - \frac{\mu_\alpha}{\mu_c} \quad \text{and} \quad K_P \geq \frac{\mu_\alpha}{\mu_c}$$

Where

$$\mu_\alpha = \frac{57.3 C_{N\alpha} A q L_p}{I} = 0.48 \text{ sec}^{-2}$$

$$\mu_c = \frac{\tau L_c}{I} = 1.47 \text{ sec}^{-2}$$

$$\frac{\mu_\alpha}{\mu_c} = 0.326$$

III, E, Control System (cont.)

Because $C_{N\alpha}$, L_p and L_c do not change very much during boost, μ_α/μ_c is clearly maximum when q is near its maximum value. The maximum value of μ_α/μ_c is the worst case for stability purposes so the value used in this example is an upper bound. To obtain at least a 6 db gain margin, let

$$K_p = 2 \mu_\alpha / \mu_c.$$

for the maximum value of μ_α/μ_c .

The open loop transfer function becomes

$$GH = - \frac{2 (1 + K_R s/0.65)}{[1 - (s/0.69)^2] (1 + s/5)}$$

If $K_R = 1$ the phase margin is more than adequate, and the gain crossover frequency is at 1.0 rad/sec. If a 6 gain margin and adequate phase margin are maintained for the least stable flight condition, a crossover frequency of at least 1 rad/sec appears to be a requirement.

III, E, Control System (cont.)

Only the case of rigid-body pitch control at maximum dynamic pressure has been included in this discussion. This analysis should be repeated for all flight conditions and should also be applied to pitch control of the second-stage vehicle and roll control of the system in all phases of flight.

b. Propellant Sloshing Effects

No attempt is made here to present a detailed stability analysis of the control system with the combined effects of propellant sloshing and body bending. The stability of a vehicle such as the Sea Dragon, which is controlled by an autopilot control system, is dependent on the interaction of the elastic fuselage, liquid propellant, and feedback control system.

The fundamental frequencies for the propellant slosh modes, as derived in Section V, B, 9, may be seen to be in the same range of frequencies as the control frequency. However, this

III, E, Control System (cont.)

situation does not appear to cause instability when one considers the approximate root locus of the control loop with undamped sloshing dipoles as shown in Figure III-E-3. This analysis assumes no interaction between body bending and slosh modes, which is reasonable for a preliminary analysis because the body bending frequencies are at least three times the first sloshing mode frequency. The particular case shown is for a rigid vehicle at $t = 33$ sec with the assumption made that the second-stage tanks are so full that only the sloshing of the first-stage propellants need be considered. In conclusion, it may be said that stability problems caused by sloshing during first-stage firing do not appear troublesome; however, a more detailed study of all flight conditions is necessary.

c. Body Bending

- (1) The body mode frequencies are derived in Section IV.
- (2) For this example, the body mode frequencies are approximately: first mode = 14 rad/sec, second mode = 24 rad/sec, third mode = 33 rad/sec.

III, E, Control System (cont.)

The above discussion assumed a rigid body. However, missile flexibility induces adverse effects upon vehicle loads, vehicle stability, and bending mode coupling through instruments in the missile control system. Airloads are induced by local increases in angle of attack caused by missile bending which in turn results in additional deflection and loads. Because Sea Dragon is aerodynamically unstable, gusts will produce attitude perturbations that amplify the aerodynamic loading. To minimize the loading, a fast control system is needed. This implies high loop gains that almost assure a coupling problem with one or more elastic modes.

The presence of bending makes it impossible to sense pure rigid body motion with the position and particularly the rate gyros. The first mode is the most pronounced and is generally compensated for by placing the rate gyro slightly aft of the antinode, resulting in phase stabilization. Amplitude compensation may be required for the higher modes, since the instrument placement is fixed by the first mode requirements.

III, E, Control System (cont.)

In any case, a detailed study is required of the many structural modes to ensure the stability of the control loop. This must also include details of the hydraulic actuation system since its characteristics at body mode frequencies are very important.

Detailed simulations are required to determine the effect of nonlinearities, coupling between sloshing modes and bending body modes, and many other complicating details.

d. Steering Loop Dynamics

Several factors effect the stability of the steering loop and must be considered in the system design. The inertial platform accelerometers respond to the missile pitching rate if it is not located on the c.g. A location forward of the c.g. is preferable to an aft location but in any case its effect should be considered. Sampling rates and quantization errors also effect the steering loop stability. The autopilot response and variations in its response must be considered along with the above mentioned factors.

III, E; Control System (cont.)

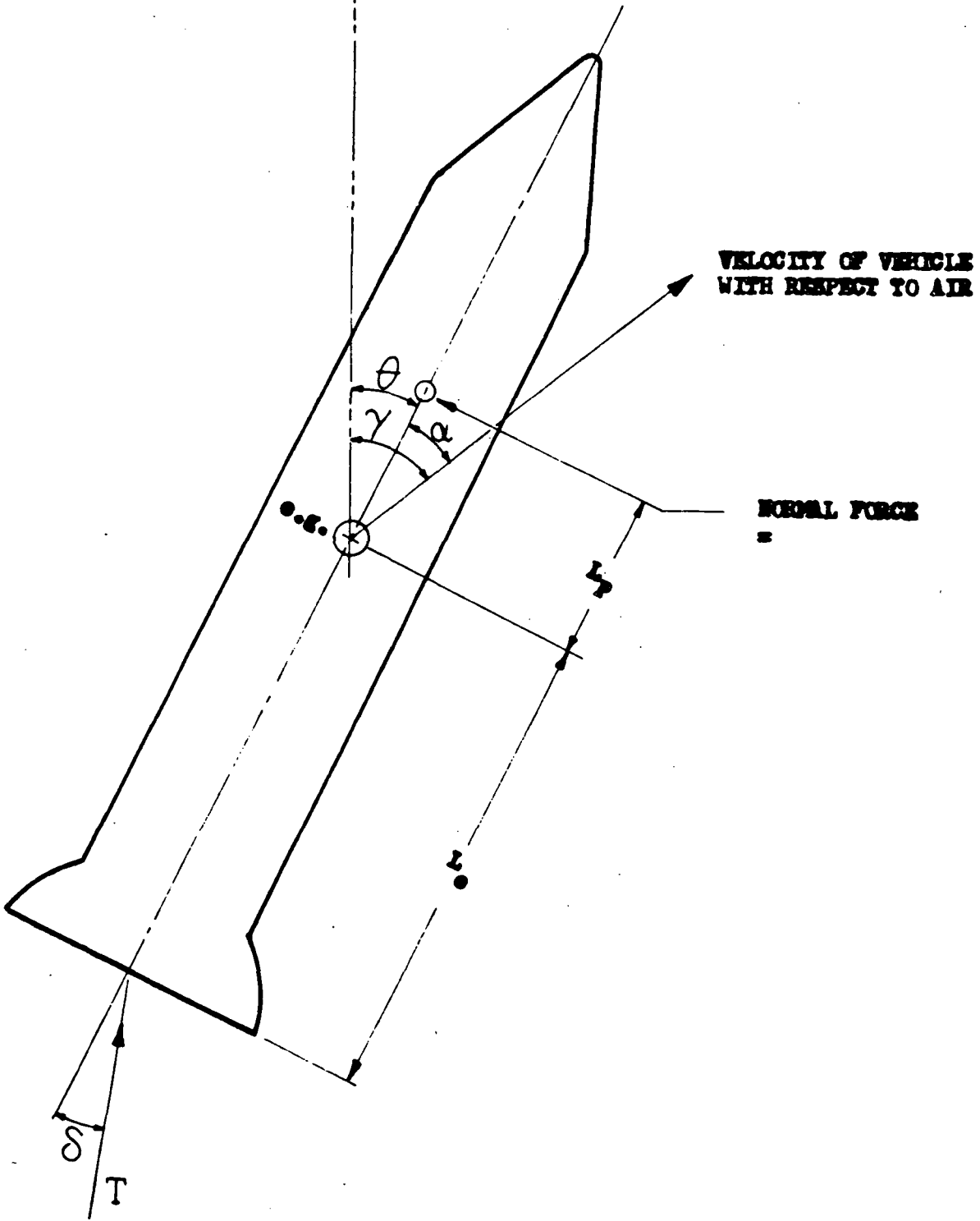
Various sources of errors can be evaluated within the context of the steering loop such as rate sensor null errors, thrust misalignments, center of gravity notions, etc., that can cause actual or effective attitude errors.

5. Measurement of Gimbal Angle

Several concepts have been considered to provide an effective gimbal action for the first stage engine. Whatever configuration is used it is important that a direct accurate measure of the engine orientation with respect to the missile be provided. If the actuator displacement were used as an indirect measure of the engine orientation then the actuator linkage compliance would have a destabilizing effect on the gimbal actuation servo. Furthermore, steady state errors could prohibit this approach.

REFERENCE

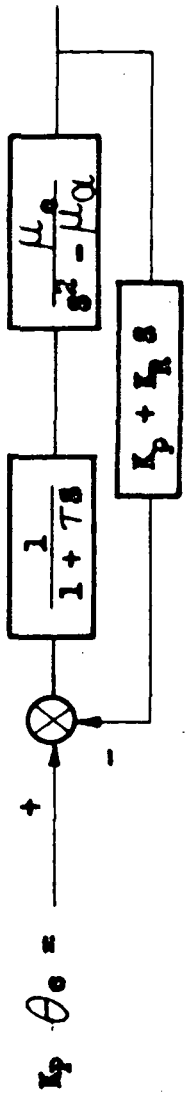
AEROJET-GENERAL CORPORATION



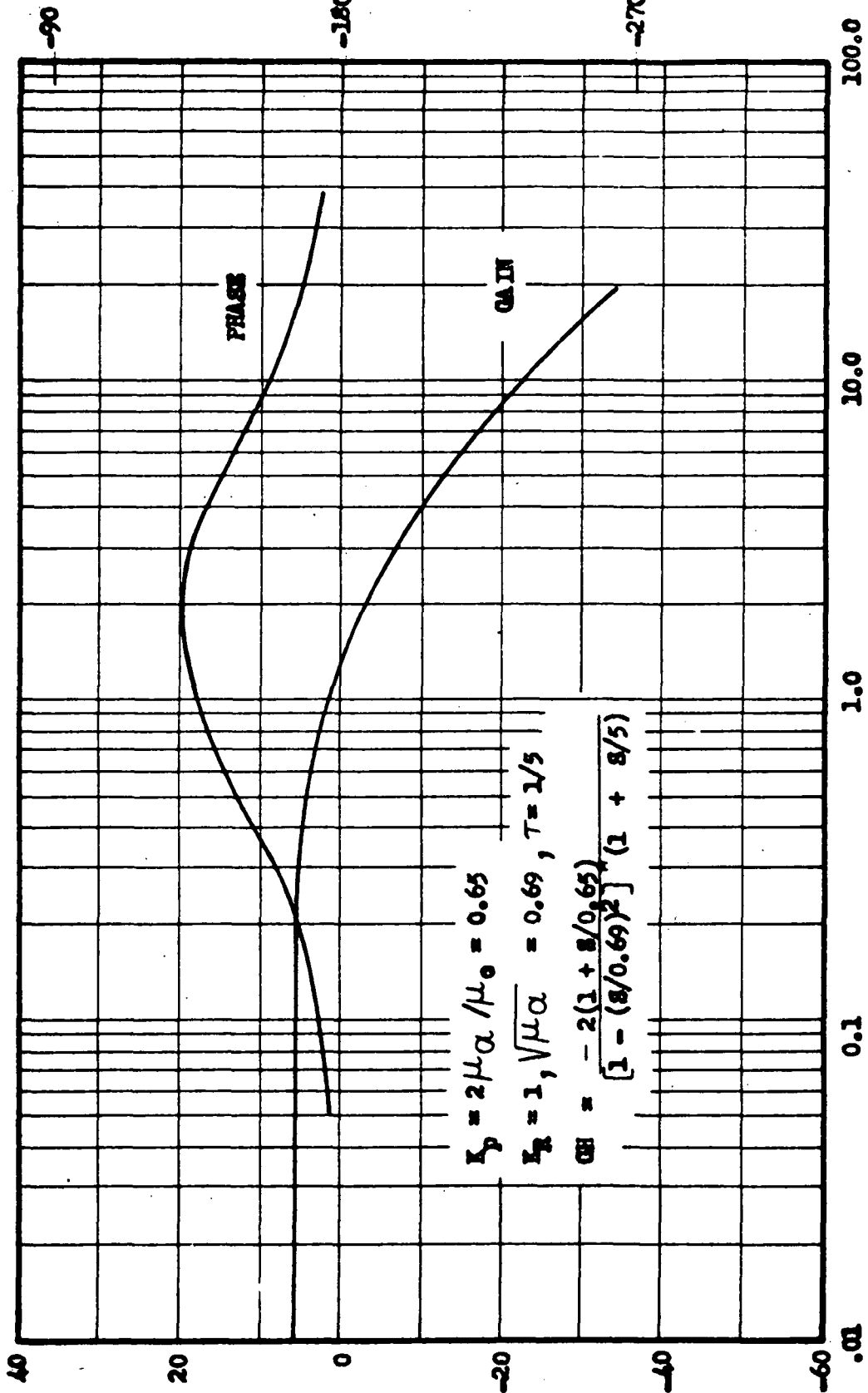
THRUST

Angles and Forces Acting on Vehicle

Figure III-E-1



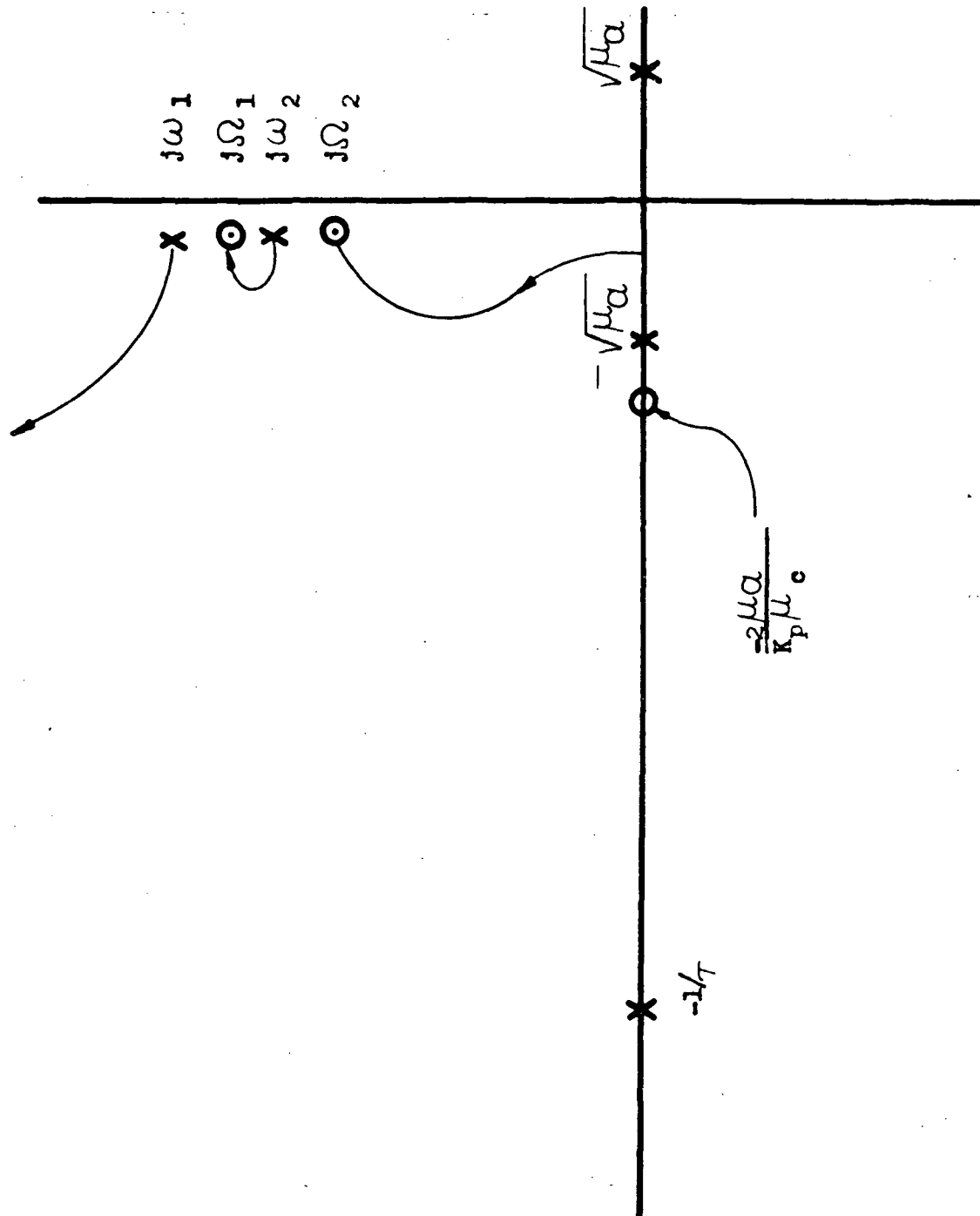
SIMPLIFIED CONTROL BLOCK DIAGRAM



RADIANS/SEC.

Characteristics of Simplified Autopilot

(8)
Figure III-E-2



Root Locus for Autopilot with Undamped Sloshing Dipoles

Figure III-E-3

III, Vehicle Subsystems (cont.)

F. GUIDANCE SYSTEM

1. Summary

a. System Performance and General Characteristics

The fully inertial guidance system proposed for the Sea Dragon launch and orbital injection vehicle has been specially adapted for vehicles launched at a sea site sufficiently close to shore Loran installations. The system is characterized by: (1) capability for full self-alignment at sea, both in azimuth and vertical directions, through gyrocompass and stable-vertical search modes, under the conditions of existing roll and pitch while afloat; (2) necessity for a prelaunch insertion of initial position and velocity conditions obtained from shore installations, monitored continuously and mechanized in the vehicle guidance system; (3) a fully self-contained inertial performance during the flight mode of the vehicle from launch to injection into orbit.

III, F, Guidance System (cont.)

The analyzed accuracy of the guidance system is expected to be such that the injection of the payload into a nominal circular orbit of 300-nm altitude will be achieved with a confidence of 98% that the following tolerances will not be exceeded:

- (a) Orbit altitude at injection: 300 ± 4.27 nm
- (b) Eccentricity established orbit: 0.005 max
- (c) Difference between altitude at apogee and perigee; that is maximum change in altitude of injected satellite for one full orbital circle is 37.5 nm

The injection into orbit will be accomplished at a point about 4,100 nm downrange from the launch site, 22.4 min after countdown 0.

The error budget drawn up by the performance analysis has assigned the following component and parameter tolerances, which are based on the foregoing injection requirements:

III, F, Guidance System (cont.)

Uncompensated gyro drift rate = $0.022^{\circ}/\text{hr}$

Initial platform misalignment = $1/3$ min of arc

Accelerometer error = 10^{-4} g

Initial position determined error = 2,000 ft =
0.33 nm

Initial velocity determination error = 3.16
knots

These values are within the state-of-the-art, except for the initial alignment accuracy, in a self-aligning mode and at sea. Consequently, this mode of operation will require a rather heavy gyrocompass and stable-vertical erection system, more of a naval-ordnance type than of an avionics type.

Systems growth capability will include the addition of radio-command guidance and possibly stellar monitoring as a further improvement in system accuracy and reliability and for mission growth. Further, in the orbital mode, the addition of a horizontal scanner and other auxiliary equipment is anticipated as a necessity for adequate attitude control.

III, F, Guidance System (cont.)

A significant factor influencing the study of guidance concepts is that there may be a human crew aboard. Accordingly, the system reliability must be man-rated, and provisions must be made for the crew to become an important link in the orbital mode of operation.

While an entirely automatic operation is envisioned, the crew must be able to provide certain overrides, to insert radioed guidance information and to take action in possible mission abort situations.

b. Physical Characteristics

The guidance system proposed for the Sea Dragon consists of two main assemblies, one containing the miniaturized guidance computer and associated electronics, and the other, a relatively heavy stable platform. This equipment will be located in the command modules of the vehicle.

III, F, Guidance System (cont.)

The computer, which uses transistor components and solid wiring, weighs 100 lb, occupies 1.0 ft³, and consumes 100 watts of electric power, and has a storage capacity of about 8,000 words. This may be compared to an existing prototype digital computer using printed circuitry weighing 35 lb, occupying 0.3 ft³, and consuming 30 watts of electric power. The actual choice will be primarily determined by reliability considerations. The entire computer and electronics package is thermal- and shock-insulated, and its estimated physical characteristics are as follows: weight, 200 lb; and volume, 7 ft³. The estimated power requirements are: 300 watts at 26v, 400 cps. The design of the package will be such as to allow operation in the space environment.

The accuracy requirements for self-alignment of the stable platform call for gyros with very high angular momentum, and therefore high moments of inertia. This requirement will lead to a considerably increased size and weight of stable platform by comparison with existing units for avionics applications. Anticipated

III, F, Guidance System (cont.)

physical characteristics for a stable platform unit located within the pressurized capsule are: weight, 400 lb, volume 6 ft³, and 1 kw peak power demand. By comparison, a typical fully developed miniature platform for avionics applications weight 33- $\frac{1}{2}$ lb, occupies 0.65 ft³ of space, and consumes 230 watts peak power.

In addition, a certain allowance for radio equipment and for a telesextant to be used by the astronauts may be included. A horizon scanner, probably mounted on a secondary stable platform slaved to the master unit, will be used in the orbital mode to establish the local vertical.

c. Special Features

The rather special conditions existing at the launch of the vehicle floating at sea in the vertical position impose the requirements of an accurate self-alignment of the stable platform

III, F, Guidance System (cont.)

in the required azimuth and vertical directions. Such an alignment cannot be performed in a conventional manner through an optical alignment system based outside of the vehicle. Instead, the highly accurate gyropendulum self-erecting system of the vehicle stable platform will operate during this mode as a self-contained north and vertical seeking element. A simplified block diagram of the self-alignment mode is shown in Figure III-F-1.

During the flight-navigation mode of the inertial guidance system after launch, which is diagrammed in Figure III-F-2, the use of the all-inertial system will obviate the necessity for a network of ground stations along the ephemeris of the inertial 4,100 nm downrange flight of the vehicle till its injection into orbit. Moreover, the guidance system of the type proposed here will provide complete freedom of selection of orbital planes of the vehicle and of the injection trajectory. In fact, it is expected to be sufficiently flexible to accommodate future growth or expansion to the required modes of operation, mission and maneuverability requirements, orbital navigation with full attitude control, and finally a re-entry with or without active participation of the crew.

III, F, Guidance System (cont.)

The location of the guidance system, i.e., of the stable platform, the associated electronics and digital computer packages, the horizon scanner and radio transponders, in the command module of the Sea Dragon vehicle will ensure a complete recoverability of this expensive precision equipment, because the command module will be designed with full capability for controlled re-entry.

An essential simplification of the overall system is expected to be achieved through a judicious application of the multifunction principle to various system elements, networks, subsystems, etc., so that they could be switched sequentially into different modes of operation, as required. On the other hand, the demand for a very high level of reliability may, in general, require an emphasis on overdesign in some areas as well as a planned redundancy of the most critical subsystems and channels of operation. For example, marked simplification of the guidance and control equipment is achieved by using the vehicle-borne equipment to perform in sequential modes of

III, F, Guidance System (cont.)

operation the various prelaunch checkout and alignment functions and the airborne guidance. Test and checkout equipment is simplified by using the airborne digital computer to check itself functionally and to monitor the performance of the guidance system during all modes of operation.

2. General Considerations of Guidance Problems

a. Introduction

By guidance is generally meant the totality of operations required to: (1) locate the position of a vehicle during flight; (2) determine the magnitude and direction of its velocity; (3) compute from this data, and from the known location of the destination, what corrective steering action, if any, is required.

The major phases into which these operations can be grouped are: (1) prelaunch mode including self-alignment; (2) injection mode during which the principal rocket engines of the vehicle

III, F, Guidance System (cont.)

are in operation; (3) orbital mode, carried out by on-board propulsion system; and (4) terminal phase consisting of re-entry and touchdown of the command module.

Even though the Sea Dragon is an ascent vehicle, the guidance system specifications must reflect requirements generated for all these phases.

Devices able to generate guidance information fall into two classes: those that make the measurements from within the vehicle itself (self-contained guidance); and those that make the measurements with the aid of guidance stations external to the vehicle. As with navigation in the past, different methods are not competitive but complementary. Classification by different guidance techniques such as "zero-draft" or adaptive guidance may also be used.

Special computer techniques are required for coordinate conversion of the basic input information into coordinates more useful for later computations, or into coordinates more appropriate

III, F, Guidance System (cont.)

for referencing missile steering commands. Computers are also required to compare the actual behavior with the standard program, calculate the correct time for initiation of such actions as rocket shutoff, calculate the direction and magnitude of command corrective maneuvers, and perform stability and attitude control computation for the autopilot. The computer also performs noise-reduction signal shaping for continuous signals used within a closed-guidance loop. Analog and digital computers have been used in the past. The heart of the guidance scheme may be thought of as the set of highly specialized equations of motions that must be resolved to fit the idiosyncrasies of the particular mission. The beam-riding and proportional-navigation techniques developed for ground to air guided missile applications and the rendezvous and orbital correction guidance schemes may be cited as examples. For ballistic missile and ascent vehicles, three schemes are generally recognized, viz: Q , Δ and explicit, and of these the explicit guidance scheme has been chosen (Section III, F, 5).

III, F, Guidance System (cont.)

In general, much of the computation, being of a nonlinear variety on noise contaminated signals, requires that very careful consideration be given to the order of performing filtering and computing. However, if small deviations of a vehicle from its nominal kinematic conditions can be assumed; it is often possible to avoid noise-filtering problems by using only the first order on linear terms.

From a system cost effectiveness point of view, a definite trend exists at present to use major guidance subsystems for many prelaunch checkout and control systems operations. In addition, the choice of technique used to determine the initial kinematic conditions of the launch vehicle affects the requirements for the guidance system of the vehicle, and vice-versa.

III, F, Guidance System (cont.)

b. Selection Criteria and Advantages of Inertial Guidance

First it should be mentioned that a variety of different guidance schemes such as radio-inertial, fully inertial, and possible stellar-monitored inertial guidance systems have been found conceptually feasible for application to the Sea Dragon. The selection then proceeded on the basis of possible extensions needed in proven techniques, and development of new components, particularly in the event that required accuracies or speeds of response would exceed present-day capability. In addition a rudimentary cost evaluation study, especially taking into account ground-support equipment and checkout needs for accommodating a variety of orbital missions, served as one of the criteria for recommendation of a particular injection guidance scheme for the Sea Dragon vehicle.

The missions for a large sea-launch orbital space vehicle may require changes in flight profiles and trajectories as a function of launch time, particularly in the case of a rendezvous

III, F, Guidance System (cont.)

requirement. Correspondingly, flexibility in the mode of operation and capability to execute a wide spectrum of flight programs is desirable. Because of the large size and cost of the vehicle and its probable application to manned missions, a high degree of reliability is required in the guidance and control systems.

The guidance and control system selected is a fully inertial one with growth potential to include stellar inertial or radio command inertial capabilities. As in the Saturn vehicle, the guidance system is located in the payload and will be available to the command module after second-stage separation.

The necessary degree of accuracy during the ascent flight and orbit injection can be achieved by this self-contained system independent of ground station support. Continuous radio-inertial guidance, which can in general achieve a higher accuracy with given equipment tolerances, is not required but does demand a large number of ground tracking station if various launch directions are

III, F, Guidance System (cont.)

considered. Additionally, and especially in the case of a sea-launch operation like the Sea Dragon, a sizeable portion of the guidance stations would have to be provided in the form of tracking and guidance ships. These ships must be very accurately located on the geographical grid and with respect to velocity, or their tracking measurements will be meaningless from the guidance standpoint. Nevertheless, even in the case of all-inertial guidance, provisions in the system can be made for discrete corrections in later guidance phases, necessary to compensate for errors in the inertial sensors in the form of RF commands through a guidance processor to the initial guidance system. These commands can be based on radar, interferometer, and radio-doppler systems as processed by a ground based computer. Alternatively, star-track monitoring on the motion of the vehicle in inertial space can be used.

3. Nominal Trajectory Concerning Guidance Requirements

The following table summarizes those characteristics of the nominal trajectory that have a direct bearing on the performance analysis of the guidance system. This study was based on preliminary data but is essentially unchanged by the new trajectory.

III, F, Guidance System (cont.)

Basic Parameters of Nominal Trajectory

Description of Parameter		Magnitude
Payload Weight		1,119,000 lb
Termination Time	Stage I	66.58 sec
	Stage II, High Thrust	267.47 sec
	Stage II, Low Thrust	1,010.04 sec
	Total	1,344.09 sec = 22.4 min
Initial Kick Angle Used*		19.74° at V = 280 ft/sec
Kinematic Conditions at High Thrust Termination of Stage II	Velocity, V	23,434 ft/sec
	Flight Path Angle (to Horizontal),	6.26 degrees
	Altitude, h	150.0 nm
Kinematic Conditions at Injection	Velocity, V	24,890 ft/sec
	Flight Path Angle (to Horizontal)	0°
	Altitude, h	299.8 nm
	Central Range Angle,	69 degrees
Characteristic Velocity, for Injection of Low-Thrust Engines		2,556 ft/sec

* In subsequent studies the kick angle was reduced to approximately 7 degrees.

III, F, Guidance System (cont.)

The vehicle is launched at sea in a vertical direction, and during the initial phase of the flight, a very coarse type of guidance is in operation. The autopilot receives preprogrammed command signals based on a predetermined time and attitude program. Thus, during the vertical ascent of the vehicle, after clearing the water, the vehicle is rotated about its roll axis to ensure that the pitch axis of the vehicle becomes perpendicular to the plane of the trajectory. The maneuver is performed by means of four auxiliary control rockets, while the attitude control in yaw and pitch is performed by the main thrust vector control system of the first stage. Even so, the coarse adjustment in roll is done by rotation in the water, before launch. This is in contradistinction to the conditions for a land launch, which by necessity, must launch with a fixed roll attitude with respect to the ground site installations.

After the performance of the rotational trimmaneuver, and upon obtaining the "kick-over velocity" as determined by the guidance system, a command signal is sent to the autopilot to initiate

III, F, Guidance System (cont.)

the pitch-over program, which is a series of commanded pitch rates approximating the kick angle and subsequent gravity turn (near zero angle of attack, autopilot stabilized flight).

The magnitude of the kick angle should be held to about six or eight degrees for structural reasons. This means that the initiation of the kick angle should be at low velocities, allowing less time for roll maneuvering. Subsequent trajectory analysis will be performed using the more realistic profile, but it is not expected to markedly change the vehicle performance.

Guidance system output is next used by the autopilot at a certain instant during the operation of the second stage, typically about 180 sec after launch, when guidance command signals based on vehicle altitude samplings are sent (Section III, F, 5, C).

III, F, Guidance System (cont.)

4. Definition of System Design

a. Summary of Injection Accuracy Requirements

Since the mission of the Sea Dragon has been initially defined as that of injecting payload into an essentially circular orbit at a given altitude, only the permissible errors in orbital eccentricity have been investigated. Once the mission spectrum has been completely specified, comparable analyses for the other parameters (inclination, position of the nodes and apsides, epoch, and period) will be made.

Assuming that the eccentricity error at orbital injection is caused by equal contributions from errors in injection radius and horizontal velocity, it is shown in Appendix II-12 that the permissible error in horizontal velocity at injection is:

$$\Delta v_h = \frac{R \Delta e_{\max}}{4 \sqrt{-\log (1-P)}} \sqrt{\frac{g_s}{r_o}} \quad (\text{Eq 1})$$

III, F, Guidance System (cont.)

and the permissible error in position (radius, or altitude) at injection is:

$$\Delta r_o = \frac{r_o \Delta e_{\max}}{2 \sqrt{-\log(1-P)}} \quad (\text{Eq 2})$$

where:

Δv_n = maximum permissible error in horizontal velocity at injection

Δr_o = maximum permissible error in position (altitude) at injection

R = radius of earth

g_s = acceleration due to gravity at earth's surface

r_o = nominal radius at injection

Δe_{\max} = maximum permissible error in orbit eccentricity

P = Probability of not exceeding the maximum permissible error in eccentricity

On the basis of Equation 1 graphs of the maximum permissible error in velocity at injection, Δv_h , versus probability of "successful" injection, P, are plotted in Figure III-F-3 for several different values of maximum error in eccentricity,

III, F, Guidance System (cont.)

$\Delta e_{\max} = 0.001, 0.005, 0.01, 0.025$, representing the criteria of "success." Similarly, from Equation 2 plots of maximum permissible simultaneous errors in position (altitude) are given under the same conditions of injection into a circular, 300 nm orbit (Figure III-F-4).

Somewhat arbitrarily assuming a permissible variation in orbital altitude of 32 nm or $\Delta e = 0.005$ (Appendix II-12), with a probability of 99%, it can be seen directly from Figures III-F-3 and -4 that the maximum permissible injection errors are 15 ft/sec in horizontal velocity and 26,000 ft = 4.27 nm in altitude.

b. Operational Airborne Equipment

A general block diagram of the inertial guidance and control system is shown in Figure III-F-2. The main physical units of the system are as follows:

III, F, Guidance System (cont.)

(1) Inertial Measurement Unit

A four-gimbal gyro-stabilized platform provides the necessary freedom of motion for any kind of flight maneuvers and delivers three-axes attitude information to the guidance and control computer. Also, mounted on the platform are three properly aligned accelerometers. Provisions are also made for later installation of a horizon scanner and possibly star scanners.

(2) Airborne Electronics

This block includes gimbal servo amplifiers and signal-shaping networks, integrators, power supplies, accelerometer electronics and gimbal-angle resolver signal conversion electronics, with provision for inclusion of horizon and star scanner electronics as a growth future.

III, F, Guidance System (cont.)

(3) Vehicle-Borne Digital

A high-speed, high-capacity generalized digital computer needed for the wide range of guidance and control operations in the pre-launch, ascent, as well as orbital modes is represented by this block. A tentative selection of the computer now in prototype development at Librascope, designated L-90, was made on the basis of a preliminary needs and availability evaluation. The only other computer whose announced specifications were compared directly with the L-90 unit is the AC Spark Plug product using Fairchild semiconductor microcircuits. In addition, specifications for somewhat less advanced computers by IBM and Texas Instruments were available. This tentative selection was made on the basis of announced memory capacity, presumed expansion capabilities, word time, power consumption, and component count. Naturally, this tentative selection will be carefully reviewed and reconsidered in the follow-on phases of the Sea Dragon design and program definition study.

III, F, Guidance System (cont.)

(4) Airborne Power Supply

In unmanned ballistic vehicles, on-board requirements are largely related to the guidance and control needs so that it is usual to provide a power supply as a component part of the guidance and control system. However, in the case of a manned vehicle, the presence of life support systems aboard will dictate an additional large and still undefined electric power requirement. Section F,6,a summarizes the guidance and control power requirements.

(5) Rate Gyro Assembly

This assembly consists of a package of three low threshold, miniature, spring-constrained rate gyros in each stage, which provide an anticipation signal for attitude stabilization. The stable platform should not be used as the attitude control reference for the first stage because flexure and bending of the missile would produce erroneous pitch and yaw axis attitude indications at the stabilized platform location.

III, F, Guidance System (cont.)

5. Inertial Guidance Performance Analysis

a. Discussion of Operation of Guidance System

(1) General Description of Guidance System

The fully inertial guidance system to be used for injection of the Sea Dragon payload into a nominal 300-nm circular orbit will consist of the following three major subsystems:

- (a) The stable platform
- (b) The stable-platform electronics
- (c) The guidance-equations computer

The purpose of the stable platform is to establish within the vehicle an inertial rectangular reference system properly aligned during the prelaunch period, and maintaining its initial alignment during the powered flight through the operation of platform gyros and gimbal system properly fitted with servo-mechanisms.

III, F, Guidance System (cont.)

Briefly, the stable platform, which is the heart of an inertial guidance system, will consist of a structural element gimbaled by means of four gimbals to the frame of the vehicle. Four gimbals (three basic plus one "redundant") are necessary to avoid any possible gimbal lock particularly during the orbital operations of the system after the injection. Two two-degree-of-freedom or three single-degree-of-freedom, high-precision floating gyros will be mounted on the platform that constitutes the inner gimbal of the system.

The gyros will be capable of being torqued so that they could be erected through precession in the required direction in space. The platform will be always slaved to the gyros through high accuracy gimbal servos operating each gimbal through properly resolved gyro pickoff signals.

In addition to the gyros, three precision accelerometers are mounted on the stable platform so that each of the accelerometers has its sensitive axis oriented precisely along the corresponding axis of the platform.

III, F, Guidance System (cont.)

Additional electronic equipment and subsystems essential to the operation of the stable platform and the inertial guidance system are:

- (a) Platform gimbal servo amplifiers and shaping networks
- (b) Integrators of accelerometer outputs
- (c) Gravity terms computer which closes the inertial guidance loop
- (d) Analog-to-digital converters.

These elements and subsystems are located outside the platform and form what might be called the stable-platform electronics system.

Further, the third major subsystem of the inertial guidance is the guidance-equations computer. This computer performs the coordinate transformation operation. The position and velocity components (time functions) in the x-y-z inertial Cartesian coordinate system, obtained from the inertial system, are translated into polar coordinates so that these polar equations can be input to the autopilot of the vehicle. The guidance-equations computer may be

III, F, Guidance System (cont.)

combined with the inertial-guidance computer (platform electronics) into one integral physical unit.

The general simplified block diagram of the guidance and control system is shown in Figure III-F-2.

The overall operation of the guidance system of the Sea Dragon vehicle can be divided into three basic modes:

- (a) the prelaunch mode
- (b) the injection flight mode
- (c) the orbital and re-entry mode

(2) Prelaunch Mode

During the prelaunch mode, while the vehicle is being towed, fueled, and erected at sea, the inertial guidance system operates continuously in properly damped stable-vertical and gyrocompass mode. The gyros of the stable platform are continuously torqued by proper signals obtained from pendulous accelerometers and

III, F, Guidance System (cont.)

from the platform-erection computer so that the three platform axes are to be aligned continuously with a high degree of accuracy with the directions north, east, and vertical at any location of the vehicle. Thus, a self-alignment of the stable platform is obtained and continuously maintained during the entire prelaunch period.

Another variant of the self-aligning, prelaunch mode of the operation is the alignment in which one horizontal axis, x , of the platform forms a given angle θ in azimuth (with respect to north) such that this axis lies in the plane of the planned trajectory. The other horizontal axis, y , is perpendicular to x , and the third platform axis, z , is vertical at the point of launch. This alignment has the advantage of leading to a considerable simplification of the coordinate transformation equations during the flight mode of operation of the guidance system.

It must be remembered that the self-aligning mode of operation may become a relatively lengthy procedure requiring several hours if sufficient accuracy is to be obtained. On the

III, F, Guidance System (cont.)

other hand, the time of self-alignment can be appreciably reduced if, before initiation of the self-aligning mode, a coarse alignment of the platform through external means (such as magnetic compass, for example) is performed.

During the prelaunch mode, the data pertaining to initial conditions of position and velocity of the vehicle at the instant preceding the actual launch must be introduced and mechanized in the inertial guidance computer. This data must be obtained from outside the vehicle with the information on the direction of launch in azimuth and other pertinent data on the nominal injection trajectory of the vehicle. It is envisioned that the initial conditions data for the sea launch of the Sea Dragon will be continuously monitored from Loran shore installations, so that the exact instantaneous location of the launch site at sea, as well as the exact horizontal velocity components at launch are measured, properly transformed, and introduced into the vehicle guidance system. The horizontal vectors of the vehicle inertial velocity just before launch are primarily results of the rotation of the earth, and in part caused by any drifting of the vehicle

III, F, Guidance System (cont.)

at sea currents. The water velocity in Gulf Stream may have a magnitude of 2 to 4 knots depending upon the location.

The self-alignment mode of the vehicle guidance system is illustrated in Figure III-F-1, which represents a general block diagram of the prelaunch, self-alignment mode.

(3) Flight Navigation Mode

The flight-navigation mode of operation of the guidance system is the actual active mode during which the inertial guidance system generates continuous, instantaneous data on the position and velocity of the vehicle in inertial space and computes kinematic equations that are to be satisfied at injection, through the operation of autopilot, TVC actuators, and the gradual response of the vehicle in space of these control functions (Figure III-F-6).

The flight-navigation mode is automatically initiated at the instant of vertical launch of the vehicle, and

III, F, Guidance System (cont.)

is characterized by free (nontorqued) operation of the previously aligned gyros. The stable platform is slaved to the gyros through its gimbal servos and, therefore, maintains its inertial (nonrotating) orientation in space with an accuracy nearly equal to that of the gyros themselves.

The three accelerometers with their sensitive axes oriented respectively along the x , y , z axes of the platform are sensing the total acceleration in each direction in space. These accelerations, of course, contain gravity terms that must be subtracted by means of gravity computer operating in a closed-loop fashion on the basis position data of the vehicle obtained from the guidance system. Each accelerometer output is integrated once to obtain velocity,* and the second time to obtain position. The data on position is used to compute the corresponding gravity term that is subtracted from the accelerometer output (Figure III-F-5). As a result, continuous signals representing x , y , z , \dot{x} , \dot{y} , \dot{z} are produced by the inertial guidance

* This first integration may be performed within the accelerometer. Such an accelerometer is called integrating accelerometer or velocity meter.

III, F, Guidance System (cont.)

system, providing continuous data on the instantaneous position and velocity of the vehicle.

These inertial position and velocity signals are fed into the guidance-equations computer that performs all the required coordinate translations and generates basic guidance equations as well as the input signals to the autopilot. Then, through the operation of the autopilot and the TVC system of the vehicle, the guidance equations must be satisfied at the instant of injection of the vehicle into orbit.

A guidance and control system that operates in a general manner discussed here, so that it assures the satisfaction of the guidance equations at the crucial injection (or cutoff) point of the powered trajectory, while permitting, in general, trajectory deviations from the nominal pattern at the intermediate points, is called an adaptive guidance and control system. The more rigid "zero-drift" system cannot be regarded as superior in operation, while being much more difficult to realize in practice.

III, F, Guidance System (cont.)

A more detailed discussion of the flight-guidance problems, injection dispersion and guidance equations is given in the subsequent sections.

(4) Orbital and Re-Entry Guidance

Although the present phase of the Sea Dragon study is not concerned with detail investigation of the orbital and re-entry guidance of the service and command module of the vehicle, it is necessary to mention several significant points relating to the required modifications of the system operation and to some auxiliary equipment necessary for proper orbital navigation and ultimate re-entry.

Once the payload (with the service and command module) is injected into the orbit, the most significant problem is to maintain the attitude of the orbital vehicle with a sufficient degree of accuracy. As far as the command module is concerned, a proper attitude maintained during its orbital mode is necessary to assure the required direction of retro-thrust for de-orbiting at the

III, F, Guidance System (cont.)

beginning of re-entry, and for other functions such as observation, photography optical and infrared, communications, telemetering, etc. It is apparent that the payload space station itself must be attitude stabilized for the purpose of any future rendezvous with it by other orbital vehicles coming in for refueling, etc.

Normally, the attitude of an orbiting vehicle will be maintained so that its yaw axis is always colinear with the local vertical; its roll axis will always lie in the orbital plane, and its pitch axis will be perpendicular to the plane of the orbit.

It must be recognized that an inertial guidance system of either Schuler-tuned or fully inertial type cannot be used successfully during the orbital mode, during which the outputs of accelerometers will always be zero. Therefore, independent sensing devices must be used in addition to the gyro-stabilized platform.

Specifically, an optical or infrared horizon scanner must be used to establish the direction of local vertical at each instant of time, whereas the stable platform will be

III, F, Guidance System (cont.)

slaved, through the appropriate torquing of its gyros, to the local vertical realized by the horizon scanner. Further, the vehicle frame will be slaved to the platform through pitch and roll attitude-control jets.

While the horizon scanner and the yaw axes of both the platform and the vehicle frame will thus continuously track the local vertical, a definite angular velocity about the pitch axis must exist. Under these conditions, if the roll axis is exactly in the plane of the orbit, the average angular velocity of the vehicle about the roll axis should be zero. If however, there is some angular displacement of the roll axis of the vehicle about the yaw axis, a definite mean angular velocity in roll will be registered by a high-sensitivity roll rate gyro properly mounted on the vehicle frame. The output signal of this rate gyro will be fed into the yaw attitude control channel which will operate the yaw-control jets to return the roll axis to the orbital plane of the vehicle.

III, F, Guidance System (cont.)

Further, radio command and communication equipment will be used in the command module to maintain continuous communications and possibly telemetering links with the ground stations and to provide the capability of initiating the de-orbiting operation for final re-entry by ground radio command.

If the orbiting module is to be provided with any space maneuvering capability such as trimming and corrections of the existing orbit, transferring to different coplanar orbits, or changing the orbital-plane inclination angle, additional guidance and control and space propulsion equipment will be required.

b. Summary of Inertial Guidance Accuracy Requirements

It can be shown (Appendix II-12) that the errors in position and velocity determination of the vehicle in the x-direction (Figure III-F-6) are given by the following explicit functions of time:

III, F, Guidance System (cont.)

Error in position:

$$x = x_i - x = + \frac{g_s \eta}{\omega^3} (\omega t - \sin \omega t) + \delta R (1 - \cos \omega t) + \frac{a}{\omega^2} (1 - \cos \omega t) + \Delta x_0 \cos \omega t + \frac{\Delta \dot{x}_0}{\omega} \sin \omega t \quad (\text{Eq 1})$$

Error in velocity:

$$\Delta \dot{x} = \dot{x}_i - \dot{x} = + \frac{g_s \eta}{2} (1 - \cos \omega t) + \delta \omega R \sin \omega t + \frac{a}{\omega} \sin \omega t + \Delta x_0 \omega \sin \omega t + \Delta \dot{x}_0 \cos \omega t \quad (\text{Eq 2})$$

where

$$\omega = \sqrt{\frac{g_s}{R}}$$

t = time counted from the instant of launch

Δx_0 = initial error in position

$\Delta \dot{x}_0$ = initial error in velocity

a_{xi} = actual reading of the x-accelerometer
(a general function of time)

\dot{x} = kinematic acceleration in the x-direction

$\frac{g_s}{R}$ x = gravity component in the x-direction

δ = initial vertical misalignment of the stable platform

III, F, Guidance System (cont.)

g_s = acceleration due to gravity

\mathcal{N} = gyro drift rate

ϵ_a = error of accelerometer

Using the results of the injection accuracy requirements analysis, the position and velocity dispersion at injection are:

$$\delta_{\Delta x} = \frac{\Delta x_{\max}}{-2 \log (1-P)} = 8567 \text{ ft}$$

$$\delta_{\Delta \dot{x}} = \frac{\Delta \dot{x}_{\max}}{-2 \log (1-P)} = 4.94 \text{ ft/sec}$$

Noticing that the ascent trajectory time is approximately one quarter of the period of the guidance system, each contribution to position error and velocity error at injection can be written as:

$$\Delta x_x = \frac{\delta_{\Delta x}}{2} = 4283 \text{ ft}$$

$$\Delta \dot{x}_n = \frac{\delta_{\Delta \dot{x}}}{2} = 2.47 \text{ ft/sec}$$

III, F, Guidance System (cont.)

Further, considering the expressions for individual contributions to error in Equations 1 and 2, the expressions for maximum component tolerances and initial condition inaccuracies follow immediately (Table 1 of Appendix II-12).

From the standpoint of position accuracy at injection,

$$\mathcal{N} = 0.08 \text{ }^\circ/\text{hr, gyro drift rate}$$

$$\delta = 0.64 \text{ minutes of arc, initial platform misalignment}$$

$$\epsilon_a = 0.00019g, \text{ accelerometer error}$$

$$\Delta \dot{x}_0 = 5.3 \text{ ft/sec} = 3.16 \text{ knots, initial velocity error}$$

From the standpoint of velocity accuracy at injection,

$$\mathcal{N} = 0.022 \text{ }^\circ/\text{hr, gyro drift rate}$$

$$\delta = 0.33 \text{ minutes of arc, initial platform misalignment}$$

$$\epsilon_a = 0.0001g, \text{ accelerometer error}$$

$$\Delta x_0 = 2000 \text{ ft} = 0.33 \text{ nm, initial position error}$$

III, F, Guidance System, (cont.)

c. Guidance Equations

During the vertical and programmed pitch-over portion of the flight, which includes a predetermined roll maneuver to define the pitch plane, only coarse guidance signals are sent to the autopilot, but the complete kinematic guidance equations, developed in Appendix II-12 are continuously generated as mentioned in Section III, F,5,a,(3). After the initiation of the first stage, the actual vehicle altitude will be periodically sampled (by means of Equation 16, Appendix II-12) and compared with the nominal altitude at that instant, to generate the altitude error which produces a signal to the autopilot for a change in pitch attitude. An additional criteria (Equation 23, Appendix II-12) will ensure that the flight path angle becomes small, a degree or two. When the actual altitude of the vehicle approaches the nominal altitude by several miles, the guidance will be switched to the flight path angle mode, Equation 1.

$$x \dot{x} + (z + R) \dot{z} = 0$$

III, F, Guidance System (cont.)

While the guidance Equation 1 will be satisfied and continuously maintained through the autopilot by means of the pitch control system, a signal to cut off the auxiliary (vernier) engines will be given at the instant at which the injection velocity Equation 2 is reached.

At injection of the vehicle into the nominal orbit, then, kinematic conditions should ideally be:

$$\text{Inertial velocity, } V = \dot{x}^2 + \dot{z}^2 = R \sqrt{\frac{g_s}{x^2 + (z+R)^2}}$$

$$\text{Altitude, } h = h_n = \sqrt{x^2 + (z + R)^2} - R$$

$$\text{and flight path angle} = 0$$

which will imply Equation 1.

6. Airborne Guidance Design Considerations and Sub-system Description

a. Evaluation of Physical Characteristics

III, F, Guidance System (cont.)

(1) Packaging and Location

A guidance compartment structure is needed to contain the airborne equipment, providing mechanical support and environmental conditioning. Provision for windows to provide the star scanner a free line of sight to selected stars should be incorporated for future growth in system capability.

In addition, special airborne test equipment such as signal conditioners, necessary for the evaluation of the guidance and control system during flight tests will be mountable on the structure. It is anticipated that the flight tests with guidance evaluation missiles, as well as sled tests, will be necessary to check out the system. This is particularly true in the case of the star-tracking component.

The entire guidance package is insulated with glass fiber and placed in a specially coated monocoque enclosure, which will be designed to have the stiffness and damping coefficients

III, F, Guidance System (cont.)

to aid the serious vibration problems connected with missile guidance computer design.

To provide cooling for the avionics equipment, the sealed container is filled with helium. It also contains a circulating fan and a liquid-type heat exchanger in its base.

The exact location in the command and service module is not critical, and in fact from the producibility point of view may be in the shirt-sleeve environment or vacuum outer space portion, depending on detailed capsule design and operational considerations not yet resolved. Placement of flight control system sensors is separately discussed.

(2) Weights, Dimensions, and Power Requirements

The Litton L-90 digital computer weighs 35 lb, occupies about 0.3 ft³, and consumes 30 watts. The Litton L-3009 platform weighs 33.5 lb, occupies 0.65 ft³ and consumes 230 watts

III, F, Guidance System (cont.)

under high torque conditions. If an astro-inertial platform is not selected, radio trim commands would probably be supplemented by telesextant data in orbital and, especially, possible lunar modes. Possible telesextant characteristics would be 20-lb weight, 0.65-ft³ volume, and 20-watt power requirements. An astro-inertial platform may be expected to weigh about 55 lb, need 1.3 ft³ of space and 250 watts of power. The average power consumption, including associated airborne electronics, is estimated at 500 watts, weight (including compartment) about 200 lb, and compartment volume about 10 ft³, of which perhaps 3 ft³ is actually taken up by pertinent guidance equipment. Power is furnished at 26v, 400 cps \pm 1% rms.

However, the extreme accuracy requirements of alignment in the vertical mode when no radio or astro corrections are made during ascent leads to a relatively heavy, naval type, gyro compassing system. In this case, which is selected as the preferred method to date, the guidance and control system will weigh an extra 200 to 300 lb, with corresponding increase in space and power required. It will be recalled that an increase of this magnitude is not a significant event in the Sea Dragon weight budget.

III, F, Guidance System (cont.)

b. Stable Platform

The unaided inertial guidance scheme selected will require development of a platform featuring high inertia gyros delivering high angular momentum. Further advances in powdered metallurgy, including magnetic high density materials of high tensile strength, are expected to aid this effort. If, however, the alternative guidance treatment involving stellar monitoring during the ascent phase is used, platforms presently under development for avionics applications would be suitable. In this mode of operations the errors in alignment, which if uncompensated would be unacceptably large, are obtained from the star tracking fix and appropriate steering corrections are generated in the guidance computer.

A number of miniature inertial platforms were considered, and the Litton P-300G has been selected as typical and capable of fulfilling Sea Dragon requirements under these conditions. Much of the discussion which follows, based on Air Force miniature platforms, is applicable also to the heavier platform, but detailed

III, F, Guidance System (cont.)

design analysis affecting the large units will not be available for the study. A detailed component description of the P-300G platform is given in Appendix II-13.

(1) General Description

The inertial subsystem consists of an inertial reference unit and an inertial reference electronics unit. These are the major units of the subsystem.

A summary of P-300G subsystem physical characteristics is presented in Table 1 of Appendix II-13. The environmental capabilities of the subsystem are summarized in Table 2 of the same appendix.

(2) Inertial Reference Unit

The inertial reference unit consists of a stable element employing two floated, two-degree-of-freedom gas bearing gyros and three floated, torque-balance accelerometers supported by

III, F, Guidance System (cont.)

a set of gimbals permitting vehicle angular freedom in azimuth, pitch, and roll. The stable element can be maintained in a prescribed orientation by torquing the gimbals with angular error signals derived from the gyro pickoffs. A redundant inner roll gimbal is provided to prevent gimbal lock; this allows the vehicle complete maneuverability without affecting the stable element. A summary of P-300G characteristics is found in Table 3 of Appendix II-13.

(a) Gyros

In a stabilized platform employing two-degree-of-freedom gyros, the gyro instrument errors are the limiting factors in stabilization accuracy (since there are no cross-coupling errors caused by rotor precession). It is therefore of extreme importance that the design configuration be highly accurate. The development of self-acting, gas-lubricated bearings makes it possible to improve the performance of the precision gyro by approximately one order of magnitude. Basically, the gas-lubricated bearing assembly consists of simple sleeve bearings and thrust pads similar to the oil-lubricated

III, F, Guidance System (cont.)

bearing used on large machinery. The difference between gas and oil-lubricated bearings is that a gaseous lubricant requires a much smaller clearance between the bearing surfaces. About one-twentieth the clearance commonly used in oil-lubricated bearings is used in the gas bearing.

(b) Accelerometers

Typically, a miniature, single axis, torque balance, pendulous accelerometer is used. The sensitive element is a floated pendulum mounted on a pair of jewel-and-pivot bearings and equipped with an electromagnetic pickoff and torquer. The sensitive axis of the instrument is perpendicular to both the pivot axis and to the line joining the center of mass and the center of buoyancy; hence, an acceleration along the sensitive axis results in a torque acting upon the floated pendulum, which tends to rotate the pendulum about the pivot axis. This rotation, however, is immediately sensed by the pickoff that generates a signal to control the accelerometer torquer current by means of an external amplifier so that the pickoff signal is continuously maintained at null. As a result, the current through the torquer coils becomes a precise measure of the applied acceleration. The high

III, F, Guidance System (cont.)

pickoff sensitivity and restoring amplifier gain keep the relative rotation of the pendulum with respect to the case limited to a small fraction of a milliradian even in the presence of maximum acceleration. As a result, the directional accuracy of the sensitive axis is maintained, and cross-coupling effects are negligible. A calibrated precision resistor, mounted externally to the instrument, converts the torquer current to a voltage that is a precise measure of acceleration. This voltage is applied to the input of the digital conversion circuit.

(c) Gimbal System

The gimbal system for the inertial reference unit employs a four-gimbal, three-axis configuration, including one redundant gimbal to eliminate the possibility of gimbal lock during vehicle maneuvers. The azimuth, pitch, and outer roll gimbals have unlimited freedom about their respective axes, but the inner roll gimbal is limited to $\pm 20^\circ$ of freedom. The resultant system, when servo-stabilized, allows unlimited maneuverability of the carrier vehicle.

III, F, Guidance System (cont.)

Typically, the signal generators and torquer motors are direct drive, gearless units. This arrangement permits higher angular output accuracy within minimum size and without the need for special, low-backlash gearing in the case of the signal generators. The torquer motors approach the high efficiency of geared units by proper design and application of the direct drive components.

(3) Electronics

The inertial data subsystem electronics unit contains all the circuitry necessary for operation of the inertial reference unit and for communication with a digital computer. The inertial reference electronics unit contains the gimbal servo amplifiers, accelerometer restoring amplifiers, redundant azimuth gyro axis caging amplifier, the various power supplies for the subsystem, platform temperature control circuits, the digital converter, and various switching functions.

III, F, Guidance System (cont.)

The digital converter contains the analog-to-digital conversion circuits for converting accelerometer analog outputs to binary incremental velocity data for a digital computer, the precision gyro pulse torquing circuits that are controlled by torquing commands from a digital computer, and the emergency pendulous leveling circuits for the platform.

c. On-Board Digital Computer

The predesign study described here is intended to result in a computer that will have the capability to navigate and guide the Sea Dragon vehicle from launch to landing completely automatically (Figure III-F-7.) Also, in case of abort, it has the capability of guiding the vehicle to a safe landing at any of several pre-selected sites. Other functions to be performed by the computer are to provide information for various guidance displays, to make decisions regarding fuel management or the need to abort, and to assist in the telemetry link. In addition, the crew must be able to manually insert data and commands into the computer.

III, F, Guidance System (cont.)

The operation of the computer is generalized by discussing the four operational phases: preflight, launch, orbital, and re-entry. On the basis of previous experience, the numbers of words of computer memory required has been estimated at 8,000. This includes 4,500 for equations of motion and launch corrections, and 1,250 words for re-entry subroutines (target selection; navigation computations to determine h , v , x , Y path angle, q ; energy management; landing commands). The memory capacity is conserved by the assumption that a judicious organization of instruction words has resulted in using two instructions per word.

The initial phase of the computer operation is preflight and is combined with the launch phase since the computations are the same. Such computations as gravity corrections, position and velocity are performed during these phases. This portion of the mission requires a high solution rate for accurate determination of position and velocity. The incremental portion of the computer is ideally suited for this purpose.

At cutoff of the rocket booster, the computer

III, F, Guidance System (cont.)

automatically switches to the programs associated with orbital mode guidance.

The computer selected for Sea Dragon is designed around a delay line memory. In Appendix II-13 the computer requirements are discussed and followed by a description of a computer with a delay line memory that will fulfill these requirements. The many advantages of delay lines are discussed in detail.

Alternatively, for comparative purposes, a computer design using a wired fixed program-core memory with a 512 word erasable core memory was considered. An advantage is that only one core is needed for each instruction word.

7. Checkout and Ground Service Equipment (GSE) Summary

The GSE consists of operational and maintenance units. The operational unit includes flight checkout equipment to prepare and maintain the airborne equipment ready for launch and a guidance control

III, F, Guidance System (cont.)

panel required on the ship during the earth-fixed modes of system operation. While the in-flight guidance computer performs many system checks, the ship-board equipment monitors the computer for malfunctions. Maintenance ground equipment includes:

- a. Handling equipment
- b. Interface and isolation console
- c. Component test equipment
- d. Computer load-test console

Detailed descriptions and methodology of the support equipment required by the guidance (and other) systems is included in the section on support operations of this volume. In addition, the results of the preliminary study made specifically for guidance system ground support and checkout is presented as Appendix II-14. Section B of this appendix, it should be noted, presents a method and justification of finding the initial position data needed for orbital injection computations.

The requisite telemetry and associated antenna systems are discussed in Section III of Appendix II-14.

III, F, Guidance System (cont.)

8. Comment on Reliability and Redundancy

a. General Discussion

The development of the Sea Dragon design will be based on the results of a comprehensive reliability design analysis. The reliability design analysis approach proposed for the Sea Dragon program will be reflected primarily by analytical techniques that will ensure that reliability becomes inherent in the design. Concurrent with design efforts, analysis will be done. In logical sequence these steps are: functional analysis, analysis of environments, malfunction mode review, system analysis, alternative analysis, reliability prediction and establishment, and allocation of system goals.

b. Electronics Reliability Factors

The design analysis procedure selected for the Sea Dragon guidance computer development will in general follow the worst case analysis concept using the tolerance analysis briefly outlined in the following: (1) specify in complete detail and with

III, F, Guidance System (cont.)

tolerances all the basic functions that the circuit is required to perform; (2) determine all conditions (primarily tolerances, damaging stresses, noise, and handling) that tend to prohibit the circuit from performing each function as required; (3) prove that the circuit will perform each function as required, even though all failure-causing tendencies occur simultaneously at their maximum values (unless some are mutually prohibitive; in this case each set of failure-causing tendencies is considered separately).

It can be proved that the necessary and sufficient condition for a component never to fail is that the tolerance analysis criteria above be met, assuming zero intrinsic parts failure.

The engineer performing the analysis has the responsibility for determining all the required functions of the component (states, input-output, errors, tolerances, internal functions, etc.) and all failure-causing tendencies. The effectiveness of a tolerance analysis is dependent on the accuracy, completeness, and

III, F, Guidance System (cont.)

reasonableness with which these items are specified. If the procedure given here is not completely adequate for all circuits, the analyzing engineer should add a procedure that proves the tolerance analysis criteria are met in full.

Maximum consideration will be given to the use of semiconductor microcircuits for logic and gating functions. The potentially high reliability of these devices made possible partly by the decrease in the number of hand made connections among parts, and partly because of the inherent potential advantages of semiconductor technology make this approach highly desirable. In some documented cases the parts count in guidance computer applications has been reduced by as much as 80% through the use of semiconductor microcircuits. Thus, reliability should be improved by the attempt to minimize the number of components and by the introduction of microcircuits.

Prelaunch testing of guidance and flight control systems have generally required extensive ground-based equipment. This equipment, usually digital in operation, also had an important but brief role that ends when the missile is launched.

III, F, Guidance System (cont.)

Recent advances have designed the guidance computer so it could serve a dual function. The computer can be used also to test the complete guidance system before launch. This technique, which is used in the Sea Dragon design, enables the missile computer to be continuously exercised independently of the ground installation with an obvious increase in reliability.

c. Inertial System Reliability Factors

Not too many years ago in guidance planning, inertial guidance ran a poor third behind radio and radio inertial systems as a system most likely to succeed. Today, however, this system is the most generally accepted. The break-through of inertial guidance was made possible primarily as a result of inertial component performance and reliability improvement.

d. Redundancy Concepts

Redundancy might be defined as the existence of more than one means of accomplishing a given task, where all means

III, F, Guidance System (cont.)

must fail before there is an overall failure of the task. As applied to reliability, redundancy concerns the practice of paralleling two or more elements, such as parts, circuits, components, modules, equipments, or even complete systems, such that, ideally, they will independently perform the same function. Failure of any one or more of the elements should neither cause failure of the desired function nor affect the probability of successful operation of any of the remaining paralleled elements. It is obvious that the use of redundancy in design should improve the probability of accomplishing a given task beyond that which would be experienced with a single element, the failure of which would cause an immediate loss of the desired function. However, the use of redundancy does introduce certain practical problems, such as requirements for additional weight, space, and power and the need for a decision making process as a means of assigning the failure to the appropriate redundant unit. This switching system must perform with an overall improvement in system reliability.

Redundancy may be further classified as functional and standby, which are defined as follows:

III, F, Guidance System (cont.)

(1) Functional redundancy exists when two or more means are operating simultaneously to accomplish a task, and less than the total number is capable of performing the function in the event of failure of less than all of the primary and alternate means.

(2) Standby redundancy provides one or more alternative means of accomplishing a task. The task is switched or transferred into operation by a malfunction sensing device when the primary means fail.

AEROJET-GENERAL CORPORATION

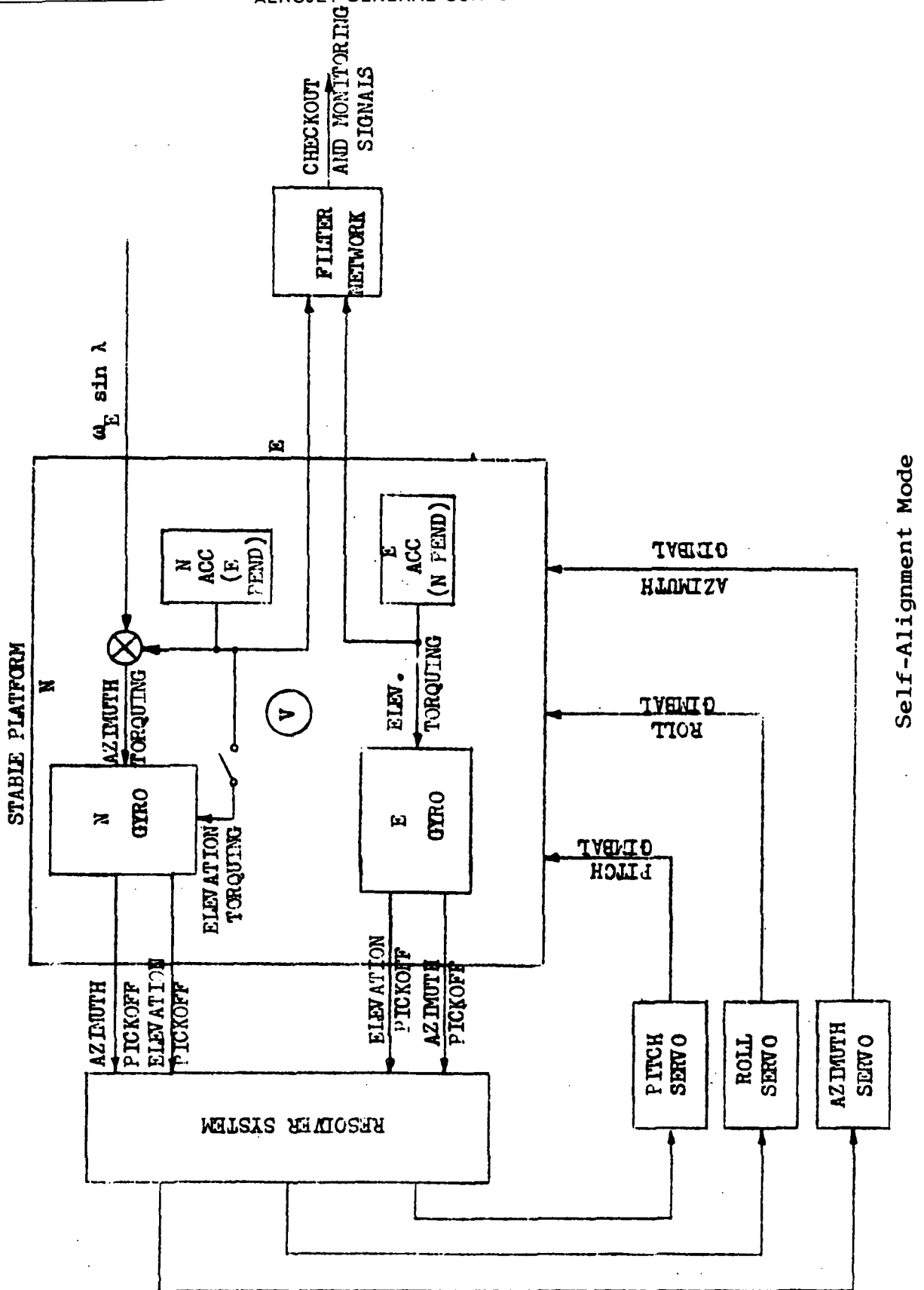
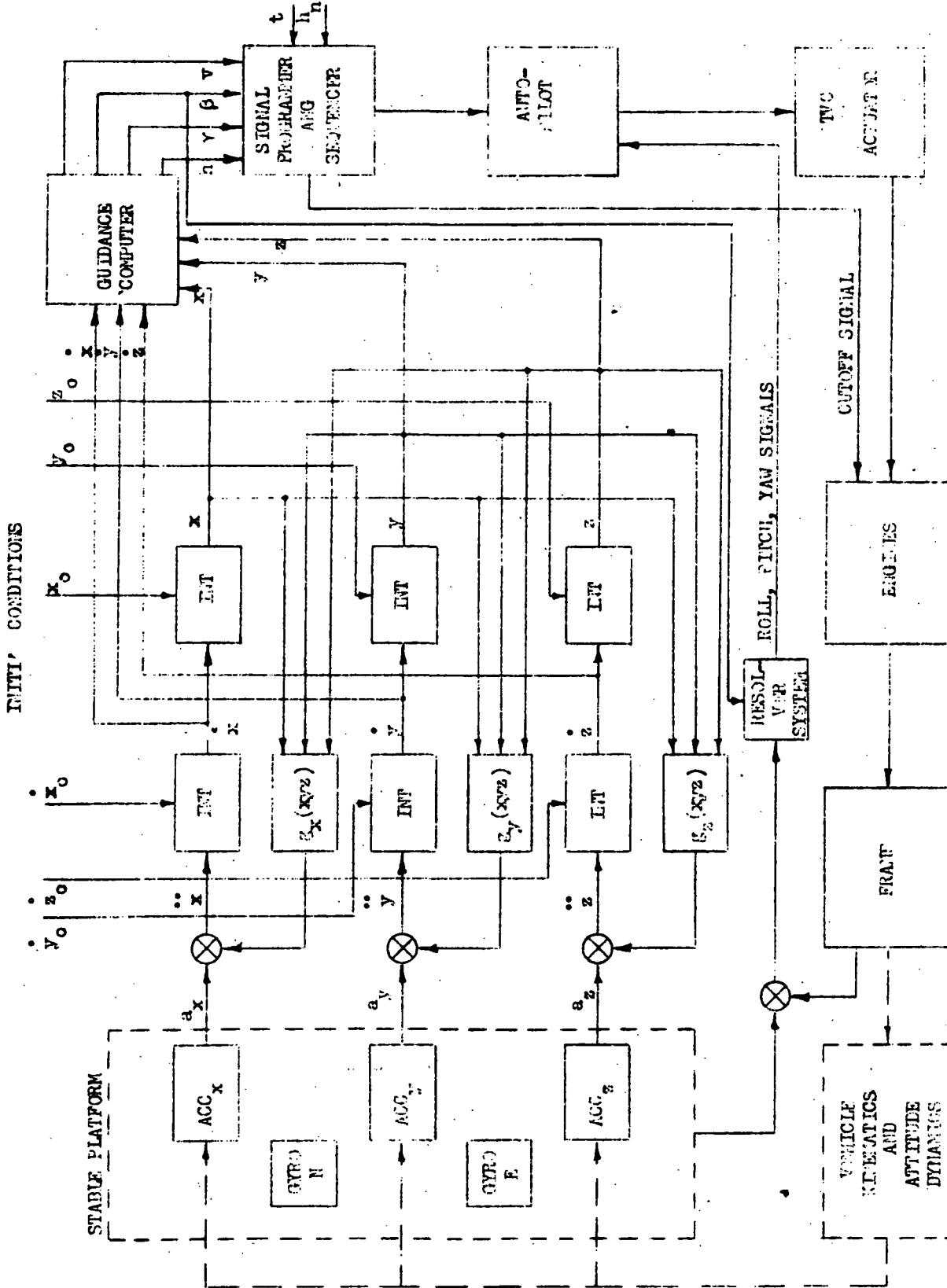


Figure III-F-1

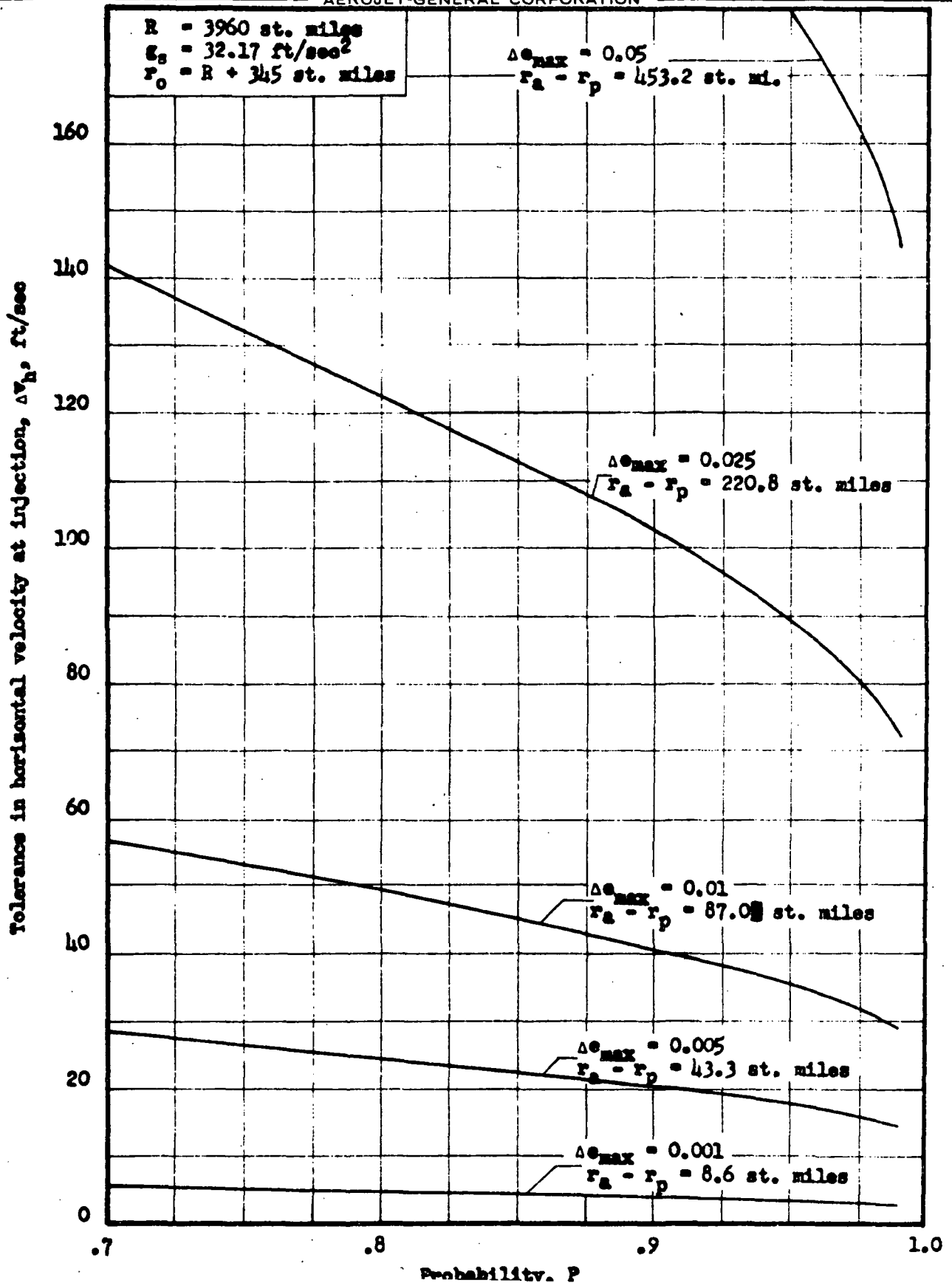


SIMPLIFIED BLOCK DIAGRAM OF INERTIAL GUIDANCE AND CONTROL SYSTEM IN FLIGHT-NAVIGATION MODE

Flight Navigation Mode

Figure III F-2

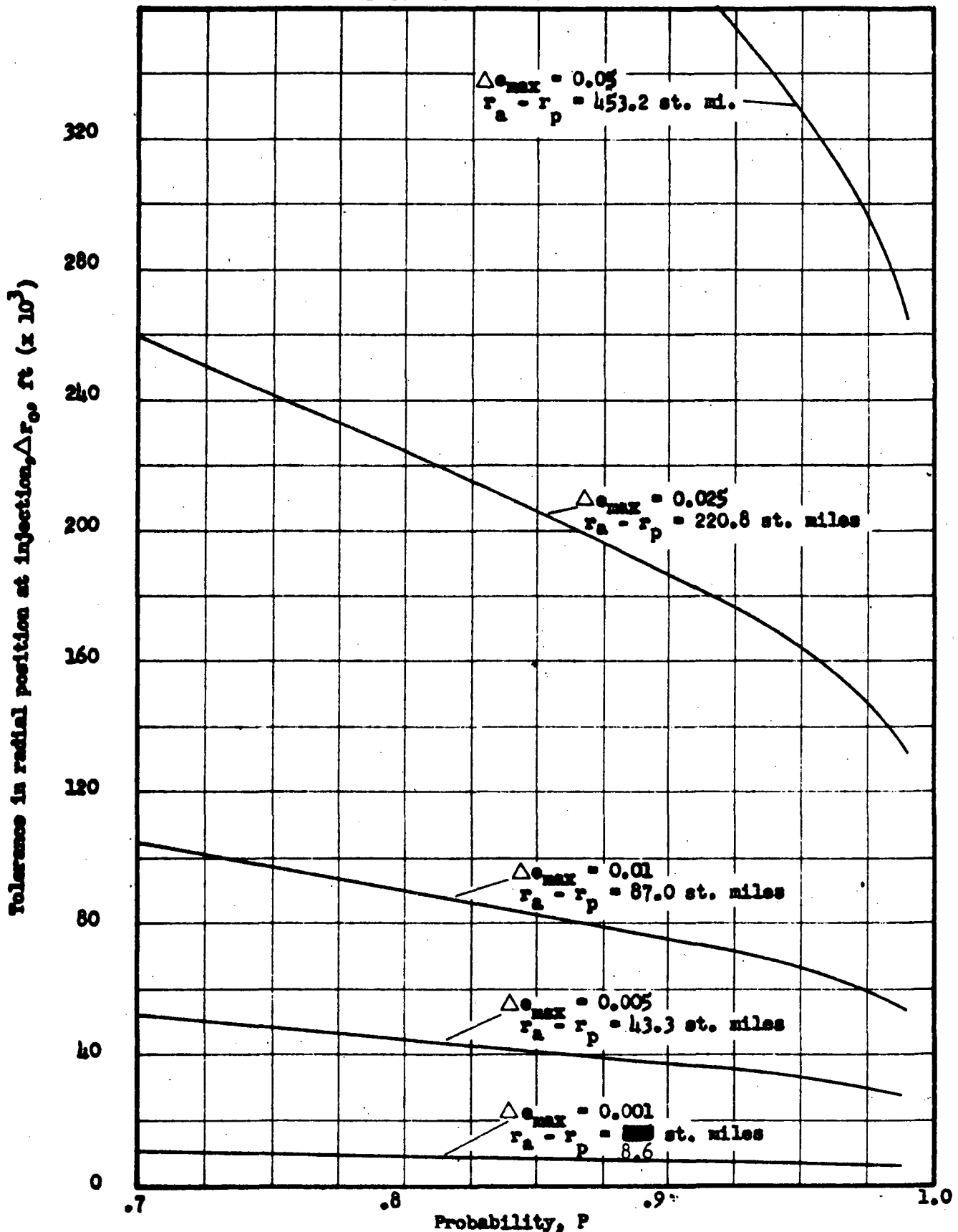
AEROJET-GENERAL CORPORATION



Permissible Error in velocity at Injection Versus Probability of Not Exceeding Tolerances in Eccentricity

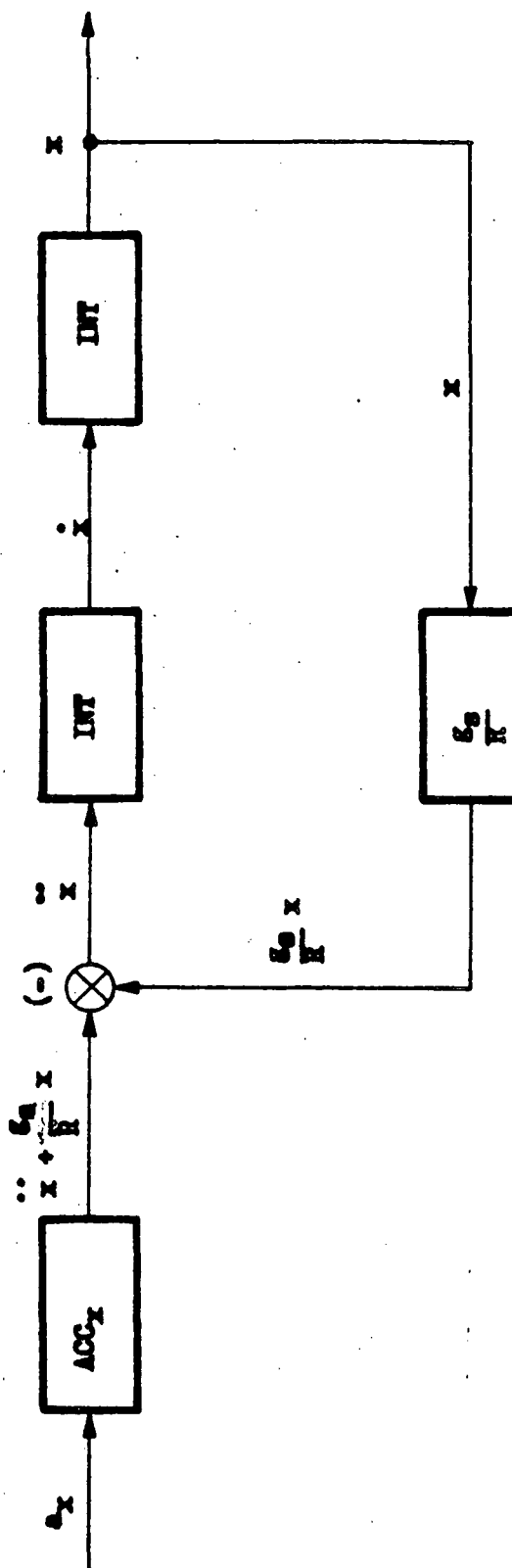
Figure III F-3

AEROJET-GENERAL CORPORATION



Tolerance in Radial Position at Injection Versus Probability of Not Exceeding Given Eccentricity

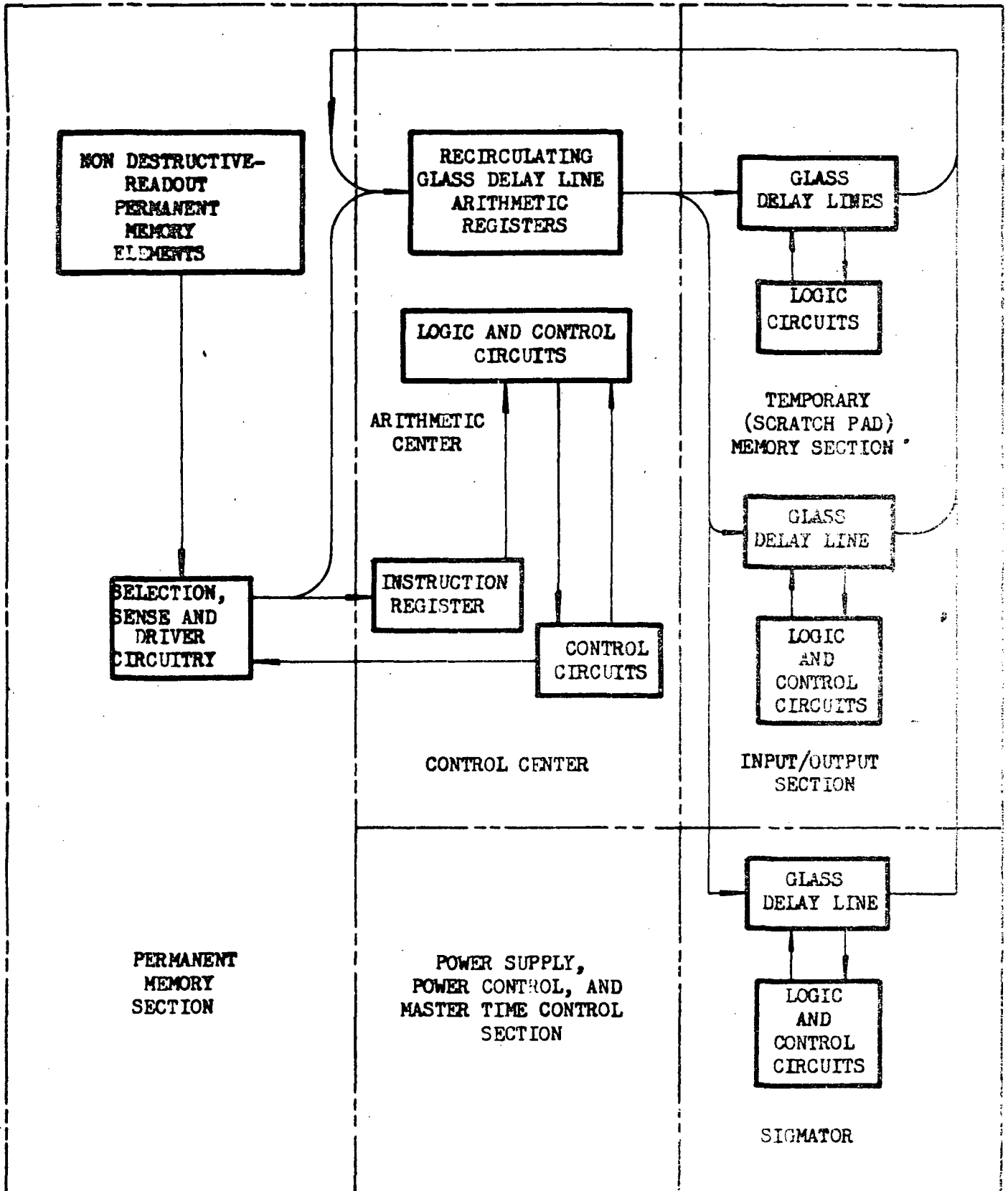
Figure III F-4



Basic Loop of Inertial Guidance System

Figure III-F-5

AEROJET-GENERAL CORPORATION



Block Diagram of L-90 Computer
Figure III-F-7

III, Vehicle Subsystem (cont.)

G. RECOVERY SYSTEM

1. Summary

A recovery system for the Sea Dragon Stage I vehicle has been selected on the basis of operational simplicity and reliability. In choosing the recovery method, advantage was taken of the increased strength of the pressurized booster in overcoming adverse scale effects that tend to make very large vehicles less adaptable to conventional recovery methods. Consideration of this size scale effect showed that for vehicles that are aerodynamically decelerated to a given landing velocity, that the ratio of required "drag diameter" (size of accessory drag device) to vehicle diameter increases as vehicle size increases. Deceleration of the Sea Dragon vehicle to normal let-down velocities of 20 to 25 ft/sec would require a drag device, for example, a parachute 3,000 ft. in diameter. To overcome this problem use was made of the inherent structural strength of the Sea Dragon (a result of using a pressure-fed propellant feed system).

III, G, Recovery System (cont.)

Since the booster tanks are in a pressurized condition (with ullage pressurant) they can react landing loads most efficiently in an axial direction. Therefore, final water impact of the vehicle, regardless of the method used to reach terminal velocity, was restricted to a nose-down, vertical position. Since final deceleration of the vehicle will be caused by water impact forces, analyses of the hydrodynamic pressures and decelerations were carried out so that limiting impact velocities could be established. Pressure distributions over the conical nose of the vehicle were quantitatively predicted and compared with experimental results (Appendix II-22). Deceleration-time histories were developed. For an impact velocity of 600 ft/sec a maximum deceleration of 90g is encountered, and for 300 ft/sec the maximum is 22g (see Figure III-G-1). Assuming a cone half-angle (θ) = 30° analysis of the structural response to impact loads at various velocities showed that for velocities less than 600 ft/sec no dynamic load amplification will occur. Using these facts an allowable impact velocity-tank pressure criterion was established, relating water entry velocity to tank pressure available for axial load reaction, i.e. for a LOX tank pressure of 400 psi an impact velocity of 600 ft/sec can be

III, G, Recovery System (cont.)

accepted. For 100 psi (which is the burnout pressure actually achieved with Sea Dragon) the allowable impact velocity is slightly less than 300 ft/sec (Figure III-G-2).

The basic recovery sequence consists of two main operations: an atmospheric entry phase and a terminal or impact phase. At Stage I burnout the propellant valves in the booster are closed and the pressurant gases are trapped in the tank (somewhat in excess of 100 psi in the LO₂ tank and approximately 290 psi in the RP-1 tank). After staging occurs the first stage coasts upward along its ballistic trajectory and then re-enters the atmosphere. During atmospheric flight drag and stabilization forces are produced such that vertical impact at the proper terminal velocity is achieved.

Three different aerodynamic deceleration methods were considered: parachutes, large first stage nozzle skirt, and inflatable aerodynamic decelerator. Parachutes were excluded because of potential deployment and attachment problems. The large nozzle skirt concept, which made use of a very large area ratio first-stage engine, had the

III, G, Recovery System (cont.)

highest estimated reliability because of its passive operation as a decelerator. However, because of relatively high drag losses during ascent flight, possible nozzle vibration caused by the high degree of over-expansion and separation at low altitude, and adverse reaction to sea operation towing loads, this concept was discarded for the present time.

The inflatable flare decelerator was selected for the Sea Dragon because it provides a high degree of reliability, ease of operation and minimizes the drag penalty during ascent. This device is attached, in deflated package form, to the first-stage thrust chamber. The device is in the form of a large conical flare 300 ft in diameter with a flare half angle of 55° (Figure III-G-6).

The flare is made up of a large, 30-ft diameter torus rigidized with smaller inflatable tubes 10 ft in diameter and covered with a surface generating outer skin. The torus and supporting tubes are constructed of rubberized nylon-dacron reinforced fabric and are protected from any thermal environment by the outer skin. The outer skin

III, G, Recovery System (cont.)

is an ablating rubberized asbestos fabric and is expendable (i.e., it is replaced for each flight). The outer skin is kept in tension and reacts the air loads (design aerodynamic external pressure was 5 psia) by the reaction of the tubes on the torus structure.

The flare structure is inflated to a maximum of 30 psia with pressurant gas from the first-stage fuel tank (the pressurant gas is CH_4). Thus, the need for separate gas supply to inflate the flare is eliminated. The volume of the torus and tubes is such that the fuel tank still has sufficient pressure to react the impact loads.

Maximum temperature on the flare skin during re-entry is approximately $1,000^\circ\text{F}$; however, the asbestos cloth with its ablative covering can resist this temperature pulse without failure.

The flare device represents a weight penalty of 3.8% of recovered weight. This weight increase corresponds to a payload penalty of approximately 1.7%. Total payload penalty due to recovery is 2.5%.

III, G, Recovery System (cont.)

The following sections provide discussion of Sea Dragon stage recovery in more detail.

2. Introduction

Since booster recovery and reuse can play an important role in achieving the low payload delivery costs required for the establishment of truly large scale space programs, emphasis has been placed on developing a recovery concept for Sea Dragon that is simple and reliable in operation and represents a low weight penalty for the vehicle.

The size, weight, and, in part, the complexity of a vehicle recovery system are functions of the allowable touchdown or impact velocity. Conventional boosters require very "soft" landings because of their basic structural design. The Sea Dragon, by virtue of its pressurized tanks, has considerable more structural strength than other proposed vehicles. As a result, it can, in general, withstand higher impact velocities and associated load environments. Thus, the

III, G, Recovery System (cont.)

complexity and weight of the Sea Dragon recovery system should be much lower relative to other systems.

The ability of the Sea Dragon Structure to accept higher impact velocities is a fortunate one since the scale effect for very large boosters, in general, places much higher requirements on a given recovery system. This size-scale effect can be shown quite simply: for recovery methods, which depend on aerodynamic deceleration to final velocity, the ratio of accessory drag device diameter to the vehicle diameter can be expressed as follows:

$$\frac{D_a}{D_v} = \sqrt{\frac{8W}{C_{da} \rho V_i^2 D_v^2} - \frac{C_{dv}}{C_{da}}}$$

where ρ is the atmospheric density, V_i is the impact velocity, C_d is the drag coefficient, W is the recoverable inert weight, and subscripts a and v refer to the accessory device and the booster vehicle, respectively. For geometrically similar bodies with comparable structural efficiencies, we can now write the same diameter ratio as:

$$\frac{D_a}{D_v} = \sqrt{K_1 D_v - K_2}$$

III, G, Recovery System (cont.)

Thus, the drag diameter to body diameter ratio, for a fixed impact velocity, goes up as vehicle size goes up. If the Sea Dragon used conventional low pressure tanks whose inherent lower structural strength required an impact velocity of 20 to 30 ft/sec, the necessary diameter (e.g., a parachute) of the mechanism would be approximately 3,200 feet.

Since the Sea Dragon operation is based on the sea launch concept, final vehicle recovery and retrieval will take place at sea. Thus, in general, final deceleration of the expended booster will be caused by water impact forces. Because the Sea Dragon booster vehicle will take advantage of its increased strength in accepting higher impact velocities, it is important to know quantitatively, the water impact pressures and decelerations.

An analysis of the water entry load environment and vehicle structural response (assuming vertical nose first entry) was conducted. The following sections show a summary of this analysis.

III, G, Recovery System (cont.)

3. Water Entry

a. Pressures and Deceleration During Water Entry

The pressure distribution over the conical nose as a function of immersion depth is shown in Figure III-G-3. This particular graph was computed for an initial impact velocity of 600 ft/sec. The graph may be used for any initial impact velocity merely by using the nondimensional pressure $P' = \frac{P}{\frac{1}{2} \rho_w \mu_o^2}$ where P is the actual static pressure, ρ_w is the density of sea water and μ_o is the initial water entry velocity. As a result, it is seen that the pressure can be scaled according to the square of the initial impact velocity ratio. Thus, the maximum pressure for an initial velocity of 300 fps is approximately 650 psia, and occurs at the apex. Figure III-G-4 shows, for the cone immersion portion of entry, the nondimensional depth of penetration, velocity, and deceleration versus nondimensional time. The immersion depth (I) shown in Figure III-G-3 can be correlated to the proper time of immersion (this is a critical factor in determining the structural response of the cone to the

III, G, Recovery System (cont.)

pressure loads). Figure III-G-1 illustrates the deceleration-time history, during flow establishment over the cone, for several initial entry velocities. Figure III-G-5 shows the complete deceleration history during the entire water entry phase, from initial penetration to maximum penetration.

b. Determination of Allowable Impact Velocities

(1) Propellant Tank Stresses

Using the deceleration-time data from Figure III-G-1, a criteria for determining allowable impact velocity was established: the structural response of the empty booster was analyzed, and it was found that the first mode longitudinal natural frequency was 30 cps and the first mode bending frequency was 13 cps. Comparing these frequencies with the impact frequency of the water entry loading (Figure III-G-5) we see that no dynamic load amplification is probable for velocities less than 500 ft/sec (Section V,B,9 gives a more detailed analyses of the dynamic response of the booster structure

III, G, Recovery System (cont.)

during water entry). Therefore, using a dynamic load amplification factor of one, we can establish a general criterion relating impact velocity with internal tank pressure required to react the associated water entry loads. This criterion is based on the assumption that the cylindrical tank wall cannot accept any compressive stresses. Thus, we equate the compressive stresses, caused by the maximum deceleration inertia loads to the longitudinal tension stresses due to internal pressure. Figure III-G-2 shows the results of this calculation. Using this graph we can select the proper impact velocity for the available internal pressure. For the pressurization system used in this design, the LO₂ tank pressure at burnout is approximately 100 psia. From Figure III-G-2 it is seen that an impact velocity of 300 ft/sec must be obtained. Based on this velocity and the associated pressures and acceleration, the remaining vehicle structure (nose cone and components) were examined.

III, G, Recovery System (cont.)

(2) Conical Nose

(a) Stresses

Using Figure III-G-3 and reducing the pressure for an impact velocity of 300 fps, the dynamic stresses in the conical nose were analyzed. Preliminary results show that the stress levels in the tank wall during impact are below the yield value, except in an area near the cone apex.* Stresses at this point may exceed the failure point and a reinforced apex may be required. However, the extent of the area over which this condition exists is small (approximately 10 feet) and the weight penalty is negligible.

(b) Stability

Experimental results from the Aerojet-General water entry test facility show that material failure is

* It was also shown that membrane stresses, rather than bending stresses, are predominant.

III, G, Recovery System (cont.)

not the design criteria for nose cones such as used on Sea Dragon but rather that geometric or buckling instability is the mode of failure (as might be expected). While complete mathematical analysis of the buckling problem has not been completed, it has been shown by a simplified analysis that some stiffening will be required to stabilize the cone under the transient pressure loading. However, the weight penalty due to installing circumferential T-type stiffeners is small; 8% of total cone shell weight and approximately 2.2% of the first-stage inert weight. For stability purposes, it was found that approximately ten stiffener rings were required. Spaced equally between a point approximately $6\frac{1}{2}$ ft from the apex and the cone base. The stiffeners were of thickness t , equal to the shell skin thickness, and depth of $10 t$ and flange width of $5 t$.

(c) Vehicle Components

A major factor in the structural integrity of vehicle subassemblies is the amplification of the input acceleration pulse by vehicle resonances. For subassemblies whose

III, G, Recovery System (cont.)

mass is small relative to the vehicle, the input is more easily described as an acceleration pulse at the base of their tie-down structure. This acceleration is a function of the amplification in the longitudinal mode and the location of the tie-down structure in the mode shape. Components and subassemblies that are highly sensitive to these loads will be located as close to the nodal point of this mode as possible. Preliminary study of the subassembly attachments under a 22g deceleration pulse showed that stiffening and beefup structure would be required, which would impose a weight penalty of 2.0% of booster inert weight. Consideration of the thrust chamber dynamic interaction with the gimbal joint and tankage indicated that structural stiffening of the gimbal joint would be required. The weight penalty due to the required increased structural strength is approximately 0.5% of booster inert weight.

4. Selection of Aerodynamic Deceleration Device

After preliminary investigation, three basic recovery systems were selected for study: inflatable aerodynamic decelerator;

III, G, Recovery System (cont.)

large nozzle flare; and parachute. All of the systems studied, with the exception of the large nozzle, were required to yield impact velocities of 300 ft/sec, the allowable velocity based on available tank pressure for structural stability (Figure III-G-2). In each case the same basic recovery operation was followed: the first-stage vehicle after burnout continues along its ballistic trajectory, re-enters the atmosphere and impacts on the ocean surface at terminal velocity. The basic objective in selecting a particular recovery system is to provide means for attaining the proper aerodynamic stabilization and drag for the given impact conditions. The aerodynamic decelerator was chosen as the most promising system based on overall reliability, weight, and performance. A brief discussion of each concept is presented below.

a. Parachutes

For recovery of the Sea Dragon first stage booster with a single parachute, a diameter of 270 feet would be required to attain the required impact velocity. Preliminary estimates indicate that a complete recovery system weight, including a 45 foot drogue

III, G, Recovery System (cont.)

parachute and tank reinforcement would be approximately 3.0% of the total recovered weight. Supersonic deployment, at Mach number 1.8 to 2.0 of the drogue chute was assumed. Use of several smaller chutes was considered, but the total weight of a clustered system was approximately the same as a single chute system. It was also concluded that the deployment reliability of a clustered system was lower than for a single chute.

Even though the parachute system appeared very favorable from a weight standpoint, some important disadvantages were found in the area of initial atmospheric entry and deployment: the Sea Dragon booster, without accessory devices, has poor aerodynamic stability and at best is neutrally stable. Thus with a tumbling re-entry, as must be the case because of staging tipoff torques, the problem of parachute deployment is a serious one. The prediction of tumbling rates during entry is very difficult. Whether or not stable equilibrium at some angle of attack is reached before impact also poses an involved analysis program. Thus, attitude and rate sensors must be used in the booster so that parachute ejection and deployment

III, G, Recovery System (cont.)

can be sequenced properly. If low drag fin type stabilization devices are used to provide sufficient stability for a stable flight path, the rapid descent of the booster allows insufficient time for parachute deployment, i.e., for a stabilized (with fin) descent, a Mach number of 1.8 is reached 105 sec after initial entry. At 113 sec impact occurs. Thus, there is a very short time interval in which parachute deployment, even at supersonic Mach numbers, can occur. Deployment at higher speeds presents severe problems in parachute stability and deployment (NASA TN D752). Therefore, based on overall ease of operation and reliability, the parachute, for purposes of this effort, was not considered further.

b. Large Nozzle Flare

In seeking a recovery system with the highest reliability possible, a system with almost complete passive operation was investigated. The configuration studied was the basic Sea Dragon first-stage with a very large area ratio nozzle. The function of the large nozzle was to provide re-entry stabilization and drag forces that

III, G, Recovery System (cont.)

would give the proper velocity and attitude at impact. For this particular system, the exit diameter required for 300 ft/sec was impractically large from a structural and thrust coefficient standpoint so a modification in pressurization system was assumed and a tank pressure of 400 psi was assumed to be available. Thus, from Figure III-G-2 we see that a velocity of 600 ft/sec can be accepted. For this case, a nozzle diameter of 175 ft is required (for a 20° half angle conical nozzle). The payload penalty associated with the additional drag losses during ascent, increased nozzle weight, additional beefup of components, I_s loss caused by over-expansion, and increased outage gas weight was approximately 18%. It was decided, for this study, that the payload penalty and the additional fabrication and other associated problems over-shadowed the high recovery reliability available with this system. However, a final selection of any recovery system will rest upon the results of a detailed cost effectiveness study for each recovery method.

III, G, Recovery System (cont.)

c. Inflatable Aerodynamic Decelerator

Based on (a) and (b) above, a recovery system was designed which attempts to incorporate a high degree of reliability with reasonable weights and deployment simplicity. As a result, an inflatable aerodynamic decelerator was chosen to provide the necessary drag and stability during atmospheric entry and still enable the Sea Dragon to have a reasonably high performance capability. The detail design of this device is described in Appendix II-15. Basically, it is an inflatable conical flare attached to the thrust chamber of the booster (see Figure III-G-6). The base diameter of the flare is 300 ft and provides an impact velocity of 300 ft/sec. The flare is made up of a large, 30-ft diameter torus made rigid with smaller inflatable tubes 10 ft in diameter and covered with a surface generating outer skin. The torus and supporting tubes are constructed of rubberized nylon-dacron reinforced fabric and are protected from any adverse thermal environment by the outer skin. The outer skin is an ablating rubberized asbestos fabric that is replaced for each flight. The outer skin is kept in tension and reacts the air loads (design aerodynamic external pressure was 5 psia, by the reaction of the tubes on the torus structure.

III, G, Recovery System (cont.)

The flare structure is inflated to a maximum of 30 psia with pressurant gas from the first stage fuel tank (the pressurant gas is CH_4). Thus, the need for separate gas supply to inflate the flare is eliminated. The volume of the torus and tubes is such that the fuel tank still has sufficient pressure to react the impact loads.

This concept was chosen as the Sea Dragon booster recovery system. It provides low terminal velocity and high aerodynamic stability yet presents no drag penalty during ascent. The weight of the complete flare system constitutes approximately 3.8% of the total recovered weight. The basic vehicle can withstand the impact loads without additional stiffening*, however, some stiffening will be required in component attachments and gimbal joint which should be charged to the recovery system. This weight amounts to approximately 2.5% of inert weight. Therefore, the percentage of total recovery system weight to recovered weight is approximately 8.5%.

* With the exception of the nose stiffeners which constitute 2.2% of inert weight.

III, G, Recovery System (cont.)

This is a lower figure than those reported for other types of recovery systems (15% of inert weight and higher) and derives from the fact that the requirement on impact velocity is drastically reduced here due to the structural design of the Sea Dragon. Thus, this recovery system will have an associated payload penalty (for a 300-min orbital mission) of 2.5%. The advantage in using a vehicle whose strength allows higher impact velocities is readily apparent. In addition, the use of a pressure fed fuel system eliminates the need of carrying separate flare inflation gas since, in the case of the Sea Dragon, the tank pressurant gas required for the propulsion phase is available for flare inflation.

(1) Operational Sequence

(a) Flare Deployment

Upon attainment of first stage burnout conditions (velocity 5,800 ft/sec, altitude 125,000 ft), the staging sequence occurs and the expended booster coasts upward along

III, G, Recovery System (cont.)

its ballistic trajectory. Immediately after staging the forward extended skirt is detached and the outer fabric cover which contains the deflated flare structure is ejected. When the dynamic pressure has reached a value of 10 lb/ft^2 (17 sec after staging) inflation of the flare structure begins. Methane gas from the fuel tank is passed through a pressure regulating valve and into the flare. The structure is fully inflated, to a pressure of 1 psi, in approximately 100 sec. At this time, the vehicle has reached its apogee (335,000 ft). Pressurization of the flare continues and at approximately 200 sec from inflation initiation, the flare is pressurized to its design value of 20 psia. At this time, the altitude is 182,000 ft, the trajectory flight path angle is 33° below the local horizontal, the velocity is 5,450 ft/sec and the dynamic pressure is 15 lb/ft^2 .

(b) Atmospheric Entry

Atmospheric entry of the Sea Dragon booster stage "effectively" occurs at an altitude of 200,000 ft. At this point, the velocity is 5,350 ft/sec and the flight path angle is

III, g, Recovery System (cont.)

30° below the local horizontal. Tumbling of the vehicle, due to initial tipoff forces at staging will begin to affect the vehicle trajectory at this point; however, because of the high aerodynamic stability and damping of this configuration, the tumbling motion will subside rapidly and the vehicle will attain a stable flight path at, or around a zero angle of attack. As mentioned above, the flare structure is not fully pressurized to its design pressure of 20 psia until the vehicle reaches an altitude of 182,000 ft. The flare, however, is fully inflated at all times during entry and the internal pressure at all times far exceeds the external flow field static pressures.

During the subsequent descent trajectory, the following maximum conditions are experienced by the vehicle. The maximum stagnation radiation equilibrium temperature (on the 7-ft diameter blunt nose cap) is 1,390°F. Temperatures on the flare structure, assuming no ablative materials, are not expected to exceed 900°F. If an ablative outer skin is used, temperatures within the flare on the torus and tubes will be in the order of 250°F maximum. The maximum dynamic pressure is 300 psf and the maximum deceleration is 6.5g's.

III, G, Recovery System (cont.)

(c) Impact Conditions

An impact velocity of 300/sec and a flight path angle of 89° from the horizontal (1° off vertical) are the end conditions for the atmospheric trajectory described above. Oscillatory motions of the booster are damped out; thus, for a still air condition, the water entry angle of attack is zero prior to impact. The effect of surface winds in the splash area could conceivably give rise to an angle of attack in the order of six degrees for a 30 ft/sec surface wind, however, due to the slow response of booster to such drift effects, the angle of attack will never be greater than 3.0 degrees.

(d) Maximum Underwater Penetration

Since the effective density of the empty booster is quite low, the penetration of the vehicle for an initial velocity of 300 ft/sec will be relatively small, approximately 45% of total first stage length.

III, G, Recovery System (cont.)

density is defined here as total weight divided by the cube of the tank radius times the density of water. Thus, the flare structure will not be subjected to hydrodynamic loads.

The action of buoyant forces will eject the vehicle upward after maximum penetration. The cone apex will rise approximately 30% of one body length above the surface.

Reimpaction will occur at a velocity of 35 ft/sec. Structural loading due to reimpaction will be very low. Angular rotation of the booster during this "pop up" period will cause lateral as well as axial loading; however, the combined effects are not expected to be nearly as severe as those at first impact.

5. Second-Stage Recovery

Recovery and reuse of the second stage vehicle has been studied. The general method that was used to effect recovery of

III, G, Recovery System (cont.)

the first stage could be applied to upper stage recovery as well. In this case, a conical nose would be incorporated in the second stage.

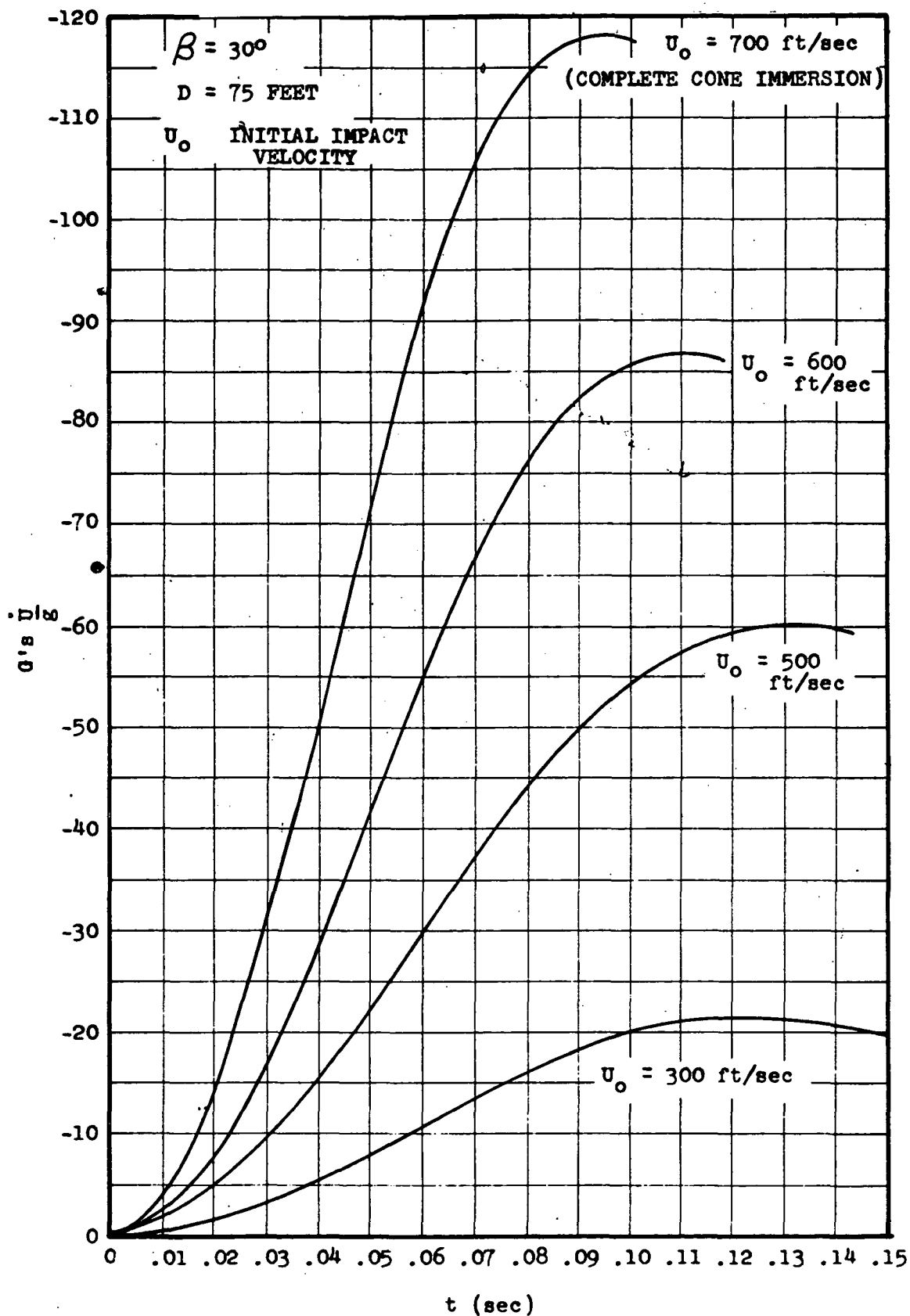
Since the second stage auxiliary engines provide orbital injection thrust for the payload, the second stage will go into orbit with the payload. During ascent into orbit and after the second stage main engine has ceased firing, the expandable nozzle skirt will be separated and ejected from the vehicle. After attaining orbital condition, the payload and expended second stage will be separated. When the second stage has reached the proper position, small retro rockets in the nose will be fired to eject the vehicle out of orbit. A velocity impulse of 480 ft/sec will be required to give an initial re-entry angle of 2.0° from the local horizontal.

Aerodynamic stabilization and deceleration of the vehicle will be attained with an inflatable flare identical to the one used for first stage recovery. However, the size of the flare will be smaller than the device used on the first stage since, even

III, G, Recovery System (cont.)

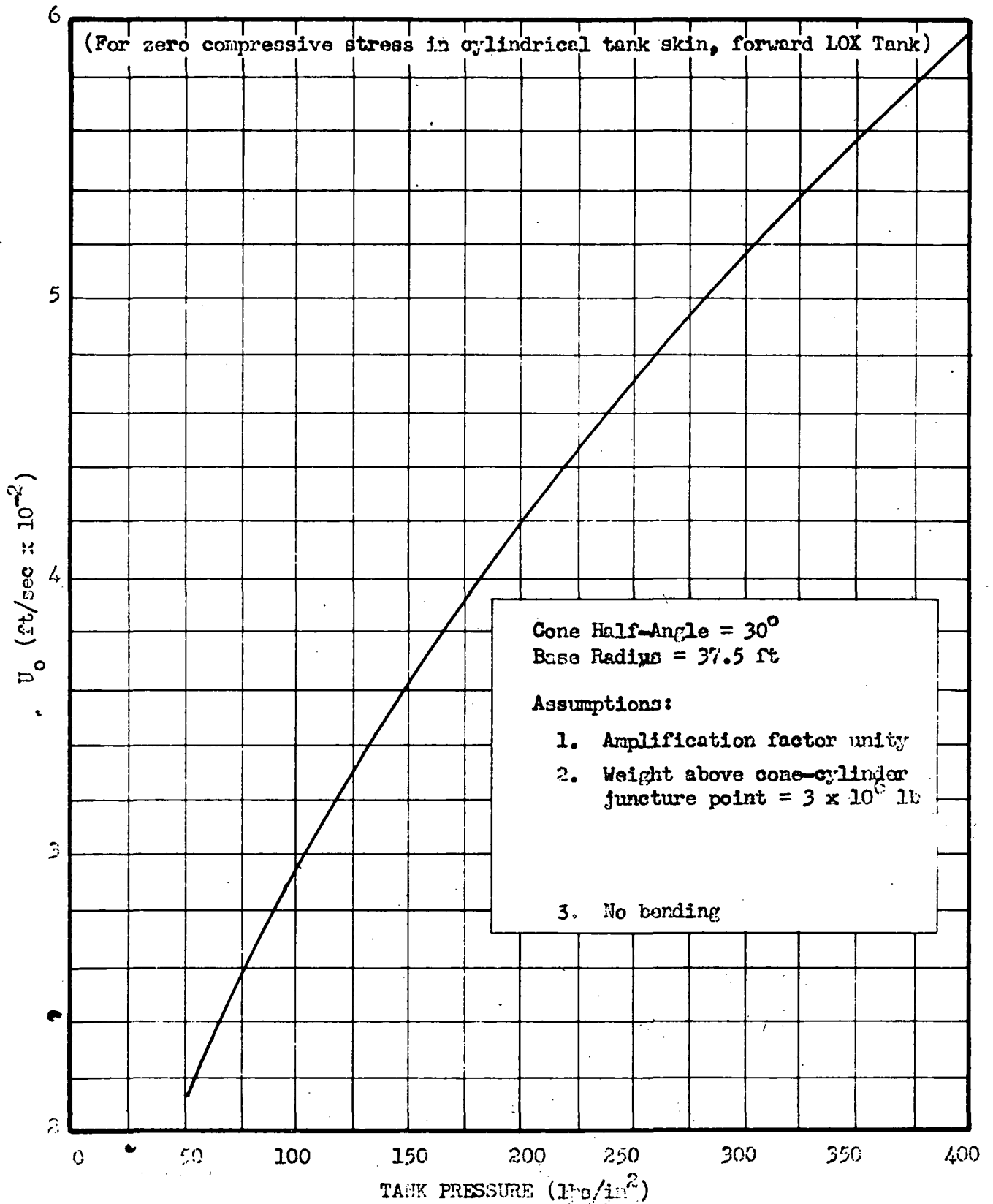
though the estimated available tank pressure is lower, 50 psi, the recovered weight is also lower, 1.2×10^6 lb. With 50 psi tank pressure available for axial load reactions at impact a terminal velocity of 210 ft/sec can be allowed. The flare diameter required is 240 ft.

Aerodynamic heating for second stage recovery will of course be more severe than for first stage. Use of material with higher thermal resistance, such as Rene 41 mesh and ablative coatings, will be necessary.



Deceleration versus Time

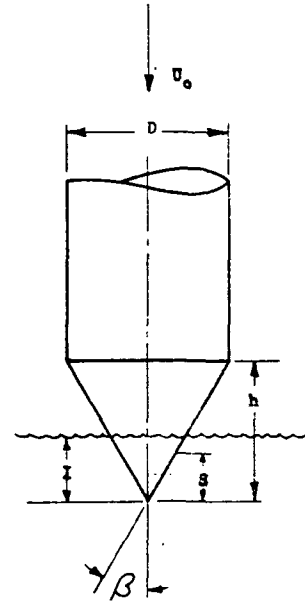
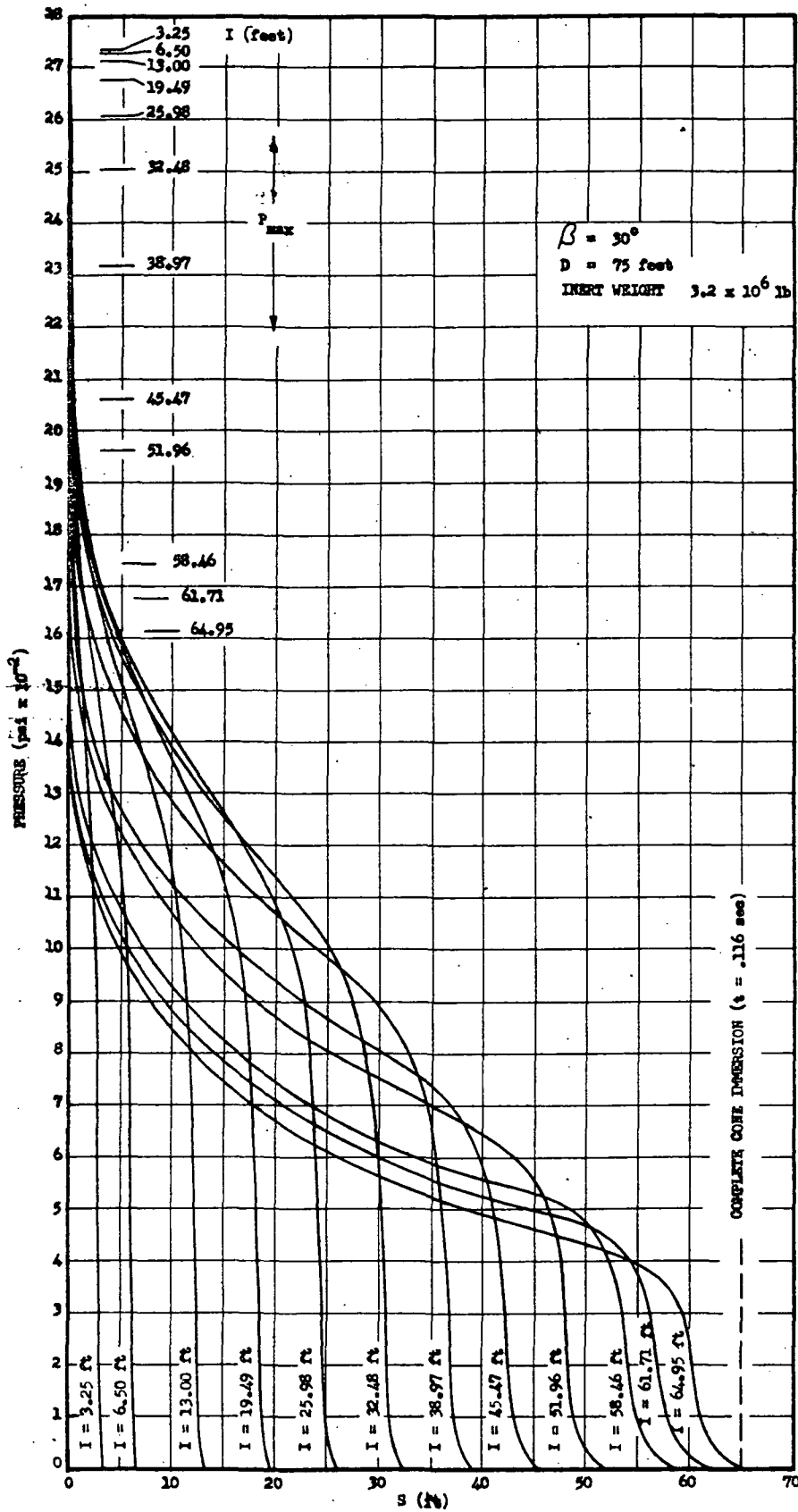
Figure III-G-1



Tank Pressure versus Critical Impact Velocity

Figure III-G-2

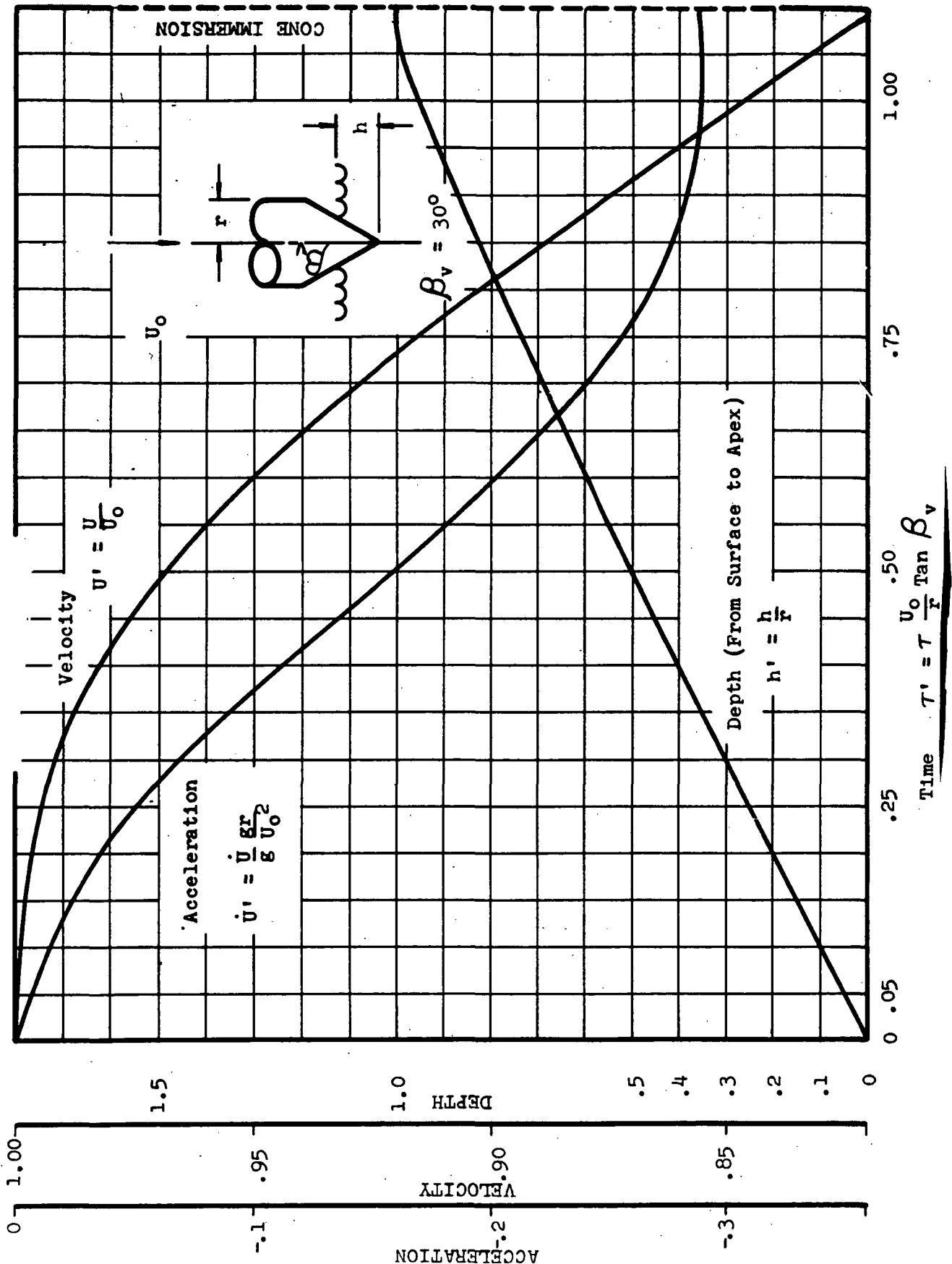
AEROJET-GENERAL CORPORATION



Pressure Distribution at Various Core Immersion Depths

Figure III-G-3

AEROJET-GENERAL CORPORATION



Water Entry Parameters versus Entry Time

Figure III-G-4

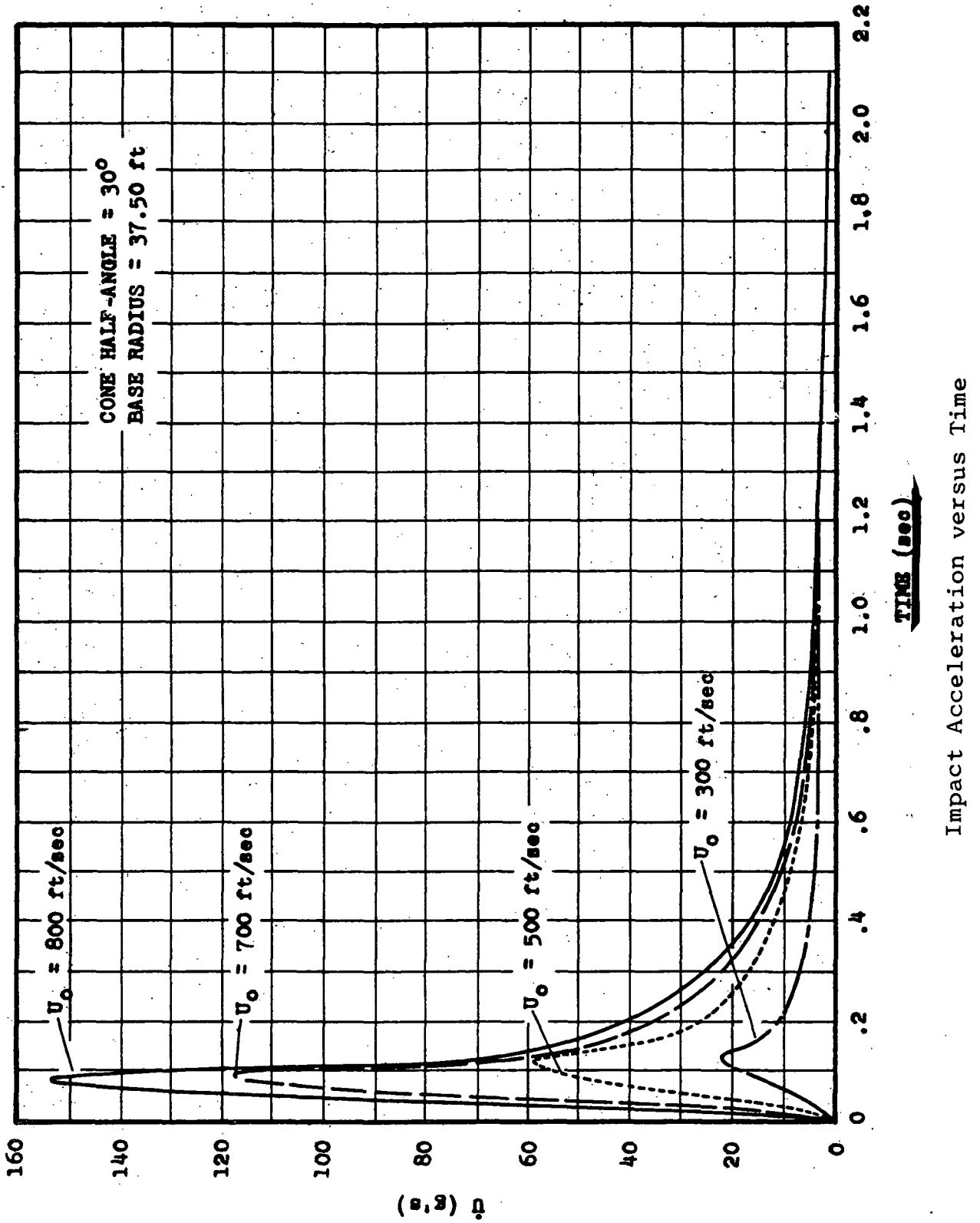
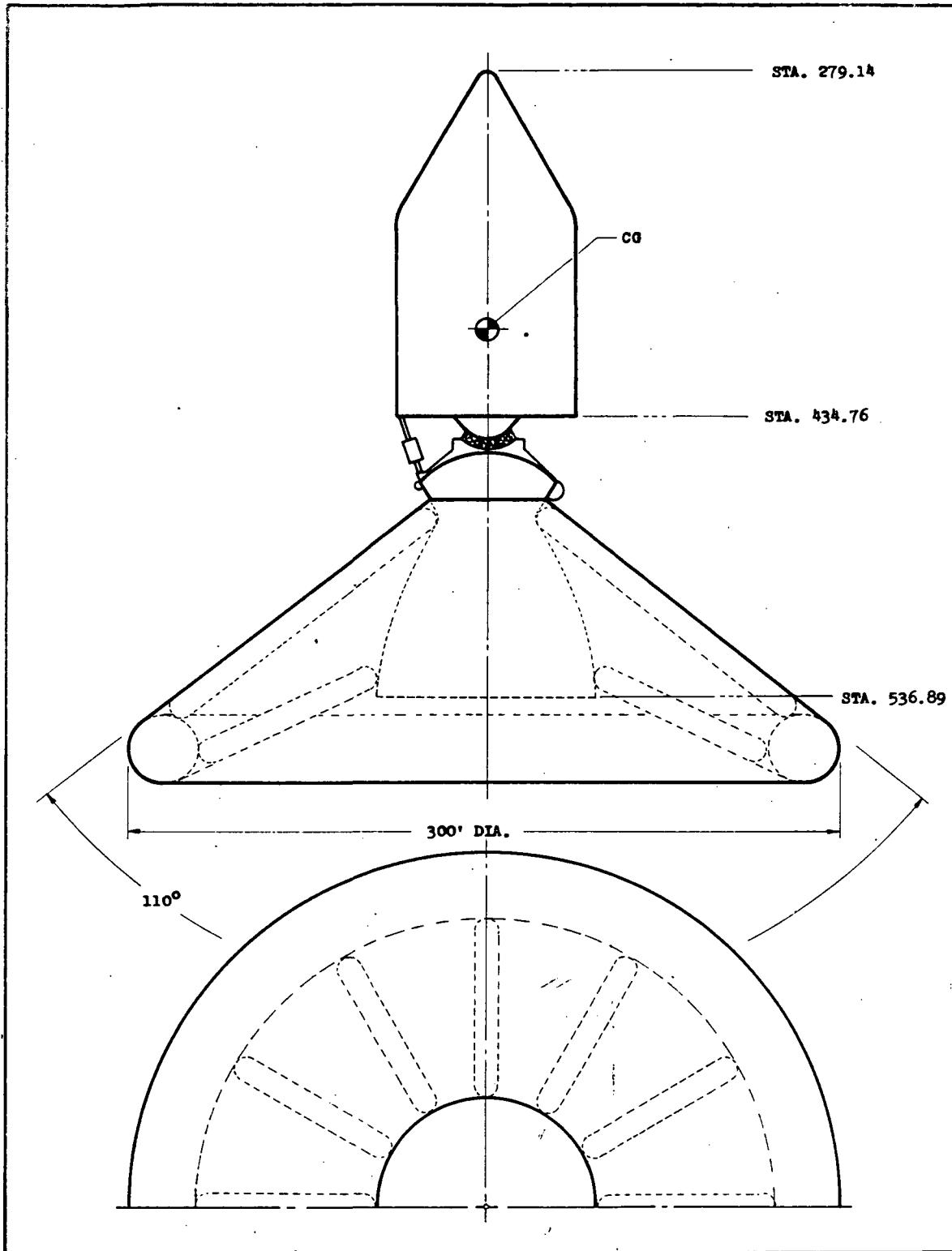


Figure III-G-5



Stage I Recoverable Configuration

Figure III-G-6

III, Vehicle Subsystems (cont.)

H. SECONDARY SUBSYSTEMS

1. Summary

This section concerns power supplies and the ordnance systems because their functions extend throughout the vehicle.

Batteries have been tentatively selected for use as the electrical power source for this vehicle; there is no need for a central hydraulic or pneumatic power supply. The first-stage engine gimbal actuator utilizes RP-1 fluid power and no separate hydraulic supply is required. The use of hydrogen-oxygen fuel cells or other electrical power systems may be indicated after the total vehicle power requirements are determined. No attempt was made to develop this data for this study. The ordnance system will be integrated for optimum safety, check-out, and reliability. Positive mechanical safe-arm mechanisms will be provided for each ordnance item.

III, H, Secondary Subsystems (cont.)

It has been assumed that many of the minor subsystems and some of the major ones will have hardware and operational techniques developed and available from current space programs by the time the Sea Dragon program starts, and that these will be adapted for this program. Therefore, some of the concepts portrayed in this section and throughout the report will later be influenced by future developments in the state of the art and will be improved accordingly. However, the currently available techniques can be adapted to make adequate and feasible subsystems without development of new techniques.

2. Power Supplies

The main power supplies for the vehicle during flight will be located in the compartment between the forward end of the second stage and the aft end of the payload. Power converters will be used to convert the direct current battery power into alternating current as required for the various subsystems of the vehicle. Separate power supplies will be provided in the command module and its service module for their operation after separation from the vehicles. Also a separate power supply will be provided on the first stage for recovery operations.

III, H, Secondary Subsystem (cont.)

During the towing of each individual stage, electrical power will be supplied externally from the towing ship. After assembly into the complete vehicle, power will continue to be supplied from an external source until the service vessel leaves the erected vehicle late in the countdown.

Before final prelaunch checkout, the vehicle power supply batteries will be activated and the external power supply disconnected. This final checkout will be performed using vehicle flight power; the external power for vehicle functions will not be reconnected except during an extended delay in flight operations.

The first-stage power supply for recovery purposes will be a battery pack that will be checked out prior to launch, but will not be used until after separation of the first stage. This power supply will provide power for all functions of the onboard recovery system.

III, H, Secondary Subsystems (cont.)

The main functions that will be controlled by the sequencing equipment are jettisoning of the forward interstage structure by means of explosive charges; inflation of the recovery flare bag; telemetry throughout the recovery phase including impact; and signalling of the location of the first stage after impact by active location aids.

The onboard equipment for the first stage will be rugged enough to withstand the landing impact. The battery pack will be made of dry cells potted in plastic; the sequencing equipment will be especially designed for the purpose and will be shock mounted to attenuate the shock.

All major external electrical wiring will be contained in conduits that are pressurized with dry nitrogen gas, and a replenishment system will maintain the pressure. The replenishment rate will be monitored to assure there are no leaks in the system.

III, H, Secondary Subsystems (cont.)

3. Ordnance System

Several vehicle and propulsion systems functions that will be accomplished by means of various types of ordnance items are:

- a. Command module abort propulsion system
- b. Posigrade and retrograde propulsion systems in the service module for the command module.
- c. Command module abort separation system
- d. Command module re-entry separation system
- e. Interstage (Stage I/II) separation system
- f. Propulsion system valve operating devices
- g. Ballast staging devices
- h. First-stage recovery operation devices

There will be an integrated ordnance system that includes provisions for checkout of all items and for operations as commanded by the guidance computer and sequencing equipment.

III, H, Secondary Subsystems (cont.)

Positive mechanical safe and arm provisions will be made for all ordnance items to prevent inadvertent firing. These safe and arm mechanisms will be operated remotely by electrical signals and will be monitored as to position. These mechanisms will be reversible to provide for operational checkout and for safety after checkout.

The first-stage recovery operation devices will operate after separation from the vehicle, and therefore will operate separately with its own sequencing system and power supply. However, the checkout procedures and equipment will be integrated with those of the vehicle.

III, Vehicles Subsystems (cont.)

I. BALLAST UNIT

1. Summary

The ballast unit consists of a structural assembly of six cylindrical tanks and support struts. The forward structural element is an orifice that provides a control of thrust chamber environment for underwater operation. The ballast unit as attached to the first-stage thrust chamber assembly and with struts to the aft skirt provide aft-end flotation for sea handling of the vehicle. The ballast tankage when filled with a heavy fluid (specific gravity =2) provide balancing mass that erects and stabilizes the vehicle in the vertical launch attitude. Provisions exist for staging the ballast during the ignition sequence as shown in Figure II A-2.

2. Description and Function

The ballast unit as shown in the Stage I drawing consists of a structure that interfaces with the aft end of Stage I thrust chamber assembly at Station 536. A structural separation

III, I, Ballast Unit (cont.)

point is provided. The forward support structure for the ballast tanks includes reaction points for the struts. The ballast support struts are four A-frame links that span from reaction points on the ballast structure to fittings on the aft skirt of the vehicle at Station 432. The function of the ballast and strut assembly is illustrated in Figure II-A-2.

a. Forward Structure

The forward ring structure of the ballast interfaces with the internal surfaces of the thrust chamber assembly at Station 516 where it is sealed and aft to Station 536. The ring is ported at its center at a diameter of approximately 46 ft., which provides a port area ratio relative to the engine throat of 1.2. This port will be sized to produce pressures in the skirt area of the thrust chamber that are higher than the ambient pressure. The ring is ported at six places for duct access to each of six ballast tanks. The ducts admit chamber gases to the ballast tank ullage during ballast

III, I, Ballast Unit (cont.)

fluid expulsion. The forward port on the ballast tanks (aft end of the duct) will be sealed with a diaphragm that ruptures when exposed to pressures in excess of design values or when failure is initiated by explosive means.

b. Ballast Tanks

Six ballast tanks are attached at their forward end to the forward ring structure. The tanks are sized to contain a fluid of specific gravity of 2 and produce, when fully loaded, an underwater weight of 10×10^6 lb. The 28 ft diameter cylindrical tanks are 24 ft long between tangents of the hemispherical end closures. The ballast tanks are designed to withstand an internal pressure of 150 psig and will be pressurized to avoid crushing pressure differentials. The aft closure on each ballast tank is ported and sealed with a diaphragm that will rupture when design pressures are exceeded, or when failure is initiated by explosive means. The aft port will be sized to control heavy fluid expulsion at rates desired for the underwater trajectory. Each tank provides the mounting for structure that distributes concentrated loads from the ballast support struts. Attachment

III, I, Ballast Unit (cont.)

fitting are provided for plumbing lines as required to fill and vent the ballast tankage. Flotation devices will be installed that enable returning the ballast unit to a buoyant condition following vehicle launch. These devices can be flotation bags inflated with air from ground equipment.

c. Ballast Support Struts

The ballast support struts are A frames constructed of tubular elements interconnected by webs. The base of aft end of the A frames attach to pins on the ballast assembly; the forward ends attach to fittings on the aft skirt of the vehicle. The struts transmit all axial and shear forces developed during all handling modes to the aft skirt. The A frames are provided with hydrodynamic plates inclined to the longitudinal axis of the vehicle, which rotate the struts outboard during the underwater trajectory after separation of the struts at their forward end from the fittings on the aft skirt of the vehicle.

III, I, Ballast Unit (cont.)

3. Evaluation and Recommendations

The functions provided by the ballast unit are necessary for the handling and launching of the Sea Dragon Configuration 135. Additional functions that are felt to be desirable if not necessary, have not been attainable at this point in the design development of Sea Dragon. Ballasting, in flotation and in weighing are enabled by the unit; hard points for towing and protection for accessory flotation devices are provided. It is estimated that 50% of the aft skirt weight is necessary to provide the structural reactions for the ballast unit. This is equivalent to a payload penalty of 3000 lb.

Although the present design allows several seconds between main engine ignition and commitment to flight, it would be desirable to add a thrust spoiling capability. During the ignition transient, it is considered desirable to maintain the vehicle in a stable condition at zero velocity until engine performance quality is established. Thrust spoiling would enable shutdown with the vehicle in a manageable condition if ignition transient criteria are not met.

III, I, Ballast Unit (cont.)

a. Alternative Approaches

The design of the ballast unit is on the basis of requirements derived from the vehicle design and its environment; flexibility appears to exist only in its operational sequence. Alternate ballast designs exist primarily for different vehicle designs.

b. Struts and Strut Staging

The ballast unit design for Configuration 135 includes struts that serve the purpose of avoiding a weight penalty on the vehicle for the structure required to react the gimbal loads associated with handling. The flight gimbal moments are estimated to be 62×10^6 ft lb. The gimbal moments resulting from handling of the vehicle with the ballast attached to the trailing edge of the thrust chamber assembly only (no struts) will be 1000×10^6 ft. lbs. This moment would have to be reacted with the vehicle structure and actuation components at a significant weight penalty. The requirement for struts exists only where the thrust chamber is articulated. The

III, I, Ballast Unit (cont.)

current operational concept for the ballast staging is illustrated in Figure II-2. The struts are retained in structural interface with the ballast and vehicle to the point in the ignition sequence where an orderly shutdown could be accomplished. The attached struts prevent structural damage to the chamber on such a shutdown.

An alternate possibility involves staging the struts prior to the initiation of the first-stage main engine ignition sequence. Staging of the struts early simplifies the underwater trajectory, but affords limited potential for orderly shutdown after the main engine ignition sequence has started.

c. Ballast Design and Thrust Chamber Loads

The current ballast concept includes an orifice plate located near the trailing edge of Stage I thrust chamber assembly. The orifice plate will be designed to maintain positive pressures in the thrust chamber during the underwater trajectory. The ambient pressure at start is 135 psig and pressure control must be maintained to the sea surface where the pressure is 0 psig. The thrust

III, I, Ballast Unit (cont.)

chamber skirt must be designed for the highest pressure differential, or for 150 psig. The weight increment for the structure required is approximately 100,000 pounds which is equal to a 14,000 pound payload penalty. While it is expected that an orifice plate could be designed to control pressures in the Stage I thrust chamber during its underwater trajectory, the starting transients may introduce flow instability. Alternate means for reacting the loads on the expansion section of the thrust chamber have been considered.

Where the ballast is designed not to provide control of the thrust chamber environment, the thrust chamber must be able to withstand the loading imposed by the separated exhaust gas flow. The estimated loads on the thrust chamber during start and for the underwater trajectory consist of a crushing pressure differential, over a limited length of the chamber, of approximately 50 psi. This crushing pressure level exists over short lengths of the thrust chamber and moves from the throat region to the trailing edge as part of the base pressure on the vehicle. Flow separation resulting from the high ambient pressure produces the negative pressure. The weight

III, I, Ballast Unit (cont.)

of structure to react to these loads is estimated as 190,000 lb. This is equivalent to payload penalty of approximately 23,000 lb.

Structural support for the gimbaleed DeLaval thrust chamber can be provided by a ballast element that provide a duct within the thrust chamber that extends from the trailing edge to the throat. The duct is sized to avoid overexpansion of the engine exhaust flow, and supports the thrust chamber skirt for external loads. The plug is sealed at its forward end. The plug type of ballast, because it counteracts all loads associated with the underwater trajectory, provides the least incremental structural weight penalty. The primary disadvantage of the approach is that staging of the ballast requires a relative motion of the annular body (plug ballast) of nearly 100 ft; the analytical prediction of the dynamics of this system is not too precise.

d. Ballast Considerations and Alternate Thrust Chamber Design Type

Ballast requirements for thrust chamber design types applicable to Sea Dragon were considered qualitatively. Of

III, I, Ballast Unit (cont.)

primary interest are the requirements for a single fixed DeLaval thrust chamber, where thrust vector control is provided by secondary injection and for a plug nozzle with a truncated spike.

A fixed DeLaval chamber simplifies the ballast design in regards to the support struts. Support struts are not required to counteract handling loads developed by the ballast unit. It is felt that the fixed nozzle can be reinforced, with a minor weight increment, to counteract ballast loads; there are no actuator elements in the ballast reaction structural path. Structural considerations in regard to the expansion section are similar to that for the gimbal engine.

The plug thrust chamber assembly with truncated spike provides attractive features for design of the ballast and enables a thrust spoiling capability. Because the plug engine will compensate for the back pressure, no modification of the exhaust flow or structural support of chamber surfaces is required. The ballast unit can be interfaced structurally with the truncated spike on a face

III, I, Ballast Unit (cont.)

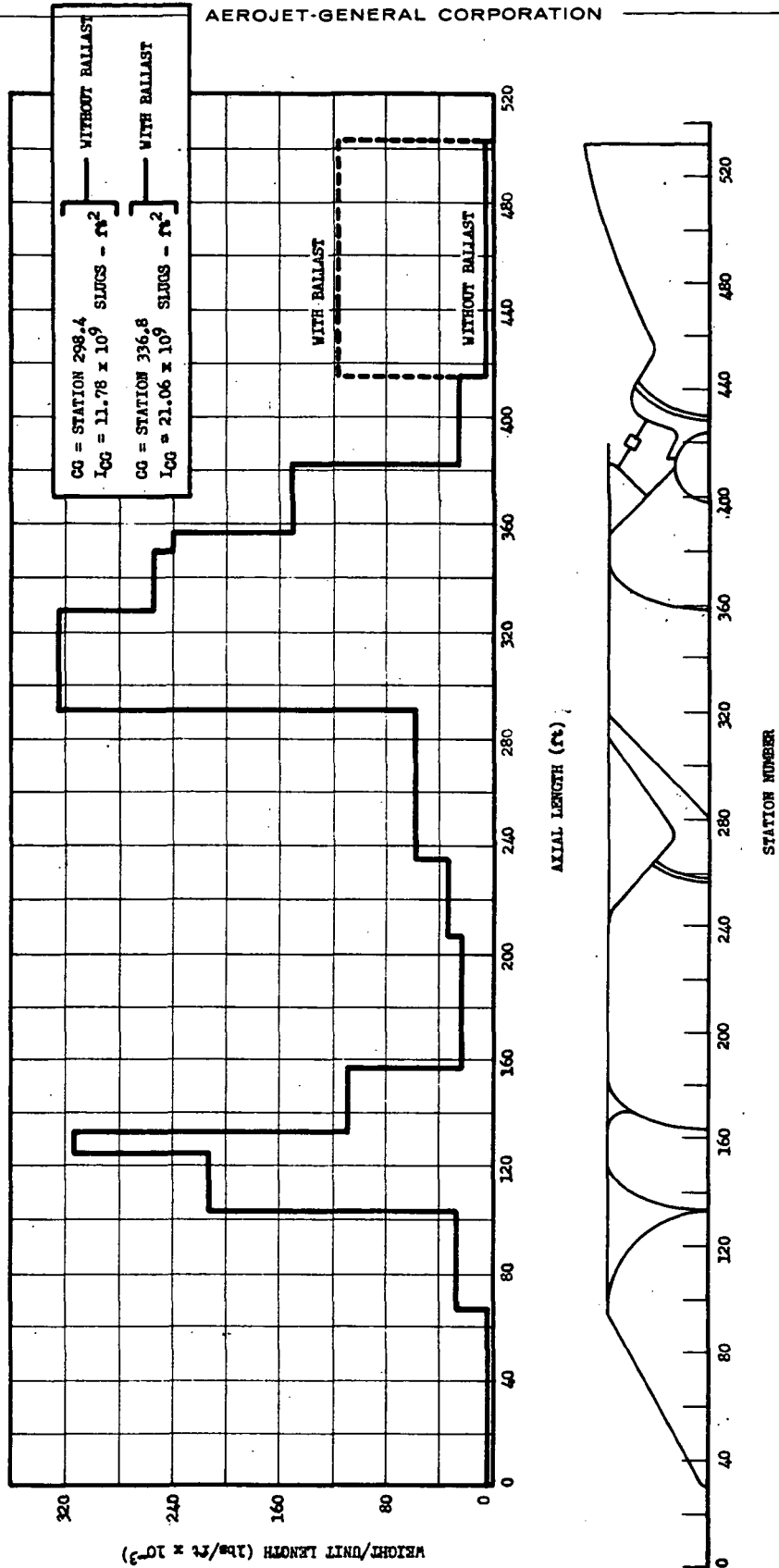
engagement. Ballast staging will not require a telescoping of parts between the vehicle and the ballast. The ballast could provide a thrust spoiling function by redirecting flow outboard at the trailing edge of the truncated spike.

IV. VEHICLE STRUCTURAL CHARACTERISTICS

Airframe stiffness and mode shapes of the vehicle were computed for many different vehicle conditions, such as towing, fueling, launch, flight, and impact. Results of the weight and stiffness distribution calculations are given in Figures IV-1 -2, and -3.

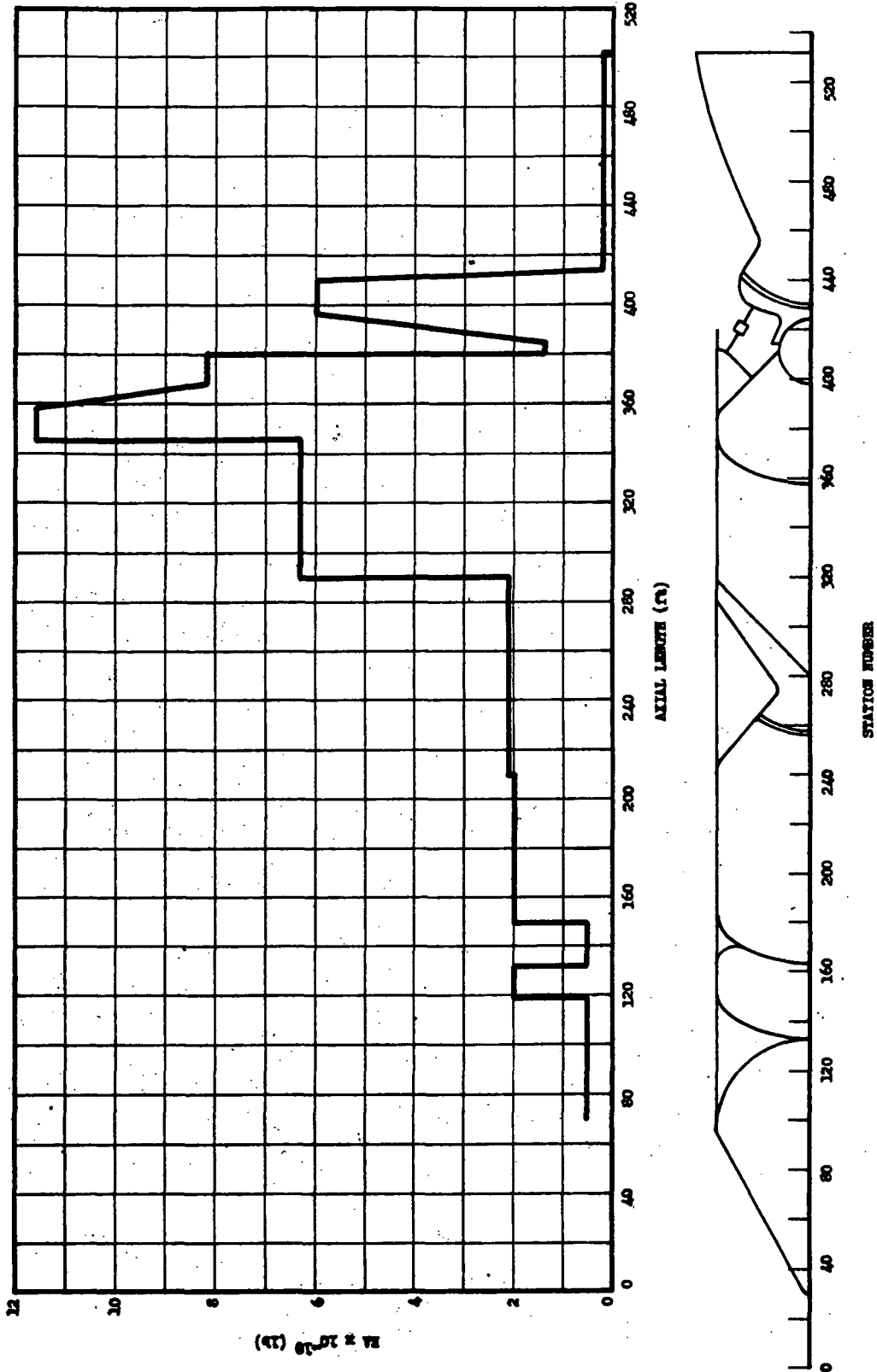
From these results, modal analyses were made using a modified Mylkestad technique, mechanized for digital computation. The mode shapes and frequencies for two vehicle conditions were thus determined; these are shown in Figures IV-4 and IV-5. Although used primarily for launch and towing dynamics analyses, these modal data were also used in considering the autopilot-control-body loops and instrument locations.

AEROJET-GENERAL CORPORATION



Weight Distribution at Liftoff

Figure IV-1



EA versus Length

Figure IV-2

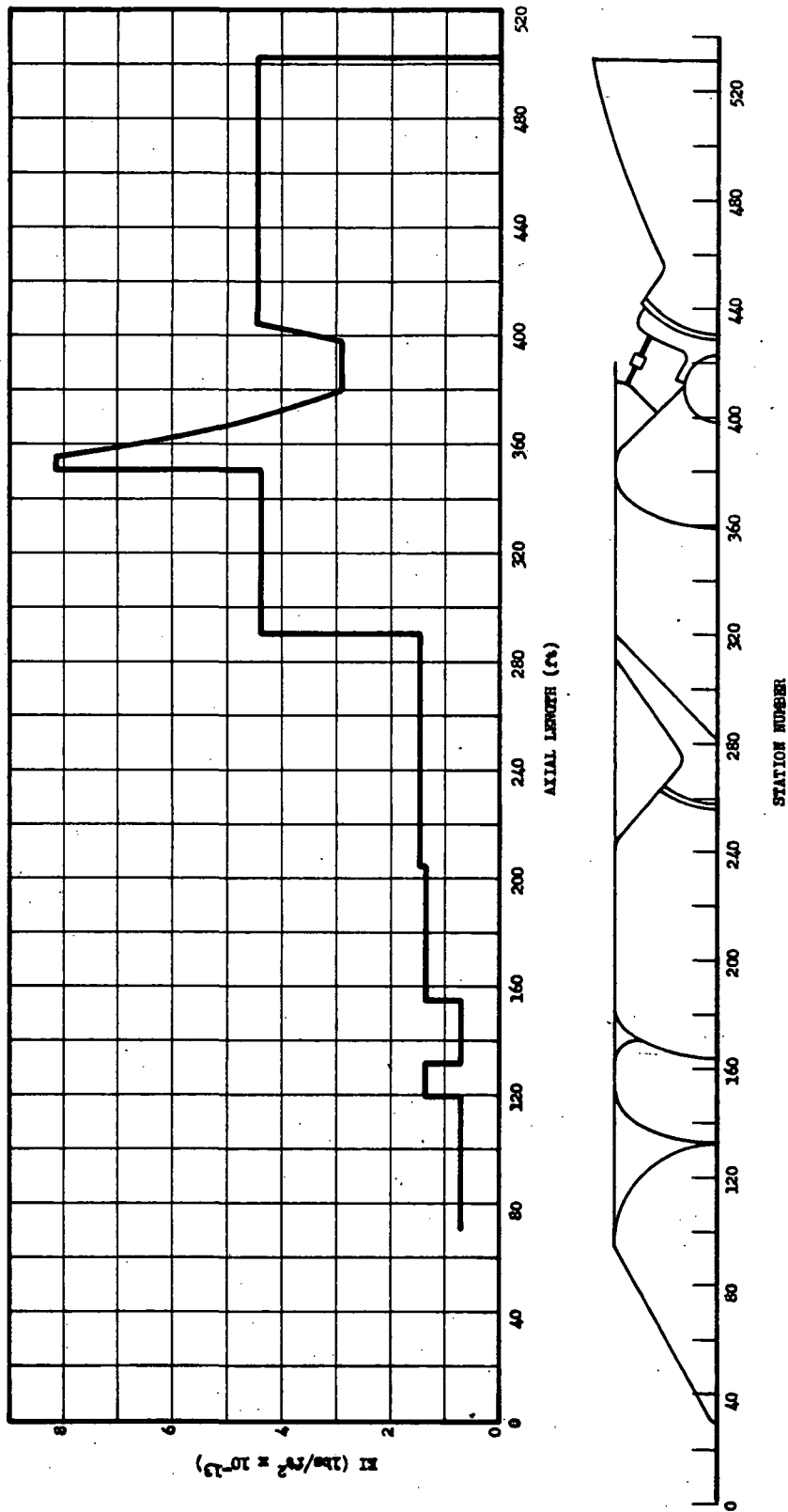


Figure IV-3

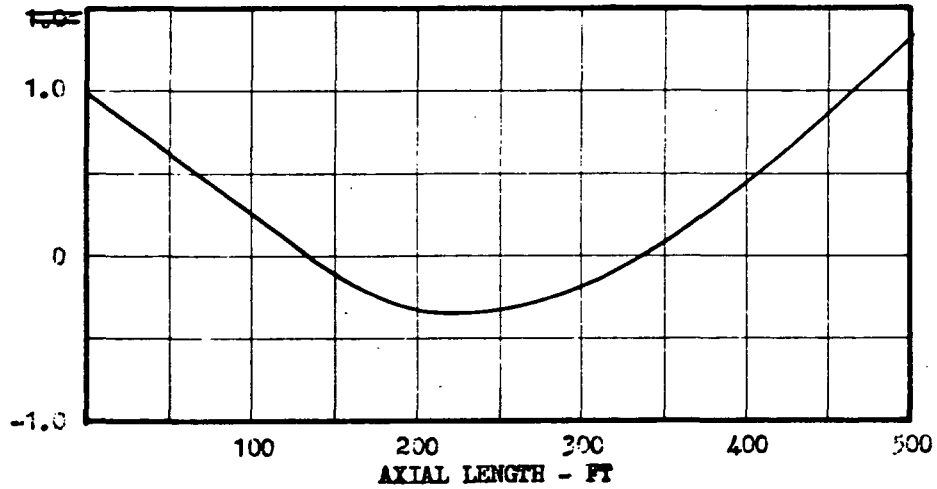
EI versus Length

AEROJET-GENERAL CORPORATION

CONFIGURATION 134

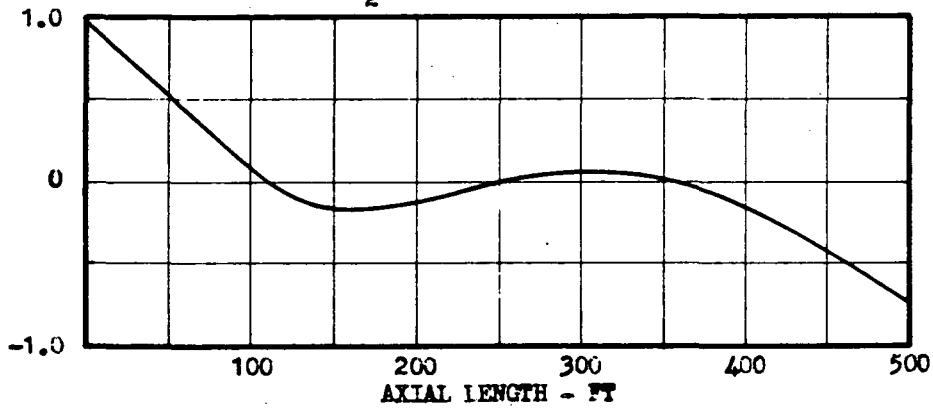
First Mode $f_1 = 2.01$ cps

$M_1 = 7.05 \times 10^4$ Slugs



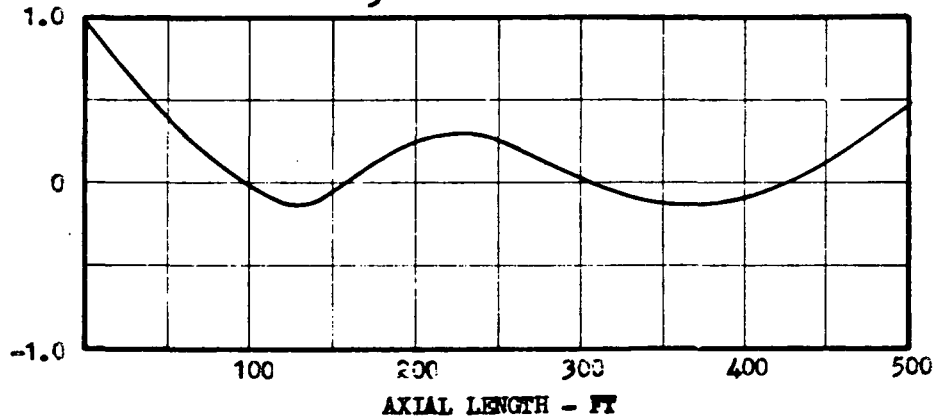
Second Mode $f_2 = 3.23$ cps

$M_2 = 1.99 \times 10^4$ Slugs



Third Mode $f_3 = 4.25$ cps

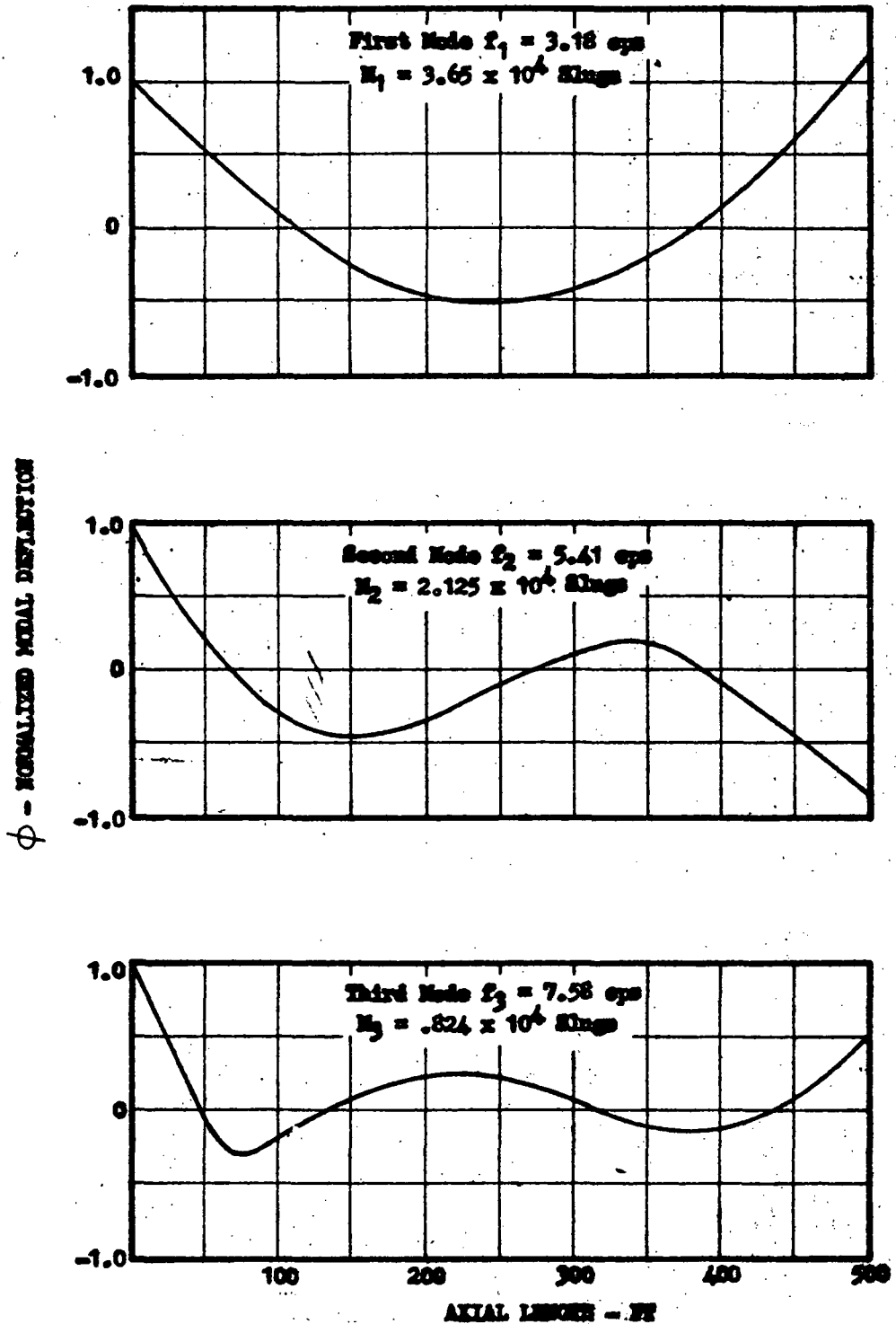
$M_3 = 4.87 \times 10^4$ Slugs



Bending Modes at Launch

Figure IV-4

CONFIGURATION 134



Bending Modes while Empty

Figure IV-5

V. VEHICLE ANALYSIS

A. SYSTEM PERFORMANCE

1. Summary

The Sea Dragon recoverable vehicle configuration No. 135 has a capability to deliver 1.10 million lb of payload to a circular earth orbit of 300 nm altitude when sea launched from Cape Canaveral in an Eastward direction. A preliminary optimization study established the following design parameters: first-stage nozzle area ratio of 5.0:1; thrust to weight ratio of first stage of 2.0:1; and staging ratio (mass ratio second stage/mass ratio first stage) of 1.9:1.

To accomplish sea launch, the first-stage engine operates under water for approximately 5 sec until total emergence of the vehicle from the sea. During this period the variations in thrust, drag, buoyancy, and ballast weight can combine to produce an inflection in the acceleration time history. The large ambient hydrostatic pressure and its subsequent decline is accommodated by a self-compensating

V, A, System Performance (cont.)

plug ballast unit. An analysis of these effects is presented in Section V,A,3. When the vehicle has reached 100 ft/sec it undergoes a pitch-down maneuver (kick) of approximately 7° rotation. Then it merges into a gravity turn and continues to orbit. The first stage burns out at an altitude of approximately 125,000 ft and a velocity of 5,800 ft/sec. The first stage is immediately separated and the second stage ignited, with minimum coasting. At the end of the second stage burning, 260 sec later, the altitude is 150 nm and the velocity 23,430 ft/sec. The auxiliary engines continue burning for a total time of about 22.4 min. During this low thrust period, the altitude increases to 300 nm and the trajectory is shaped to reduce eccentricity. The entire trajectory is illustrated in Figure II-3.

Many other trajectories were studied with variations in propellant utilization rate, kick angle, and payload. For comparison some cases involving coast and restart were also examined. The best of these indicates that a payload gain (by restart) of 86,000 lb is possible; however, additional weight required to realize restart capability was not evaluated and would reduce the advantage. Section V,A, 3 and Appendix II-16 present these studies in detail.

V, A, System Performance (cont.)

Analyses of staging dynamics show that the relative lateral motion between the first and second stages is sufficiently small to preclude damaging contact or severe perturbations to the flight path. Although the stages are aerodynamically unstable at the time of staging, the dynamic pressure and angle of attack are low enough to avoid appreciable rotation being developed before the longitudinal separation has proceeded past its critical point. This is made possible by the use of pressure-driven separation which results in a total staging time of 3 sec.

The first stage unit recoverable and reusable. The recovery operation starts after staging with the inflation of a drag device of flared shape that stabilizes the unit and reduces its velocity for sea impact.

A parametric study of re-entry and impact conditions showed that an impact velocity of 300 ft/sec was required by structural considerations of the first-stage tankage at a terminal pressure of 100 psi. Analyses of various configurations for drag effectiveness

V, A, System Performance (cont.)

showed that a conical flare of 300-ft dia was required to achieve the impact velocity. An inflatable flare was chosen after a weight/payload tradeoff study of this, parachutes, and fixed structures. These studies are discussed in Section III, G.

2. Propulsion Parameter Optimization

A preliminary performance optimization was carried out for the Sea Dragon launch vehicle Configuration No. 132. These studies were made more current as more precise performance data became available. Three vehicle design parameters were studied: first-stage area ratio, liftoff thrust to weight ratio, and staging ratio. Interactions between the various parameters were neglected and the mass fractions were assumed constant for each stage (Figure V-A-1, -2, and -3). As a result of this study, the following values were selected: first-stage area ratio: 5.0:1, thrust-to-weight ratio: 2.0:1, and staging ratio (mass ratio second stage/mass ratio first stage): 1.92:1. The nominal payload obtainable with these vehicle parameters and the Configuration No. 135

V, A, System Performance (cont.)

propellant mass fractions is 1.10×10^6 lb (based on eastward launch from Cape Canaveral). The assumptions and procedures used to arrive at these vehicle parameters are discussed in the following sections.

a. Introduction

The primary purpose of the Sea Dragon performance optimization analysis was to provide a set of reference parameters for establishment of vehicle design and evaluation of the Sea Dragon launch vehicle concept.

When attempting to design a vehicle system that is optimum from an economic standpoint, it is obvious that the performance parameters, such as the thrust-to-weight ratio, staging ratio, etc., are materially affected by the economic constraints imposed. Thus, the best performing system may or may not be the most economic on terms of total program costs.

As a basis for vehicle design and economic study, this section illustrates the results of a preliminary performance optimization analysis.

V, A, System Performance (cont.)

b. General Procedure and Assumptions

In proceeding with the optimization procedure, the results of an earlier Aerojet-General study were utilized in selecting the nominal operating first stage chamber pressure of 300 psi. (The actual chamber pressure history is shown in Figure III-A-4, Section III; A.) The 2.3:1 mixture ratio for first-stage propellants was selected on the basis of maximum ideal exhaust velocity. Second-stage mixture ratio was chosen on the basis of other vehicle studies which have indicated that a mixture ratio of 5:1 is near optimum when considering the specific impulse and vehicle mass fraction trade-off. These assumptions have not been verified for the vehicle size discussed here. On the basis of these assumptions, three design variables were selected for optimization: first-stage thrust-to-weight ratio, staging ratio (mass ratio upper stage/mass ratio booster), and first stage nozzle area ratio.

V, A, System Performance (cont.)

c. Computational Procedure

The boost trajectories considered were analyzed on an IBM 7090 computer. A two-dimensional, nonrotating earth was assumed, (the effect of an eastward launch from Cape Canaveral would be to add approximately 18% to the payload delivered). The trajectory was a typical idealized boost flight; vertical ascent until a velocity of 100 ft/sec was reached and then an instantaneous kick angle applied that, with the subsequent gravity turn, gives the second-stage burnout conditions required to establish a 300-nm circular orbit. Staging was instantaneous and the second stage was permitted to coast to the proper orbital altitude and angle after burnout. The circularization of the orbit occurred at this point with the assumption made that the second stage had a restart capability to supply the small velocity increment required to complete injection. The use of the auxiliary engines to inject the vehicle into orbit does not change the optimum values of the various parameters to any extent.

V, A, System Performance (cont.)

Because this preliminary optimization was for the purpose of establishing a basic set of design parameters, any interaction between area ratio, staging ratio, and thrust-to-weight ratio was ignored (i.e., each parameter was investigated independently of the other three, using past experience as to the value of the fixed quantities in each case). Also neglected is the variation in mass fraction with the various parameters. The values of mass fraction used initially were from the basic Sea Dragon design Configuration No. 132. First-stage mass fraction was 0.89 and second stage 0.91. As more accurate design information became available the optimizations were rerun when it was felt a significant change would occur. The first-stage area ratio study was not rerun because of the relative insensitivity of area ratio optimization to small changes in mass fraction. The staging and thrust/weight ratio studies were rerun with Configuration No. 135 data, although the information was not used to change the design, so that the degree of inefficiency could be determined.

Engine performance parameters C_F and C^* were modified with efficiency factors of 0.97 and 0.96 respectively. Theoretical vacuum thrust coefficients for the first and second stages

V, A, System Performance (cont.)

were 1.67 and 1.84 respectively. (Correction for atmospheric back pressure is performed at each altitude by the computer.) The values of theoretical C^* for each stage are: first stage 5883 ft/sec and second stage 7688 ft/sec.

In all computations, the vehicle drag forces were calculated using the maximum cross sectional area of the vehicle (i.e., the drag area calculated on the basis of tank diameter or nozzle exit diameter, whichever was the greatest). The variation in drag coefficient (based on tank diameter) with Mach number is shown in Figure V-A-4.

A second stage thrust-to-weight ratio of 1.25:1 was selected on the basis of earlier trajectory studies.

d. Results

Figure V-A-1 through V-A-3 illustrate the results of this study. Figure V-A-1 shows the variation in payload

V, A, System Performance (cont.)

weight with liftoff thrust/weight ratio. A thrust-to-weight ratio of 2.0:1 was chosen based on limiting water exit loads and burnout acceleration loading of the interstage and tanks. The effect of selecting a thrust-to-weight ratio of 2.0:1 rather than the optimum value reduces the payload approximately 2.5%. Figure V-A-2 shows the variation in payload weight with staging ratio (mass ratio second stage/mass ratio first stage).

An optimum value of 1.4:1 is shown. During the earlier phases of this study an optimum staging ratio of 1.92:1 was computed. However, this value was based on a first-stage mass fraction of 0.89 and a second-stage mass fraction of 0.91 (Configuration No. 132). When the final mass fraction of 0.888 and 0.887 were defined, the optimum staging ratio was redetermined, the results of which are shown in Figure V-A-2. Since the staging ratio determines the amount of propellant each stage shall carry it was not possible within the time available to redesign the tanks for this new value. The effect of decreasing the staging ratio is to add more propellant to the first stage (since the structural efficiency of second stage is now less); the amount of

V, A, System Performance (cont.)

propellant increase in going from a staging ratio of 1.92:1 to 1.4:1 is approximately 9.3%. The first-stage burnout velocity would increase from 5,866 ft/sec to 7,310 ft/sec and the payload would increase by 7%. The burnout dynamic pressure drops from 115 lb/ft² to 80 lb/ft² however the burnout acceleration increases from 4.02g to 5.0g. Thus, while a decrease in staging ratio would give a higher payload the burnout structural loading would also increase. It was concluded therefore, for purposes of this effort, that the value of 1.92:1 would be retained. Later optimization work should include this effect.

Figure V-A-3 shows an optimum first-stage area ratio of 5.5:1. A nominal ratio of 5.0:1 was selected. This particular optimization was made using the early values of mass fraction. The effect of lower mass fraction is negligible.

3. Trajectory Analyses

In following sections are presented brief discussions of the studies made to date on the Sea Dragon trajectory. Each of the

V, A, System Performance (cont.)

principle phases of the vehicles flight (i.e. launch, atmospheric flight, staging, injection, re-entry, and impact) were examined. In some cases preliminary optimization of events or design features affecting the phase was performed; in others, only a nominal definition of the phase was completed. Particular attention was given to those phases that are unique to the basic concept, namely, the underwater launch and water impact after re-entry. For the most part, the trajectory analyses discussed in sections immediately following, dealt with forces influencing the longitudinal acceleration of the vehicle primarily, rather than with forces causing lateral dispersion. The latter are presented separately in Section V.

a. Underwater Performance

The underwater performance can be divided into two sections: engine operation and vehicle trajectory. These topics will be discussed separately.

V, A, System Performance (cont.)

(1) Engine Operation

The engine operation underwater is dominated by the presence of the annular ring at the nozzle exit. The purpose of this ring is to maintain a gas pressure in the nozzle skirt sufficient to keep the nozzle from collapsing because of external hydrostatic and hydrodynamic pressures.

The general operation of the nozzle-ring combination can be described as follows. The gas passes through the nozzle throat and enters the skirt under supersonic condition. Because of the high back pressure in the skirt, the gas jet separates from the nozzle wall with an accompanying oblique shock. The oblique shock turns the flow towards the nozzle axis. This separated supersonic jet then exits through the hole in the ring.

The nozzle-ring flow system is self-regulating. Should the hole in the ring be too small to pass all the flow, the pressure in the skirt area will rise. This will result in flow separation occurring at a smaller area ratio, reducing the diameter of

V, A, System Performance (cont.)

the separated jet. This self-adjusting process will continue until the separated jet is small enough to pass through the ring. Obviously the hole in the ring must be larger than the nozzle throat.

Similarly, if the separated jet is too small to fill the hole, the skirt area will vent around the edges of the jet, reducing the pressure in the skirt and causing the jet to separate at a larger area ratio. The separated jet will thus increase in diameter until it fills the hole. This self-regulating feature of the system may give rise to oscillatory flow.

The real difficulty in determining the steady-state operation of this system is in predicting the point of separation. The ordinary empirical separation correlations developed for nozzle flow are not valid at the pressure and area ratios encountered. The criteria used in this analysis is one developed by Magar (J. Aero Sc., February, 1956) for turbulent boundary layers. The pressure ratios and Mach numbers to which Magar's criteria correlates data are considerably lower than those covered by most other criteria. To cover very

V, A, System Performance (cont.)

low values of Mach number Magar's criteria was combined with normal shock theory, since the shock must approach a normal shock as the upstream Mach number approaches 1.0.

The basic method of calculation used for this report is as follows. A gas pressure is assumed for the separated region in the skirt and the point of separation is determined. With the pressure ratio across the shock and the initial Mach number known the downstream conditions can be calculated using oblique shock theory. The flow downstream of the shock is assumed to be axial, so that the jet cross section at the exit is essentially the same as that at the separation plane. No attempt was made to investigate the shock pattern initiated by the separation shock, as most of it will occur outside the nozzle and will not affect the vehicle performance.

It is recognized that a much more rigorous approach to the flow problem is possible, obtaining the complete flow field with the method of characteristics. However, it is also felt this would be rather futile as the uncertainties involved in the

V, A, System Performance (cont.)

prediction of separation are much greater than those resulting from use of the simpler theory to predict the remainder of the flow.

Variations in chamber pressure do not change the flow pattern within the nozzle. Thus the chamber pressure decay and recovery during the first 7 sec of flight do not affect the performance of the nozzle and ring provided the pressure in the separated region remains greater than the ambient. Chamber pressure variations do affect the thrust.

Ejection of the water from the chamber at ignition was not considered in this study. However, conservative calculations indicated that the LO_2 -TEA lead might reasonably be expected to clear the chamber of water by ignition.

(2) Vehicle Trajectory

To determine the vehicle trajectory underwater all vertical forces acting on the vehicle must be known at all

V,A, System Performance (cont.)

points in time. For convenience these forces will be classed as either frictional, gravitational, thrust, hydrostatic, or hydrodynamic.

Frictional drag is the result of viscous shearing forces acting on the vehicle skin. Frictional drag was neglected for this vehicle as calculations performed on a similar vehicle indicated this force was negligible in comparison with the other forces involved.

Engine thrust was calculated by combining the momentum flux with the net pressure area term of the exhaust jet. The properties of the exhaust jet were obtained by the method given in the preceding section.

The net hydrostatic force could be calculated by integrating the vertical components of the pressure times area forces over the whole vehicle*. To do this rigorously would be extremely difficult if not impossible. These terms were instead calculated by representing the complex vehicle shape with a combination of conical

*With the exception of the exhaust jet and its projected area of the vehicle nose. Those pressure times area terms were included in the engine thrust.

V, A, System Performance (cont.)

sections and a cylinder. The mode which was chosen was also felt to be a reasonably good model for the calculation of the dynamic loads.

The accuracy of the model was checked by comparing the free floating model and ballast with the calculated water line of the vehicle and ballast. This check indicated the model had a buoyant force 7×10^6 lb greater than the vehicle and ballast unit weight. This discrepancy is not an error but actually represents the weight of the water trapped between the injector and the RP-1 tank. To make the calculations accurate while using this model, this water must be included in the vehicle weight until this portion of the vehicle clears the water.

The ballast unit was not included directly in the calculation of hydrostatic forces. The net static effect of the ballast was known as a function of time and this was included in the summation of hydrostatic forces.

V, A, System Performance (cont.)

The gravitational force was taken as simply the weight of the vehicle and trapped water. The weight of the ballast unit was not included as the net effect of its hydrostatic and gravitational forces was considered in the summation of the hydrostatic forces.

The hydrodynamic forces acting on the vehicle are extremely difficult to evaluate. With the aid of the model and empirical drag coefficients drag forces were obtained for the portion of the vehicle up to the nozzle exit. As the flow around the nozzle exit is complicated by the presence of the ballast tanks and the gas jet, no attempt was made to represent it with a model. Instead the drag was calculated by applying a conservative drag coefficient to the nozzle base area less the jet area.

The drag terms are not completely accurate due to the acceleration of the system. This introduces corrections to the drag terms which make them larger. However, the inclusion of the trapped water in the vehicle inertial mass actually does correctly compensate for the acceleration corrections in the drag terms.

V, A, System Performance (cont.)

The inertial mass of the vehicle was obtained by combining the total mass of the vehicle, the trapped water, and the ballast unit. It was assumed that the ballast unit was drained of 14×10^6 lb inertial mass over a period of two seconds, and that the trapped water was shed immediately as that portion of the vehicle cleared the water.

The actual calculations were performed by taking finite increments of vehicle travel and assuming all forces were constant over that increment. Fifteen increments were used to obtain the results presented here.

(3) General Discussion

The underwater trajectory is given on Figure V-A-5. These results are for the case in which the ballast unit fluid is ejected over the first two seconds of firing. It was also assumed that the chamber pressure dropped at a uniform rate from 285 to 225 psia over the first 3.5 sec of firing and that it rose at a uniform rate to 294 psia over the next 3.5 sec.

V, A, System Performance (cont.)

The rather unusual trajectory is the result of several interacting effects. At ignition the engine thrust coupled with large buoyant forces gives the vehicle a moderately large acceleration. However, as the vehicle gains velocity and rises, the drag increases while both the buoyant forces and engine thrust decrease. This causes the acceleration to drop off and even briefly assume negative values. The decreasing engine thrust is the result of dropping chamber pressure. The drop in chamber pressure referred to here is not related to this phenomenon but rather to ullage gas pressure decay. The coupling effect of these factors will be studied in more detail in future designs. The decay in pressure can be accommodated by increased ullage volume or redesign of the pressurization system.

Finally as the lower end of the vehicle begins to clear the surface the vehicle sheds trapped water, drag decreases, thrust increases and the acceleration again becomes positive.

A plot of interest is that showing the net static pressure on the skirt at two positions as functions of depth

V, A, System Performance (cont.)

(Figure V-A-6). These curves represent the difference between the internal static pressure and external static pressure at a position near the nozzle throat and near the exit. To obtain the net total pressure a value equal to about 25 to 30% of the total external hydrodynamic pressure should be subtracted from each curve at each depth. This indicates that, except for a very short period at the nozzle exit, the nozzle is not subjected to crushing loads. Once the ballast-ring unit is staged these plots are invalid, as dropping the ring completely changes the pressure distribution within the nozzle.

No breakdown on drag forces or buoyancy forces is given. Because this particular model was used there are some net force terms that are not easily separable into drag, buoyancy, and other force components. This complication is primarily the result of the way in which the ballast unit and trapped water were handled.

b. Atmospheric Mode

The Sea Dragon vehicle is launched from a near vertical floating position in the ocean. Preliminary analysis has

V, A, System Performance (cont.)

shown that the vehicle requires a maximum of 8 sec to clear the ocean surface and emerges with a minimum velocity of 60 ft/sec if the water ballast is retained during the underwater portion of the trajectory. These values were used to determine the initial conditions of the atmospheric portion of the nominal ascent trajectory, and were based on an underwater trajectory which retained the water ballast. For this particular analysis it was assumed that no lateral launch dispersion occurred during the underwater phase of motion. A separate study of launch dispersion was made and is reported in Appendix II-21. In addition, several other trajectories were computed as described in Appendix II-16, which also contains trajectory analysis details. The ascent trajectory can be divided into two phases: (1) an initial two-stage high-thrust phase, and (2) a low-thrust phase during which a small percentage of the second stage propellant is burned to inject the vehicle into orbit. The high thrust phase has a duration of 342 sec, while final injection at low thrust requires 1,010 sec.

Table V-A-1 shows the data that was used for this part of the study. Slightly better data in some instances

V, A, System Performance (cont.)

became available near the close of the study but time did not permit a new analysis. A cursory examination of the changes, however, indicates that they would have no profound effect on the comparative results discussed herein. The performance data was obtained from theoretical shifting equilibrium data by applying a nozzle efficiency of 96% and a combustion efficiency of 94%, which are very conservative values. The weight data shown applies to the basic launch vehicle with no payload. The burn-out weight of each stage includes a propellant outage of 1%. Using the weight data of Table V-A-1, the calculated propellant fractions are 0.896 and 0.897 for Stages I and II, respectively.

The significant parameters for the continuous burn ascent trajectory are shown in Figures V-A-7 through V-A-12. Significant data is also shown in Table V-A-2, which includes a comparative restart case. Note that zero time is defined as the time when the vehicle has just cleared the ocean surface.

The first stage burns out at an altitude of 107,800 ft (17.7 nm), a velocity of 5,603 ft/sec, and γ equal to 46.33° . Referring to Figure V-A-8, the acceleration on the vehicle

V, A, System Performance (cont.)

varies from 2.09g at launch to 6.06g at burnout. The first-stage trajectory is quite flat, as evidenced by the large kick angle and rapid increase in γ , and results in a peak dynamic pressure of 1,930 lb/ft². At burnout, the dynamic pressure has dropped to 350 lb/ft². However, the trajectory analysis was based upon a constant chamber pressure in the first stage engine and a correspondingly short burning time (74 sec) and low altitude. More recent design information shows that the chamber pressure decays near burnout of the first stage, increasing burning time by approximately 10 sec. The net result is to increase the first-stage burnout altitude without appreciably changing the velocity. It has been shown that the increase in burnout altitude will decrease the dynamic pressure at staging to approximately 100 lb/ft², and the burnout acceleration to 4.2g.

Figures V-A-11 and V-A-12 show the trajectory parameters during low thrust operation of Stage II. The thrust is assumed constant at 200,000 lb for the duration of 1,010.04 sec. The altitude increases from 150.0 to 300.0 nm. The velocity decreases

V, A, System Performance (cont.)

initially from 23,430 ft/sec (note that the velocity is incremented by 1,275 ft/sec to account for the rotating earth at this point) to 23,359 ft/sec at 490 sec, and then increases to 24,878 ft/sec at burnout. This is due to the very low thrust and tangential acceleration. Acceleration on the vehicle due to thrust increases from 0.071g or 2.28 ft/sec² at initiation of this low thrust phase to 0.087g or 2.81 ft/sec² at burnout. Gamma increases from 83.72° to 90°, and thus the tangential deceleration due to gravity starts at 3.23 ft/sec² and decreases to zero at burnout. The net tangential acceleration thus varies from -0.95 to +2.81 ft/sec². The net velocity gain produced by the low thrust operation of Stage II is 1,448 ft/sec.

For the retained ballast case, the 300-nm circular orbit payload is 1,112,000 lb. If the ballast fluid is expelled, the duration of the underwater portion of the trajectory is reduced from 8 to 5.05 sec, the velocity of the vehicle as it clears the ocean surface is increased from 60 to 84 ft/sec and the payload increases to 1,173,000 lb.

V, A, System Performance (cont.)

The exchange ratio in pounds of payload per sec change in specific impulse in both stages is 17,000 lb/sec. If a specific impulse of 92% of theoretical is attained, the Stage I specific impulse increases approximately 7.5 sec, thereby increasing the payload by 129,000 lb.

c. Separation

Separation of the first and second stages is accomplished using the energy of a prepressurized interstage cavity. When the staging sequence is initiated, expansion of the gas charge in the cavity results in a relative acceleration of the two sections of the vehicle. A separation velocity between the two stages is thus developed, which is a function of the initial interstage pressure and the length of travel during which air is effectively confined to the interstage cavity. This length is referred to as the ejection stroke length.

V, A, System Performance (cont.)

In the analysis of staging dynamics, it was assumed that there is no leakage of air from the interstage during the staging sequence until the ejection stroke length is exceeded. Although there will undoubtedly be some leakage during this time, it should have no significant effect on staging time as long as the leakage rate is small. It was also assumed that the expansion of the air in the interstage is isentropic. External aerodynamic forces acting on the vehicle other than drag were neglected in computing the longitudinal motions during staging. The first-stage engine thrust is negligible when staging begins. Staging is defined as being completed when the fore end of the first stage clears the end of the second-stage expandable nozzle; however the first part of the motion is the most critical as regards potential collision between stages.

The acceleration of the first stage of the vehicle relative to the second was obtained by summing the forces acting on each of the stages caused by pressure in the interstage and to drag, and dividing by their masses. This acceleration was computed at 0.01 sec intervals, and integrated numerically to obtain separation velocity and distance. Air in the interstage was assumed to expand

V, A, System Performance (cont.)

isentropically during this process. When the ejection stroke length is exceeded, the pressure in the interstage drops to ambient, and only drag forces are considered for the remainder of the process. The results of these calculations are given in Figure V-A-13 which shows separation times as a function of ejection stroke length for initial interstage pressures of 20, 30 and 40 psi.

The major problem expected in the staging process is that of maintaining alignment of the two stages to prevent interference between the first stage and the expandable nozzle of the second stage. For a very conservative estimate of the interference potential during staging, the pressure distributions on the two stages were estimated for a dynamic pressure of 100 lb/ft^2 and an angle of attack of 1° . These pressure distributions were integrated over each of the stages to obtain a lift force, and a moment tending to rotate the stage about its center of gravity. These moments were used to obtain the angular acceleration of each stage. The angular accelerations of each stage were integrated numerically to obtain angular displacements, which were used

V, A, System Performance (cont.)

to obtain interference displacements between the expandable nozzle and the first stage fore end. The results of this calculation for an initial interstage pressure of 40 psi and an ejection stroke length of 10 feet are shown in Figure V-A-14. It was assumed in the calculation that the expandable nozzle remains essentially unexpanded, and thus contributes nothing to the aerodynamic stability of the second stage. Since the expandable nozzle will be released during the staging process (after the ejection stroke is completed) it will begin to expand under the influence of the air leaving the interstage cavity and the restraint of external flow. The time rate of expansion has not been calculated; however, only a very small amount of expansion (1.5°) will accommodate the full lateral excursion of the adjacent stage elements. During the first 20 ft of separation, less than 1 inch of relative lateral motion will occur as indicated in the curve of Figure V-A-14.

Considering that the foregoing analyses assumes that Stage II is free to pitch during staging, the results are conservative. Since the Stage II TVC system will prevent this motion, the potential interference will be substantially less than indicated in

V, A, System Performance (cont.)

Figure V-A-14. With this change the analysis showed a 65% reduction in the lateral motion. A further discussion of considerations pertaining to these factors is given in Appendix II-17.

The conclusion to be drawn from the foregoing discussion is that the relative lateral motion of the two stages is sufficiently small to avoid damaging contact between them. Pressure driven ejection will produce adequate separation velocity, essentially compensating for the drap shielding effect of the expandable nozzle on the first stage. If ultimately found necessary, the vehicle pitch rate can be programed briefly to further accommodate separation requirements.

d. Stage I Re-Entry Phase

The re-entry trajectory of the Sea Dragon first stage is described in detail in Section III, G. The important re-entry parameters (with drag flare inflated) are:

V, A, System Performance (cont.)

Apogee altitude 335,000 ft

Re-Entry Velocity 5350 ft/sec

(at 200,000 ft)

Re-Entry Angle 30°

(from local horizontal)

Maximum Re-entry Deceleration 7.1 g

Maximum Dynamic Pressure 300 lb/ft²

Maximum Heat Flux = 3.5 Btu/ft² -sec

(stagnation heating blunt radius = 7 ft)

Re-entry parameters were calculated using a two-dimensional IBM 7090 computer program for a spherical nonrotating earth model.

Dispersions of the vehicle from the point mass trajectory because of aerodynamic oscillatory motion is negligible. The Sea Dragon first stage possesses a high degree of static and dynamic stability due to the large inflatable flare structure.

V, A, System Performance (cont.)

e. Stage I Impact

Using the end conditions of the atmospheric trajectory described above, parameters were determined for the Sea Dragon expended first stage. An impact velocity of 300 ft/sec (using a slightly conservative drag coefficient curve) was found. The point mass trajectory flight path angle was 89° from the horizontal. Vehicle angle of attack due to surface winds of 30 ft/sec was approximately 5.5° .

TABLE V-A-1

SEA DRAGON WEIGHT AND PERFORMANCE DATA

PERFORMANCE DATA

	<u>Stage I</u>	<u>Stage II</u>	
		<u>High Thrust</u>	<u>Low Thrust</u>
Propellants	LO ₂ /RP-1	LO ₂ /LH ₂	LO ₂ /LH ₂
Vacuum Thrust (lb)	94,450,000	14,600,000	200,000
Nozzle Exit Area (ft ²)	6828	15,644	-
Vacuum Specific Impulse (sec)	275.19	404.80	382.00
Flow Rate (lb/sec)	343,217	36,067.2	523.560
Burning Time (sec)	74.579 (atmospheric)	282.133 (max.)	1050 (approx)
Cross-Sectional Area (ft ²)	4418	4418	-

WEIGHT DATAWithout Payload (lb)

Stage II at Burnout	1,168,400
Stage II Useful Propellant	<u>10,175,700</u>
Stage II at Liftoff	11,344,100
Stage I at Burnout	<u>2,983,900</u>
Vehicle at Stage I Burnout	14,328,000
Stage I Useful Propellant Wt. At Time of Water Emergency	<u>22,851,200</u>

TABLE V-A-1 (cont.)

<u>WEIGHT DATA</u>	<u>Without Payload (lb)</u>
Vehicle Gross Wt. at Start of Atmospheric Trajectory	37,179,200
Stage I Useful Propellant Wt. Consumed Before Water Emergence	<u>2,745,700</u>
Vehicle Gross Wt. at Ignition	39,924,900

INITIAL CONDITIONS FOR ATMOSPHERIC TRAJECTORY

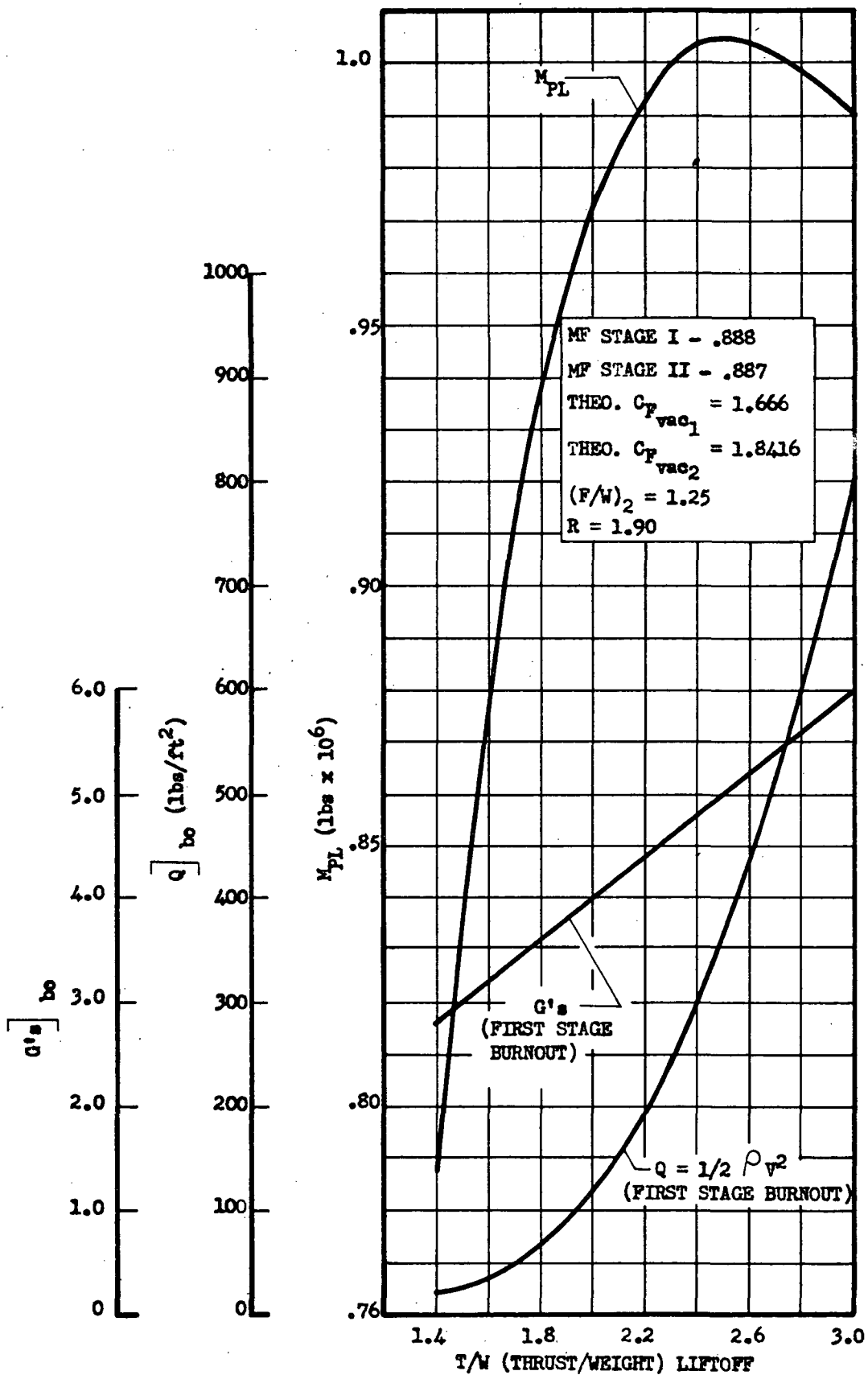
Velocity 60 ft/sec
Time from Ignition 8 sec

TABLE V-A-2COMPARISON OF CONTINUOUS BURN ASCENT
TRAJECTORY TO RESTART TRAJECTORY

<u>Parameters</u>	<u>Continuous Burn</u>	<u>Restart</u>
Payload (lb)	1,119,000	1,204,770
Stage I Duration (Above Water) (sec)	66.579	66.579
Stage II Duration (High Thrust) (sec)	267.471	277.968
Coast Time (sec)	0	1,156.412
Stage II Duration (Low Thrust) (sec)	1,010.04	0
Stage II Restart Duration (High Thrust) (sec)		<u>4.169</u>
Total Time to Orbit (sec)	1,344.090	1,505.128
Initial Kick Angle (degrees)	19.74	20.75
Stage II Burnout Conditions (Before coast or low thrust period)		
Altitude (nm)	150.0	130.7
Gamma (degrees)	83.74	86.48
Velocity (ft/sec)	23,434	25,277

TABLE V-A-2 (cont.)

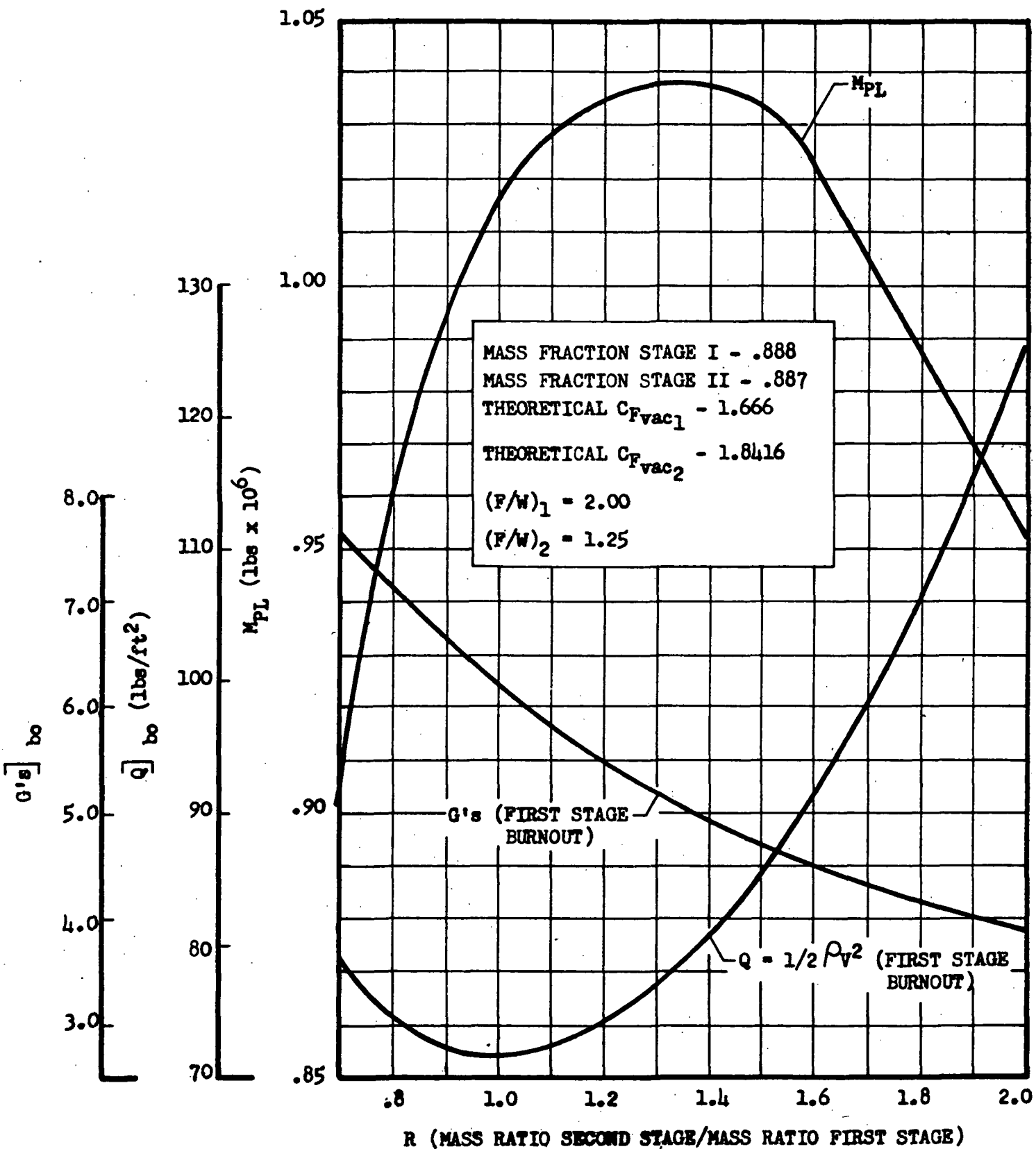
<u>Parameters</u>	<u>Continuous Burn</u>	<u>Restart</u>
Vehicle Burnout Conditions		
Altitude (nm)	299.8	299.8
Gamma (degrees)	90.00	90.00
Velocity (ft/sec)	24,890	24,889
Angular Displacement from Launch Vertical, Beta (degrees)	69.00	81.41
Restart or Low Thrust Parameters		
Propulsive Velocity Increment (ft/sec)		
Stage II Low Thrust	2,556	-
Restart at Apogee	-	800
Decrease in Velocity Due to Gravity (ft/sec)		
Stage II Low Thrust	1,100	-
Coast	-	1,188
Net Velocity Gain (ft/sec)	1,456	-388



Thrust-Weight Optimization

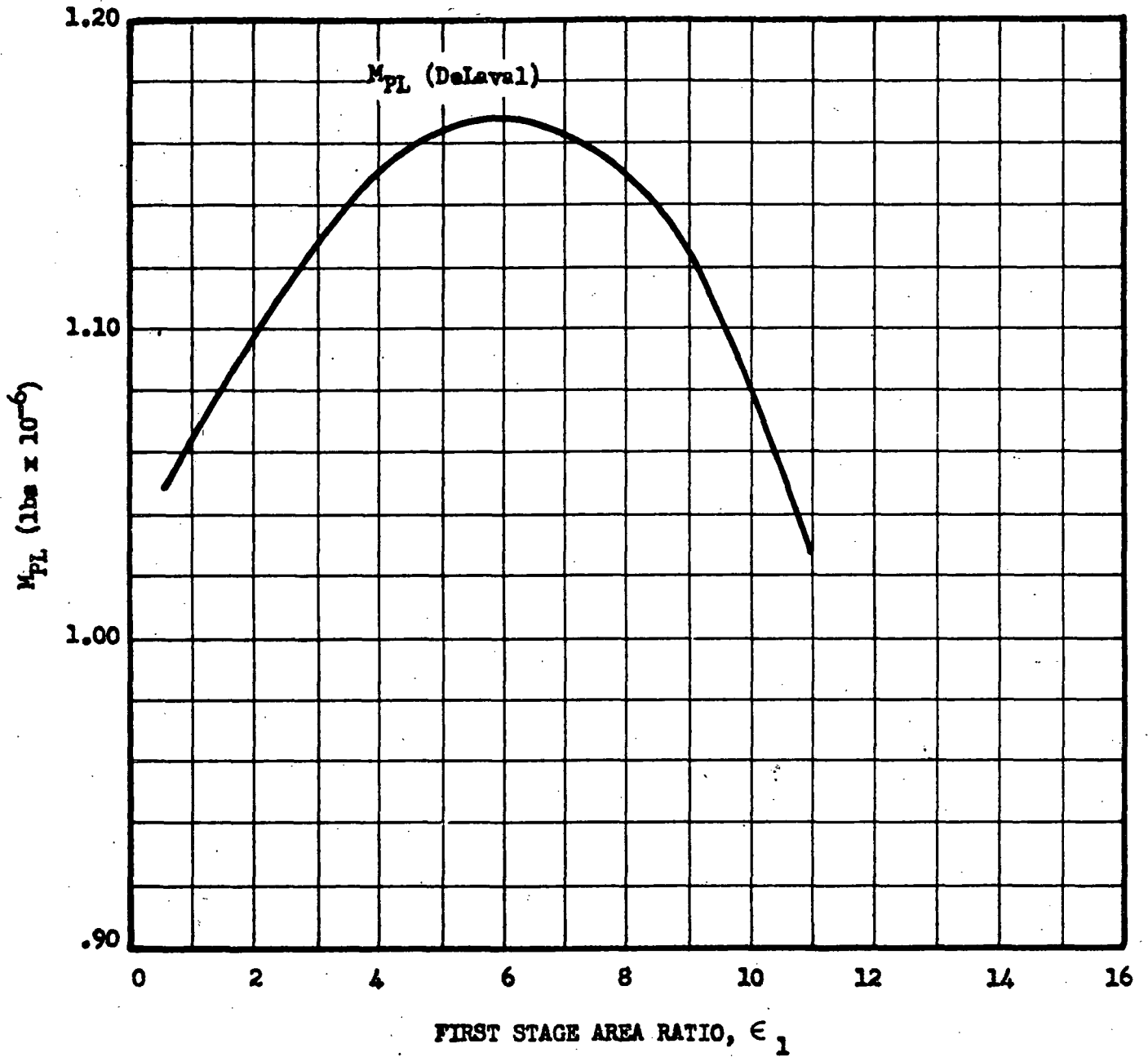
Figure V-A-1

AEROJET-GENERAL CORPORATION



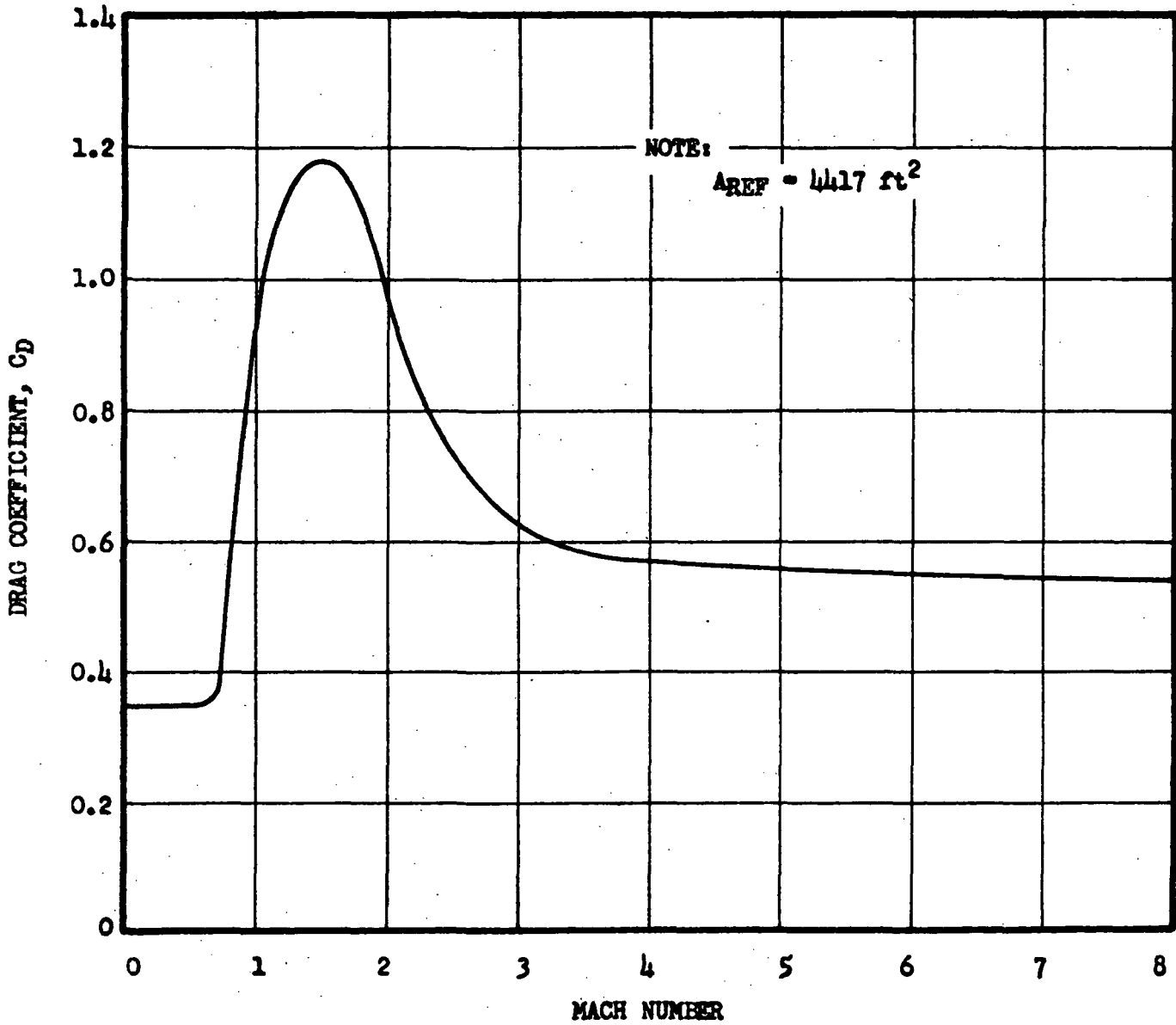
Staging Ratio Optimization

Figure V-A-2



Stage I Area Ratio Optimization

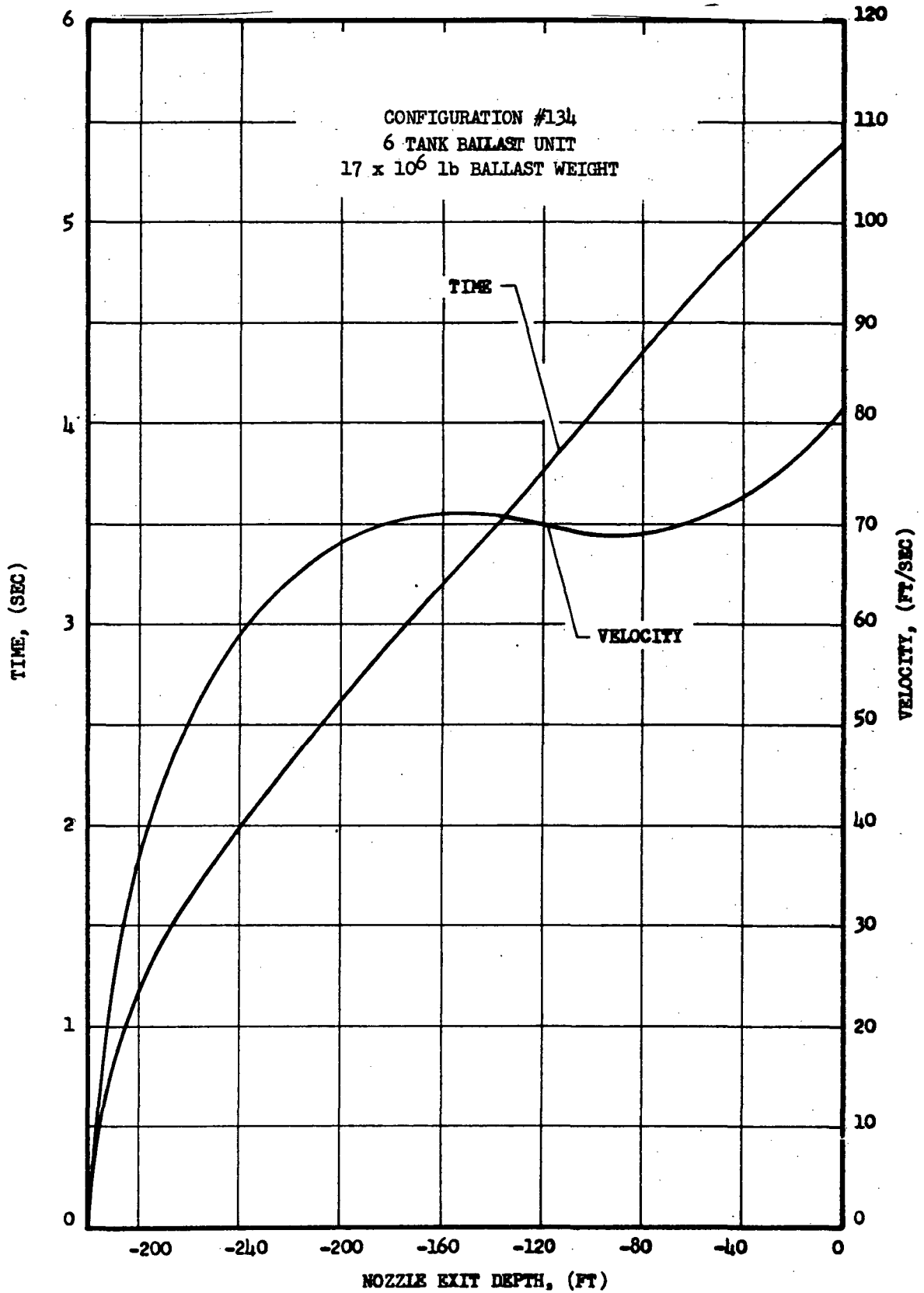
Figure V-A-3



Drag Coefficient versus Mach Number

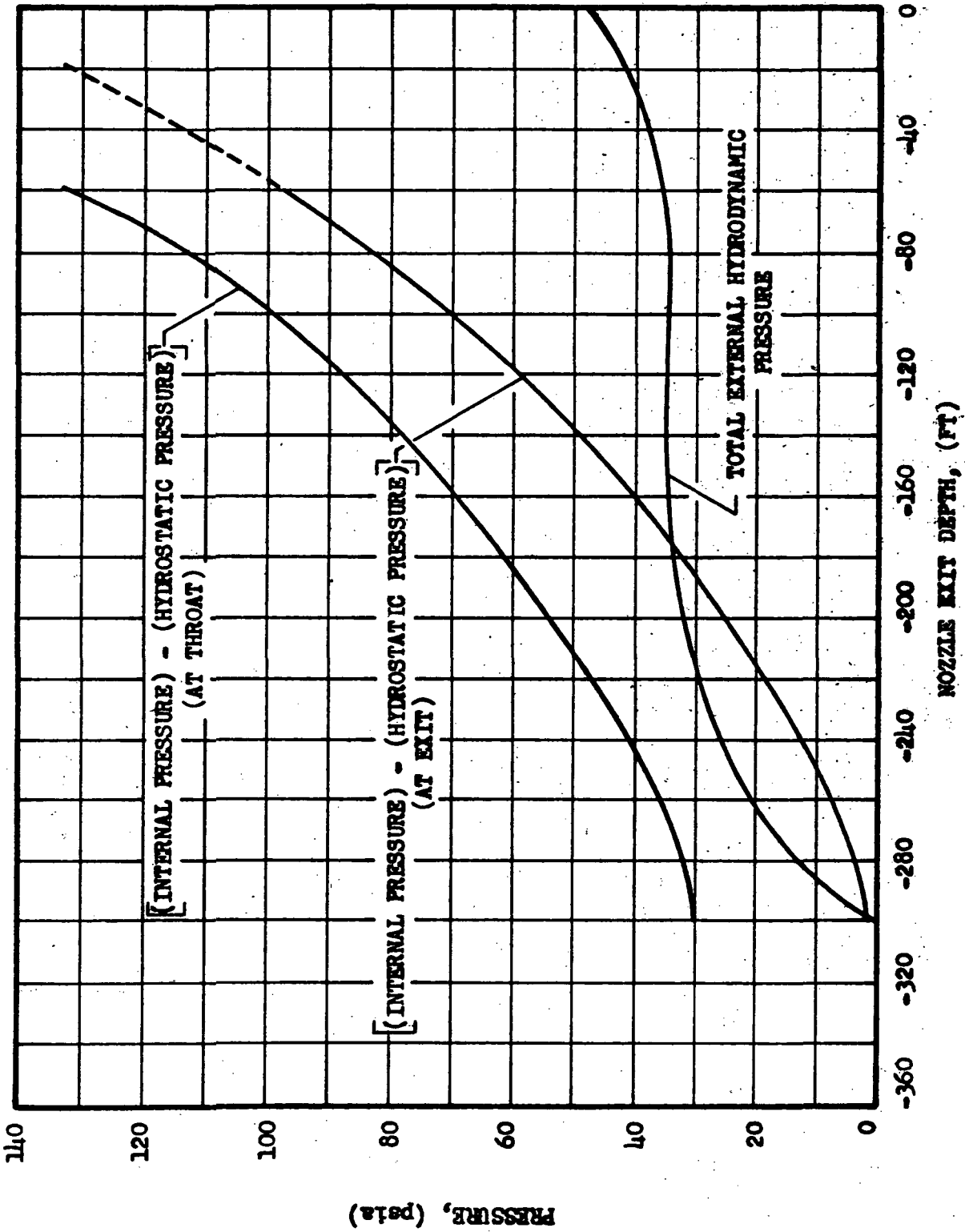
Figure V-A-4

AEROJET-GENERAL CORPORATION



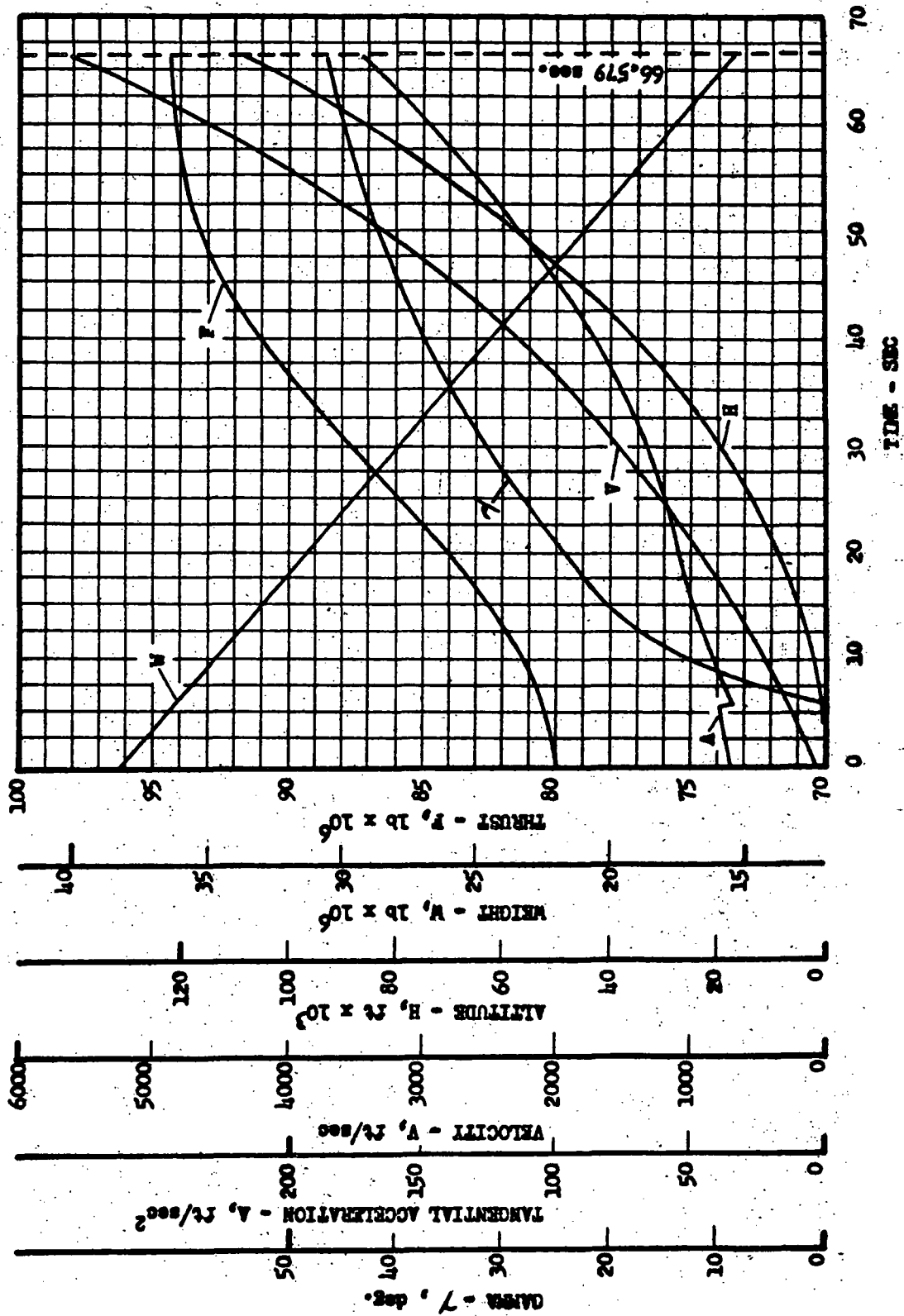
Underwater Trajectory

Figure V-A-5



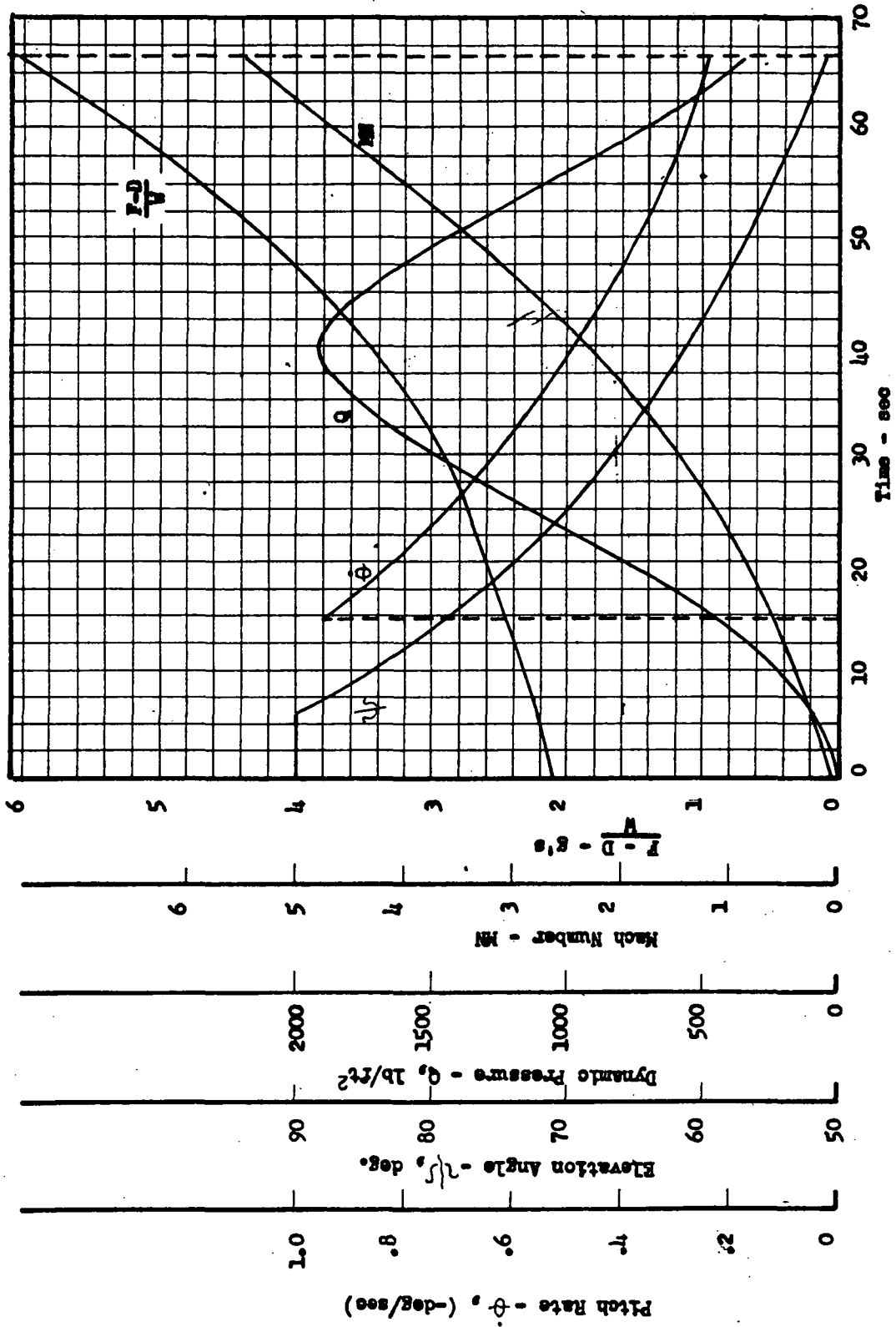
Net Pressure on Skirt

Figure V-A-6



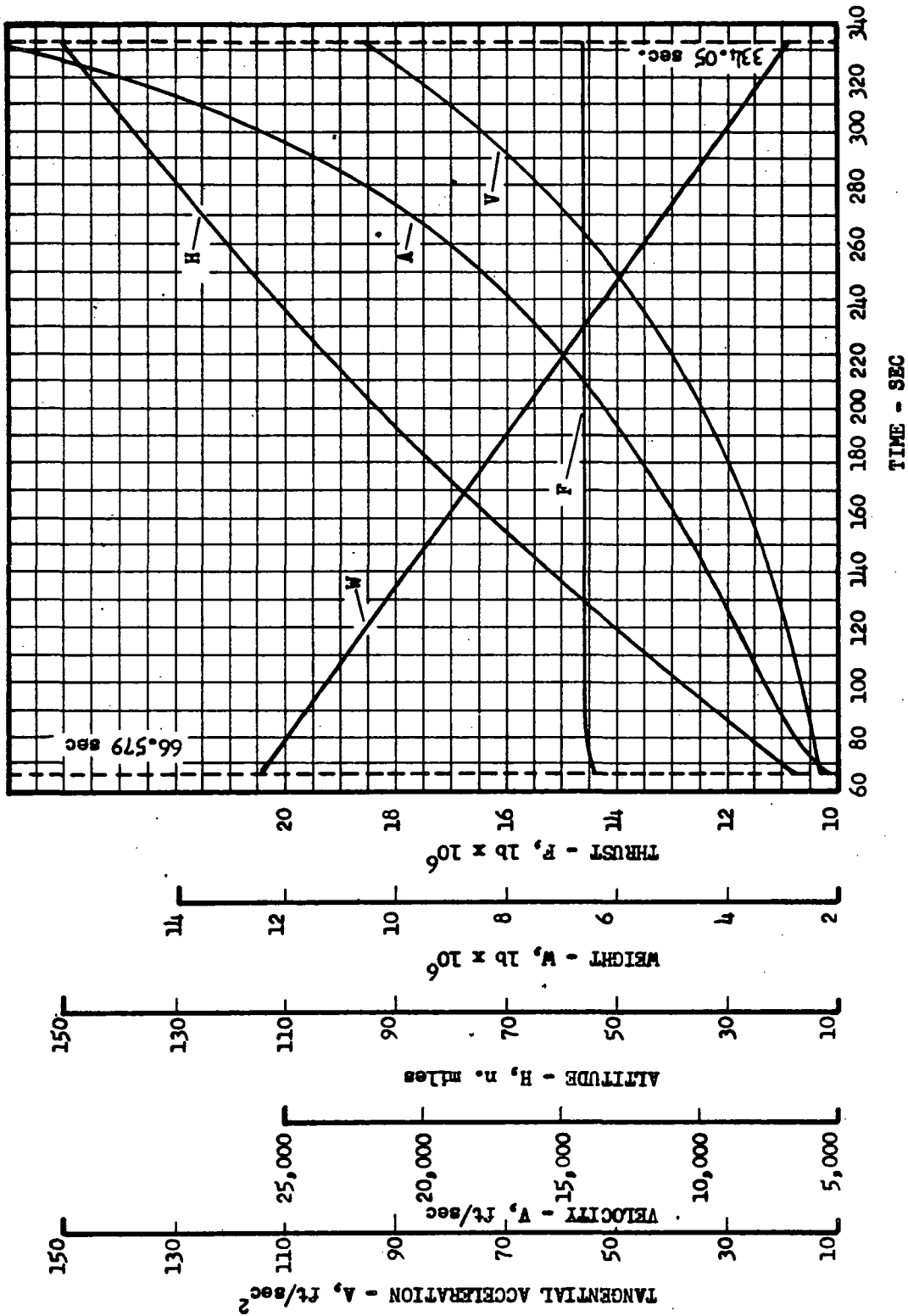
Performance Parameters Stage I

Figure V-A-7



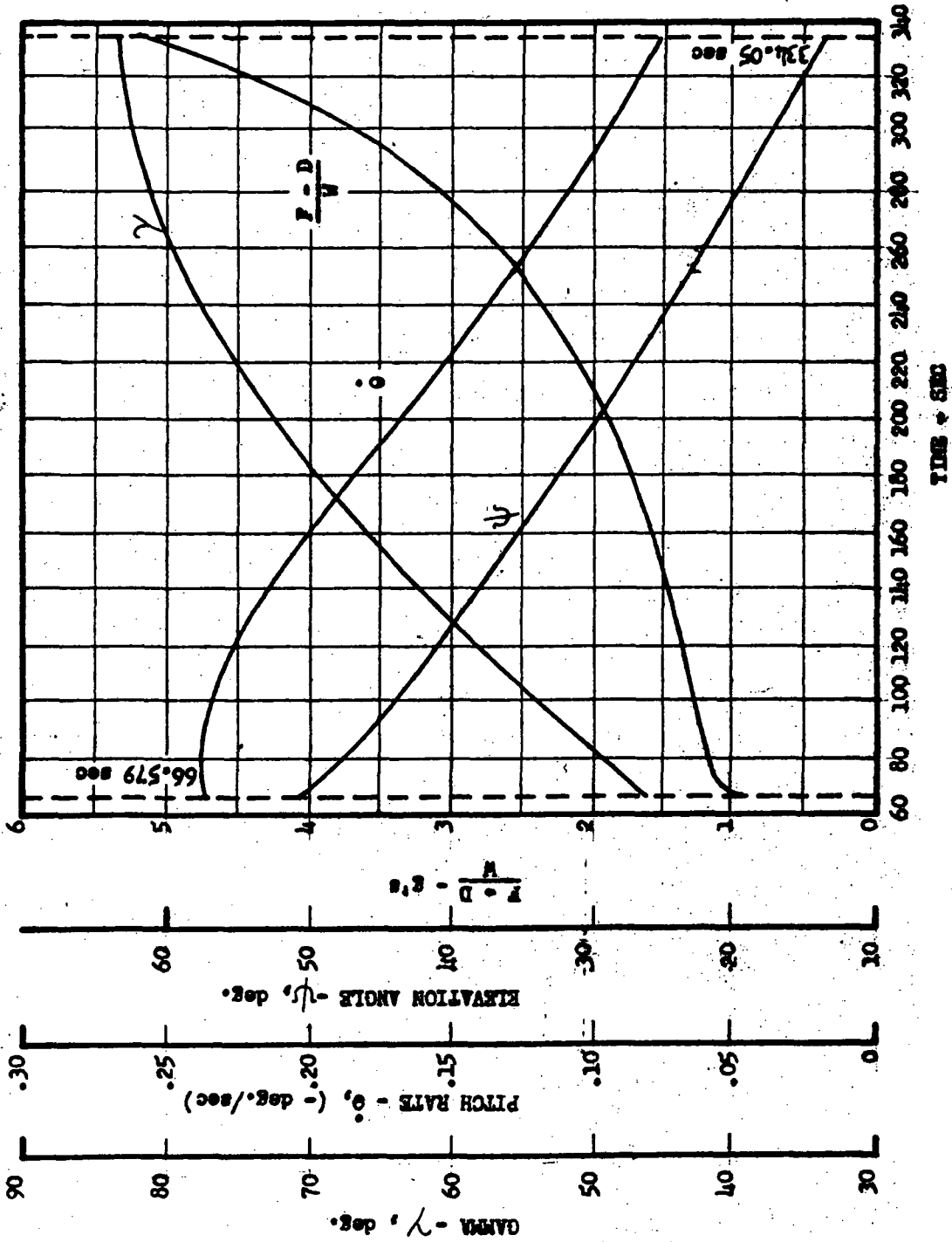
Trajectory Parameters Stage I

Figure V-A-8



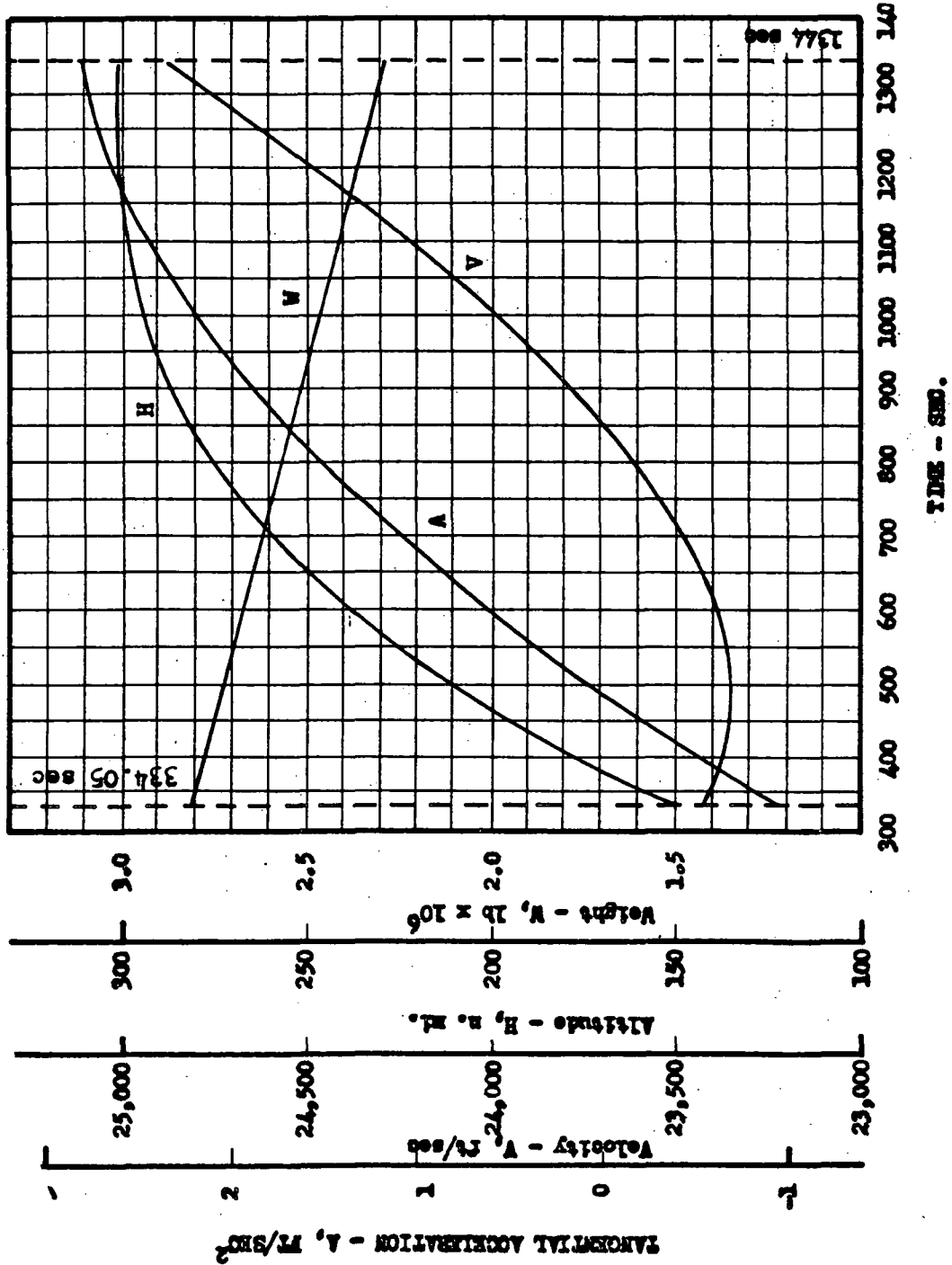
Performance Parameters Stage II, High Thrust

Figure V-A-9



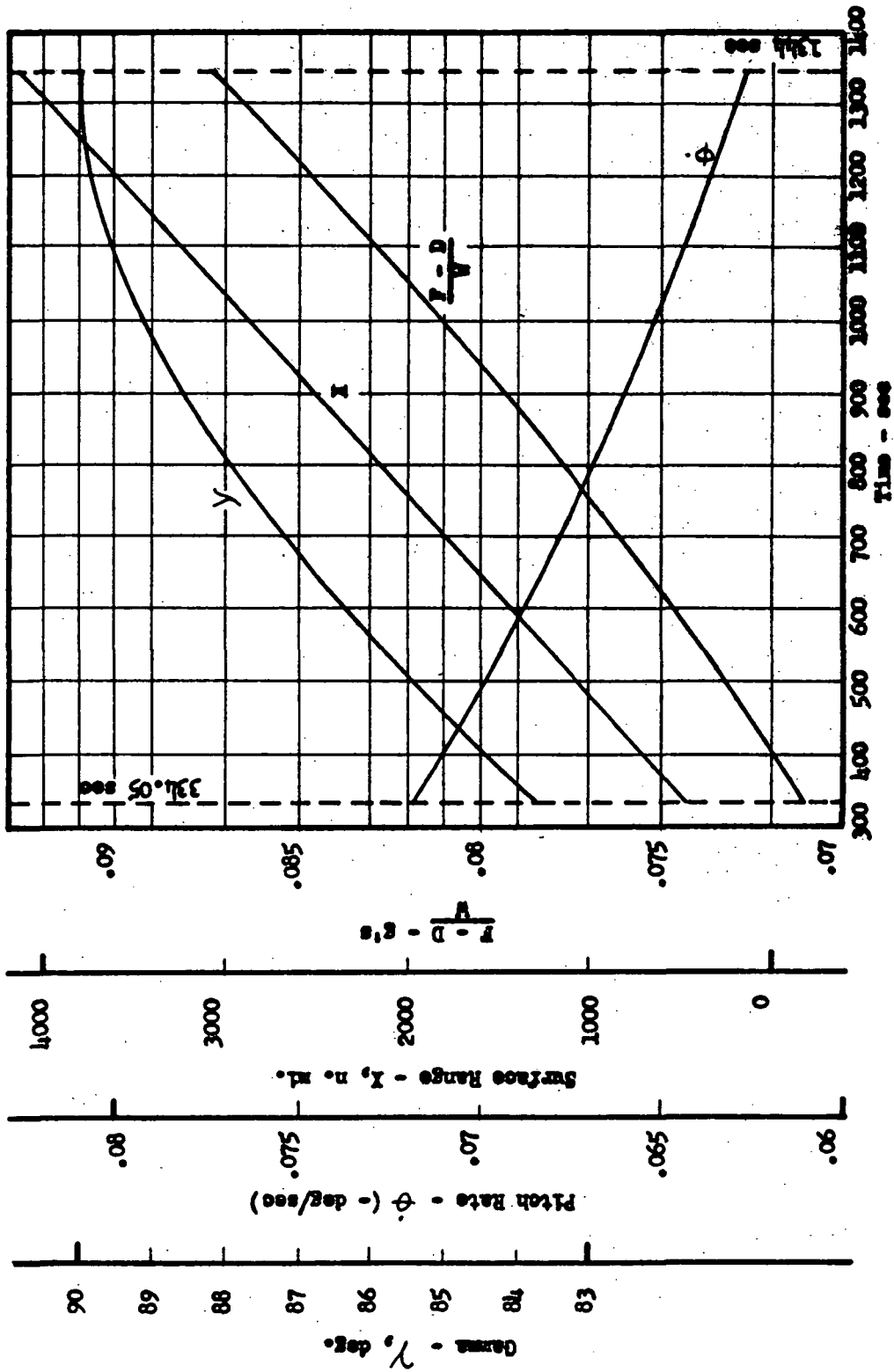
Trajectory Parameters Stage II, High Thrust

Figure V-A-10



Performance Parameters Stage I, Low Thrust

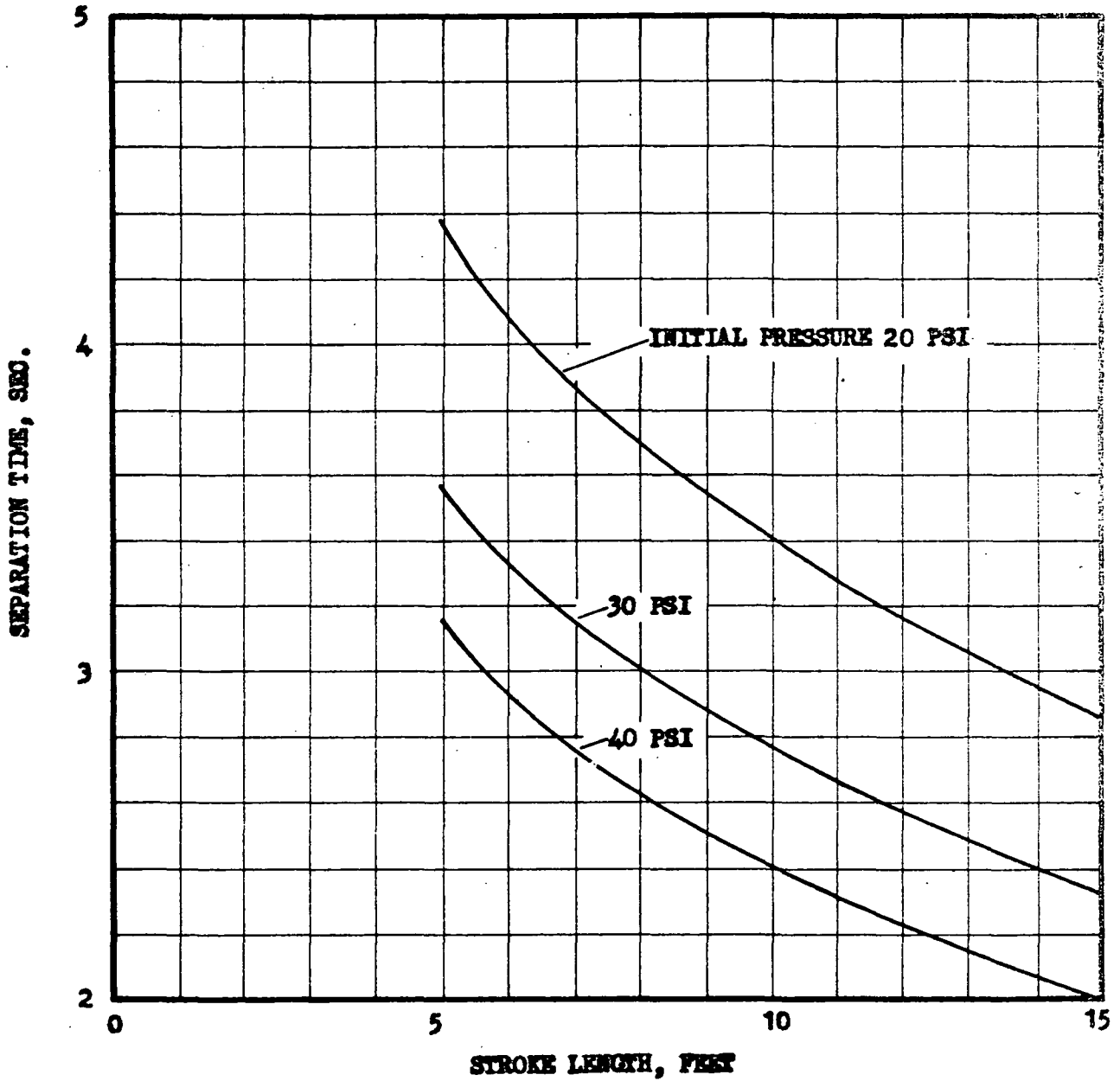
Figure V-A-11



Trajectory Parameters Stage I, Low Thrust

Figure V-A-12

$q = 100 \text{ PSF}$



Staging Data, Separation Time versus Stroke Length

Figure V-A-13

AEROJET-GENERAL CORPORATION

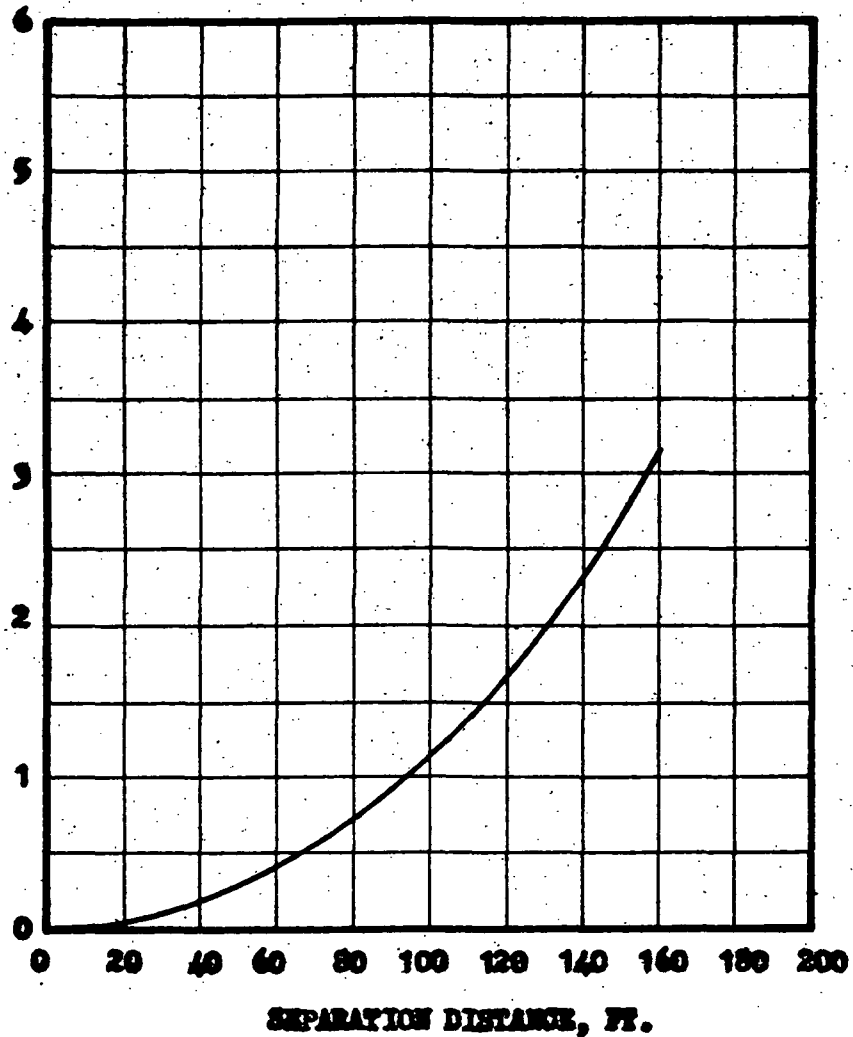
$q = 100 \text{ MP}$

Angle of Attack = 1°

Nozzle Stroke Length = 10 Ft.

Initial Inboard Stage Pressure = 40 psi

INTEGRATED DISPLACEMENT OF EXPANDABLE
NOZZLE AT FIRST STAGE FOR 100 - FT.



Staging Data, Displacement versus Separation Distance

Figure V-A-14

V, Vehicle Analysis (cont.)

B. VEHICLE LOADS AND DYNAMICS

1. Summary

a. Introduction

A wide variety of problems associated with static and dynamic loads, vehicle kinematics and dynamics, and the Sea Dragon environment have been investigated with differing degrees of completeness. The principal result of this work, however, has been the identification and definition of problems in the area of vehicle loads and dynamics which will require more attention in the next design phase of the program.

In many instances, the findings of this preliminary work have indicated that phenomena associated with the Sea Dragon concept (large size, water environment, etc.) do not give rise to insurmountable engineering problems with respect to present technology and conservative estimates of future advances. For example, launch dispersion magnitudes and water re-entry loads can be readily handled.

V, B, Vehicle Loads and Dynamics (cont.)

In other areas it has been recognized that the problems are not yet fully defined or that methods of solution are not readily available, e.g., the acoustic environment and resulting vehicle response.

The more significant results of loads and dynamics studies conducted to date are summarized in the following paragraphs.

b. Sea and Wind Environments

Wave lengths, heights, and periods are given as a function of sea state (wind velocity) in Section V,B,2,a. The concept of "sea spectra" is introduced, and a source of sea spectrum data is referenced.

The upper atmosphere wind environment used in analytical and design studies presented in this report is taken from NASA TN 1274. A maximum wind velocity of approximately 320 ft/sec at 42,000-ft altitude is thereby specified.

V, B, Vehicle Loads and Dynamics (cont.)

c. Floating Loads

The most severe loading condition for the floating vehicle is the case, "full tanks, no ballast." A bending moment of 385×10^6 ft-lb is calculated for the interstage area. This load is substantially less severe than that experienced during erection and is easily reacted by 30 psi tank pressure.

d. Towing Dynamics and Loads

Maximum bending moments of 230×10^6 and 390×10^6 ft-lbs are calculated for the "sagging" and "hogging" conditions respectively. ("Hogging refers to the condition in which the vehicle is supported near the center by an ocean swell, while "sagging" describes the condition in which each end of the vehicle is supported by a wave crest). No dynamic amplification of these loads is anticipated since the vehicle bending modes are much higher in frequency than are the significant frequencies in the sea spectra.

V, B, Vehicle Loads and Dynamics (cont.)

Difficulties in controlling the towed vehicle with respect to yaw and roll in a cross-sea environment are discussed briefly in Section V,B,4,b. A substantial analytical and model testing effort should be expended on this problem in future Sea Dragon studies.

The problem of dynamic interactions of the Sea Dragon vehicle, the towing cable, the towing vessel, and the sea environment is reviewed in Section V,B,4,c. A simplified method of analysis is also presented. A great deal of analysis and model testing remains to be done in this area.

Propellant sloshing frequencies for the vehicle in the towing attitude are found to be in the range 0.208 to 0.722 cps for the first three modes (tanks 90% full). These sloshing frequencies will couple with wave forces when sea state 5 conditions exist (see Section V,B,2). The effects of this slosh coupling on the complete towing configuration remains to be evaluated. However, since the cryogenic tanks will be completely full (97% full for RP-1 tank) during most towing operations of the complete vehicle, no problem is anticipated.

V, B, Vehicle Loads and Dynamics (cont.)

e. Vehicle Erection Loads

The process of erecting the vehicle gives rise to the largest bending moments experienced by the structure, primarily because the Stage II LO₂ tank was placed forward to achieve better aerodynamic characteristics. A maximum bending moment of 1.0×10^9 ft-lb is calculated for the case of a 5.0×10^6 lb effective ballast weight. An internal gas pressure of approximately 30 psi in the first-stage LO₂ tank and second-stage LH₂ tank is required to react the erection bending moment.

It appears that large propellant sloshing forces will not occur during erection due to the fact that the tanks will be nearly full.

f. Prefire Loads and Motions

Dynamic loads due to wave action calculated for sea states up and including Sea State No. 7 are found to be relatively

V, B, Vehicle Loads and Dynamics (cont.)

small. Heaving motion, however, becomes quite violent for sea states above five due to strong coupling between sea spectra and the vehicle heaving mode. There also appears to be possibility of encountering pitch-heave instability for wind velocities above 30 knots (Sea State No. 6). It appears that launching should be restricted to Sea State No. 5 or less, for which a maximum pitch amplitude of 0.17° and maximum heave excursion of 3.0 ft are calculated. This area also requires additional study to determine if the same conditions exist for other configurations and to investigate ameliorating devices such as the use of different ballast unit configurations to change the dynamic characteristics of the vehicle. Forces due to wave induced vortex shedding will not be a problem for the Sea Dragon vehicle. Atmospheric vortex shedding, however, may result in significant responses of the erected vehicle due to coupling with the rigid body pitch mode. A rough calculation indicates an angular excursion of 1.75° for a 25 ft/sec wind velocity.

Propellant sloshing loads are not felt to be of importance during the prefire stage due to fullness of the propel-

V, B, Vehicle Loads and Dynamics (cont.)

lant tanks and frequency separation between sloshing modes and other forcing and natural frequencies of the environment and vehicle.

g. Launching Dynamics

"Launch dispersion" (motions of the vehicle as it leaves the water) are calculated for several disturbing forces. Wave forces in Sea States No. 5 and 6 result in maximum angular deflections and rates of 4.55° and $2.41^\circ/\text{sec}$ respectively. A thrust misalignment angle of 0.25° was found to give rise to maximum dispersions of 1.56° displacement and $1.70^\circ/\text{sec}$ rate. A 33-knot wind gives rise to 5.77° angular dispersion and $1.17^\circ/\text{sec}$ angular rate dispersion. Combined effects are also evaluated. Maximum dispersion displacement and rate for all cases considered were calculated to be 5.82° and $2.41^\circ/\text{sec}$ respectively. It appears that the control system can easily handle these dispersions if activated at the time the vehicle leaves the water.

V, B, Vehicle Loads and Dynamics (cont.)

The possibility of large loads being generated by propellant sloshing response during launch seems remote, since only the higher (fifth and sixth) sloshing modes will couple with the fundamental vehicle bending mode.

The maximum bending moment experienced during the underwater phase of launch (control system inactive) is found to be 201.5×10^6 ft-lb, which is less than the maximum erection load.

h. Flight Loads

The most significant flight load on the Sea Dragon vehicle occurs at maximum dynamic pressure conditions ($q = 1866$ lb/ft, altitude = 34,600 ft). For this condition a wind-induced angle of attack of 4° is found to give rise to a bending moment of 120×10^6 ft-lb in the interstage area.

First-stage tank pressures of 80 psi are required to react the 4.2g longitudinal acceleration which occurs at

V, B, Vehicle Loads and Dynamics (cont.)

burnout. Although larger decelerations occur at re-entry, the resulting axial loads are smaller than those encountered for the burnout condition noted above.

i. Impact Dynamic Loads

The response of the first-stage structure (including the fundamental longitudinal vibration mode) to impact loads is calculated in Section V,B,9. Impact velocities of 300 ft/sec and 600 ft/sec have been considered. The relatively long rise time of the 300 ft/sec impact force results in very little dynamic amplification. However, the rise time of the 600 ft/sec impact shock is sufficiently short to cause 93% dynamic overshoot in the acceleration felt at the nose.

Analysis of the effects of impact shock on the nose cone, cylindrical tanks, and the nozzle involves considerations of dynamic buckling. A large testing and analytical effort should be directed toward this area in future Sea Dragon studies. Response of specific subsystems to impact loads also remains to be investigated.

V, B, Vehicle Loads and Dynamics (cont.)

Based on results of impact studies to date, it appears that impact problems can be handled with presently available technology. A balanced combination of nose cone geometry and impact velocity (accomplished by use of an appropriate drag mechanism) will result in a practical first stage structure. The problem of isolating sensitive components is compatible with present packaging techniques.

j. Special Aeroelastic Effects

In Section V,B,10 the problems of flutter of the first- and second-stage nozzles and the possibility of encountering oscillatory side loads during underwater operation are discussed.

k. Propellant Sloshing

Propellant sloshing frequencies have been calculated for several flight conditions. Fundamental mode frequencies ranging from 0.520 to 0.609 cps are noted.

V, B, Vehicle Loads and Dynamics (cont.)

The primary importance of the excitation of propellant sloshing modes is in connection with autopilot stability. It is possible that sloshing motions will be reinforced by spurious attitude error signals resulting from sloshing forces. This closed-loop reinforcement is particularly acute on Sea Dragon, since the propellant sloshing frequencies are in the range of control frequencies.

It will probably be necessary to design damping devices to preclude closed loop instability; the design process should be guided by a complete analog simulation of the autopilot.

1. Acoustics

A discussion of the Sea Dragon acoustic environment and its effect on the vehicle is presented in Section V,B,12. The principal sources of acoustic environment are found to be (1) generated by the first-stage rocket engine (185 db); (2) caused by the aerodynamic boundary layer (150 db); and (3) created by towing turbulence (155 db).

V, B, Vehicle Loads and Dynamics (cont.)

The predominance of low frequencies in the rocket engine noise spectrum will result in levels of roughly 150 db at distances of 10 to 15 mi from the source for a duration of one minute. A more detailed summary of acoustic environments is given in Table V-B-1.

Vibrational accelerations of 10 to 15g rms are anticipated for the airframe vibration modes. High-damped materials may have to be used to preclude intolerable panel responses.

2. Sea and Wind Environments

a. Sea and Surface Wind Environments

The following chart gives wind velocity, wave height, wave period, and wave length as functions of sea state as listed in Reference A.

V, B, Vehicle Loads and Dynamics (cont.)

Sea State	1	2	3	4	5	6	7	8
Wind Velocity (knots)	4-7	7-12	12-16	16-20	20-24	24-32	32-47	47-66
Wave Height (ft) (2X amplitude)	0-1	1-3	3-5	5-8	8-12	12-18	18-40	40-100
Period (sec)	0-2	2-3.4	3.4-5	5-6.3	6.3-7	7-8.5	8.5-15	15➤
Length (ft)	0-20	20-60	60-100	100- 250	250- 300	300- 400	400- 900	900➤

This chart illustrates the limited value of the term "sea state" in describing sea environment; since a particular sea state will encompass a range of wind velocities, wave heights, periods and, wave lengths. A more significant representation is one utilizing "sea spectra" to describe the sea condition as a random phenomenon. Sea spectra corresponding to various sea states are given in Reference B. Further description of the concept of sea spectra is contained in an appendix to this volume.

References

- A. Carsola, A. J., "Sea State Versus Sea Spectrum", presented at SNAME Meeting, La Jolla, Calif., 14 April 1962.

V, B, Vehicle Loads and Dynamics (cont.)

B. Observing and Forecasting Ocean Waves, USN Hydrographic Office Publication No. 603.

b. Upper Atmosphere Wind Environment

The upper atmosphere wind profile used to compute the Sea Dragon Aerodynamic loading was taken from NASA TN D-1274. Figure 6 in this reference, for a 99% probability of occurrence, was used, i.e., the maximum wind velocity, approximately 320 ft/sec, occurs at an altitude of 42,000 ft. (As shown in the section describing aerodynamic loads, V,B,8, the maximum dynamic pressure during Sea Dragon ascent occurs at 34,600 ft.)

3. Floating Loads

The static bending moments due to buoyant and weight distribution loading for various horizontal floating (in still sea) conditions have been derived. The following cases were considered: tanks empty, no ballast; tanks empty, ballast attached; tanks full, no ballast;

V, B, Vehicle Loads and Dynamics (cont.)

tanks full, ballast attached; and fuel tanks full, LO₂ tanks empty, ballast attached. The only ordinary floating condition that has bending moments greater than the aerodynamic moment is the case of full tanks, no ballast attached. In this condition the maximum bending moment occurred in the interstage area (Figure V-B-1) and was approximately 385×10^6 ft-lb. Since this moment is much less than that incurred during erection, the 30 psi tank pressure required for structural integrity during erection is more than sufficient for safe operation of the vehicle under the floating condition described above.

4. Towing Dynamics and Loads

a. Hogging and Sagging Loads

The terms "hogging" and "sagging" pertain to static conditions during which the vehicle is supported near the center by an ocean wave (hogging) or supported at each end by two crests (sagging).

V, B, Vehicle Loads and Dynamics (cont.)

Static internal shear and bending moments along the length of the vehicle were determined in the following manner:

The vehicle was supported horizontally on a trochoidal wave with a length to height ratio equal to $L/20$ where L = length of the vehicle. The pressure load, as distributed in the hogging and sagging conditions, is reacted by the weight distribution, and the resultant shear and bending moment distributions are derived. The trochoidal wave profiles were determined through the use of Bonjean curves. The shear and bending moment distributions were then found by an iterative technique.

Shear and bending moment curves are presented in Figures V-B,2,3,4,5. Maximum shear and bending moments are tabulated below:

	Shear (lb)	Bending Moment (ft-lb)
Hogging	8,000,000	390,000,000
Sagging	5,100,000	230,000,000

V, B, Vehicle Loads and Dynamics (cont.)

The maximum internal bending moment from the hogging conditions appears to be approximately twice as large as the maximum moment due to sagging. The slight irregularity of the curve shapes are due to the irregularities in load distribution. No dynamic amplification of the internal shear and moments is indicated since the exciting frequencies of the wave spectra are sufficiently lower than the nature (free-free beam) frequencies. (The first free-free bending mode frequency of the towing configuration is 1.35 cps. Wave periods giving rise to significant hogging and sagging loads will be greater than five seconds; thus the exciting frequencies will be below 0.2 cps.)

b. Cross Sea Effects

The Sea Dragon vehicle, being cylindrical in shape, will have tendencies to spin about its longitudinal axis in a cross-sea environment. The sponsons on Stage II will prevent any vehicle roll.

V, B, Vehicle Loads and Dynamics (cont.)

Another complication is that the vessel will be driven to a steady yaw angle; it is also possible that yaw oscillation may result from the cross-sea forces, causing the towed vessel to swing from one side of the towing course to the other, imparting surging loads to the towing lines.

c. Towing Cable Dynamics

The dynamic interactions between the elastic towing cable, the Sea Dragon vehicle, the towing ship, and the sea environment may be one of the more important considerations in the evaluation of system towing dynamics. The primary consideration here is one of excitation of the mass-spring-mass system by long ocean swells resulting in a whip-cracking motion between the vehicle and towing vessel.

The solution to the towing dynamics problem should combine analysis with model testing. Parametric variations in towline elasticity and length, towing configurations, damping devices, etc., may then be carried out to arrive at a satisfactory towing scheme.

V, B, Vehicle Loads and Dynamics (cont.)

Studies of this nature are common in marine practice; it should only be necessary to apply known techniques of analysis to the Sea Dragon case.

An example of the type of analytical work involved in the towing dynamics problem is presented in an appendix to this volume. The dynamic model is shown, and wave forcing functions are formulated.

d. Propellant Sloshing During Towing

(1) Introduction

The unsteady nature of the towing force and the wave-induced pitching motion of the Sea Dragon vehicle during the towing operation will cause fluid oscillations within the propellant tanks if the tanks are not completely full. If the sea is not calm, the suddenly applied force due to whip-lash of the towing cable will excite the fundamental longitudinal sloshing mode. The resulting

V, B, Vehicle Loads and Dynamics (cont.)

motion of the fluid will be sustained due to the periodic nature of the forcing function, and if the excitation frequency is nearly equal to slosh natural frequencies, substantial sloshing forces may result.

(2) Solution for Longitudinal Sloshing

By use of Reference A, which gives the sloshing frequency relationships for the longitudinal modes of liquid oscillation in horizontal circular cylindrical tanks, the first three modes for the four tanks may be determined.

The following natural frequencies of the contained fluids are evaluated for a fluid height to tank diameter ratio of 0.9, which corresponds to a nearly full condition.

V, B, Vehicle Loads and Dynamics (cont.)

Propellant Sloshing Modes During Towing
Operation for $h/d = 0.9$

	(cps)	(cps)	(cps)
First Stage LO ₂ Tank	0.261	0.416	0.577
First Stage RP-1 Tank	0.346	0.551	0.684
Second Stage LO ₂ Tank	0.365	0.581	0.722
Second Stage LH ₂ Tank	0.208	0.332	0.412

(3) Discussion of Results

The fundamental longitudinal modes of fluid oscillation for the propellants in the nearly full condition may be seen to be in the frequency range of 0.2 to 0.4 cps. This corresponds to an expected pitching frequency of the vehicle from 0.1 cps to 0.3 cps during Sea State No. 5. Therefore, it is expected that a resonant condition will exist during towing for certain sea conditions.

If the longitudinal propellant slosh modes are excited by the pitching motion of the vehicle, the fluid wave height within the tank will be restricted by the curved upper surface

V, B, Vehicle Loads and Dynamics (cont.)

of the cylindrical tanks. Because of the restricted fluid motion near the free surface, the slosh mass ratio (equivalent sprung mass to total propellant mass) is small, thus resulting in reduced oscillatory pressures on the tank walls. If the perturbation pressures result in too high a stress level within the tank walls, additional slosh suppression devices would be used, such as annular baffles or floating "cans."

5. Vehicle Erection Loads

a. Static Loads

The bending moments encountered during erection of the fully loaded Sea Dragon have been calculated. Erection is effected by filling of the ballast tanks after arrival at the launch site. Figures V-B-6 and V-B-8 show the weight and buoyant force distribution on the vehicle for two ballast flooding conditions; 2.5×10^6 lb effective ballast and 5×10^6 lb effective ballast. Figures V-B-7 and V-B-9 illustrate the bending moment distribution for the two respective

V, B, Vehicle Loads and Dynamics (cont.)

cases. The case of 5.0×10^6 lb effective ballast represents the maximum moment during erection, 1×10^9 ft-lb. Further flooding of the ballast causes the moment to decrease due to the rapidly increasing angle with the horizontal. The moment of 1×10^9 ft-lb is the maximum bending moment experienced by the vehicle during all loading conditions.

The internal gas pressure in the first stage LO_2 tank and second stage LH_2 tank required to resist this moment is approximately 30 psi.

b. Dynamic Loads due to Propellant Sloshing

The possibility of large sloshing forces arising during the erection operation is slight. If the tanks are completely full, the sloshing frequency is infinite and there will be no sloshing forces transmitted to the structure. Probably there will be a small ullage resulting in a high slosh natural frequency which will not be excited by the quasistatic erection operation.

Reference A: NASA TN D252, "Investigation of the Natural Frequencies of Fluid in Spherical and Cylindrical Tanks." McCarty and Stephens.

V, B, Vehicle Loads and Dynamics (cont.)

6. Prefire Loads and Motions

The purpose of this section is to determine the wind and wave induced motions of the erected vehicle, to evaluate the effects of vortex shedding (wind and ocean waves), and to discuss the effects of propellant sloshing forces in the prefire condition.

a. Wind and Wave Induced Motion

The object of this portion of the study was to determine the maximum amplitudes of position, velocity and acceleration for two principal degrees of freedom, namely, pitch and heave. Two basic conditions were considered for various sea states. The first of these is the nominal prelaunch which was assumed to occur at less than sea state 5 (wind velocity 20 knots). The main consideration in this case was the effect of the motions on launching. The second case considered was the standing condition which could occur where the sea would rise unexpectedly and it would be necessary to have the vehicle ride out the storm. In this case the main consideration was the effect

V, B, Vehicle Loads and Dynamics (cont.)

on the structure from dynamic loads. These studies were conducted to sea state 8 (wind velocity 50 knots). The method and results are discussed in the following paragraphs.

To maintain a condition of pitching equilibrium, the external forces of wind and sea acting about the center of rotation of the vehicle are balanced by an equal restoring buoyant force acting about the center of rotation so that a summation of moments about that point is equal to zero. The dynamic forces are balanced by the response of the vehicle, as discussed in the example shown in an appendix and Section V,B,6,a, (3) of this volume.

(1) Wind Force

The force exerted on the vehicle due to wind is expressed as

$$F_{\text{wind}} = \frac{1}{2} \rho V^2 S C_d$$

V, B, Vehicle Loads and Dynamics (cont.)

where ζ = air density, V = wind velocity, S = exposed frontal area, and C_d is the coefficient of drag. The wind force is constant for a particular wind velocity.

(2) Moment due to the Wind Force

The wind force produces a moment about the vehicle center of mass which reacts the buoyant restoring moment. The steady-state pitch angle (ϕ_0) is simply

$$\phi_0 = \frac{M_{\text{wind}}}{W \times \overline{CB}}$$

where W = vehicle weight, \overline{CB} = metacentric height.

(3) Sea Motion

The motion of the sea is applied to the vehicle surface below the water line as a force per unit length which decreases exponentially with depth. The moment from the water force

V, B, Vehicle Loads and Dynamics (cont.)

acting about the center of rotation may be determined by integrating the unit force along the submerged length (L) of the vehicle as follows:

$$dM = (\bar{y} - y) dF$$

$$M = \int_0^L (\bar{y} - y) (S C_d \frac{S}{2} v^2 e^{-2my}) dy$$

Therefore

$$M = K \int_0^L e^{-2my} (\bar{y} - y) dy$$

where

$$K = S \frac{S}{2} C_d v^2$$

$$y = \text{depth}$$

$$m = 2 \pi / \lambda$$

$$\beta = \text{vehicle diameter}$$

$$\lambda = \text{wave length}$$

The "static" pitch angle from water forces is

$$\phi' = \frac{M_{\text{water}}}{W \times \overline{CB}}$$

ϕ' is then divided by the wave amplitude and the quotient is squared. The squared term is then multiplied by the dynamic response factor, and the square root taken to obtain the root mean square of the dynamic pitch angle (ϕ' dynamic). The total pitch angle experienced by the vehicle from wind and water loads is $\phi' + \phi' \text{ dyn.}$

V, B, Vehicle Loads and Dynamics (cont.)

The dynamic response factor referred to above is obtained by the spectral density method explained in Reference A and B and illustrated in an appendix to this volume.

Heave amplitudes are obtained directly by the spectral density method except with a damping coefficient of 0.04.

(4) Dynamic Loads

The dynamic loads experienced in the pre-fire condition for sea states 6 and 7 are shown in Figures V-B-10, -11, -12, -13, -14 and -15. These loads are very small and will be easily reacted by internal pressure.

(5) Vehicle Motion

Vehicle motions as a function of wind velocity are presented in Figures V-B-16 and -17. A plot of sea state versus wind velocity is presented as Figure V-B-18 for correlation of vehicle motions as a function of sea state.

V, B, Vehicle Loads and Dynamics (cont.)

It appears that the Sea Dragon vehicle could be launched in conditions corresponding to Sea State No. 5 or less. The maximum pitching and heaving amplitudes for Sea State No. 5 are =

	<u>Displacement</u>	<u>Rate</u>	<u>Acceleration</u>
Pitching	0.17°	0.00034 deg/sec	0.000058 deg/sec ²
Heaving	3.0 ft	0.51 ft/sec	0.09 ft/sec ²

For environments more severe than Sea State No. 5, large responses in heave are anticipated because of excitation of the natural heaving mode of the vehicle by these sea spectra. For a 30 knot wind condition, the following responses are calculated:

	<u>Displacement</u>	<u>Rate</u>	<u>Acceleration</u>
Pitching	0.33°	0.056 deg/sec	0.0096 deg/sec ²
Heaving	18.0 ft	3.1 ft/sec	0.52 ft/sec ²

Beyond the 30 knot condition, coupling of pitch and heave is expected to present a significant problem for the present configuration. A wind velocity of approximately 30 knot would

V, B, Vehicle Loads and Dynamics (cont.)

imply 40-ft heave amplitude, which corresponds to neutral stability in pitch. Further analytical and model study is required to determine the implications of coupling and to find the best solution to the problem. The possibility of damping devices incorporated into the ballast unit or changes in the configuration should be evaluated.

References

- A. Carsola, A. J., "Sea State Versus Sea Spectrum", presented at SNAME Meeting, La Jolla, Calif., 14 April 1962.
- B. Observing and Forecasting Ocean Waves, USN Hydrographic Office Publication No. 603.

b. Prefire Vortex Shedding

(1) Atmospheric Vortex Shedding

The phenomenon of vortex shedding in the wake of a body is a familiar one to missile designers. Many instances of forced excitation of elastic structures can be found in engineering literature.

V, B, Vehicle Loads and Dynamics (cont.)

The problem of vortex induced forces on the Sea Dragon vehicle prior to launch can be broken into two categories: the excitation of the elastic body modes and excitation of the rigid pitching mode. It should be pointed out that structural response to forces produced by vortex shedding is not truly an aeroelastic phenomenon because the airloads are very nearly independent of the unsteady motion.

The vortex shedding mechanism is strongly a function of Reynolds Number (RN). In the region of low RN, vortices are produced in a regular discrete manner. As RN is increased, the resulting turbulence causes the process to become more random in nature (See References A and B). Reference B is concerned with this problem in the "supercritical" range of RN ($RN > 500,000$).

Reynolds numbers experienced by Sea Dragon, when expressed as a function of velocity, can be written

$$R.N. = \frac{\rho v d}{\mu} \quad 478,000 V$$

where

$$\rho = \text{air density} = .00238 \text{ lb sec}^2/\text{ft}^4$$

V, B, Vehicle Loads and Dynamics (cont.)

$$\mu = \text{air viscosity} = .373 \times 10^{-6} \text{ lb sec/ft}^2$$

$$d = \text{body diameter} = 75.0 \text{ ft}$$

Assuming, for example, a velocity of 50 ft/sec gives $RN = 23,900,000$, which is in the supercritical region. In Reference B, it is shown that most of the energy in the wake is concentrated in the region of nondimensional frequency, $S = \frac{d}{TV} = 0.1$, where $T =$ vortex period.

Thus

$$T = \frac{d}{SV} = \frac{750}{V}$$

Assuming that appreciable forces can be experienced only for velocities above 10 ft/sec, the range of significant periods up to a velocity of 50 ft/sec is then $15 \leftarrow T \leftarrow 75$ seconds.

The periods of body bending oscillations are much smaller than those noted above. The natural pitching period, however, is around 30 sec, and rigid body pitching will thus be excited by vortex shedding.

V, B, Vehicle Loads and Dynamics (cont.)

To obtain an order-of-magnitude estimate of pitching response, the torque is written

$$T = F\ell_F = \frac{1}{2}\rho V^2 S_{\epsilon}^1 C_L \ell \stackrel{N}{=} 1070V^2$$

$$C_L = \text{lift coefficient} = 0.3 \text{ (See Reference B)}$$

$$S_{\epsilon} = \text{exposed area} = 15,000 \text{ ft}^2$$

$$\ell = \text{moment arm} = 200 \text{ ft}$$

For $T = 30$ (pitching resonance) $U = 25 \text{ ft/sec}$, $T = 670,000 \text{ ft lbs.}$

Assuming a pitch inertia of $10^{10} \text{ slug ft}^2$ and a gain of 20 at resonance, the angular response is

$$\theta_{\max} = K \frac{T}{I} \frac{T^2}{(2\pi)^2} = .0306 \text{ rad.} = 1.75 \text{ degrees}$$

On the basis of this crude analysis, it is concluded that the pitching response caused by vortex shedding could be a significant factor in launching dynamics.

References

Reference A: Roshko, A, "On the Development of Turbulent Wakes from Vortex Shedding", NASA TN 2913, March 1953.

Reference B: Fung, Y. C., "Fluctuating Lift and Drag Acting on a Cylinder in a Flow at Supercritical Reynolds Numbers", Presented at IAS 28th annual meeting, New York, N.Y., January 1960.

V, B, Vehicle Loads and Dynamics (cont.)

(2) Vortex Shedding Caused by Wave Action

In this section, the possibility of vortex shedding on the erected vehicle caused by wave action is investigated. It is known that failures of cylindrical columns have occurred because of vortex shedding.

The authors of Reference A discuss the problem of wave-created vortices. They conclude that vortex shedding is possible only if the following condition is satisfied:

$$\frac{U_{\max} T}{r} \geq 25 = T_c \quad (1)$$

U_{\max} = maximum particle velocity

T_c = characteristic period

T = wave period

r = radius of cylinder

The maximum velocity in deep water can be written:

$$U_{\max} \cong H \sqrt{\frac{\pi g}{2L}} \quad (2)$$

V, B, Vehicle Loads and Dynamics (cont.)

where L = wave length, H = wave height (See Appendix II-21). An approximate relationship between wave length and period is given in Reference B as

$$L = 3.4T^2 \quad (L \text{ in feet, } T \text{ in seconds}) \quad (3)$$

Combining expressions (1), (2), and (3)

yields:

$$\frac{H}{r} \sqrt{\frac{g}{2 \times 3.4}} \geq 25 \quad (4)$$

Using $r = 37.5$ ft and $g = 32.2$ ft/sec², one finds $H \geq 241$ ft for vortex shedding to take place. This is highly unlikely, and it is concluded that the Sea Dragon vehicle will not experience difficulty due to wave vortex shedding.

References

- Reference A: Nolan, W.C. and Honsinger, V. C., "Wave-Induced Vibration of Offshore structures", paper presented to the Society of Naval Architects and Marine Engineers Gulf Section, 14 September, 1962.
- Reference B: Observing and Forecasting Ocean Waves, USN Hydrographic Office Publication No. 603.

V, B, Vehicle Loads and Dynamics (cont.)

c. Propellant Sloshing During Prefire

It is not expected that propellant sloshing will be a problem when the Sea Dragon vehicle is in the prelaunch condition. The vibration excitation is predominantly low frequency perturbations caused by wave action and the vehicle buoyant "heaving" mode. The frequency of the buoyant mode is approximately 0.06 cps, which is well below the lowest sloshing frequency of 0.520 cps for the prelaunch condition (assuming 5% ullage). Even if the sloshing modes are excited because of some transient disturbance, the sloshing mass (Equivalent sprung mass) is small for the nearly full condition. This is true because fluid motion is limited at the free surface because of the restricted boundary at the top of each tank.

7. Launch Condition

This section is concerned with dynamic loads experienced by the vehicle during launching caused by wave action, wind, and

V, B, Vehicle Loads and Dynamics (cont.)

propellant sloshing. A second major concern in "launch dispersion" (motions of the vehicle at the time it leaves the water) caused by the wind and sea environment, thrust misalignment, and initial motions or displacements.

a. Launch Dispersion

The motions of the Sea Dragon vehicle at the time that the nozzle exit clears the water surface ("launch dispersions") must be determined to evaluate their effect on thrust vector control requirements and on the atmospheric trajectory.

The equations of motion used to determine launch dispersion are derived in Appendix II-21. Four degrees of freedom are allowed the vehicle: y , vertical translation: X , horizontal translation: θ , pitch angle: and ξ , the generalized coordinate of the first bending mode.

V, B, Vehicle Loads and Dynamics (cont.)

Several sources of dispersion are investigated. The effects of impinging waves corresponding to environments encountered in Sea States 5 and 6 are determined; rather severe sea conditions are assumed to find a "worst" case. Wind and thrust misalignment dispersions are also evaluated.

The values of physical constants used in this study are listed below: Refer to Appendix II-21 for definition of the symbols:

$l_1 = 234 \text{ ft}$	$\zeta_B = 1.0$
$l_2 = 61 \text{ ft}$	$l_B = 234 \text{ ft}$
$l_o = 502 \text{ ft}$	$t_B = 3.0 \text{ sec}$
$l_g = 119 \text{ ft}$	$m_o = .624 \times 10^6 \text{ slugs}$
$r = 37.5 \text{ ft}$	$m = 1.240 \times 10^6 \text{ slugs}$
$d = 1000 \text{ ft}$	$S_A = 0.550 \times 10^4 \text{ ft}$
$m_B = 49.0 \times 10^3 \text{ slugs}$	$I = 1.178 \times 10^{10} \text{ slug ft}^2$
$k_B = 7.85 \times 10^6 \text{ lb/ft}$	

V, B, Vehicle Loads and Dynamics (cont.)

(1) Dispersion Caused by Sea State

The following sea conditions are considered:

Sea State 5

$$L = 61.4 \text{ ft} \quad H = 5.0 \text{ ft}$$

Sea State 6

$$L = 107.5 \text{ ft} \quad H = 9.15 \text{ ft}$$

$$L = 1275 \text{ ft} \quad H = 9.15 \text{ ft}$$

The displacements and rates in χ , θ , and ξ are tabulated below for each of these cases at the time the nozzle exit clears the water.

	$H = 5.0 \text{ ft}$ $L = 61.4 \text{ ft}$	$H = 9.15 \text{ ft}$ $L = 107.5 \text{ ft}$	$H = 9.15 \text{ ft}$ $L = 1275 \text{ ft}$
χ (ft)	-17.99	-25.25	-10.92
$\dot{\chi}$ (ft/sec)	-15.41	-14.16	-12.26
θ (deg)	3.48	4.55	2.178
$\dot{\theta}$ (deg/sec)	2.41	2.22	2.15
ξ (ft)	-.036	-.2004	-.0411
$\dot{\xi}$ (ft/sec)	.151	.5601	-.169

V, B, Vehicle Loads and Dynamics (cont.)

(2) Dispersion Caused by Thrust Misalignment

A maximum angle of thrust misalignment of 0.25° is assumed. This condition gives rise to the following dispersion values:

$$X = -5.81 \text{ ft}$$

$$\theta = 1.56^\circ$$

$$\dot{X} = -8.48 \text{ ft/sec}$$

$$\dot{\theta} = 1.70^\circ/\text{sec}$$

$$\xi = -0.0178 \text{ ft}$$

$$\dot{\xi} = -0.1009 \text{ ft/sec}$$

(3) Dispersion Caused by Initial Conditions

The dispersion caused by initial pitching and heaving motion of the vehicle and caused by the sea state are found to be very small. The pitching frequency is so low that resonance is not encountered for the relatively high exciting frequencies associated with the sea conditions under consideration. Thus the pitching response is negligible. Heaving resonances can be excited in Sea Stage No. 6. Results were obtained for the initial conditions $y(0) = -16.0$

V, B, Vehicle Loads and Dynamics (cont.)

ft and $\dot{y}(0) = -6.21$ ft/sec. Resulting dispersions were found to be very small.

The effect of wind is also contained in this section. A wind velocity of 33 knots gives rise to an initial leaning angle of 1.30° . Resulting dispersions are:

$$\begin{aligned} X &= -81.48 \text{ ft} & \theta &= 5.766^\circ \\ \dot{X} &= -21.30 \text{ ft/sec} & \dot{\theta} &= 1.17^\circ/\text{sec} \\ \xi &= -0.1348 \text{ ft} \\ \dot{\xi} &= -0.811 \text{ ft/sec} \end{aligned}$$

(4) Combined Effects, Launch Dynamics

The combined effects of sea condition, wind, and thrust misalignment on launch dispersion are listed below. Thrust misalignment of 0.25° and wind velocity of 33 knots are used.

$$\begin{aligned} \text{Sea State No. 5, } H &= 5.0 \text{ ft,} & L &= 61.4 \text{ ft} \\ X &= -81.04 \text{ ft} & \theta &= 5.58^\circ \\ \dot{X} &= -20.68 \text{ ft/sec} & \dot{\theta} &= 1.00^\circ/\text{sec} \end{aligned}$$

V, B, Vehicle Loads and Dynamics (cont.)

$$\xi = -0.1207 \text{ ft}$$

$$\dot{\xi} = -0.988 \text{ ft/sec}$$

Sea State No. 6, H = 9.15 ft,

L = 107.5 ft

$$X = -80.52 \text{ ft}$$

$$\theta = 5.66^\circ$$

$$\dot{X} = -20.41 \text{ ft/sec}$$

$$\dot{\theta} = 1.02^\circ/\text{sec}$$

$$\xi = -0.1238 \text{ ft}$$

$$\dot{\xi} = -1.023 \text{ ft/sec}$$

Sea State No. 6, H = 9.15 ft,

L = 1,275 ft

$$X = -81.57 \text{ ft}$$

$$\theta = 5.82^\circ$$

$$\dot{X} = -21.41 \text{ ft/sec}$$

$$\dot{\theta} = 1.23^\circ/\text{sec}$$

$$\xi = -0.1313 \text{ ft}$$

$$\dot{\xi} = -1.221 \text{ ft/sec}$$

Note that in some cases the combined effects of thrust misalignment, etc, are more severe than are the individual contributions.

b. Propellant Sloshing During Launch

At the instant of engine firing there is a suddenly applied pitching moment caused by an initial thrust misalignment. The transient nature of the moment will excite the fundamental

V, B, Vehicle Loads and Dynamics (cont.)

and many of the higher antisymmetric sloshing modes in all propellant tanks. However, because of the nearly full condition, the sloshing mass (equivalent sprung mass) is small and its effect on the vehicle will be slight. As the vehicle breaks the water at approximately $t = 5$ sec, the predominate excitation is caused by a structural bending mode at about 2 cps, which tends to excite the fifth and sixth sloshing modes in all tanks. Since the sloshing mass, and thus the sloshing force, is very small for modes higher than the third, there seems to be no serious structural or dynamic stability problems during the launching mode of operation.

The propellant acoustic modes (standing wave effect) may be excited by resonant burning during launch and should be investigated in some detail. The fundamental acoustic frequency for a propellant tank with large ullage at top is given by the formula,

$$f_a = \frac{a}{4h}$$

where a is the velocity of sound for the propellant and h is the height

V, B, Vehicle Loads and Dynamics (cont.)

of the propellant. Rough calculations show that the acoustic frequency is in the range of from 10 to 20 cps for the Sea Dragon vehicle. Further work should be done to investigate the effect of the compressibility of the propellant upon the longitudinal mode of the vehicle. The possibility of these pressure fluctuations coupling with the thrust oscillations of the engine should also be determined.

c. Launch Dynamic Loads

The bending moments induced in the Sea Dragon vehicle during launch are calculated in this section. These results are a by-product of the launch dispersion study of Section V, B, 7, a.

The first body bending mode is included in the launch dynamics equations. The model analysis indicates that the maximum bending moment due to body bending occurs at Station 294. The maximum bending moment per unit deflection in ξ is found to be

$$\frac{dM}{d\xi} = 9.702 \times 10^8 \text{ ft-lb/ft}$$

V, B, Vehicle Loads and Dynamics (cont.)

The stress at Station 294 is thus

$$\frac{d\sigma}{d\xi} = \frac{dM}{d\xi} \frac{r}{I_A} = 74.1 \times 10^3 \text{ psi/ft}$$

where r is the vehicle radius and I_A is the area moment of inertia at Station 294 (steel is assumed as a structural material).

The maximum value of ξ encountered in the launch dispersion studies was $\xi = 0.2,076$ ft. For this condition

$$M = 2.015 \times 10^8 \text{ ft lb}$$

$$\sigma = 15,380 \text{ psi}$$

This moment will be easily reacted by internal pressure; it is thus concluded that dynamic loads at launch will not design the structure.

8. Flight Loads

With the wind profile data from Section V, B, 2, b and the basic Sea Dragon ascent trajectory the aerodynamic loads were computed. For the maximum dynamic pressure conditions, an angle of

V, B, Vehicle Loads and Dynamics (cont.)

attack of 4° was calculated. With the calculated center of pressure location at 126 ft from the nose a thrust-vector gimbal angle of 1° was found to be required to balance the overturning moment. Figure V-B-19 shows the resultant body bending moment for this condition. The maximum moment of 120×10^6 ft-lb occurs at the interstage area.

The remaining major loads in flight are axial loads encountered during first-stage burnout (4.2g). This condition, insofar as the propellant tanks are concerned, presents the maximum loading condition. The axial load on the first stage tanks is in the order of 3 times the equivalent axial load during erection. The internal tank pressure required to resist this burnout load is approximately 80 psi.

9. Impact Dynamic Loads

The dynamic response of the first stage structure to impact loads at re-entry is calculated in this section.

V, B, Vehicle Loads and Dynamics (cont.)

a. Impact Loads, Normal Entry

The dynamic response of the first-stage of the vehicle at water entry is evaluated in this section. A rather complete analysis of the dynamic system is included in Appendix II-22.

The compliance of the gimbal ball has been computed to determine its influence on system response at impact. The stiffness of the ball in compression was found to be 68.4×10^8 lb/ft while the stiffness in tension was found to be 30.7×10^8 lb/ft. The resonant frequency of a mass-spring-mass system comprised of the gimbal ball, motor, and tank (using the tension spring) is roughly 62.7 cps. This frequency is high in comparison with the longitudinal mode frequency of the vehicle (33.1 cps). It is therefore concluded that the gimbal spring does not play an important role in the dynamic response.

V, B, Vehicle Loads and Dynamics (cont.)

The response of the first longitudinal mode of the first-stage structure is expressed by

$$\ddot{\xi} = -\frac{F_N}{m_2} \phi_N - \omega_2^2 \xi$$

ξ = generalized coordinate, longitudinal mode.

m_2 = generalized mass, longitudinal mode.

ω_2 = natural frequency, longitudinal mode.

F_N = impact force.

ϕ_N = modal displacement at the nose cone.

The force induced in the structure at any point η by elastic deformation is

$$F(\eta) = EA(\eta) \xi \frac{d\phi}{d\eta}(\eta)$$

E = Young's Modulus

A = cross-sectional area

$\frac{d\phi}{d\eta}$ = modal slope at η

The acceleration response (rigid body and elastic) is simply

$$a(\eta) = \ddot{x} + \phi(\eta) \ddot{\xi}$$

V, B, Vehicle Loads and Dynamics (cont.)

where $\phi(\eta)$ is the normalized modeshape. Since the modeshape is normalized to unity at the nose, the acceleration at that point is $\ddot{\xi}$.

The force-time histories of 300 ft/sec and 600 ft/sec impact velocities are given in Figure V-B-20. These curves are based on results of water impact tests. The rise time for the 600 ft/sec impact velocity is approximately 0.050 sec; the natural period of the longitudinal mode is 0.030 sec. Appreciable dynamic response can occur only if the rise time of F_N is approximately one fourth of the natural period of the longitudinal mode. Some dynamic response is thus anticipated for the 600 ft/sec impact velocity. The rise time for the 300 ft/sec impact force is roughly 0.120 sec; thus, large dynamic amplification is not expected.

The response of the longitudinal mode to the 600 ft/sec impact force is shown in Figure V-B-21. The rigid body and total accelerations are also given. Note that the dynamic overshoot causes a maximum acceleration at the nose of the vehicle, which is 93% larger than the rigid body value.

V, B, Vehicle Loads and Dynamics (cont.)

These results are based on a half-cone angle of 30° and total vehicle mass of 0.9662×10^4 slugs.

Compressive forces induced at the nose-to-cylinder attachment point and at the gimbal caused by rigid body deceleration and due to elastic deformation are shown in Figure V-B-22. Percent increases in maximum dynamic load due to the response of the longitudinal mode are:

at nose-to-cylinder intersection, $\Delta F = 70\%$

at gimbal, $\Delta F = 57\%$

Again it is pointed out that the amplification of loads caused by 300 ft/sec impact will be very small due to the much longer rise time.

10. Special Aeroelastic Effects

Included in this section are discussions of special aeroelastic problems pertaining to Sea Dragon operation. The problem

V, B, Vehicle Loads and Dynamics (cont.)

of flutter of the nozzle structures is dealt with in some detail. A discussion of the possibility of generating oscillatory side loads on the first-stage nozzle during the underwater trajectory is also included.

a. Nozzle Flutter

A qualitative study of the flutter possibilities of the large first-stage DeLaval nozzle has been carried to mathematical formulation of some parts of the problem. Flutter of such structures in smaller sizes has been observed during operation with overexpanded flow conditions.

Of particular interest are the nozzle bell modes and the several phases of flight conditions which may excite them. However, other modes such as those in bending, pitching and longitudinal motion require similar attention. The problem is further complicated by the thermal effects which may substantially alter the elastic properties and stress levels during the flight phase. None of these possibilities have been examined to a point where conclusions can be reached.

V, B, Vehicle Loads and Dynamics. (cont.)

b. Oscillatory Side Loads

The critical regime for nozzle flow separation occurs during the underwater portion of the engine operation. While under water the nozzle experiences back pressures substantially above those found during ordinary engine operation, so that a nozzle designed for above water operation will undoubtedly experience flow separation while operating underwater.

One of the criteria used in predicting flow separation is the ratio of chamber pressure (P_c) to ambient pressure (P_a). This ratio varies from about 2 at ignition (300 feet below the water surface) to a value of 20 at the water surface. Available data indicate that for $P_c/P_a > 10$ the separation phenomena is reasonably predictable and also reasonably stable and symmetrical.

Small oscillations in the separation point may couple with some part of the structure to produce a resonating condition. However, as the vehicle is ascending, the point of separation will be continually moving towards the nozzle exit, so that in all

V, B, Vehicle Loads and Dynamics (cont.)

likelihood the nozzle will only pass through a point of resonance rather than continually operate at such a point. There is a possibility that, because of the low natural frequencies found in a vehicle of Sea Dragon size, a transient resonant condition such as the one just described may almost be passed by unnoticed.

The region of operation with $P_c/P_a < 10$ may be somewhat serious. During this time the vehicle will not be moving as rapidly as at the time when $P_c/P_a > 10$, so the period of time in which coupling might occur is greater.

Tests on small nozzles at $P_c/P_a < 10$ have indicated that with these pressure ratios the separation phenomena may be both unstable and unsymmetrical. In addition, separation deep within a nozzle (as may be expected with $P_c/P_a < 10$) has been found to be erratic, primarily because of the ejector action of the gas jet in producing rapid pressure fluctuations in the separated region of the nozzle.

V, B, Vehicle Loads and Dynamics (cont.)

There may be some question as to the strict applicability of the above results to Sea Dragon. Separation in nozzles is primarily produced by boundary layer interactions, so that the condition of the boundary layer has a pronounced influence on the character of the separation phenomena. A gas stream with a fully developed turbulent boundary layer does not separate as easily and separates more stably than one with a laminary or transition boundary layer.

Because of the small size of the test nozzles, some of the instability of separation may have been associated with the boundary layer condition and was not necessarily a result of the low value of P_c/P_a . There is no doubt that Sea Dragon will have a fully developed turbulent boundary layer at the point of separation and thus will tend to separate more stably.

A solution to the problems associated with the unsymmetrical loads resulting from flow separation is complex. Flow separation itself can be prevented by placing a plug in the nozzle to

V, B, Vehicle Loads and Dynamics (cont.)

prevent over-expansion. Nonsymmetrical separation can be prevented by use of a separation inducing ring. If the final design allows free nozzle flow and separation, an attempt must be made to define the characteristic frequencies of the oscillating side loads and the nozzle designed such that nozzle bell mode or bending mode resonances do not fall at these frequencies.

11. Propellant Sloshing

a. Analysis of Slosh Natural Frequencies

A preliminary analysis has been performed to determine the first three antisymmetric modes for the natural sloshing frequencies of the propellant tanks in both stages of the Sea Dragon vehicle. This analysis is briefly explained in Appendix II-23. The results are presented in Figures V-5-23, 24, 25 and 26 as plots of the dimensionless frequency, $\frac{\omega n^2 r_0}{g}$, versus the fullness ratio, h/r_0 . Therefore, the sloshing natural frequencies for the first three modes

V, B, Vehicle Loads and Dynamics (cont.)

may be found if the depth of fluid and the acceleration of the vehicle is known at any instant in time.

For example, during the first instant of firing, assuming a 5% ullage in all propellant tanks and an acceleration of 2 g the natural frequencies may be determined. Using figures V-B-23, 24, 25 and 26, a simple calculation shows the natural frequencies to be:

Slosh Natural Frequencies at $t = .1$ sec

	f_1 (cps)	f_2 (cps)	f_3 (cps)
First-Stage LO ₂ Tank	0.631	1.07	1.27
First-Stage RP-1 Tank	0.520	1.07	1.67
Second Stage LO ₂ Tank	0.520	1.07	1.67
Second Stage LH ₂ Tank	0.520	1.01	1.27

At $t=33$ sec, the acceleration is 2.75 g and the fullness ratio is approximately 0.55 for the first-stage oxidizer tank, 0.50 for the first-stage fuel tank, 0.64 for the second-stage

V, B, Vehicle Loads and Dynamics (cont.)

oxidizer tank, and 2.4 for the second-stage fuel tank.*

Slosh Natural Frequencies at $t = 33$ sec

	f_1 (cps)	f_2 (cps)	f_3 (cps)
First-Stage LO ₂ Tank	0.278	0.566	0.703
First-Stage RP-1 Tank	0.266	0.533	0.706
Second-Stage LO ₂ Tank	0.609	1.25	1.95
Second-Stage LH ₂ Tank	0.609	1.18	1.49

b. General Discussion of Propellant Sloshing

The stability of a missile that is controlled by an autopilot control system depends on many parameters; such as bending frequency, natural slosh frequency, ratio of propellant mass to total vehicle mass, control frequency, control system damping and gain, and the types and location of the vehicle attitude sensors.

*Note that because of dissimilar tank shapes, the numerical value of the fullness ratio is not an indication of fluid utilization. In Appendix II-23 this seeming anomaly is clarified.

V, B, Vehicle Loads and Dynamics (cont.)

The interaction of the elastic missile fuselage, feedback control system, and liquid propellant may lead to an unstable mode of operation for any rocket vehicle with a liquid propellant under certain dynamic conditions.

To minimize the effects of the propellant oscillations, several methods may be employed. The proposed method is the introduction of annular baffles, rigidly attached to the tank walls, to disturb the flow near the free surface and create enough turbulence to provide damping. Another slosh suppression device consists of covering the surface of the liquid with floating cans to inhibit the free surface oscillations. A very effective method to prevent the coupling of the sloshing natural frequencies and control frequency is to divide the propellant tank into several longitudinal sub tanks by means of a system of bulkheads. The compartmented tank then consists of several slender tanks, thus increasing the natural slosh frequencies. Besides increasing the natural frequencies, this method effectively reduces the sloshing mass (the equivalent sprung mass), thereby reducing the propellant sloshing forces acting on the system during resonance.

V, B, Vehicle Loads and Dynamics (cont.)

If annular ring baffles are used, as the present design indicates, the optimum configuration and location should be determined. The damping due to a ring baffle has been shown analytically (Reference A), and experimentally (Reference B) to decrease with the depth of the baffle below the surface. The baffle location necessary for substantial damping is limited to a narrow range below the surface so that the optimum spacing of the baffles is dependent on the critical depths of the liquid; i.e., the depth of fluid resulting in a resonant frequency or a condition demanding an increase in damping.

Reference A: "Ring Damping of Free Surface Oscillations in a Circular Tank", Miles, Journal of Applied Mechanics, Vol.25, No. 2.

Reference B: "Experimental Investigation of the Damping of Liquid Oscillations in Cylindrical Tanks with Various Baffles", Silveira, NASA TN-D-715.

12. Acoustics

a. Introduction

The first-stage engine will produce the most

V, B, Vehicle Loads and Dynamics (cont.)

severe acoustic environment that is experienced by the Sea Dragon vehicle and the ground support equipment. Noise generated during the towing operation and aerodynamic turbulence during the atmospheric mode of flight will contribute to this environment. The high intensity noise that is produced by the first-stage engine subjects the surface of the vehicle to sound pressure levels in the order of 180 db (re: .0002 dynes/cm²) during the initial few seconds of engine firing. Aerodynamic turbulence and towing noise to levels of 150 db will constitute the longest duration excitation of the vehicle structure. Appendix II-24 reports an investigation of each of the acoustic noise sources with respect to the excitation of various modes of structural vibration. The appendix describes the method of noise generation and magnitude of the sound pressure levels, and indicates the relative response of the structure.

b. Acoustic Environment

The primary sources of acoustic environment are the first-stage rocket engine during boost phase, the noise of

V, B, Vehicle Loads and Dynamics (cont.)

turbulence during vehicle towing, and aerodynamic pressure fluctuations during flight at high dynamic pressures. The relative magnitude, frequency, duration, and characteristics of the noise caused by the various sources are presented in Table V-B-1. The near field sound level that is experienced by the expendable Sea Dragon, during the effective life of the vehicle, is illustrated by Figure V-B-27, which shows the predicted overall sound levels at a forward vehicle position versus time. Figure V-B-28 plots the contours of the near field sound pressures during launch and illustrates the interaction of the high velocity jet stream and the quiescent fluid medium. The noise levels caused by the rocket engine will be reduced as the vehicle gains velocity so that the sound pressures are maximum during the first few seconds of firing. In particular, the levels created at launch and those experienced by the vehicle at high subsonic speeds will be in the order of 175 db to 185 db. The far field noise will be propagated over large distances as the result of the predominance of the low frequencies in the rocket noise, causing sound levels of 140 to 160 db to be received 10-15 mi from launch position for a duration of about one min.

V, B, Vehicle Loads and Dynamics (cont.)

c. Structural Response

Noise produced during launch will excite the Sea Dragon air frame vibration modes, generating vibrational accelerations to 10 to 15g rms. Towing noise and aerodynamic turbulence will generate a lower level excitation for a longer duration. If correlation of the turbulence exists between the excitation and structural response, the vibration amplitudes could be amplified extensively. The use of highly damped materials is thus recommended to reduce the possibility of the fatigue caused by highly amplified flexural vibrations.

TABLE V-B-1

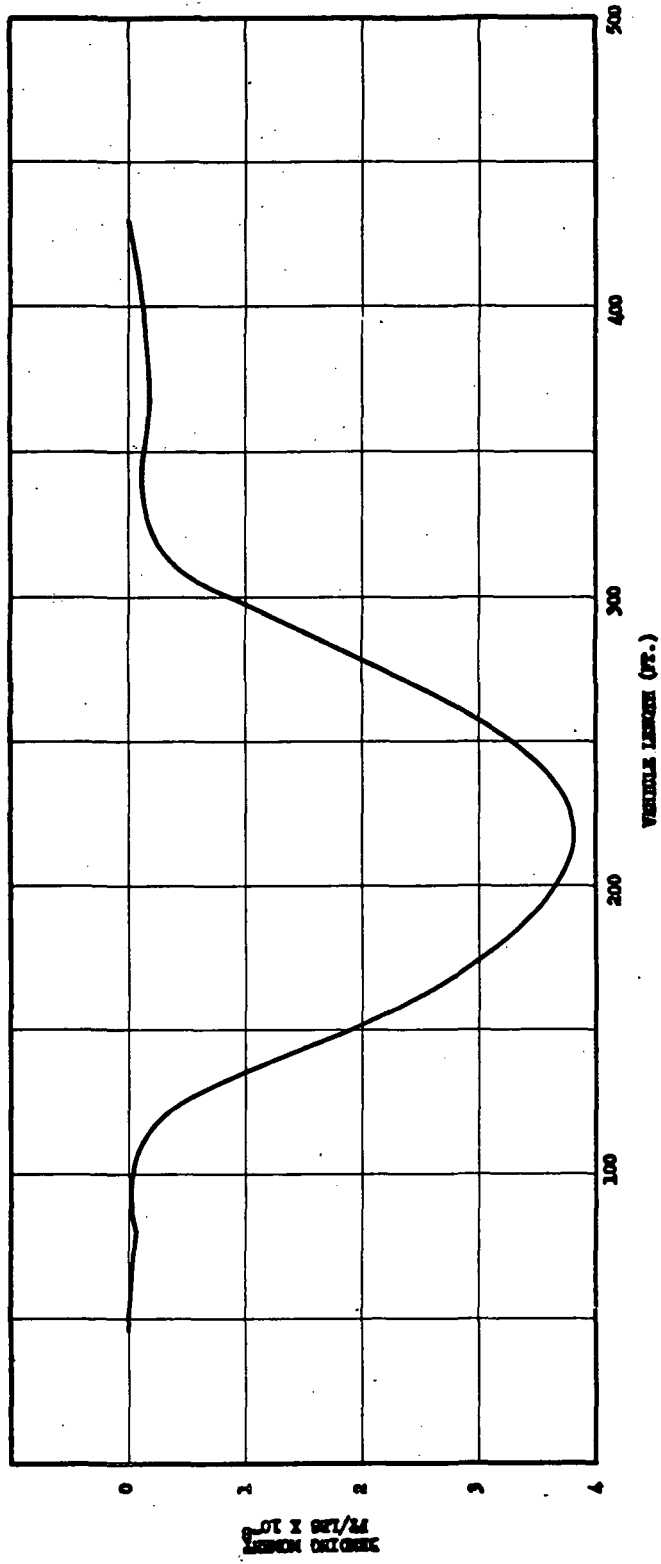
SUMMARY - SEA DRAGON ACOUSTIC ENVIRONMENT

EXPERIENCED BY VEHICLE STRUCTURE

Source Description	Type of Spectrum	Frequency Range	Approximate Duration	Sound Pressure Level db	Confidence in Estimate of SPL
Rocket Exhaust Gas Interaction with:					
a. Water	Continuous with random amplitude	4 cps to 10KC	4 to 5 sec	184 - 190	+3 -10
b. Air	Continuous with random amplitude	4 cps to 10KC	100 sec	175 - 180	+6 -6
Rocket Engine Combustion Oscillation	Discrete	1/2 to 5 cps 10 to 1000 cps	60 sec	10 to 20 db above chamber pressures	+12 -6
Surface to Bottom Reflection	Discrete	1 to 10 cps	4 to 5 sec	20 db Variations along structure	+6 -6
Towing Noise	Continuous Random Amplitude	50 cps to 5KC	5 hours	150 - 160	+10 -10

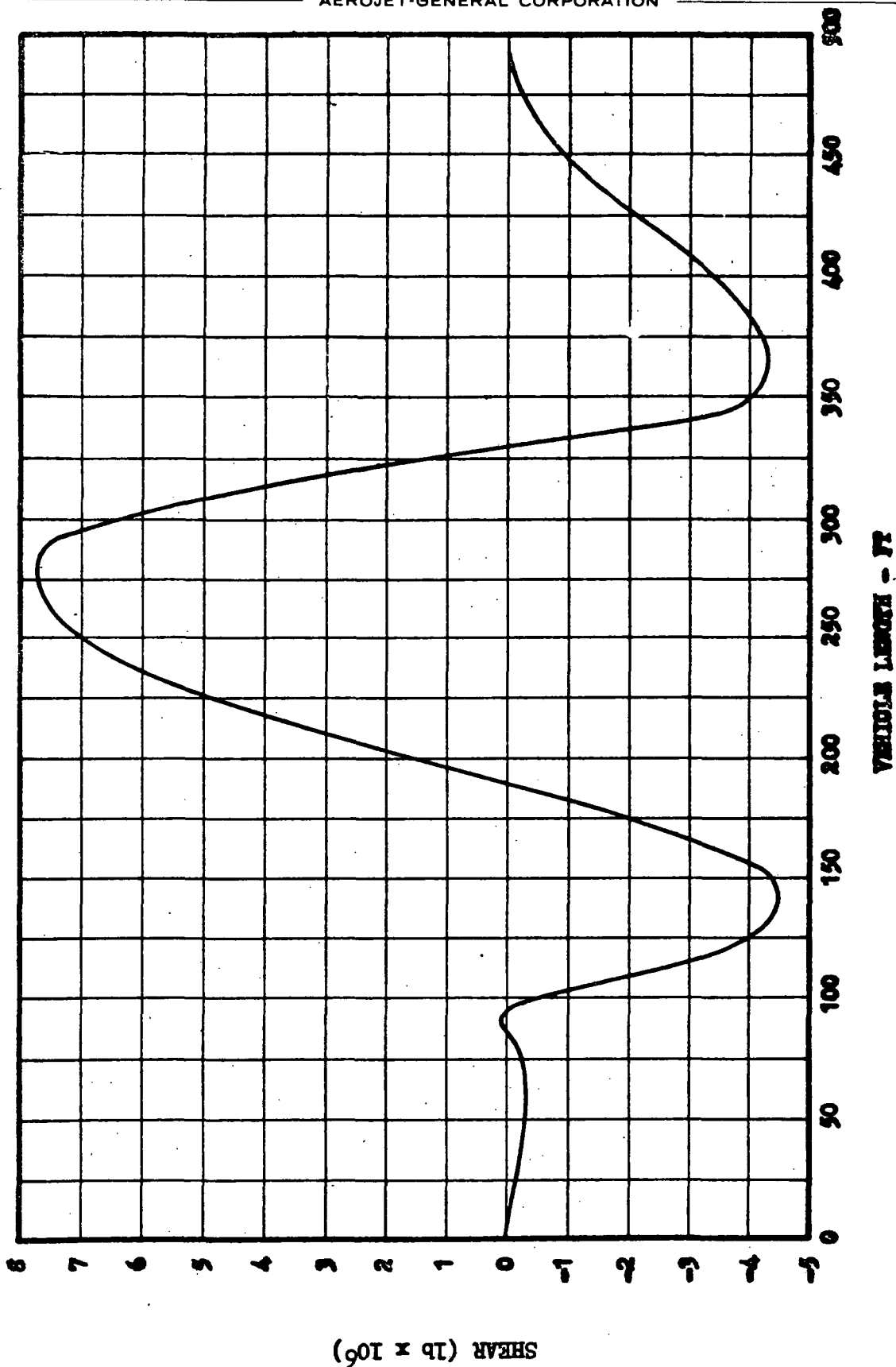
TABLE V-B-1 (cont.)

<u>Source Description</u>	<u>Type of Spectrum</u>	<u>Frequency Range</u>	<u>Approximate Duration</u>	<u>Sound Pressure Level db</u>	<u>Confidence in Estimate of SPL</u>
Aerodynamic Boundary Layer	Continuous Random Amplitude	50 to 10KC	30 sec	146	+3 -3
Base Pressure Fluctuations	Continuous and Discrete	2 to 50 cps	Flight in Atmosphere	150 - 160	+10 -10



Bending Moment Diagram--Still Water, Loaded,
Sealed Interstage

Figure V-B-1



Shear Curve--Hogging Condition

Figure V-B-2

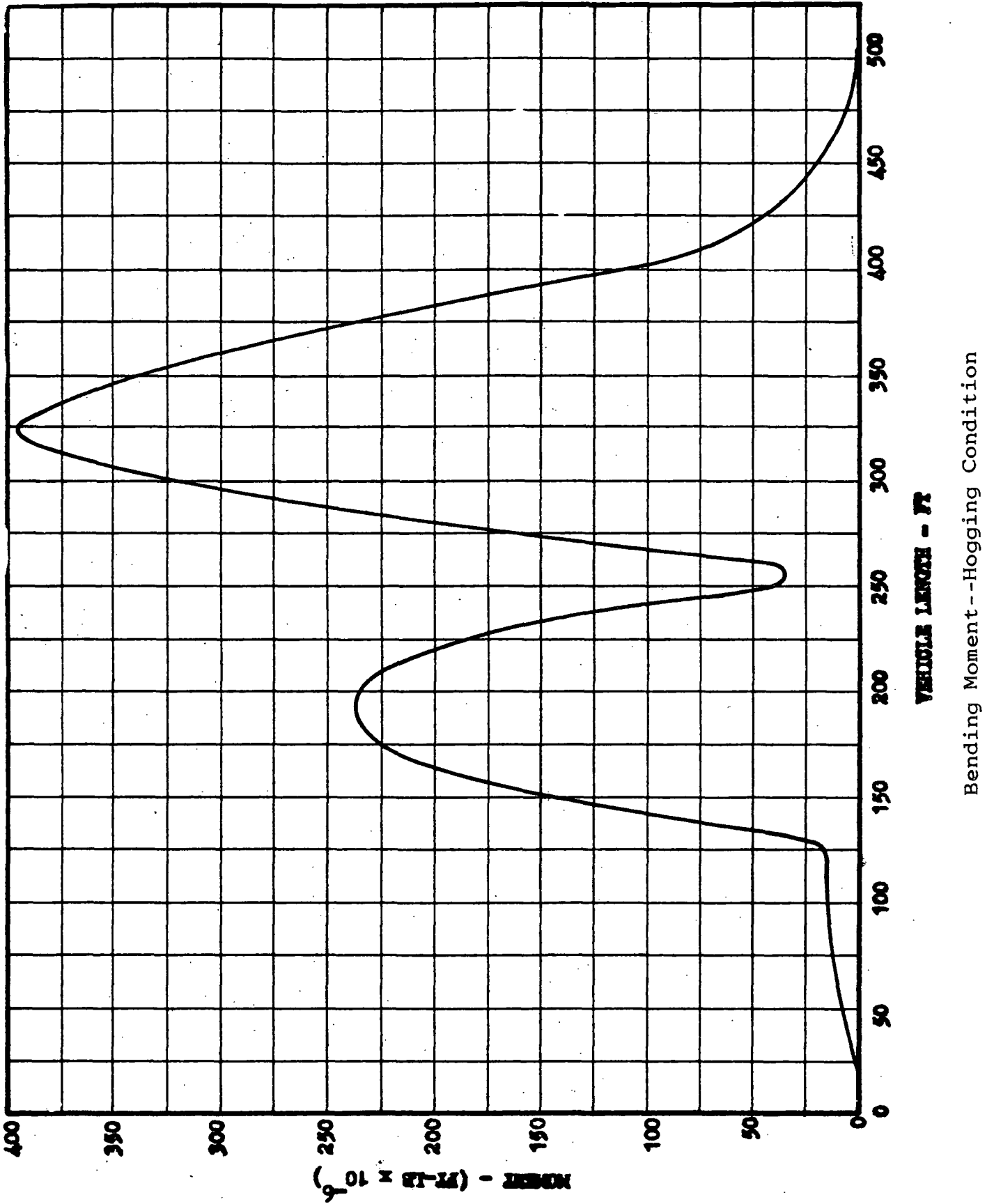
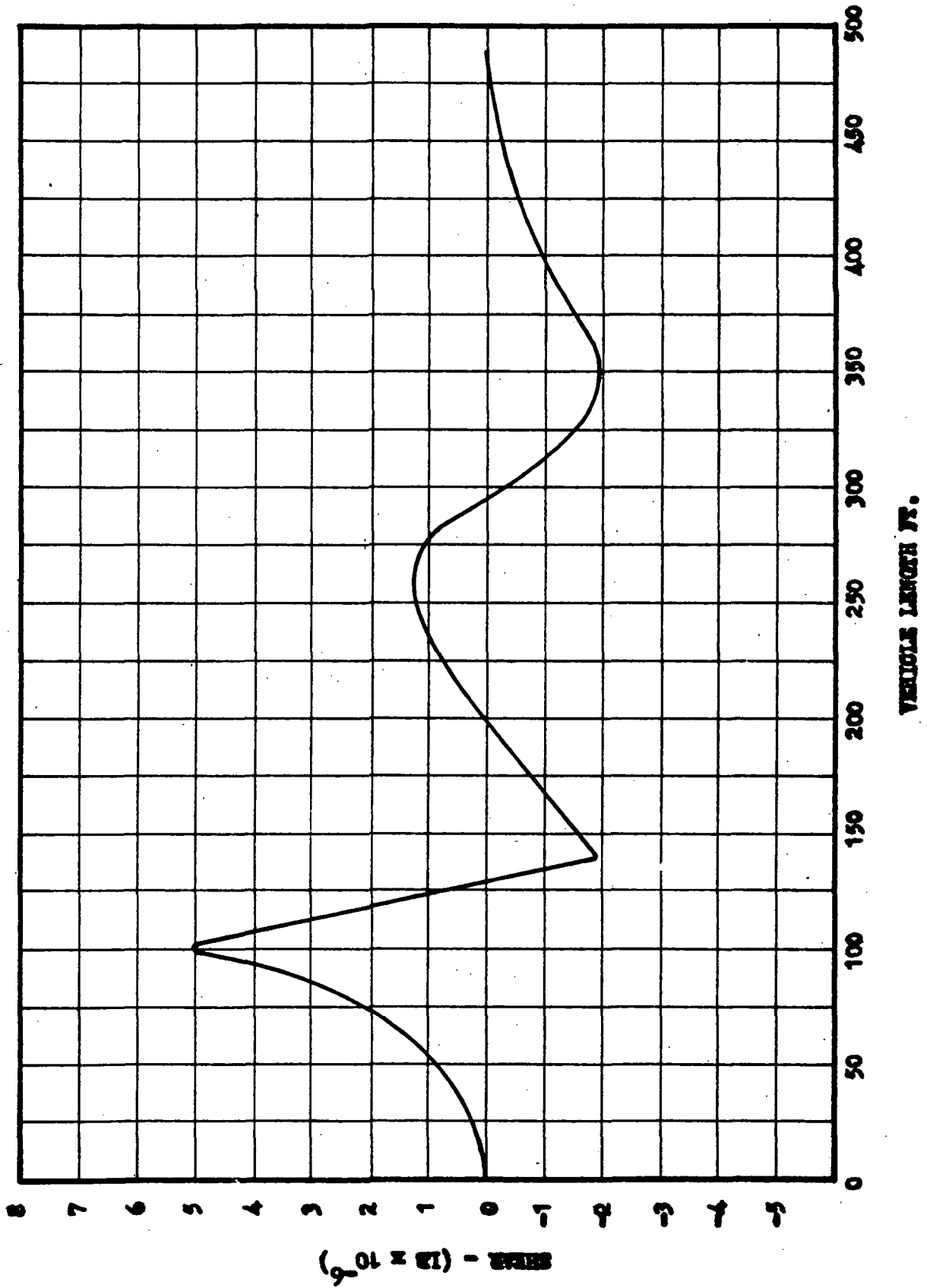
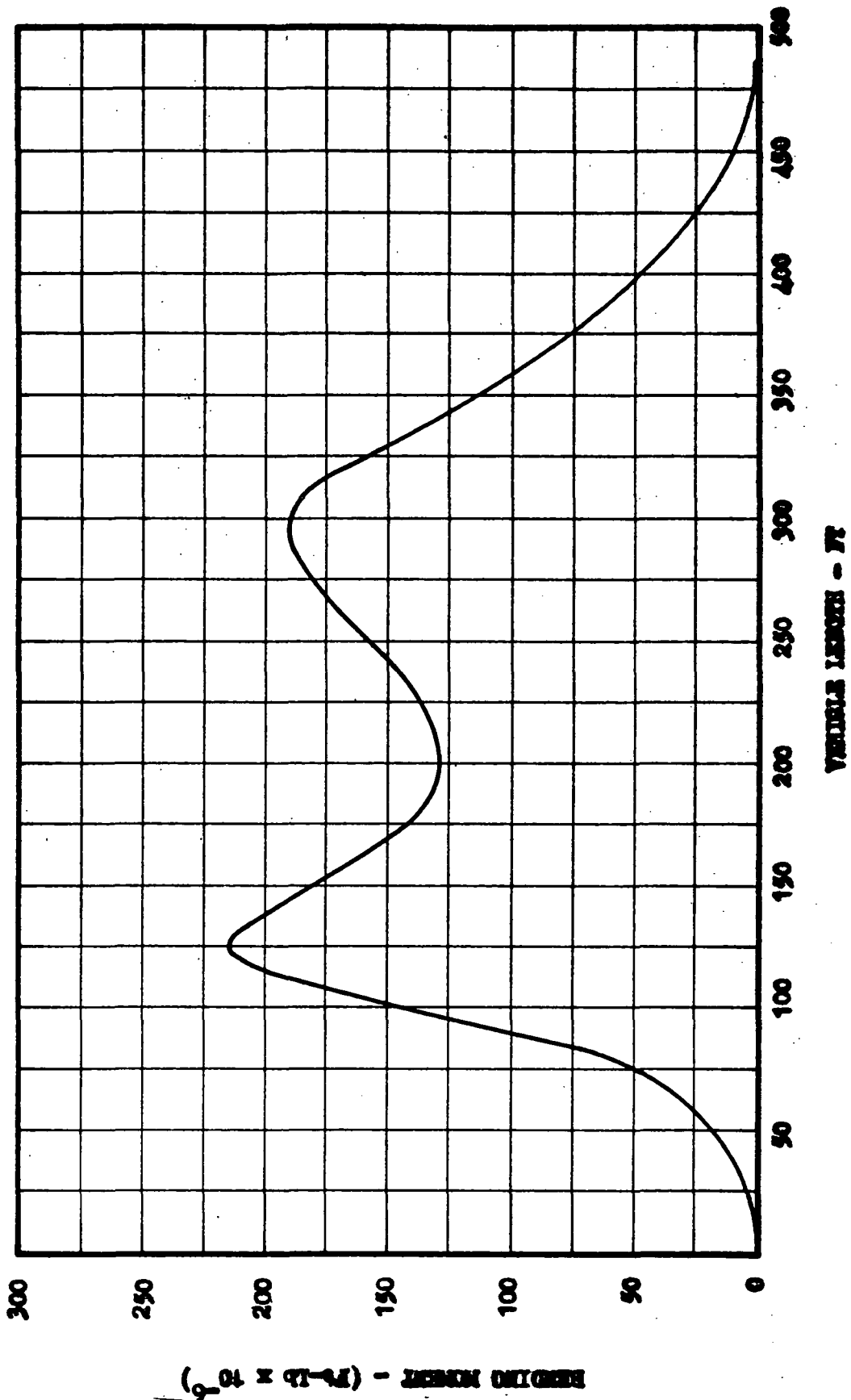


Figure V-B-3



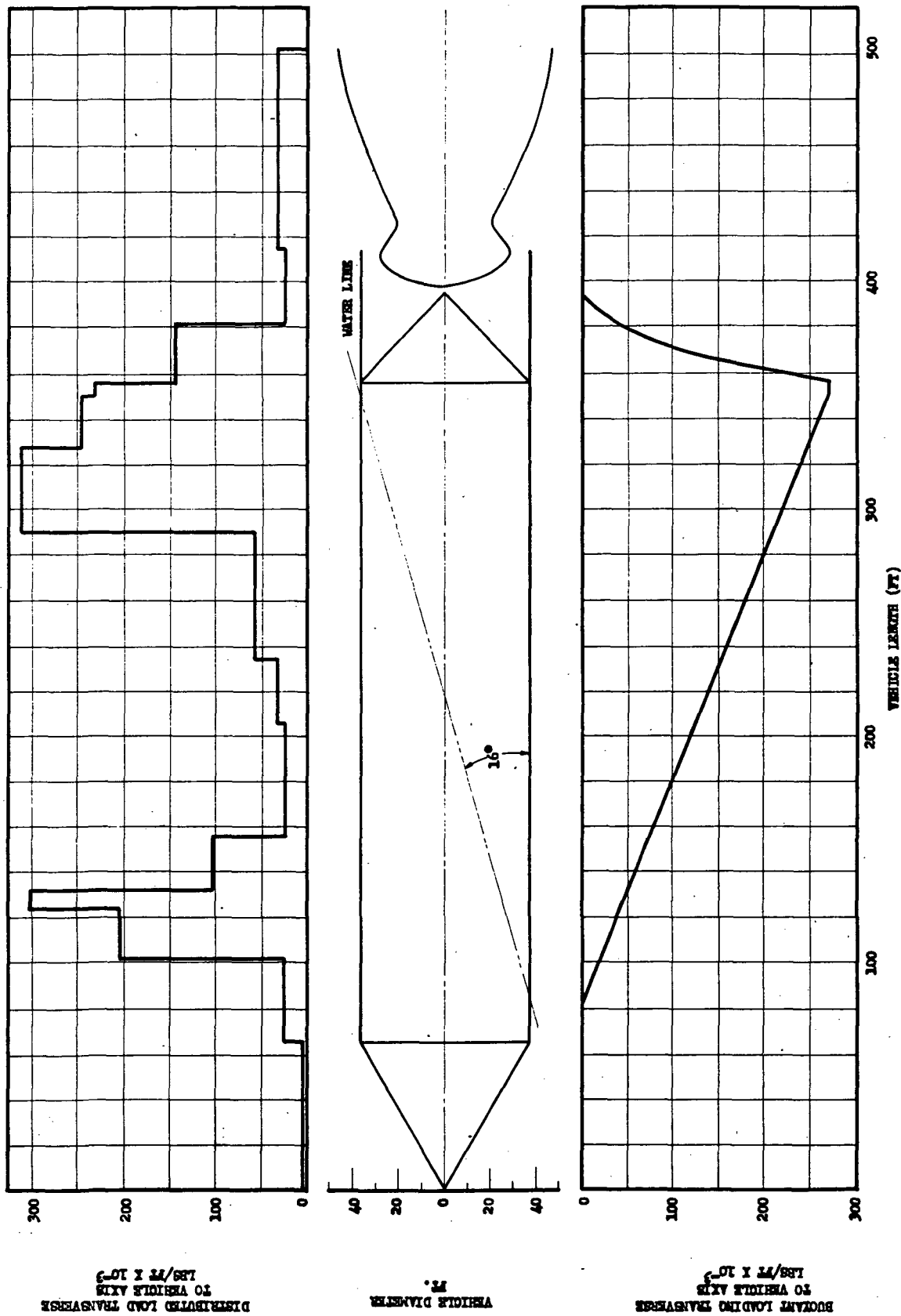
Shear Curve--Sagging Condition

Figure V-B-4



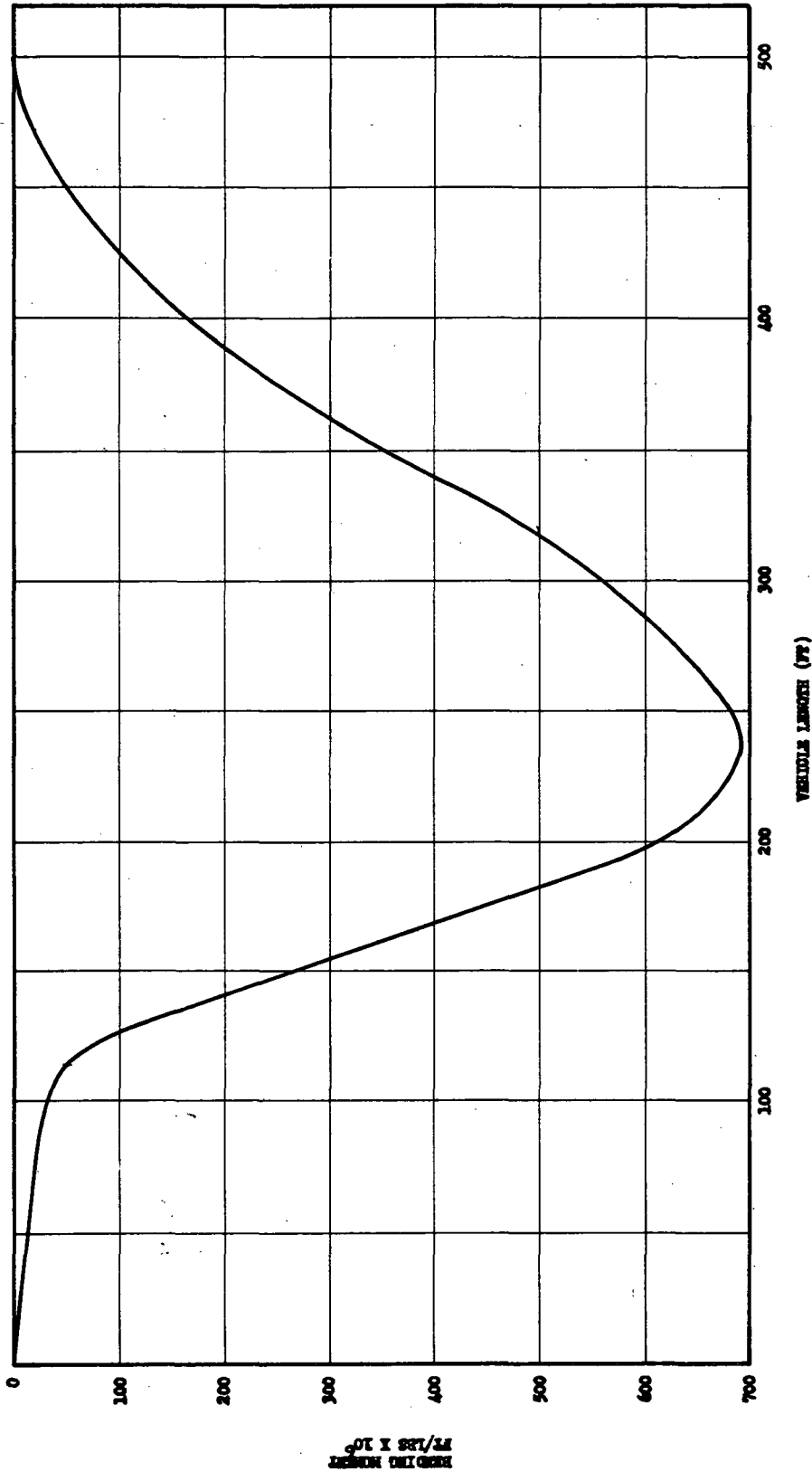
Bending Moment--Sagging Condition

Figure V-B-5



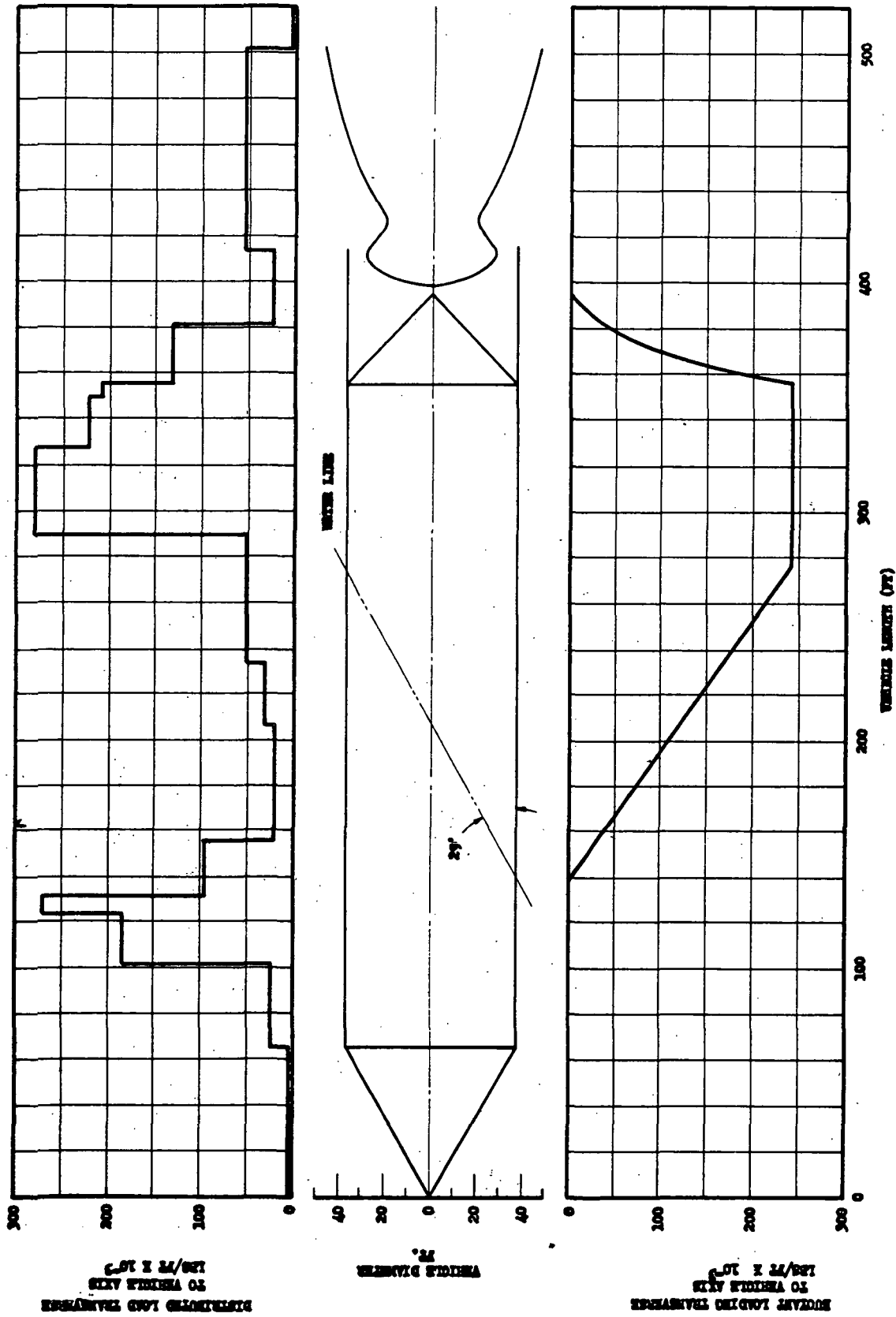
Loading During Erection (2.5 lb 10⁶ lb Ballast)

Figure V-B-6



Bending Moment During Erection (2.5 x 10⁶ lb Ballast)

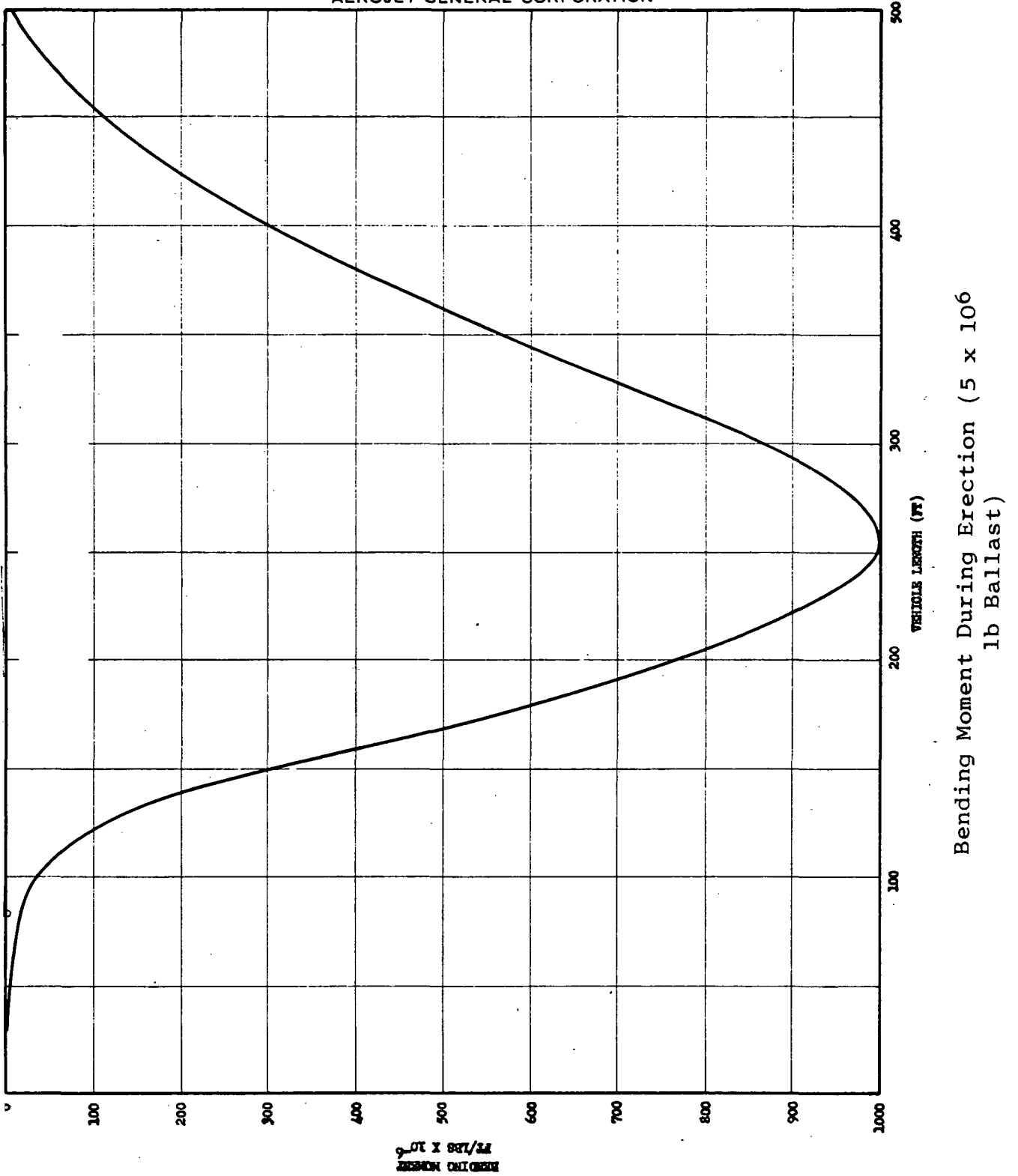
Figure V-B-7



Loading During Erection (5 x 10⁶ lb Ballast)

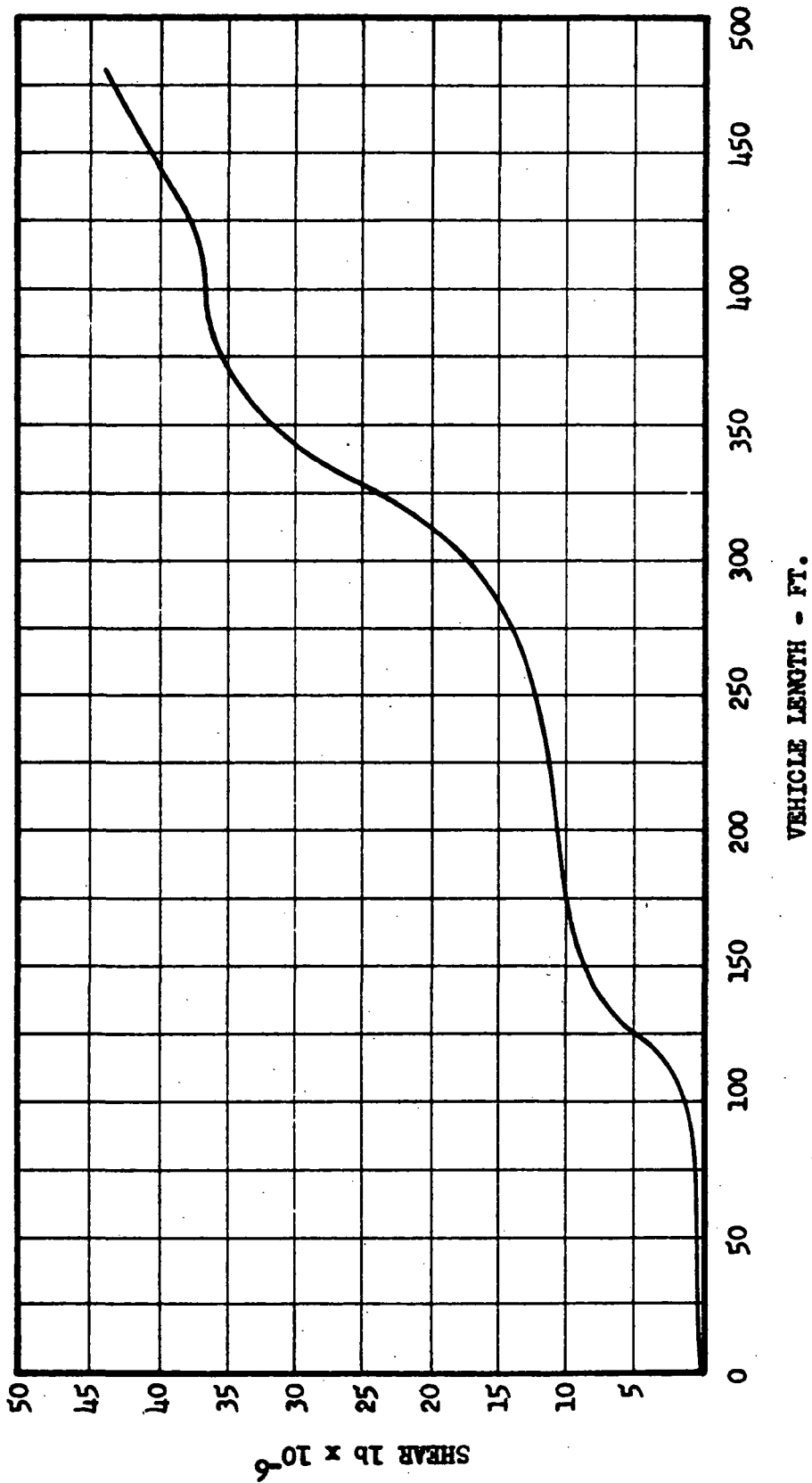
Figure V-B-8.

AEROJET-GENERAL CORPORATION



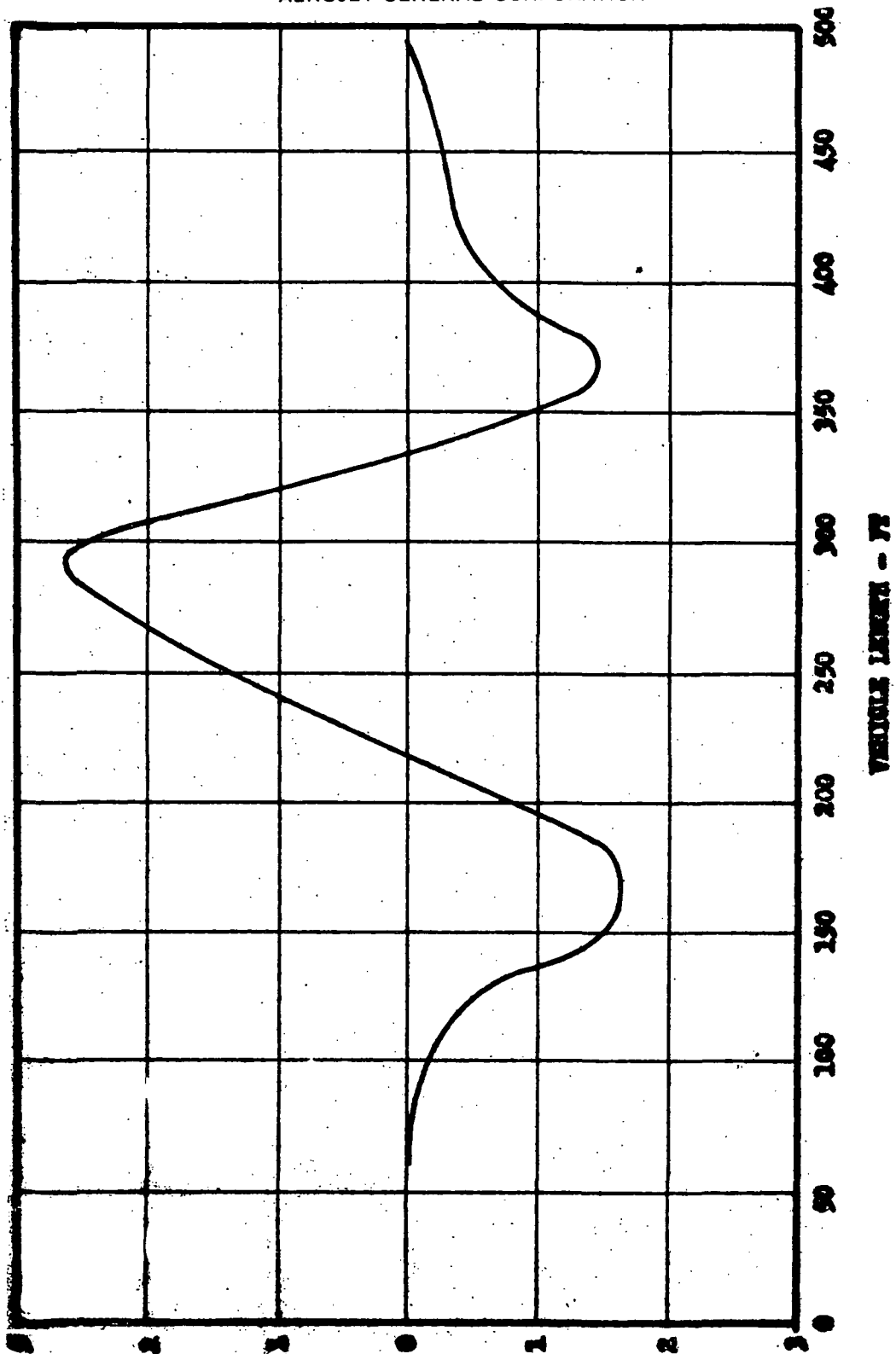
Bending Moment During Erection (5 x 10⁶ lb Ballast)

Figure V-B-9



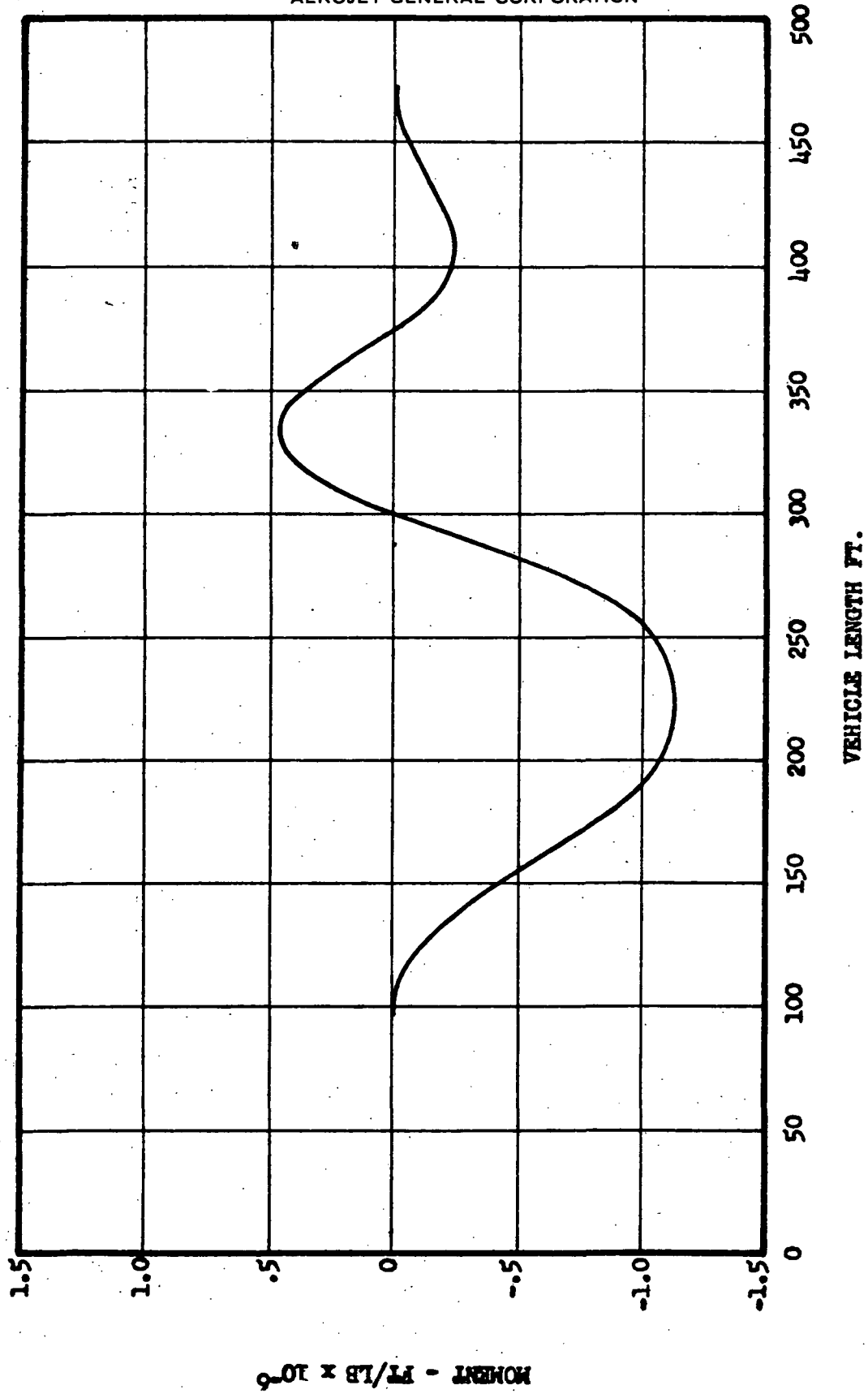
Axial Load versus Station (Sea State 6)

Figure V-B-10



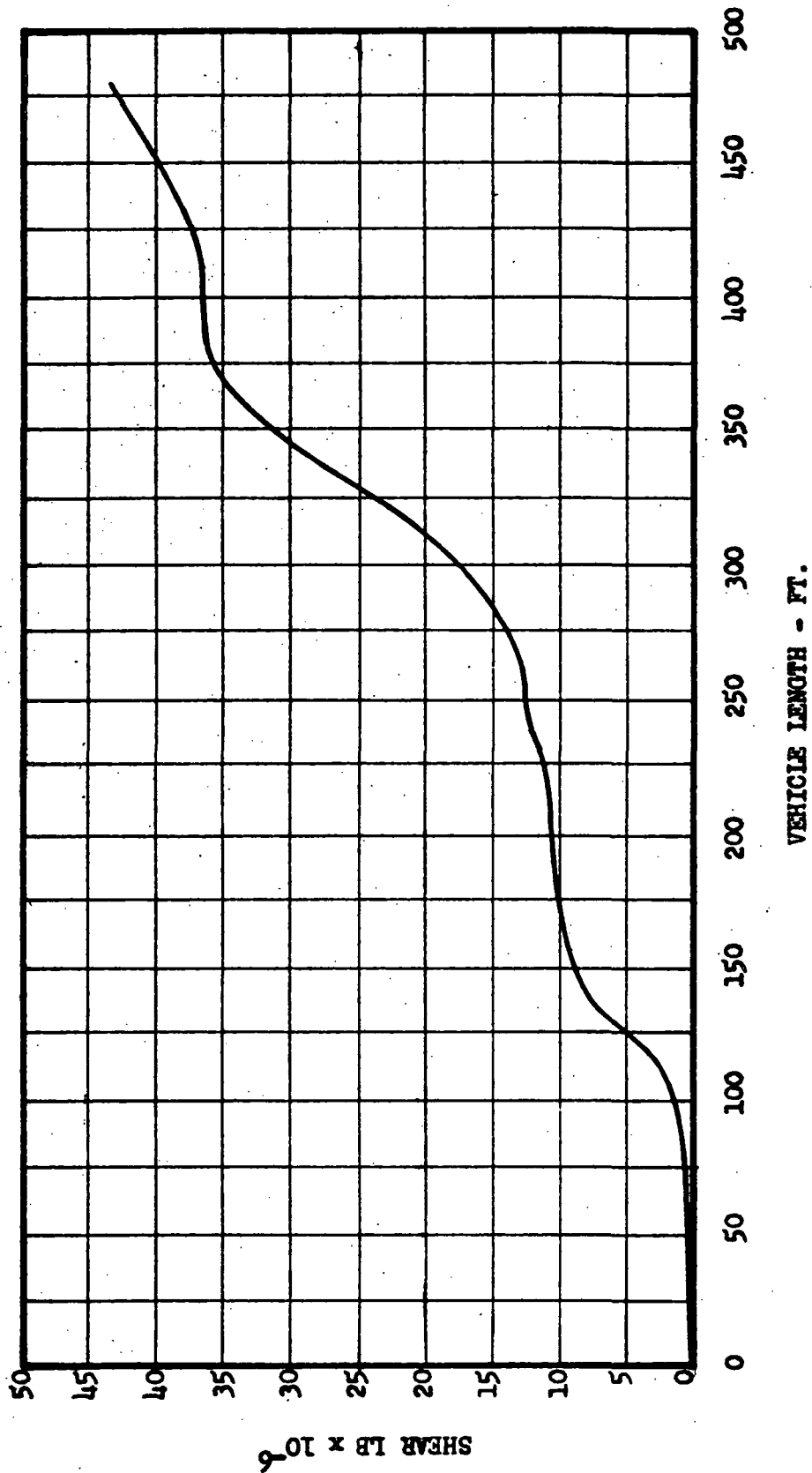
Shear versus Station (Sea State 6)

Figure V-B-11



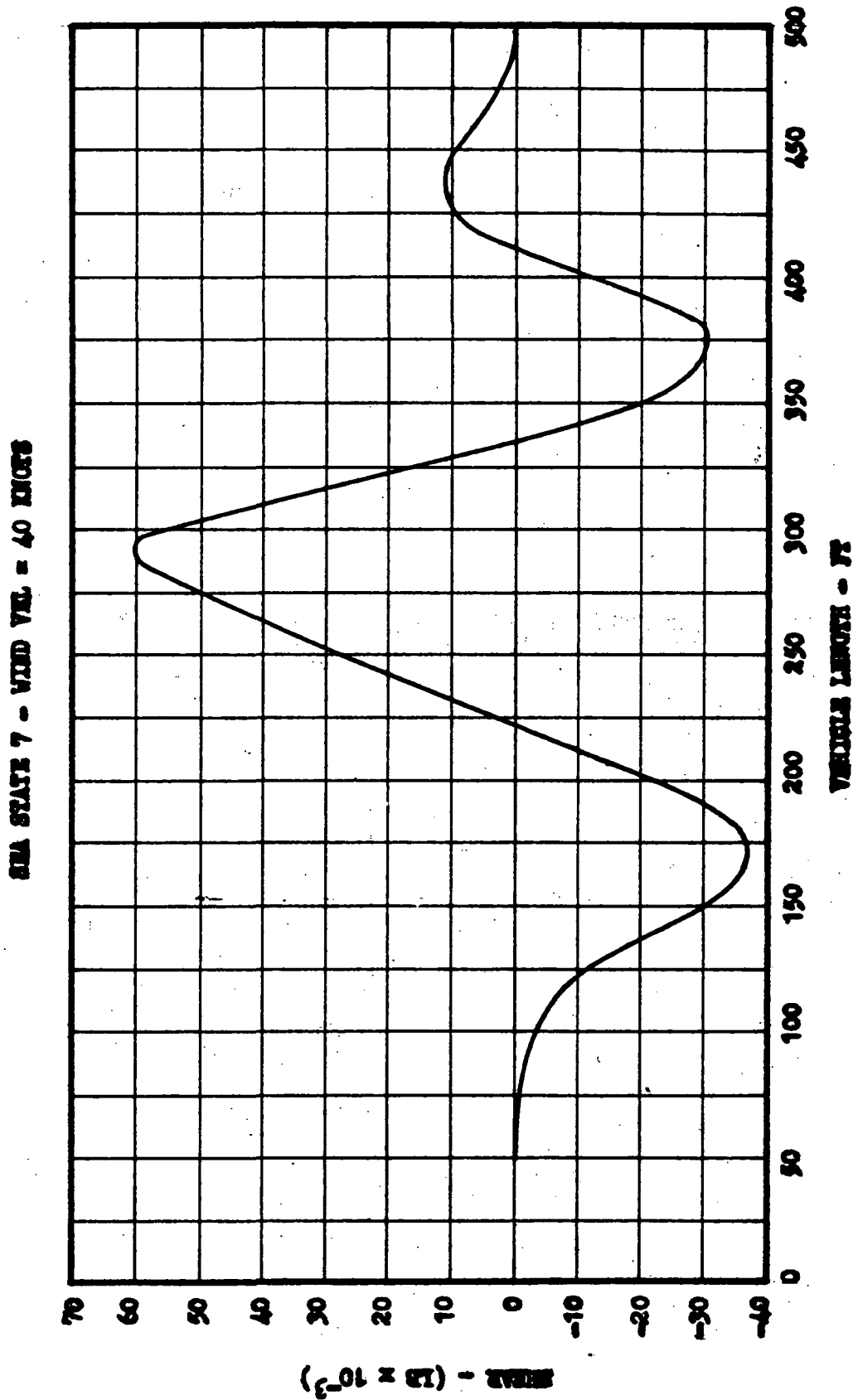
Moment versus Station (Sea State 6)

Figure V-B-12



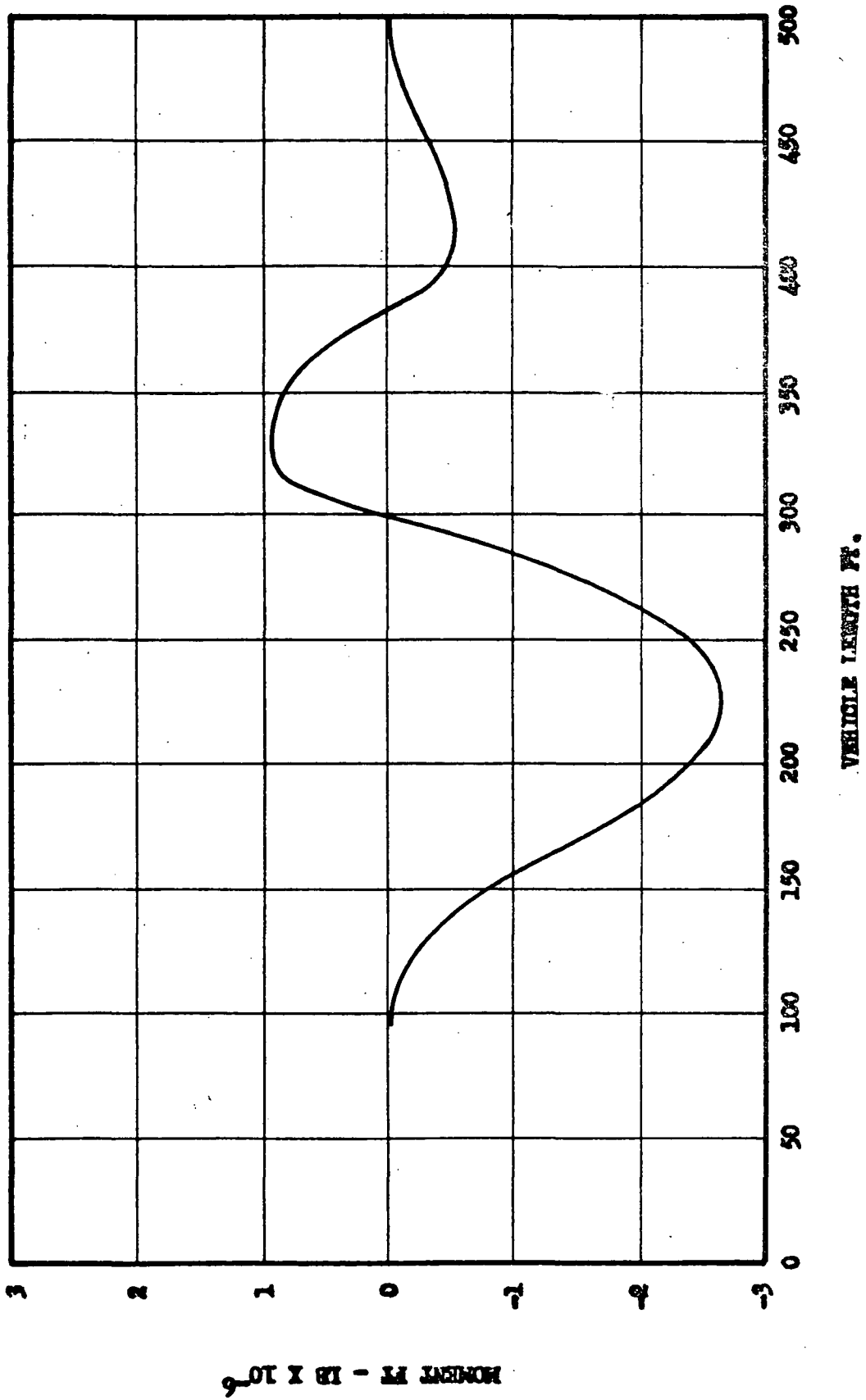
Axial Load versus Station (Sea State 7)

Figure V-B-13



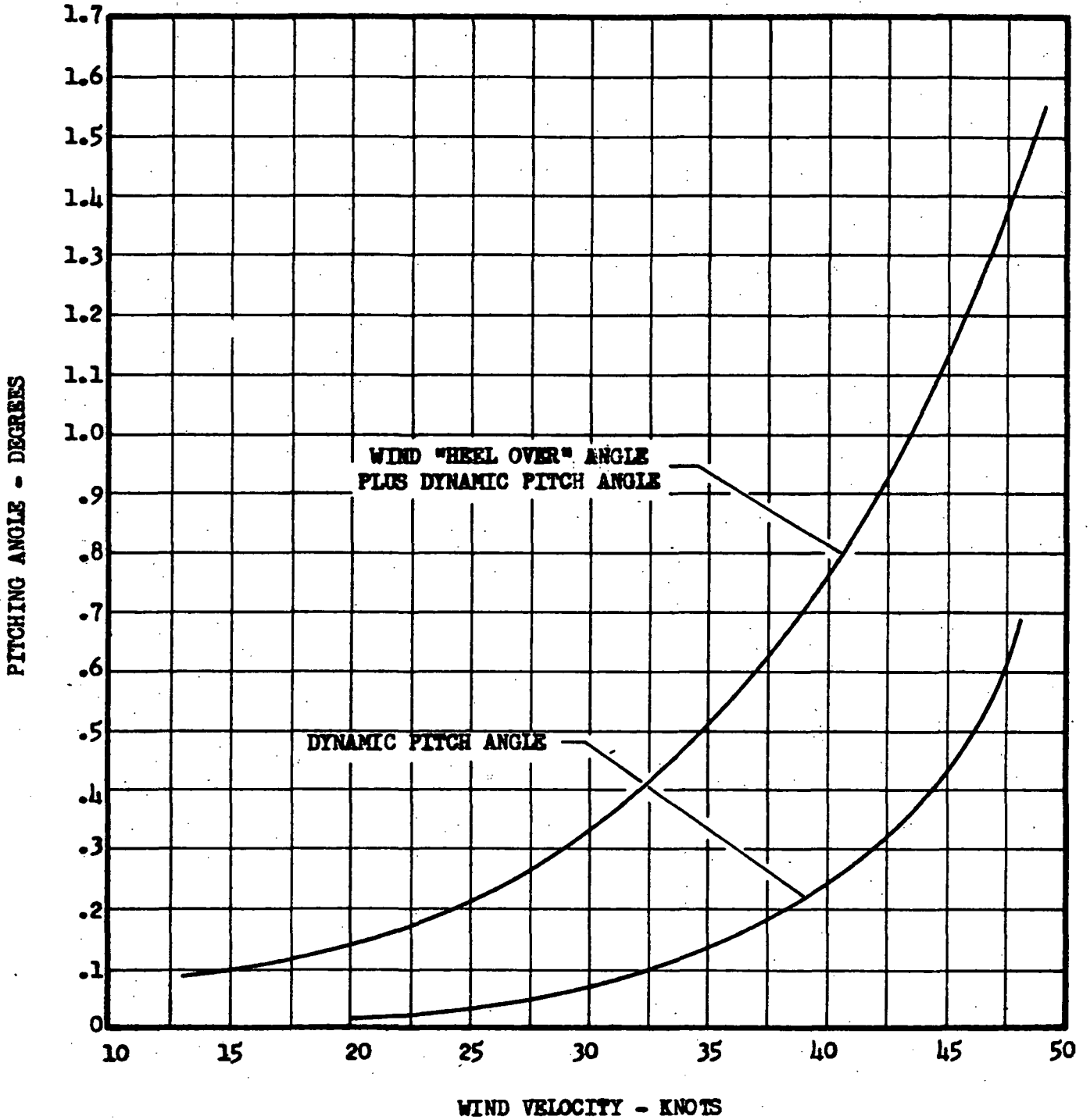
Shear Load versus Station (Sea State 7)

Figure V-B-14



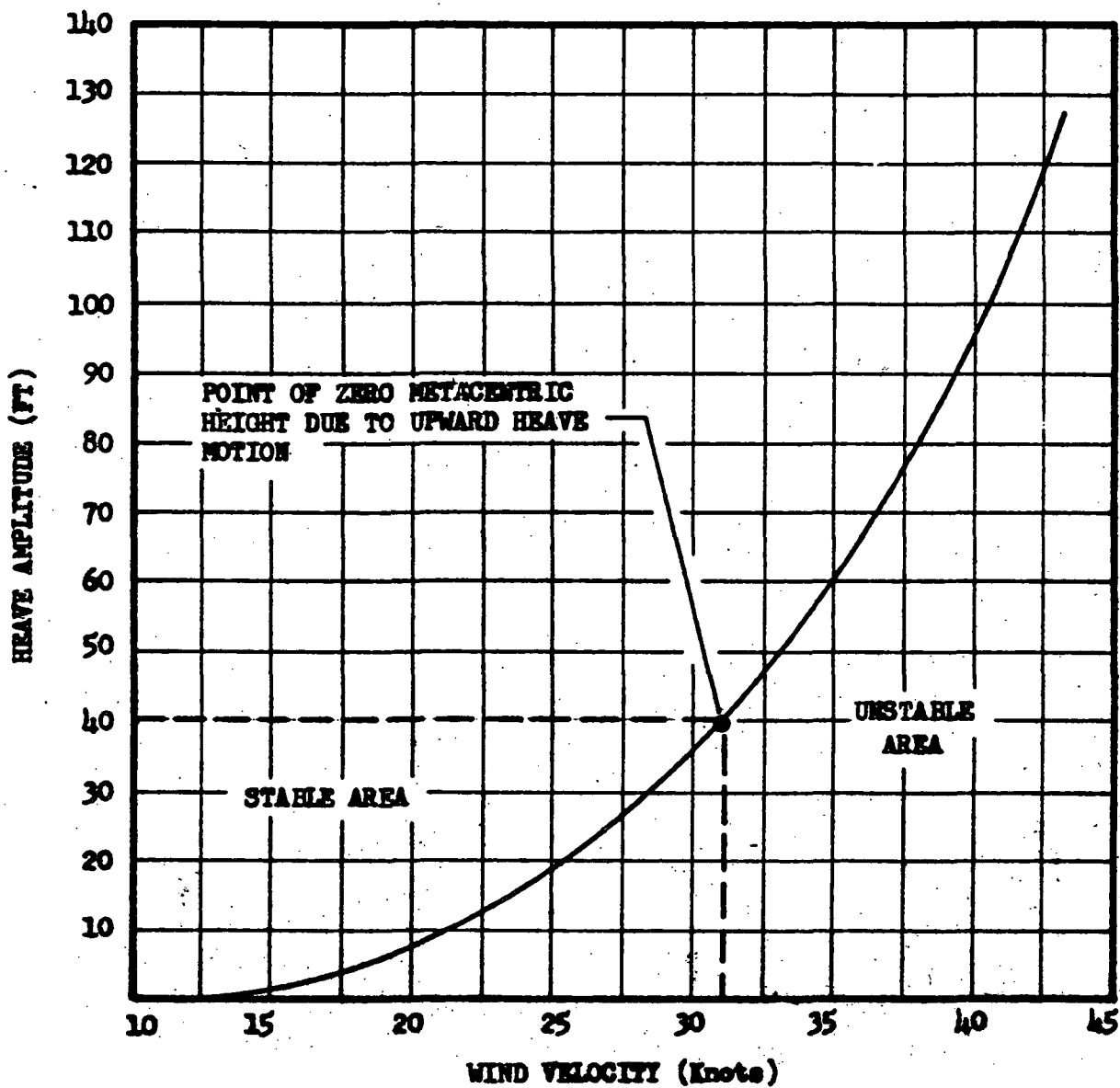
Moment versus Station (Sea State 7)

Figure V-B-15



Pitching Amplitude versus Wind Velocity

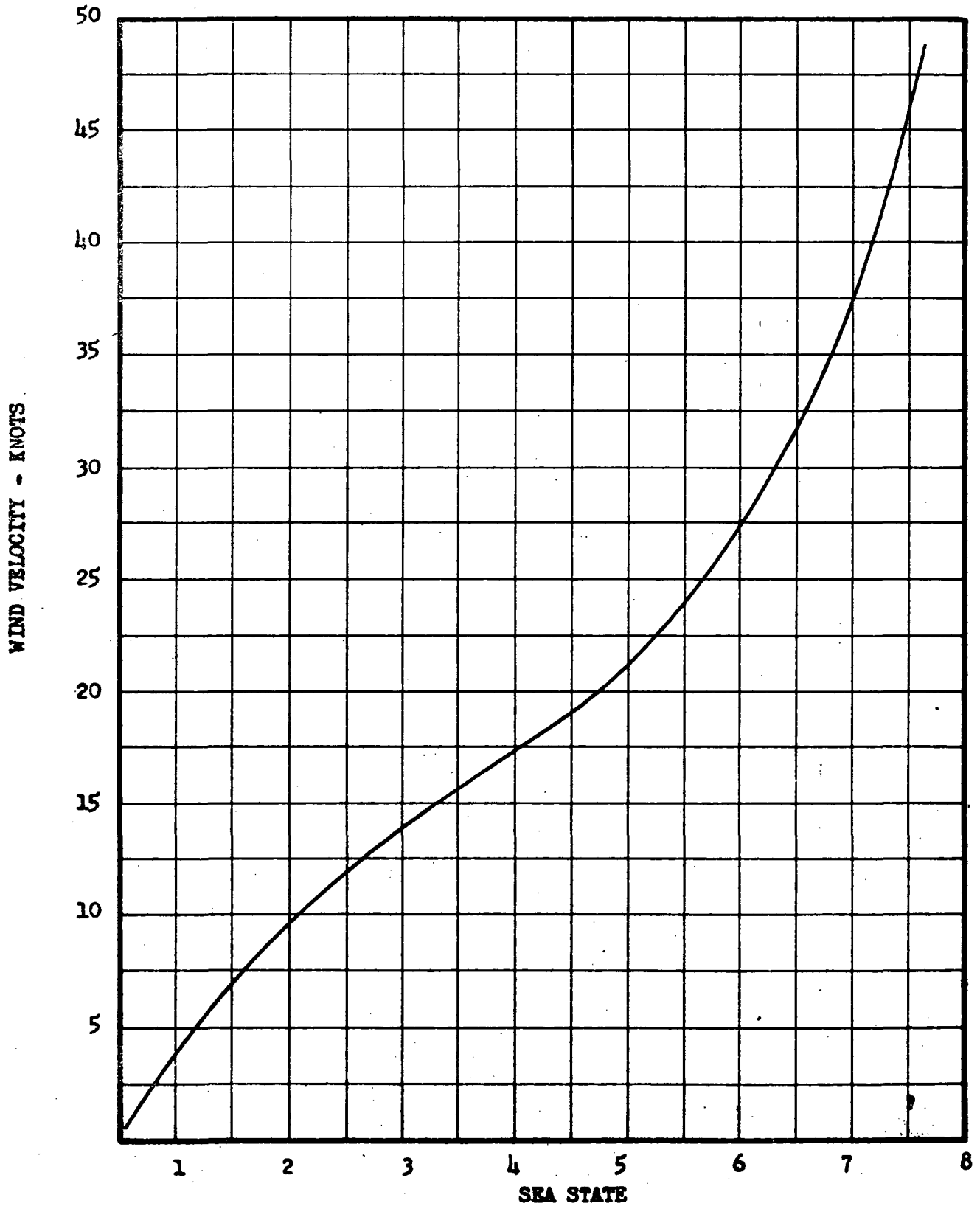
Figure V-B-16



Heave Amplitude versus Wind Velocity

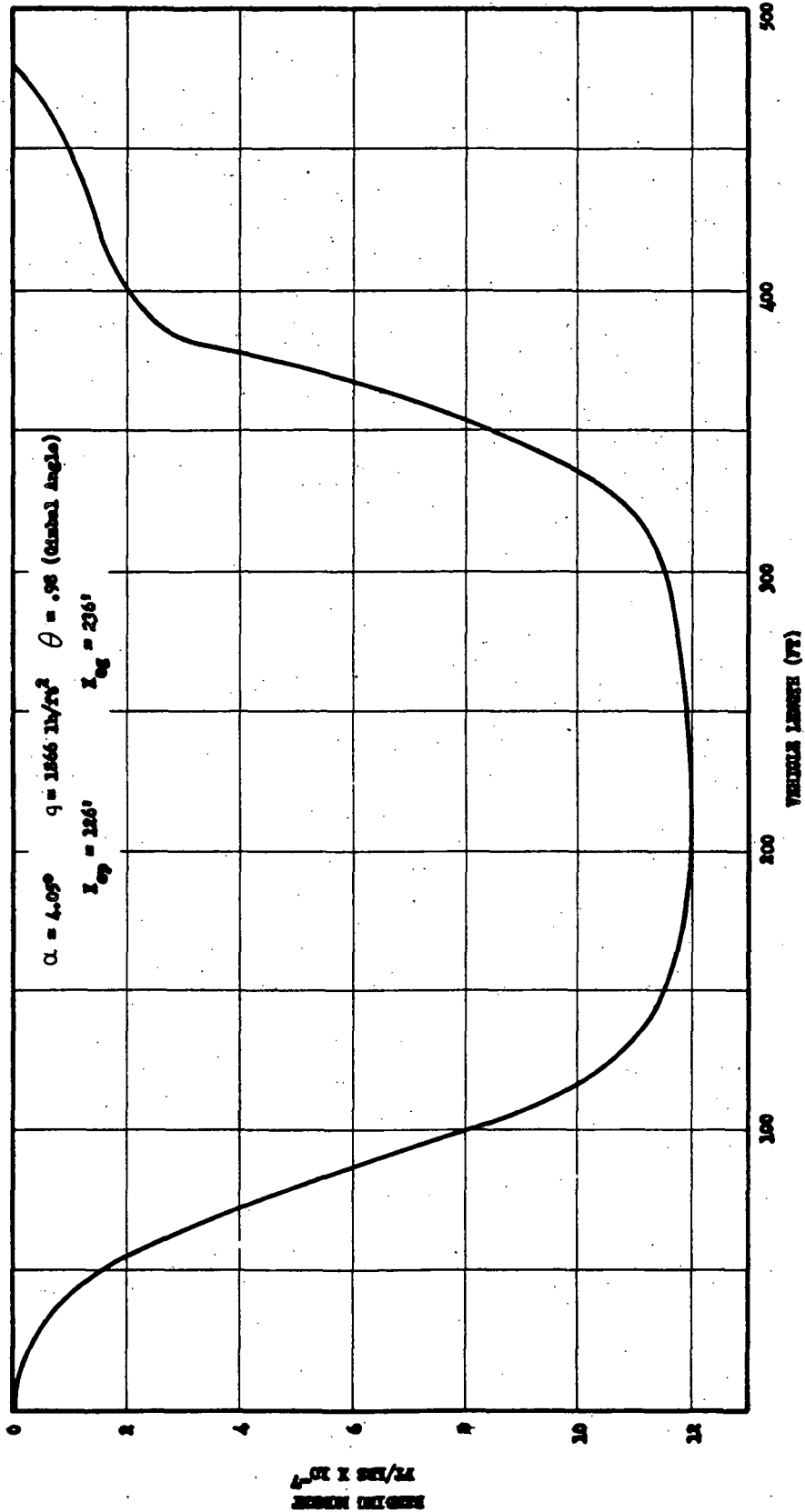
Figure V-B-17

AEROJET-GENERAL CORPORATION



Sea State versus Wind Velocity

Figure V-B-18



Bending Moment, Maximum Dynamic Pressure

Figure V-B-19

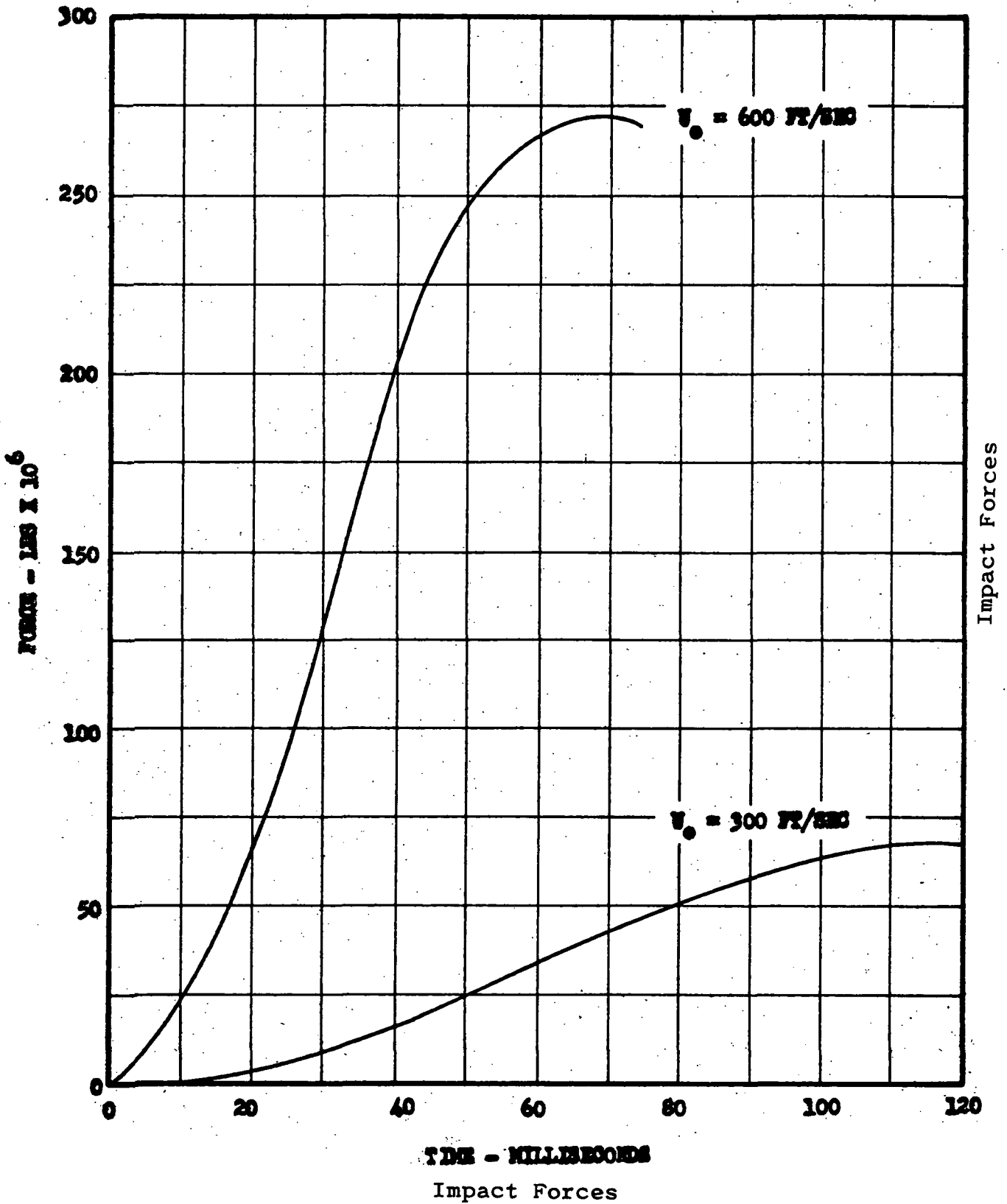
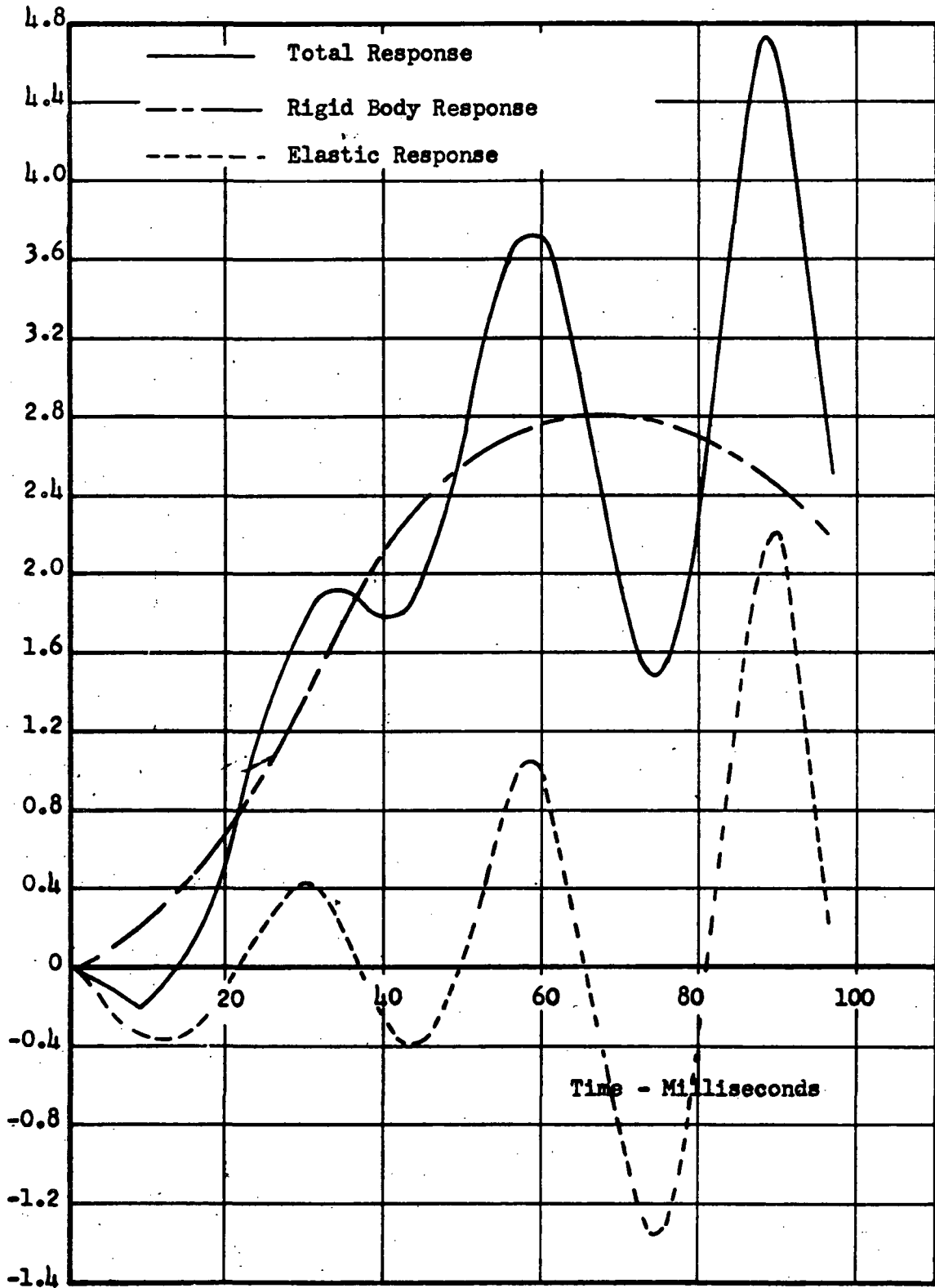
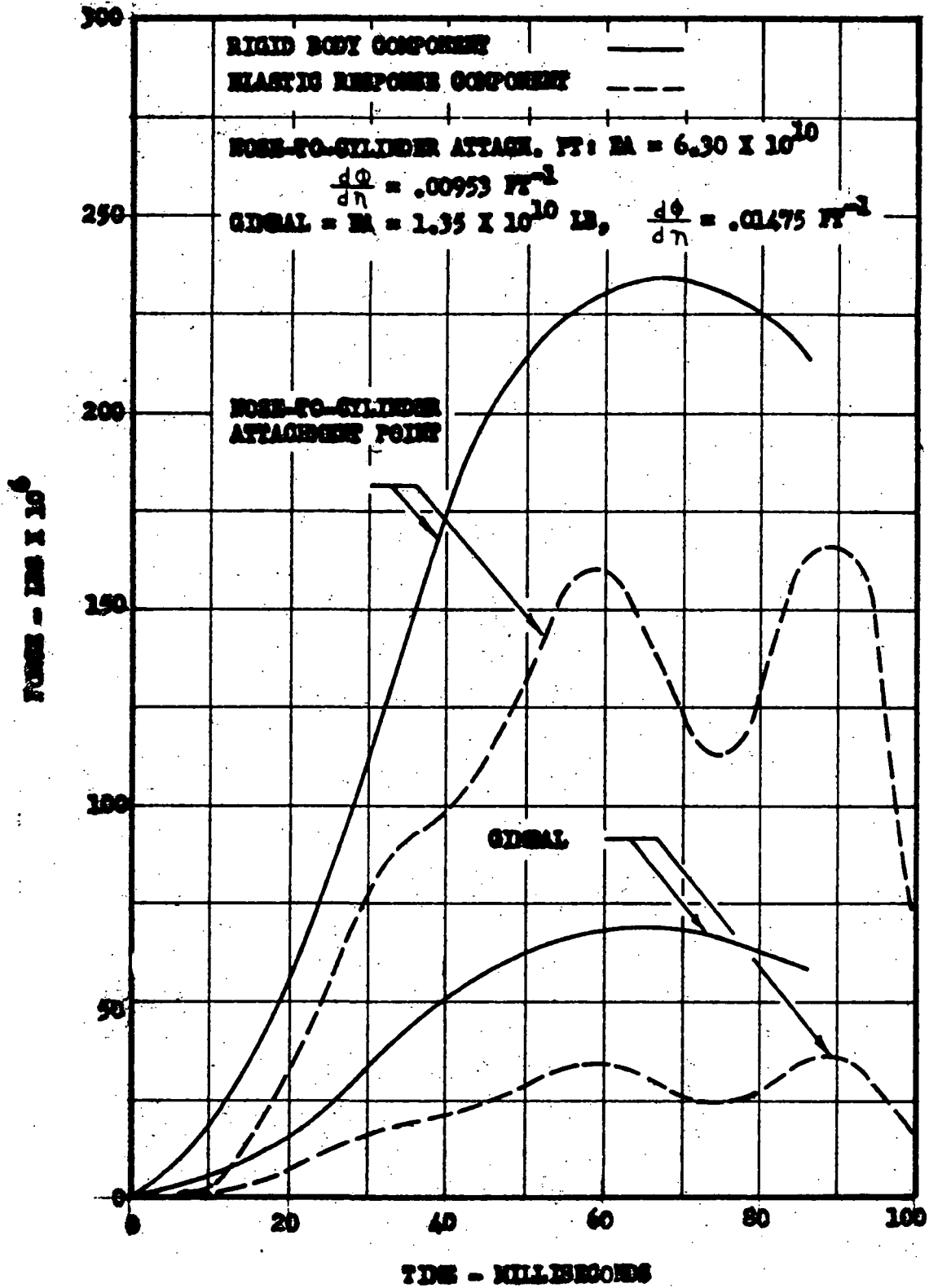


Figure V-B-20



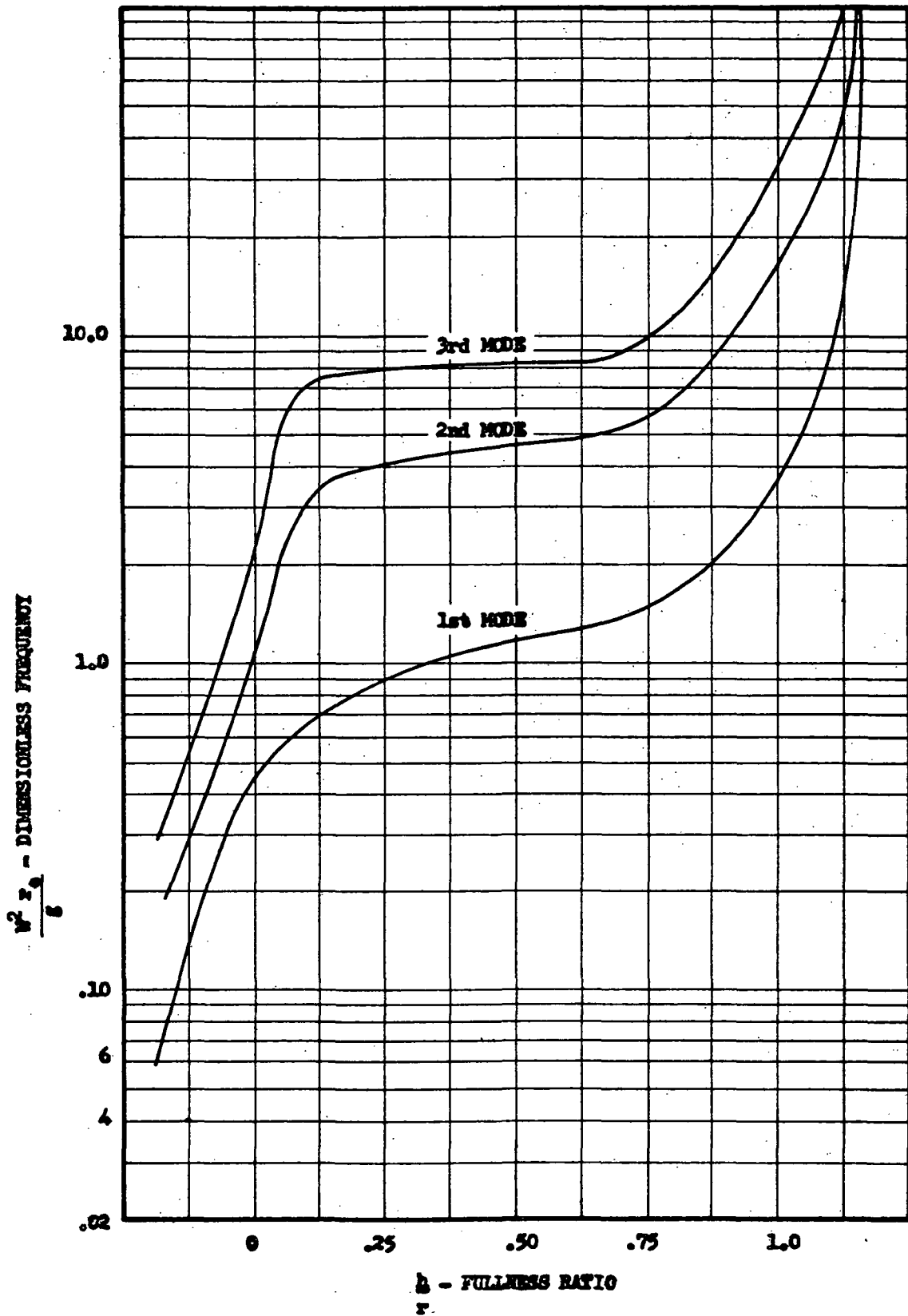
Impact Accelerations

Figure V-B-21



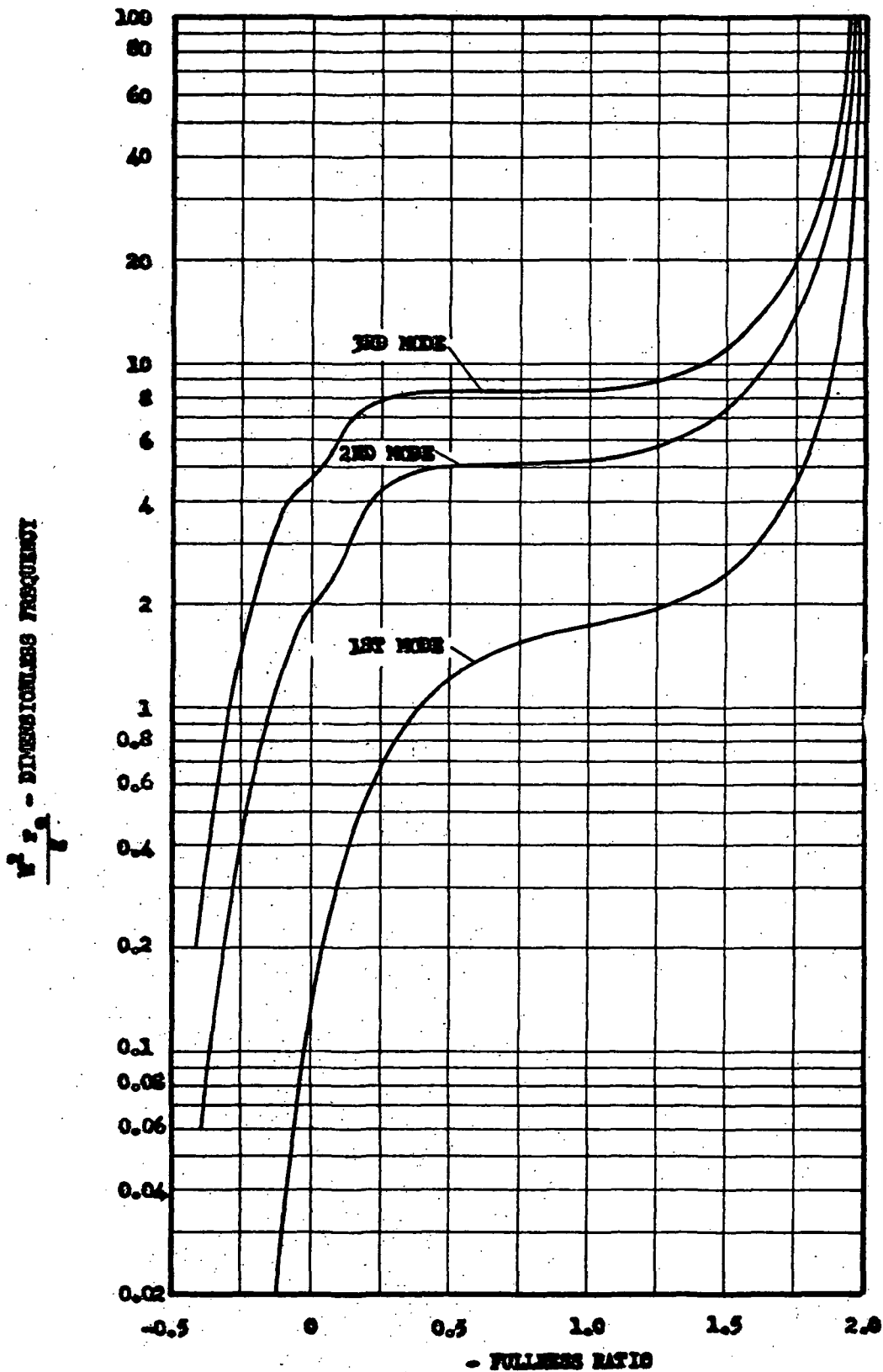
Impact Dynamic Loads

Figure V-B-22



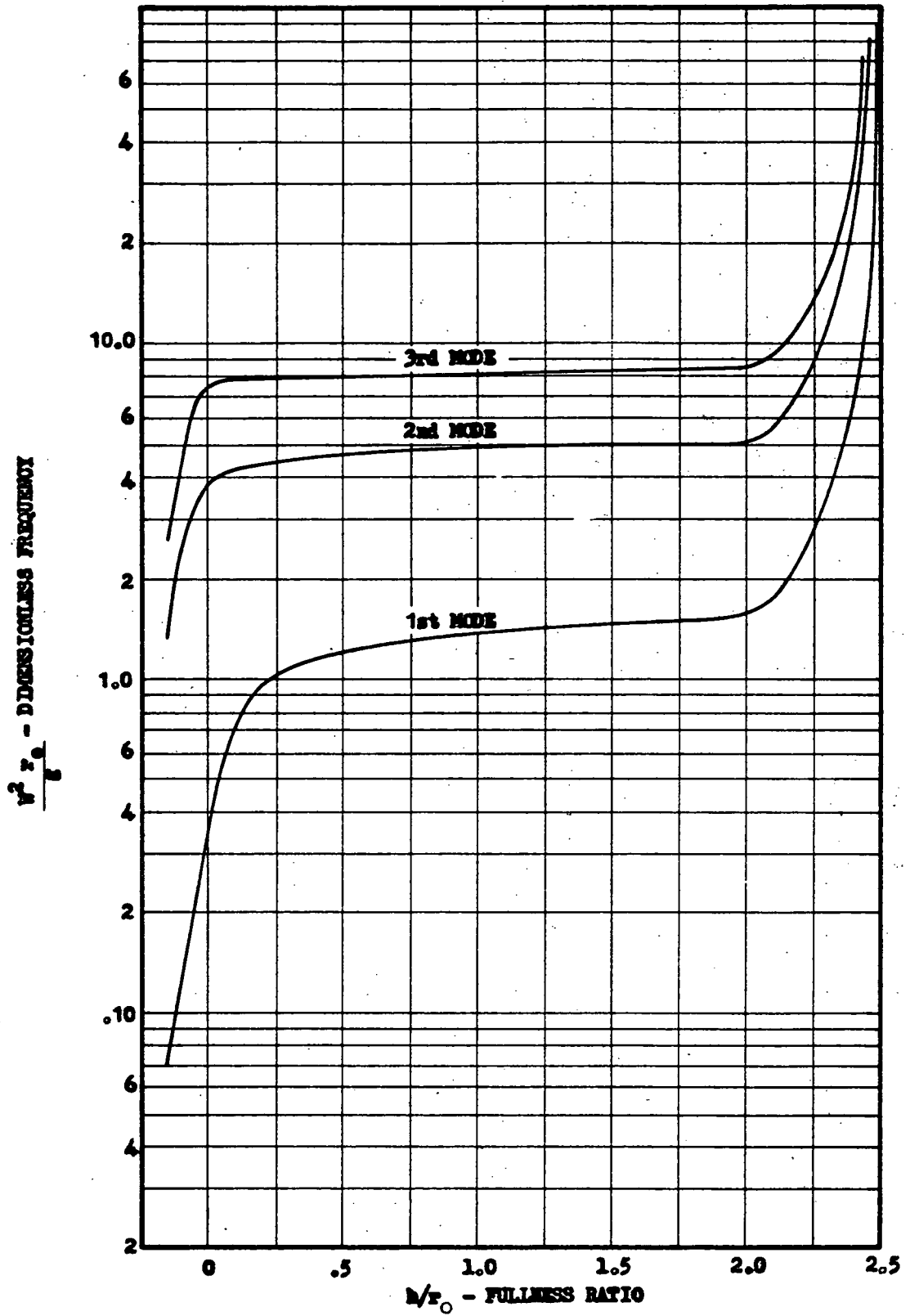
Frequency versus Fluid Depth Stage I Fuel Tank

Figure V-B-23



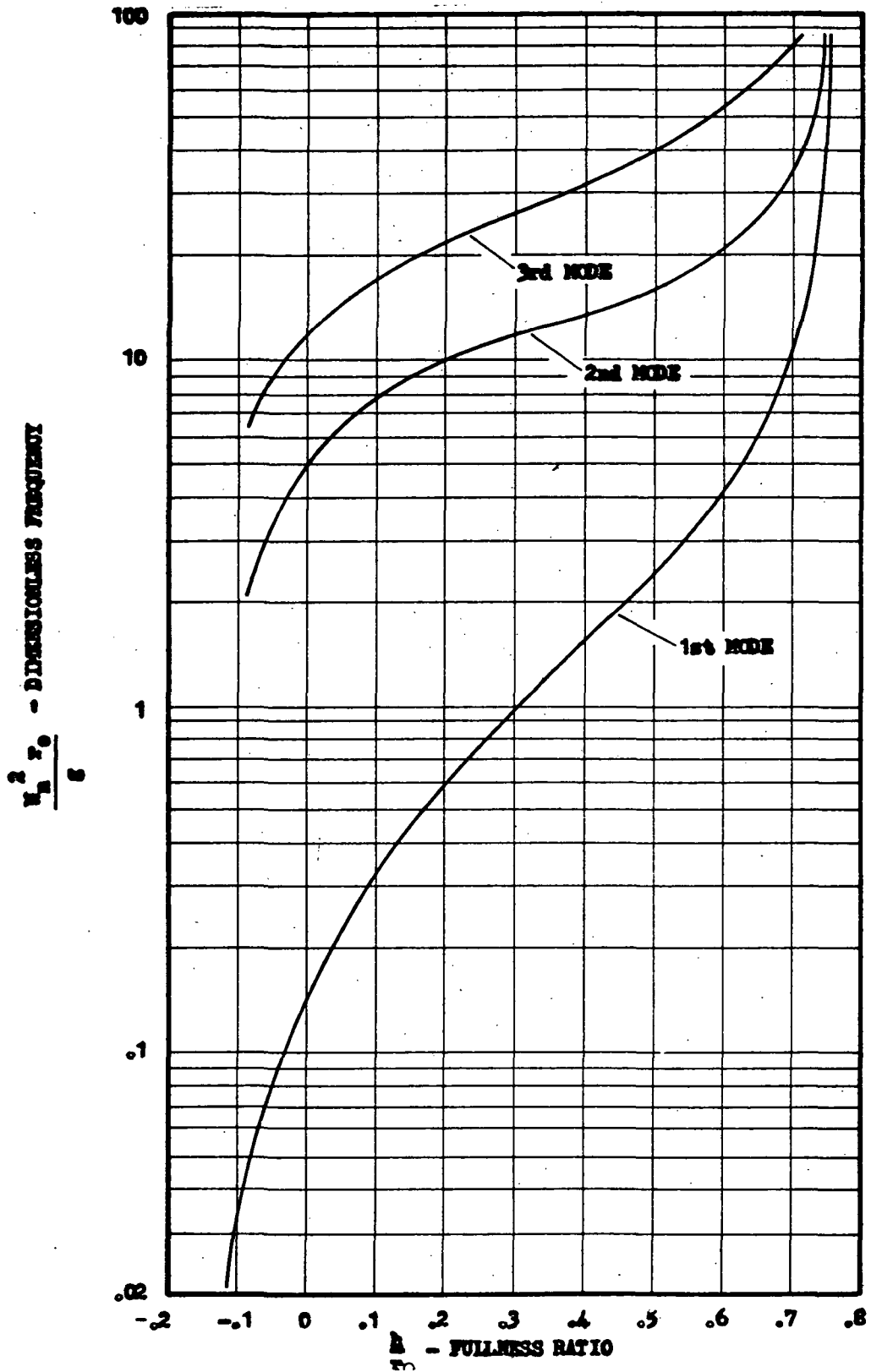
Frequency versus Fluid Depth Stage I LO₂ Tank

Figure V-B-24



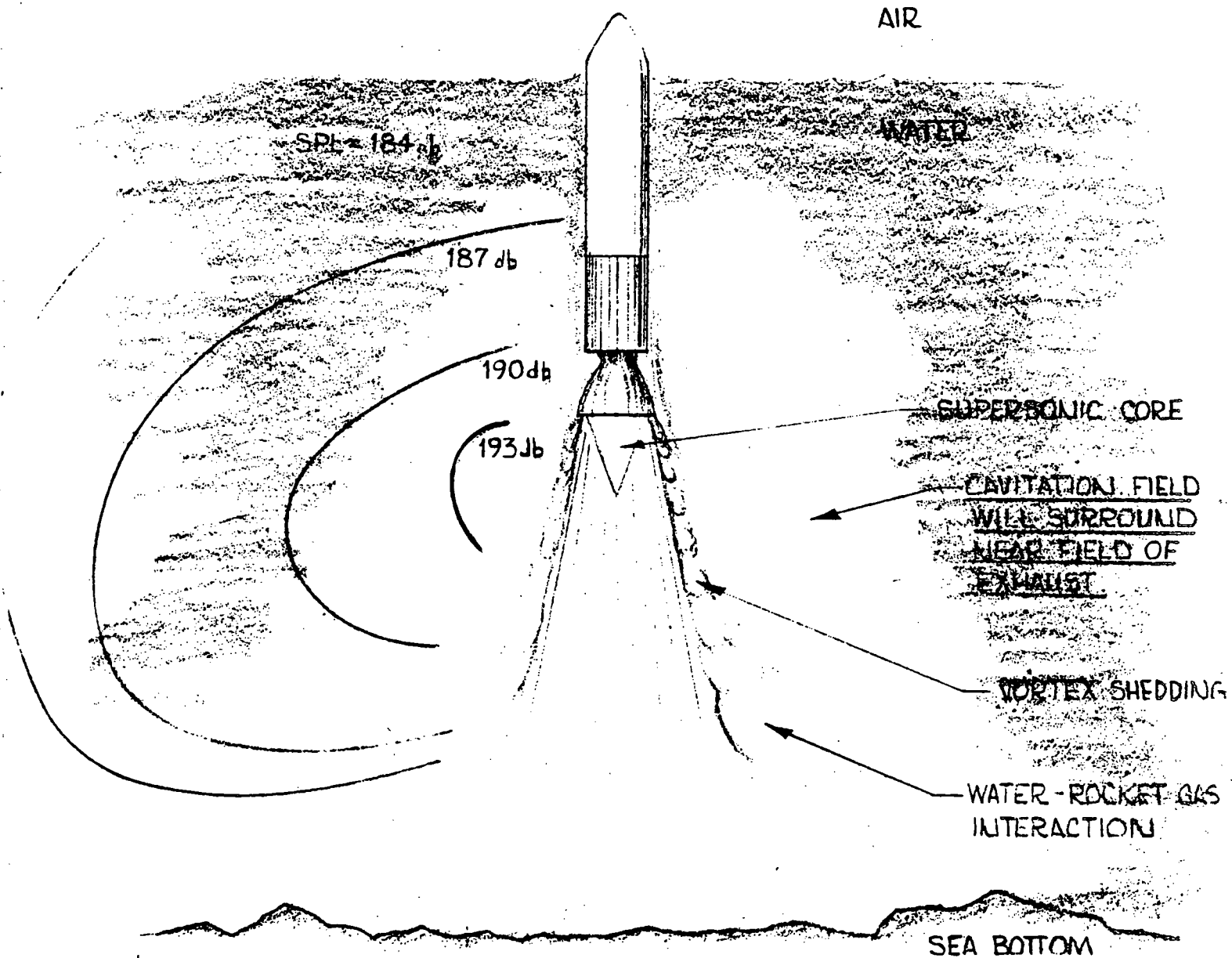
Frequency versus Fluid Depth Stage II Fuel Tank

Figure V-B-25



Frequency versus Fluid Depth Stage II Oxidizer Tank

Figure V-B-26



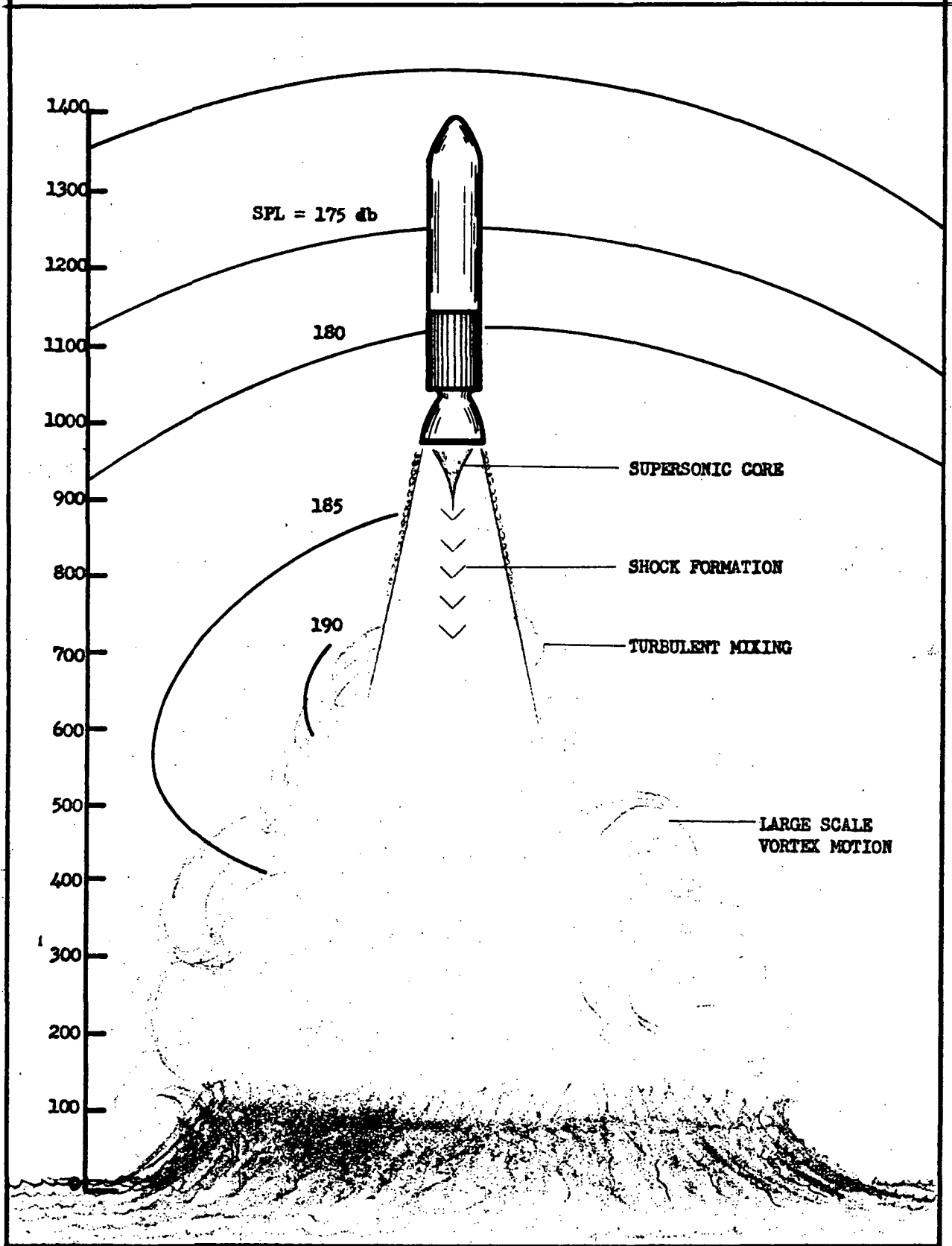
NOTE: SOUND PRESSURE LEVEL (SPL)
 [re: .0002 dyne/cm²]

$$SPL = 20 \log \frac{P}{P_0} - 10 \log \frac{\rho C}{\rho_0 C_0}$$

$$\rho_0 C_0 = \begin{cases} \text{AIR} & 42 \text{ gm/cm}^2\text{sec} \\ \text{WATER} & 1.5 \times 10^5 \text{ gm/cm}^2\text{sec} \end{cases}$$

Near Field Sound Level

Figure V-B-27



Near Noise Field after Water Exit

Figure V-B-28